

Transverse mixing of conservative and reactive tracers in porous media

Dissertation

der Mathematisch-Naturwissenschaftlichen Fakultät

der Eberhard Karls Universität Tübingen

zur Erlangung des Grades eines

Doktors der Naturwissenschaften

(Dr. rer. nat.)

vorgelegt von

Gabriele Chiogna

aus Trento

Tübingen

2010

Tag der mündlichen Qualifikation:

11.02.2011

Dekan:

Prof. Dr. Wolfgang Rosenstiel

1. Berichterstatter:

Prof. Dr. Peter Grathwohl

2. Berichterstatter:

Prof. Dr.Ing. Olaf. A. Cirpka

To Giorgia

τῷ πιθόμη]ν· ἐνὶ τοῖς γὰρ αἰείδομεν οἱ λιγὺν ἦχον
τέττιγος, θ]όρυβον δ' οὐκ ἐφίλησαν ὄνων.

Καλλίμαχος, Αἴτια (29-30)

**I obeyed him. In fact we sing among those who love the shrill sound
of the cicada, not the bray of donkeys.**

Callimachus, Aitia (29-30)

TABLE OF CONTENTS

Kurzfassung	1
Abstract	3
Introduction	5
Enhancement of dilution and transverse reactive mixing in porous media: experiments and model-based interpretation.....	13
1.1 INTRODUCTION	14
1.2 MATERIAL AND METHODS	15
1.2.1 <i>Experimental set-up</i>	15
1.2.2 <i>Hydraulic properties</i>	16
1.2.3 <i>Numerical Modeling</i>	18
1.3 RESULTS AND DISCUSSION	18
1.3.1 <i>Conservative Transport Experiments</i>	18
1.3.2 <i>Reactive Experiments</i>	25
1.4 CONCLUSIONS.....	30
REFERENCES.....	33
Transverse mixing of conservative and reactive tracers in porous media: quantification through the concepts of flux-related and critical dilution indices	37
2.1 INTRODUCTION	38
2.2 FLUX RELATED DILUTION INDEX FOR CONSERVATIVE TRANSPORT.....	40
2.3 CRITICAL DILUTION INDEX FOR REACTIVE TRANSPORT.....	42
2.3.1 <i>Reactive transport problem</i>	42
2.3.2 <i>Definition and derivation of the critical dilution index</i>	44
2.4 TRANSPORT SIMULATIONS AT DIFFERENT SCALES	46
2.4.1 <i>Results of conservative transport simulations</i>	47
2.4.2 <i>Results of reactive transport simulations</i>	49
2.5 CONCLUSIONS.....	53
APPENDIX A: Transport of the entropy density	55
APPENDIX B: Relationship between flux-related and cross-sectional dilution indices in homogeneous cases	55
APPENDIX C: Flux-related dilution index for a line source in homogeneous two-dimensional domains and analytical expressions for other remarkable cases.....	56
APPENDIX D: Uniqueness of the critical dilution index in homogeneous media	57
REFERENCES.....	61

Evidence of compound-dependent hydrodynamic and mechanical transverse dispersion by multi-tracer laboratory experiments.....	67
3.1 INTRODUCTION	68
3.2 THEORETICAL BACKGROUND.....	69
3.3 MATERIAL AND METHODS	70
3.4 RESULTS AND DISCUSSION	73
REFERENCES.....	79
S1. SUPPORTING INFORMATION: Measurements of transverse dispersion coefficient.	83
Isotopic fractionation by transverse dispersion: flow-through microcosms and reactive transport modeling study	91
4.1 INTRODUCTION	92
4.2 MATERIAL AND METHODS	93
4.2.1 <i>Experimental Setup</i>	93
4.2.2 <i>Conservative transport modeling</i>	94
4.2.3 <i>Reactive transport modeling</i>	96
4.3 RESULTS AND DISCUSSION	98
4.3.1 <i>Conservative Transport Experiments</i>	98
4.3.2 <i>Reactive Transport Experiments</i>	99
4.3.3 <i>Environmental implications and significance</i>	102
REFERENCES.....	105
S1. SUPPORTING INFORMATION: Experimental setup.....	109
S2 SUPPORTING INFORMATION: Calculation of biodegradation.....	111
Relevance of local compound-specific transverse dispersion for conservative and reactive mixing in heterogeneous porous media	115
5.1 INTRODUCTION	116
5.2 PROBLEM STATEMENT	117
5.2.1 <i>Generation of heterogeneous conductivity fields</i>	118
5.2.2 <i>Governing equations</i>	119
5.2.3 <i>Solution of reactive transport</i>	121
5.3 MEASURES OF DILUTION IN CONSERVATIVE TRANSPORT	123
5.3.1 <i>Effective dispersion coefficient</i>	123
5.3.2 <i>Flux-related effective dispersion coefficient</i>	125
5.3.3 <i>Scalar dissipation rate</i>	127
5.3.4 <i>Flux-related dilution index</i>	128
5.3.5 <i>Discussion of conservative transport results</i>	130
5.4 REACTIVE TRANSPORT.....	131
5.4.1 <i>Length of steady-state reactive plumes</i>	132
5.4.2 <i>Measures of reactive mixing</i>	133
5.5 CONCLUSIONS.....	135
REFERENCES.....	139

Conclusions	145
Acknowledgements	151
Curriculum Vitae.....	153
Ergänzungsblatt zur Eigenleistung.....	155

Kurzfassung

Die korrekte Quantifizierung des Durchmischungsprozesses ist von höchster Bedeutung zur Modellierung des reaktiven Transports in porösen Medien und um Verbleib und Verhalten von Stoffen in der Umwelt einzuschätzen. In dieser Arbeit konzentrieren wir uns hauptsächlich auf zweidimensionale Systeme unter stationären Flussbedingungen mit einer kontinuierlichen, konstant linearen Quelle. Wir untersuchen den konservativen und reaktiven Transport in homogenen und heterogenen porösen Medien und berücksichtigen hierbei Laborversuche sowie numerische Modelle auf der Darcy- und Feldskala. Unter den beschriebenen Annahmen finden die wichtigsten Durchmischungsprozesse in Querrichtung zum Hauptstrom statt. Die Hauptfragestellung dieser Arbeit ist also, wie man Querdurchmischung auf der Darcy- und Feldskala genau quantifizieren kann. Quasi-Zweidimensionale Laborversuche wurden durchgeführt um i) die Effekte der Fokussierung des Flusses in höher durchlässigen Zonen auf die Querdurchmischung bezüglich des konservativen und reaktiven Transports gelöster Stoffe zu untersuchen; ii) die Stoffabhängigkeit der mechanischen Dispersion auf der Darcyskala zu erforschen; iii) die Effekte eines stoffspezifischen lokalen Querdurchmischungskoeffizienten auf die Isotopenfraktionierung bei konservativem und reaktivem (d.h. aerobem und anaerobem Bioabbau) Transport zu studieren. Numerische Modelle wurden verwendet, um die experimentellen Ergebnisse quantitativ auszuwerten und um verschiedene Größen für Verdünnung und Durchmischung bei konservativem und reaktivem Transport auf der Darcy- und Feldskala zu studieren. Unterschiedliche feldskalige Szenarien wurden analysiert, mit dem Ziel die verstärkenden Effekte auf die Durchmischung aufgrund der Fokussierung des Flusses in hoch durchlässigen Einschlüssen zu quantifizieren und die bedeutende Rolle einer korrekten Parametrisierung des lokalen transversalen Dispersionskoeffizienten für die Definition eines effektiven Durchmischungskoeffizienten zu verdeutlichen. Die Hauptergebnisse dieser Arbeit sind: i) die Fokussierung des Flusses in höher durchlässigen Zonen ist ein zentraler Mechanismus zur Verstärkung der Durchmischung in Querrichtung und führt deshalb zu effektiven Dispersionskoeffizienten, die auf der Feldskala deutlich höher sind als die lokalen; ii) flussspezifische Größen führen zu einer Verbesserung der Quantifizierung der Durchmischung und insbesondere der neu definierte flussspezifische Verdünnungsindex könnte, durch Einführung des kritischen Verdünnungsindex, zur Quantifizierung des reaktiven Transports in Beziehung gebracht werden; iii) lokale Querdurchmischungskoeffizienten sind für einen weiten Bereich von Pécletzahlen stoffspezifisch: Stoffe mit verschiedenen Diffusionskoeffizienten in Wasser zeigen immer unterschiedliche physikalische Verschiebungen in Querrichtung. Dieses Ergebnis hat maßgebliche Konsequenzen für Mischungskontrollierte Reaktionen am Rand von Schadstofffahnen und für die Interpretation von Isotopensignaturen; iv) die Effekte von stoffspezifischen lokalen Querdurchmischungskoeffizienten sind auch auf der Feldskala relevant und sollten bei der Modellierung des Transports von konservativen und insbesondere reaktiven gelösten Stoffen in Grundwasser berücksichtigt werden.

Abstract

The correct quantification of mixing is of utmost importance for modeling reactive transport in porous media and for assessing the fate and transport of contaminants in the subsurface. In this work we mainly focus on two-dimensional systems under steady-state flow conditions with a continuous, constant linear source. We investigate both conservative and reactive transport in homogeneous and heterogeneous porous media and hereby, consider laboratory bench-scale experiments as well as numerical models at the Darcy and at the field scales. Under the specified conditions the most important mixing processes occur in the transverse direction perpendicular to the main flow. The leading question behind this work is hence, how we can properly quantify mixing in the transverse direction at the Darcy and at the field scales. Quasi two-dimensional laboratory bench-scale experiments have been performed in order to study: i) the effects of flow focusing in high-permeability zones on transverse mixing for conservative and reactive solute transport; ii) the compound-specific behavior of mechanical dispersion at the Darcy scale; iii) the effects of compound-specific local transverse dispersion coefficients on isotope fractionation for conservative and reactive (i.e. aerobic and anaerobic biodegradation) transport. Numerical models have been used to quantitatively interpret the outcomes of the laboratory experiments and to study different measures of dilution and mixing for conservative and reactive solute transport at the Darcy and at the field scales. Different scenarios have been investigated at the field scale, with the aim of quantifying the mixing-enhancement effects of flow focusing in high-permeability inclusions and the important role of a correct parameterization of local transverse dispersion on the definition of effective dispersion coefficients. The main outcomes of this work are i) flow focusing in high-permeability zones is a key mechanism for transverse mixing enhancement which leads to effective dispersion coefficients at the field scale significantly larger than the local ones; ii) flux-related quantities lead to an improvement in the quantification of mixing and in particular the newly defined flux-related dilution index may be related to the quantification of reactive mixing through the introduction of the ‘critical dilution index’; iii) local transverse dispersion is compound-specific over a wide range of Péclet numbers: compounds with different aqueous diffusion coefficients always show different transverse displacements. This finding has important consequences for mixing-controlled reactions at the fringe of contaminant plumes and for the interpretation of isotopic signatures; iv) the effects of compound-specific local-scale transverse dispersion coefficients are relevant even at the field scale and should be taken into account when modeling conservative and especially reactive solute transport in groundwater.

Introduction

Groundwater is by far the most abundant source of freshwater of the planet, if we exclude glaciers and ice caps, and in Europe, for example, 75% of the population depends on it as fresh water supply. Nonetheless, as pointed out in the forewords of the new groundwater directive of the European Union, the social and economical value of groundwater has been often underestimated in the past decades. This underestimation and the lack of overall planning of the use of this precious resource led to major environmental issues like overexploitation of aquifers, salinization and the uncontrolled spreading of diffuse and point sources of pollution in the subsurface environment. Groundwater is a “hidden resource” for which pollution prevention, monitoring and restoration are more difficult than for surface waters due to its inaccessibility. This “hidden” character makes it difficult to adequately locate, characterize and understand pollution impacts and to predict the fate and transport of the released contaminants. The consequences of anthropogenic activities may last for decades or even centuries and hence pollution that occurred somehow in the past – whether from agriculture, industry or other human activities – may still be threatening groundwater quality today and, in many cases, will continue to do so for several generations to come. The main causes for this long timescale when dealing with groundwater pollution are both the slow velocities of the flow through the subsurface porous matrix and the slow kinetic of the physical and chemical processes which may affect a contaminant.

Different processes occur at different scales and their understanding is an essential prerequisite for risk assessment studies in soils and sediments and for the design of subsurface remediation techniques [Bear, 1972; Dentz *et al.*, 2010]. In fact, it is extremely important to capture the kinetic of the mechanisms in act in order to quantify the time required for the remediation of a site: the slowest process is the limiting factor which in the end will control the whole remediation strategy. Natural attenuation of organic contaminants in groundwater and most in situ remediation technologies of contaminated aquifers (e.g. enhanced bioremediation, chemical oxidation, etc.) depend on mixing of reaction partners such as electron donors and acceptors [Lerner *et al.*, 2000]. In fact chemical reactions such as many oxidation-reduction reactions, aerobic degradation and denitrification are often fast - and in some cases may be considered instantaneous [Cirpka and Valocchi, 2007] - in comparison to the timescale of mixing processes. If we consider typical groundwater plumes, we often can address the problem of contaminant transport in porous media under the assumption of steady state conditions [Rolle *et al.*, 2009]. In this case, the most important mixing process between the contaminant plume and the surrounding clean water occurs in the transverse direction perpendicular to the mean flow [Cirpka *et al.*, 1999; Ham *et al.*, 2004; Liedl *et al.*, 2005; Maier and Grathwohl, 2006] and it is strongly affected by the porous nature of the aquifer.

A bundle of capillaries, called pore channels, connected through junctions can be assumed as a simplified model for a porous medium [Bear, 1972]. Hence, the smallest scale of interest for transport in this structure is the pore scale and here the flow of a solute is described by the Navier-Stokes equations and appropriate boundary conditions [e.g., Willingham *et al.*, 2008, 2010]. In case of laminar flow conditions, the only physical mixing process is molecular diffusion. This is the only mechanism which may lead to reaction between two initially segregated reactive species which flow in adjacent streamtubes and it is driven by a concentration gradient [e.g., Cao and Kitanidis, 1998]. At this level it is possible to capture and study the real physical and chemical processes occurring in the porous matrix but unfortunately this is a very complex system and for practical applications it is not feasible to describe it in details. Even if we aim to investigate a relatively simple and small bench scale problem it is necessary to find up-scaled quantities able to capture the main features of the microscopic processes [Bear, 1972]. We need these parameters to be easy to define, to measure and to use, in fact they should allow us to work with a model with lower resolution but still capable of predicting the fate and transport of a solute.

A typical solution strategy to obtain these quantities is to average them at the pore scale over a representative elementary volume (REV), as defined by *Bear* [1972]. After this averaging step the flow can be described by Darcy's law, and hence this scale is commonly called Darcy scale. Since the up-scaled quantities are considered locally constant over an REV, this scale is called local scale as well. Here mixing in the transverse direction is dominated by two main processes: pore diffusion and mechanical dispersion [*Saffman*, 1960; *Bear and Bachmat*, 1967]. The first term is the ratio between the molecular (aqueous) diffusion coefficient and the tortuosity of the porous medium, a geometrical parameter which accounts for the reduced volume available for molecular diffusion due to the presence of the solid matrix [*Grathwohl*, 1998]. Mechanical dispersion is a mixing process which derives from the up-scaling procedure we apply from the pore- to the Darcy scale and reflects the fluctuations of the velocity at the pore scale among an average value [*Bear and Bachmat*, 1967]. Hence, mechanical dispersion is not a physical mixing process like molecular diffusion, but a quantification of the unknown mixing generated by the flow variations through pore channels that we are not able to capture in an up-scaled model. It is possible to obtain Darcy-scale parameters from laboratory bench-scale experiments which aim to test and verify the outcomes of up-scaling theories and to investigate single physical and chemical processes under well controlled conditions [*Delgado and Carvalho*, 2001; *Klenk and Grathwohl*, 2002; *Bauer et al.*, 2009]. Researches carried out at this level are of utmost importance in terms of process understanding [e.g., *Oswald and Kinzelbach*, 2004], but real aquifer systems are orders of magnitude larger and much more complex than what it is possible to recreate in a laboratory experimental setup.

At the field scale the description of the porous medium given at the Darcy scale is often too detailed and at the same time oversimplified, even if this may seem to be a contradiction. In fact, the natural presence of heterogeneities in the porous matrix at this level would require the assignment of specific Darcy-scale parameters to the different formations present. This is impossible with the available technologies, since the characteristics of the geological structures in the subsurface remain usually widely unknown in such details. At the same time laboratory-scale experiments are not able to capture the variety of shapes, permeabilities and geochemical characteristics commonly occurring in nature. Hence a further up-scaling step is required in order to define an effective dispersion coefficient which is able to describe mixing and dilution at the field scale [e.g. *Kitanidis*, 1988; *Dagan*, 1984, 1990, 1991; *Rajaram and Gelhar*, 1993a, 1993b, 1995; *Gelhar and Axness*, 1983; *Neuman et al.*, 1987]. One additional difficulty is related to this last up-scaling step: it is very challenging or sometimes even impossible to generalize the experimental outcomes from field studies since they are not performed under well controlled and repeatable conditions. Hence, the definition and quantification of the parameters to use at the field scale is usually addressed using stochastic theories and numerical models [*Dentz et al.*, 2010]. In addition to the processes parameterized with the local dispersion coefficients, at the field scale we have to consider those mixing mechanisms associated with the larger scale heterogeneities which affect the flow of a solute. Among the advective mixing mechanisms, flow focusing in high-permeability inclusions is a key mechanism able to significantly enhance transverse mixing [*Werth et al.*, 2006]. This effect is considered as a possible reason for effective transverse dispersion coefficients at the field scale much larger than those observed at the Darcy scale [e.g., *Maier and Grathwohl*, 2006; *Prommer et al.*, 2009].

When a plume develops from a source of contamination in an aquifer, different compounds are released and transported through the porous medium and may interact with chemical species already present in the system (e.g. dissolved oxygen, nitrate, iron, sulfate etc.). Hence, it is crucial to correctly quantify reaction and degradation mechanisms when considering reactive transport of a contaminant, since they determine for example the length of contaminant plumes [*Liedl et al.*, 2005; *Cirpka et al.*, 2006]. In order to react two particles have to physically come into contact through mixing, hence the leading processes we are interested in are mainly the pore-scale ones [*Willingham et al.*, 2008, 2010]. However, due to the aforementioned limitations of a pore-scale approach to the problem (e.g., the difficulty in describing the porous medium in details), we need to use for

practical purposes (e.g., risk assessment) up-scaled parameters. The up-scaling procedure which leads to a local dispersion tensor can be verified against laboratory bench-scale experiments and the coefficients derived from conservative transport experiments [e.g., *Harleman and Rumer, 1963; Olsson and Grathwohl, 2007*] can be applied for the reactive cases at the Darcy scale [*Rolle et al., 2009; 2010*]. On the contrary, due to the increased complexity of the system and to the difficulty in capturing all the features of a field-scale experiment, up-scaled quantities at this scale are not usually able to predict correctly reactive transport scenarios [*Cirpka, 2002*] and the use of Darcy-scale parameters typically overestimate the length of a reactive plume [*Maier and Grathwohl, 2006*]. How to derive an effective transverse dispersion coefficient able to describe mixing for conservative as well as reactive species, is still a matter of debate, even if considerable research effort has been devoted to answer this relevant question [*Dentz et al., 2010*].

The present work aims to further investigate the crucial problem of transverse mixing in porous media: i) starting from the question of how to quantify mixing; ii) verifying which are appropriate measures of mixing against bench-scale experimental data; iii) improving the description of Darcy-scale processes with multi-tracer laboratory bench-scale experiments; iv) considering the influence of compound specific Darcy-scale processes on field-scale scenarios.

In the first Chapter of this thesis, the results of laboratory bench-scale experiments [*Rolle et al., 2009*] are shown both for conservative and reactive solute transport in homogeneous and heterogeneous porous media under steady-state and transient flow conditions. The experimental results are successfully reproduced with a numerical model and the enhancement of mixing, due to flow focusing in high-permeability inclusions and to non-stationary flow conditions, is quantified using measures of mixing like the second central moment, the newly introduced flux-related dilution index, for conservative solute transport, and the product mass flux for reactive transport. In the second Chapter we further develop the tool of flux-related dilution index, providing analytical and semi-analytical expressions to compute it in homogeneous porous media and, more importantly, we link it to reactive transport defining the critical dilution index [*Chiogna et al., 2010a*]. This quantity measures how much mixing is required to extinguish a contaminant plume with a given mass flux for a given instantaneous bimolecular reaction. This modeling study investigate scenarios both at the laboratory as well as at the field scale, showing that an effective transverse dispersion coefficient derived from the flux-related dilution index can be used in reactive transport simulations in order to predict the exact length of the reactive plume at both scales.

In Chapters 3 and 4 we focus our attention on Darcy-scale transverse mixing processes. First we quantify the local transverse dispersion coefficient through multi-tracer experiments with conservative solutes (oxygen, bromide and fluorescein). The goal of this study is to investigate whether mechanical transverse dispersion is affected by properties of the different compounds like the aqueous diffusion coefficient [*Chiogna et al., 2010b*]. The experimental outcomes show how laboratory bench-scale experiments are helpful to test the assumptions beyond a theory: the mechanical transverse dispersion term, in fact, was found to be compound specific in contradiction with the conclusions of random walk based theories [e.g., *Scheidegger, 1961*]. Since the aqueous diffusion coefficient is a mass dependent property of a chemical specie [*Worch, 1993*], we investigated these compound-specific effects in case of transport of different contaminant isotopologues. In particular we focused on the investigation of transverse mixing under steady-state conditions and its potential to lead to isotopic fractionation. The results of a flow-through experiment demonstrate that for conservative transport of labeled ethylbenzene a relevant fractionation is measurable due to the difference in the dispersion coefficients of the light and heavy isotopologues [*Rolle et al., 2010*]. Furthermore the same system is investigated under aerobic and anaerobic reactive conditions and it is shown how stable isotope analysis related to biodegradation of a hydrocarbon can be improved by considering fractionation due to transport mechanisms.

In the fifth Chapter we combine the main outcomes of the laboratory studies, i.e. the compound dependency of local mechanical transverse dispersion, with new (e.g. flux-related dilution index, flux-related second moment) and traditional (e.g. scalar dissipation rate [*Kitanidis, 1994*], second

moment [*Dentz and Carrera, 2003*]) measures of mixing. Field-scale conservative and reactive transport simulations are analyzed for different heterogeneous flow fields and the influence of compound-dependent local transverse dispersion coefficients on the up-scaled effective dispersion coefficient is investigated [*Chiogna et al., 2010c*].

REFERENCES

- Bauer, R.D., M. Rolle, P. Kürzinger, P. Grathwohl, R.U. Meckenstock and C. Griebler (2009), Two-dimensional flow-through microcosms: versatile test systems to study biodegradation processes in porous aquifers. *J. Hydrol.* 369, 284-295.
- Bear, J. and Y.A. Bachmat (1967), A generalized theory on hydrodynamic dispersion in porous media. IASH Symp. Artificial Recharge and management of aquifers, Haifa, Israel IASH, P.N. 1967 72, 7-16.
- Bear, J. Dynamics of fluids in porous media; Dover: New York, USA, 1972.
- Cao, J, and P. K. Kitanidis (1998), Pore-scale dilution of conservative solutes: An example, *Water Resour. Res.*, 34(8), 1941-1949.
- Chiogna G., O.A. Cirpka, P. Grathwohl and M. Rolle, (2010a), Transverse mixing of conservative and reactive tracers in porous media: quantification through the concepts of flux-related and critical dilution indices, *Water Resour. Res.*, (accepted).
- Chiogna, G., C. Eberhardt, P. Grathwohl, O.A. Cirpka and M. Rolle (2010b), Evidence of compound dependent hydrodynamic and mechanical transverse dispersion by multitracer laboratory experiments, *Environ. Sci. Technol.*, 44(2), 688-693, doi: 10.1021/es9023964.
- Chiogna G., O.A. Cirpka, P. Grathwohl and M. Rolle, (2010c), Relevance of local compound-specific transverse dispersion for conservative and reactive mixing in heterogeneous porous media, *Water Resour. Res.*, (submitted).
- Cirpka, O.A. (2002), Choice of dispersion coefficients in reactive transport calculations on smoothed fields, *J. Contam. Hydrol.*, 58, 261-282.
- Cirpka, O.A. and A.J Valocchi (2007), Two-dimensional concentration distribution for mixing-controlled bioreactive transport in steady state. *Advances Water Resour.*, 30 (6-7), 1668-1679.
- Cirpka, O.A., A. Olsson, Q. Ju, A. Rahman and P. Grathwohl (2006), Determination of transverse dispersion coefficients from reactive plumes lengths. *Ground Water*, 44 (2), 212-221.
- Cirpka, O.A., E.O. Frind and R. Helmig (1999), Numerical simulation of biodegradation controlled by transverse mixing. *J. Contam. Hydrol.* 40, 159-182.
- Dagan, G. (1984), Solute transport in heterogeneous porous formations, *J. Fluid Mech.* 145: 151-177.
- Dagan, G. (1990), Transport in heterogeneous porous formations: Spatial moments, ergodicity, and effective dispersion, *Water Resour. Res.*, 26(6): 1281-1290.
- Dagan, G. (1991), Dispersion of a passive solute in nonergodic transport by steady velocity-fields in heterogeneous formations, *J. Fluid Mech.* 233: 197-210.
- Delgado, J.M.P.Q. and J.F.R Carvalho (2001), Measurement of the coefficient of transverse dispersion in flow through packed beds for a wide range of values of the Schmidt number. *Transport in porous media* 2001, 44, 165-180.

Dentz, M, T. Le Borgne, A. Englert and B. Bijeljic (2010), Mixing, spreading and reaction in heterogeneous porous media: A brief review, *J. Contam. Hydrol.*, in press.

Dentz, M. and Carrera, J. (2003) Effective dispersion in temporally fluctuating flow through a heterogeneous medium, *Phys. Rev. E* 68 (3): 036310.

Gelhar, L.W., and C.L. Axness (1983), Three-dimensional stochastic analysis of macrodispersion in aquifers, *Water Resour. Res.*, 19 (1), 161-180.

Grathwohl, P. Diffusion in natural porous media: contaminant transport, sorption/desorption, and dissolution kinetics; Kluwer Academic Publishers: Boston, MA, USA, 1998.

Ham, P.A.S., R.J. Schotting, H. Prommer and G.B. Davis (2004), Effects of hydrodynamic dispersion on plume lengths for instantaneous bimolecular reactions. *Adv. Water Resour. Res.* 27, 803-813.

Harleman, D. and Rumer R. (1963), Longitudinal and lateral dispersion in an isotropic porous medium. *J. Fluid Mech.*, 16, 385-394.

Kitanidis, P.K. (1988), Prediction by the method of moments of transport in heterogeneous formations, *J. Hydrol.* 102(1-4): 453-473.

Kitanidis, P.K. (1994), The concept of dilution index, *Water Resour. Res.*, 30 (7), 2011-2026.

Klenk, I.D., and P. Grathwohl (2002), Transverse vertical dispersion in groundwater and the capillary fringe. *J. Contam. Hydrol.*, 58, 111-128.

Lerner, D.N., S.F. Thornton, M.J. Spence, S.A. Banwart, S.H. Bottrell, J.J. Higgo, H.E.H. Mallinson, R.W. Pickup, and G.M. Williams (2000), Ineffective natural attenuation of degradable organic compounds in a phenol-contaminated aquifer, *Ground Water*, 38, 922-928.

Liedl, R., A.J. Valocchi, P. Dietrich and P. Grathwohl (2005), Finiteness of steady state plumes. *Water Resour. Res.*, 31, W12501; DOI 10.1029/2005WR004000.

Maier, U. and P. Grathwohl (2006) Numerical experiments and field results on the size of steady state plumes. *J. Contam. Hydrol.* 85, 33-52. Mayer, K.U., S.G. Benner, E.O. Frind, S.F. Thornton and D.N.

Neuman, S.P., C.L. Winter, and C.M. Newman (1987), Stochastic theory of field-scale Fickian dispersion in anisotropic porous media, *Water Resour. Res.* 23(3): 453-466.

Olsson, A. and P. Grathwohl (2007), Transverse dispersion of non reactive tracers in porous media: A new nonlinear relationship to predict dispersion coefficients. *J. Contam. Hydrol.*, 92, 149-161.

Oswald, S. E. and W. Kinzelbach, (2004) Three-dimensional physical benchmark experiments to test variable-density flow model, *J. Hydrol.*, 290, 22-42.

Prommer, H., B. Anneser, M. Rolle, F. Einsiedl, and C. Griebler (2009), Biogeochemical and isotopic gradients in a BTEX/PAH contaminant plume: model-based interpretation of a high-resolution field data set, *Environ. Sci. Technol.*, 43, 8206-8212.

Rajaram, H., and L.W. Gelhar, (1993a) Plumescale-dependent dispersion in heterogeneous aquifers 1. Lagrangian analysis in a stratified aquifer, *Water Resour. Res.* 29(9): 3249-3260.

Rajaram, H., and L.W. Gelhar, (1993b) Plumescale-dependent dispersion in heterogeneous aquifers 2. Eulerian analysis and three-dimensional aquifers, *Water Resour. Res.* 29(9): 3261-3276.

Rajaram, H., and L.W. Gelhar, (1995) Plumescale dispersion in aquifers with a wide range of scales of heterogeneity, *Water Resour. Res.* 31(10): 2469-2482.

Rolle, M., G. Chiogna, R. Bauer, C. Griebler and P. Grathwohl (2010), Isotopic fractionation by transverse dispersion: flow-through microcosms and reactive transport modeling study, *Environ. Sci. Technol.*, 44, 6167-6173.

Rolle, M., C. Eberhardt, G. Chiogna, O.A. Cirpka, and P. Grathwohl (2009), Enhancement of dilution and transverse reactive mixing in porous media: Experiments and model-based interpretation, *J. Contam. Hydrol.*, 110, 130-142.

Saffman, P.G. (1960) Dispersion due to molecular diffusion and macroscopic mixing in flow through a network of capillaries. *J. Fluid Mech.*, 2, 194-208.

Scheidegger, A.E. (1961), General theory of dispersion in porous media, *J. Geophys. Res.*, 66(4), 3273-3278.

Werth, C.J., O.A. Cirpka and P. Grathwohl (2006), Enhanced mixing and reaction through flow focusing in heterogeneous porous media. *Water Resour. Res.*, 42, W12414; DOI 10.1029/2005WR004511.

Willingham, T., C. Zhang, C.J. Werth, A.J. Valocchi, M. Oostrom, and T.W. Wiestma (2010), Using dispersivity values to quantify the effects of pore-scale flow focusing on enhanced reaction along transverse mixing zone, *Adv. Water Res.*, 33, 525-535.kk

Willingham, T.W., C.J. Werth, and A.J. Valocchi (2008), Evaluation of the effects of porous media structure on mixing-controlled reactions using pore-scale modeling and micromodel experiments, *Environ. Sci. Technol.*, 42, 3185-3193.

Worch, E. (1993), Eine neue Gleichung zur Berechnung von Diffusionskoeffizienten gelöster Stoffe. *Vom Wasser*, 81, 289-297.

Chapter 1

Enhancement of dilution and transverse reactive mixing in porous media: experiments and model-based interpretation¹

Abstract

Transport and natural attenuation of contaminant plumes in groundwater is often controlled by transverse dispersion. The extent of mixing between dissolved reaction partners at the fringe of a plume determines its length and depends strongly on the groundwater flow field. Transient flow conditions as well as the focusing of the flow in high permeability zones may enhance transverse mixing of dissolved species and, therefore, create favorable conditions for the natural attenuation of contaminant plumes. The aim of the present study is to experimentally test the influence of these processes on solute mixing and to directly compare the results with those under analogous homogeneous and steady-state conditions. We have performed conservative and reactive tracer experiments in a quasi two-dimensional tank filled with glass beads of different sizes. The experiments have been carried out in both homogeneous and heterogeneous porous media under steady-state and transient (i.e. oscillating) flow fields. We used fluorescein as conservative tracer; whereas an alkaline solution (NaOH) was injected into ambient acidic water (HCl) in the reactive experiments. A pH indicator was added to the reacting solutions in order to visualize the emerging plume. We simulated the laboratory experiments with a numerical model and compared the outcomes of the model with the measured concentrations at the outlet of the tank and with the observed tracer plumes. Spatial moments, a newly defined flux-related dilution index, the product mass fluxes and the reaction enhancement factors were calculated to quantify the differences in mixing and reaction extent under various experimental conditions. The results show that flow focusing in heterogeneous porous media significantly enhances transverse mixing and mixing-controlled reactions, whereas temporally changing flow fields appear to be of minor importance.

¹ Reproduced from: Rolle, M., C. Eberhardt, G. Chiogna, O.A. Cirpka, and P. Grathwohl (2009), Enhancement of dilution and transverse reactive mixing in porous media: Experiments and model-based interpretation, *Journal of Contaminant Hydrology*, 110, 130-142. Copyright 2009 Elsevier.

1.1 INTRODUCTION

Mass transfer, mixing and hence reaction rates during transport of solutes in groundwater depend on dispersion processes. When contaminant plumes evolving from continuous sources approach steady-state conditions, vertical transverse dispersion controls the mixing of reaction partners (i.e. electron donors and acceptors for microbial degradation of organic contaminants) thus determining the effective reaction rates and the plume length (e.g. Cirpka et al., 1999; Mayer et al., 2001; Ham et al., 2004; Liedl et al., 2005; Maier and Grathwohl, 2006). Pore-scale mixing of the reaction partners is a necessary condition for the reaction between two or more dissolved compounds (Kitanidis, 1994; Cirpka, 2002). Experimental and modeling investigations at different scales showed that vertical transverse dispersion coefficients are typically very small (e.g. Sudicky, 1986; Klenk and Grathwohl, 2002; Cirpka et al., 2006; Olsson and Grathwohl, 2007). As a consequence, mixing-controlled reactions of dissolved compounds can only take place in narrow stripes at the fringes of contaminant plumes. Evidence that important reactive processes are restricted to the fringe of contaminant plumes were given both at the laboratory (Huang et al., 2003; Willingham, 2006; Cirpka et al., 2006; Rees et al., 2007; Rolle et al., 2008a; Willingham et al., 2008; Bauer et al., 2008, 2009a, 2009b) and at the field scale (Davis et al., 1999; Lerner et al., 2000; Tuxen et al., 2006; Rolle et al., 2008b; Anneser et al., 2008, Prommer et al., 2009). In detailed field investigations of an aquifer contaminated by phenolic compounds, Lerner et al. (2000) showed the occurrence of fringe degradation reactions between the plume contaminants and the dissolved electron acceptors in the background groundwater. Similar findings were obtained at a landfill site (Tuxen et al., 2006) and, recently, at a site contaminated by petroleum hydrocarbons (Anneser et al., 2008). The latter study showed, by means of high resolution multi-level sampling devices, the presence of narrow (mm-cm) reactive zones and the occurrence of steep concentration gradients of reactive biogeochemical species at the plume fringe.

All these studies show that mixing processes are of utmost importance in determining the fate and transport of contaminants in groundwater and they often represent the limiting factor to the overall degradation. For these reasons considerable attention should be dedicated to the investigation of processes possibly enhancing the mixing of reactants in porous media, in particular in the transverse direction.

Transient flow conditions have been indicated as a possible source of mixing enhancement. For transport of non-reactive chemicals in homogeneous porous media, it was shown (Kinzelbach and Ackerer, 1986; Goode and Konikow 1990) that fluctuations in the groundwater flow direction due to transient conditions can lead to an increase of transverse dispersion. In modeling studies of organic contaminant plumes, Schirmer et al. (2001) and Prommer et al. (2002) investigated the influence of transient flow conditions on contaminant transport and biodegradation in homogeneous porous aquifers. Both studies found just slightly increased transverse dispersion and therefore degradation enhancement. The latter authors suggested that the presence of transient flow combined with sorption processes could lead to a more significant mixing enhancement. Similar conclusions were obtained by Cirpka (2005) for solute transport and kinetic sorption in a spatially homogeneous flow field undergoing sinusoidal fluctuations in time.

Many studies based on both deterministic and stochastic approaches, investigated the importance of sediment heterogeneities in determining the flow field in saturated porous media and, therefore, the transport of dissolved compounds. Linear stochastic theory predicts only small enhancement of transverse effective dispersion by heterogeneity (Dentz et al., 2000; Fiori and Dagan, 2000). This theory results in an enhancement of transient mixing in heterogeneous media of approximately one order of magnitude under transient flow conditions (Cirpka and Attinger, 2003; Dentz and Carrera, 2003). However, the appropriateness of linear stochastic theory for transverse dispersion may be questioned (Attinger et al., 2004), since higher-order effects such as the enhancement of transverse mixing by flow-focusing (Werth et al., 2006) may be dominant.

Experimental studies of transverse mixing in heterogeneous media are scarce, and the interpretation of individual transverse concentration profiles may be impeded by the deformation of the flow field (Rahman et al., 2005).

In this study, laboratory bench-scale experiments were performed, in quasi two-dimensional flow-through systems, to deepen the understanding of vertical transverse dispersion in porous media and to quantify the influence of transient flow fields and heterogeneities on mixing and reactions. We carried out transport experiments in saturated unconfined porous media under steady-state and transient flow fields using both conservative and reactive tracers. The same experimental set-up was used for both uniform and heterogeneous porous media, thus allowing a direct comparison between the different experiments. In the latter experiments, the heterogeneities consisted of two well-defined high permeability zones (coarse material) embedded into a lower permeability matrix.

Numerical simulations of the conservative and reactive tracer experiments may help interpreting the laboratory results. We compared model results with the measured concentrations at the outlet of the tank and with the observed conservative and reactive color plumes. A quantitative evaluation of the experimental and modeling results was performed through the calculation of spatial moments, dilution indexes, mass fluxes of reaction product and reaction enhancement factors.

1.2 MATERIAL AND METHODS

1.2.1 Experimental set-up

The experiments were carried out in a quasi 2-D acrylic-glass flow-through tank with inner dimensions of 77.9 cm length, 15.0 cm height and 1.1 cm width (Fig. 1.1). The tank was equipped with 13 equally spaced ports (1.1 cm distance) as inlets and outlets on both sides. The ports were made of pierced rubber septa, and the injection needles were directly connected to tygon pump-tubing (ID 0.57 mm, Ismatec, Glattbrugg, Switzerland). For the experiments performed under steady-state flow conditions, two 12-channel high precision peristaltic pumps (IPC-N, Ismatec, Glattbrugg, Switzerland), one for the inlet ports and the other for the outlet ports, were operated at identical pumping rates.

The tank was filled with glass beads up to a height of approximately 14 cm. The top of the domain was kept unsaturated to avoid an upper shortcut of the injected tracer solutions. In the experiments with a homogeneous filling, we used glass beads of uniform grain size of 0.25–0.3 mm (Sartorius AG, Goettingen, Germany).

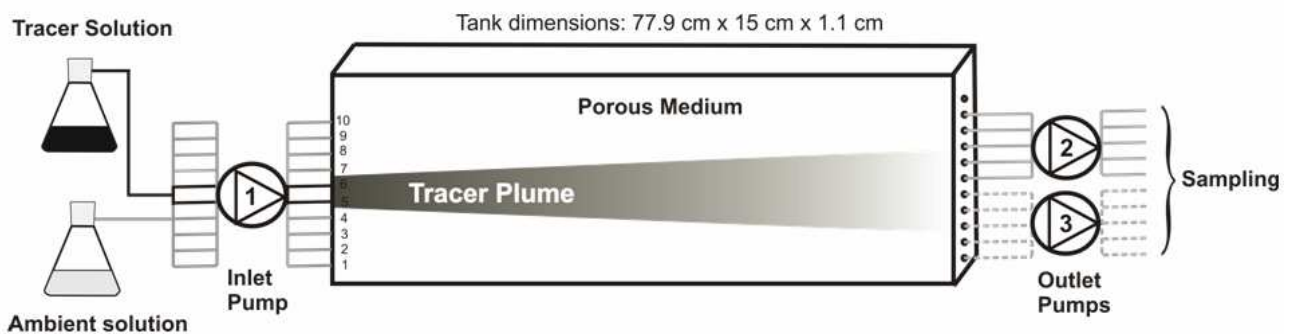


Figure 1.1: *Experimental setup*

Transient flow conditions in the homogeneous porous medium set-up were established by using three peristaltic pumps. While the inlet ports 2-8 were connected to pump 1 and operated with a flow rate of $q_{\text{port}} = 7.083 \times 10^{-4}$ mL/s for each port, inlet port 1 was connected to pump 2 and set to the double flow rate ($2 \times q_{\text{port}}$) and inlet port 10 was connected to pump 3 set to no flow rate ($q_{\text{port}} = 0$). At the outlet, the water was withdrawn from the uppermost 5 ports, which were connected to pump 2 with the double flow rate ($2 \times q_{\text{port}}$), while the lower 5 ports were connected to pump 3. At a subsequent stress period the flow rates were changed symmetrically: the flow rate of inlet port 1 and the outlet ports 6-10 were set to 0, while the ports connected to pump 3 (inlet port 10 and the outlet ports 1-5) were operated at a double flow rate ($2 \times q_{\text{port}}$).

To create a heterogeneous porous medium, two inclusions of higher permeability made of glass beads of a grain size of 1-1.5 mm (Fisher Scientific GmbH, Schwerte, Germany) were embedded into the finer glass beads (0.25-0.3 mm). The two high-permeability zones were placed directly in line with the central plume's injection port and their thickness was equal to the port spacing (1.1 cm). The length of the inclusions was 20 cm, the distance of the first zone from the injection port was 15 cm and the distance between the two inclusions was 8 cm.

In the experiments with conservative color tracer, a sodium fluorescein solution with a concentration of 30 mg/L was injected through the central inlet port (port 6), while clean water was injected through the other ports to establish parallel flow. After the displacement of two pore volumes, when the plume reached steady-state conditions, samples were taken at each outlet port and the fluorescence signal was measured using a fluorescence spectrometer (Perkin Elmer LS-3B). Conservative experiments were repeated under transient flow conditions in the homogeneous porous medium.

In the reactive experiments, a solution of 0.004 mol/L NaOH (pH = 11.49) was injected through two middle inlet ports into an ambient solution of 0.01 mol/L HCl (pH = 2.03), which was injected through the surrounding ports. Both solutions were prepared from deionized water and contained the pH indicator bromophenol blue at a concentration of 5.92×10^{-6} mol/L. The indicator changes its color from yellow to blue in the pH interval 3-4.6. In the heterogeneous setup, the reactive experiments were repeated with increasing concentrations of the alkaline solution (0.008, 0.022 and 0.030 mol/L). Pictures of the alkaline plume were taken at different times in both the experiments carried out under steady-state and transient conditions.

1.2.2 Hydraulic properties

The most important parameters determining the flow field in the tank systems (i.e. hydraulic conductivity, porosity) and the transport of conservative and reactive solutes (i.e. longitudinal and transverse dispersivities) were determined experimentally and are summarized in Table 1.1.

Permeameter tests were conducted to determine the hydraulic conductivities of the fillings with different grain sizes used as porous media in the two-dimensional flow-through systems, resulting in average values of 6.14×10^{-4} m/s and 1.27×10^{-2} m/s for the fine (0.25–0.3 mm) and coarse (1-1.5 mm) glass beads, respectively. Thus, the ratio of the hydraulic conductivities between the two different porous media in the heterogeneous system was 20.7. This parameter determines the amount of water flow that is focused in the two high-permeability inclusions of the heterogeneous setup and therefore plays a very important role for the mixing enhancement in the heterogeneous system compared to the equivalent homogeneous setup (Werth et al., 2006).

Transverse dispersivities for the two different grain sizes were determined in separate homogeneous tank experiments with fluorescein by measuring the tracer distribution at the outlet ports. In the tank filled with fine glass beads an average linear velocity of 1.1 m/day was established, whereas in the tank with the coarser grain size a higher value of linear velocity (10 m/day) was set in order to closely match the expected conditions in the high permeability inclusions

of the heterogeneous setup. In these homogeneous systems the simplifying assumption of uniform parallel flow could be considered valid. The simplified two-dimensional analytical solutions of the transport equation for a line source under steady-state (1) and transient conditions (2) (Domenico and Palciauskas, 1982; Domenico and Robbins, 1985) could be applied since the constraints pointed out by Srinivasan et al. (2007) are satisfied:

$$\frac{C(x, y)}{C_0} = \frac{1}{2} \left\{ \operatorname{erf} \left[\frac{(y+Y/2)}{2(xD_T/v)^{1/2}} \right] - \operatorname{erf} \left[\frac{(y-Y/2)}{2(xD_T/v)^{1/2}} \right] \right\} \quad (1.1)$$

$$\frac{C(x, y, t)}{C_0} = \frac{1}{4} \operatorname{erfc} \left[\frac{(x-vt)}{2(D_L t)^{1/2}} \right] \left\{ \operatorname{erf} \left[\frac{(y+Y/2)}{2(xD_T/v)^{1/2}} \right] - \operatorname{erf} \left[\frac{(y-Y/2)}{2(xD_T/v)^{1/2}} \right] \right\} \quad (1.2)$$

where D_T and D_L [L^2T^{-1}] are the transverse and longitudinal hydrodynamic dispersion coefficients, C [ML^{-3}] is the tracer concentration, C_0 [ML^{-3}] is the tracer concentration at the source, Y [L] is the source width, y [L] is the spatial coordinate in lateral direction, x [L] is the spatial coordinate in longitudinal direction, t [T] is the time and v [LT^{-1}] is the pore water velocity. In order to determine the transverse dispersion coefficient D_T , the analytical solution of equation 1.1 was fitted to the fluorescein concentrations measured at the outlet ports, minimizing the sum of the squared residuals. Successively, the transverse dispersivity, α_T [L], was calculated according to the standard linear model for saturated porous media (Scheidegger, 1961):

$$\alpha_T = \frac{D_T - D_P}{v} \quad (1.3)$$

in which the effective pore diffusion coefficient D_P [L^2T^{-1}] can be approximated as $D_P = D_{aq} n$ (Grathwohl, 1998; Boving and Grathwohl, 2001), where D_{aq} is the aqueous diffusion coefficient [L^2T^{-1}] and n [-] is the porosity. A value of $\alpha_T = 1.4 \times 10^{-5}$ m was determined for the glass beads with 0.25-0.3 mm diameter at a seepage velocity $v = 1.1$ m/day, and $\alpha_T = 5.1 \times 10^{-5}$ m for the coarse glass beads (1-1.5 mm) at $v = 10$ m/day.

Parameter	Value
Tank inner dimension (m)	0.779×0.15×0.011
Average fine grain diameter (mm)	0.275
Average coarse grain diameter (mm)	1.25
Number of inlet/outlet ports used (-)	10
Total flow rate (mL/s)	7.083×10 ⁻³
Average linear pore water velocity (m/s)	1.27×10 ⁻⁵
Porosity fine grain (-)	0.42
Porosity coarse grain (-)	0.40
Hydraulic conductivity fine material (m/s)	6.14×10 ⁻⁴
Hydraulic conductivity coarse material (m/s)	1.27×10 ⁻²
Hydraulic conductivity ratio (-)	20.7
Longitudinal dispersivity, α_L fine material (mm)	0.183
Longitudinal dispersivity, α_L coarse material (mm)	0.767
Transverse dispersivity, α_T fine material (mm)	0.014
Transverse dispersivity, α_T coarse material (mm)	0.051
Effective pore diffusion coefficient for fluorescein (m ² /s)	2.72×10 ⁻¹⁰
Effective pore diffusion coefficient for NaOH and HCl solutions (m ² /s)	1.41×10 ⁻⁹

Table 1.1: Summary of flow and transport parameters.

To determine the longitudinal dispersion coefficient D_L the analytical solution of equation 1.2 was fitted to the measured breakthrough concentrations of fluorescein at the central outlet port.

Successively, longitudinal dispersivities were calculated as:

$$\alpha_L = \frac{D_L - D_p}{v} \quad (1.4)$$

A value of $\alpha_L = 1.83 \times 10^{-4}$ m was obtained for the fine grain size, whereas $\alpha_L = 7.67 \times 10^{-4}$ m was determined for the coarse glass beads.

Porosity values of 0.42 and 0.40 were calculated from the specific discharge and the mean arrival time of the tracer in the homogeneous tank system for the fine and coarse grain size, respectively.

1.2.3 Numerical Modeling

In order to analyze the experimental results, we simulated flow and transport in the different flow-through systems with a numerical model. The model domain was discretized into 35 530 cells with a varying spacing ($\Delta x_{\min} = 1 \times 10^{-3}$ m, $\Delta x_{\max} = 5 \times 10^{-3}$ m) along the flow direction and a constant spacing ($\Delta z = 7.5 \times 10^{-4}$ m) in the vertical direction.

The flow field was simulated using MODFLOW (McDonald and Harbaugh, 1988) and particle tracking simulations were performed using MODPATH (Pollock, 1994). The flow-through systems were simulated as unconfined aquifers using the hydraulic parameters reported in Table 1.1. Neumann boundary conditions were applied and active cells, with a distance equivalent to the ports spacing in the experimental set-up, were used to simulate the inlet and outlet ports.

Non-reactive tracer experiments were simulated using MT3DMS (Zheng and Wang, 1999) with a third order total variation diminishing (TVD) scheme to solve the advection problem and an implicit finite difference scheme for the remaining terms of the advection-dispersion equation.

The reactive transport simulations of the acid/base systems were carried out with the multi-component reactive transport code PHT3D (Prommer et al., 2003), which combines MT3DMS (Zheng and Wang, 1999) with the geochemical model PHREEQC-2 (Parkhurst and Appelo, 1999).

1.3 RESULTS AND DISCUSSION

1.3.1 Conservative Transport Experiments

Steady-state plumes. In the homogeneous system the steady-state conservative tracer plume is characterized by a thin lateral extension which broadens with increasing distance from the inlet (Fig. 1.2a). The picture also shows low color intensity at the plume fringe and close to the outlet of the tank, corresponding to a decrease of tracer concentration as a result of dispersive processes. The fluorescein concentrations measured at the outlet ports show a characteristic Gaussian-type shape. The plume shape is quite different in the heterogeneous system. Here the permeability contrast between the two different porous media induces focusing of flow into the high-permeability inclusions. This behavior is shown in Fig. 1.2b by the computed flowlines which converge within the coarser inclusions. In the homogeneous tank the observed plume is just moderately thicker than

the region occupied by the computed streamlines originating from the central inlet reflecting the plume boundary in purely advective transport. This difference can be attributed to the contribution of transverse dispersion to the plume spreading in the homogeneous porous medium at a velocity of 1.1 m/day. On the contrary, in the heterogeneous setup, the small distance among the streamlines in the high-permeability inclusions favors the diffusive exchange of solute mass and enhances transverse mixing. Therefore, the fluorescein plume close to the outlet of the heterogeneous setup appears to be spread over almost the complete aquifer thickness and exhibits lower concentrations, as shown in the profiles reported in Fig. 1.2b. For both the homogeneous and heterogeneous setup a good agreement between observed and simulated results was obtained. Triplicate measurements of fluorescein at the outlet ports of the tanks are compared with the results of the numerical transport model at the virtual outlet ports and with simulated vertical profiles taken inside the porous medium at 2 cm from the right boundary of the homogeneous and heterogeneous flow-through systems.

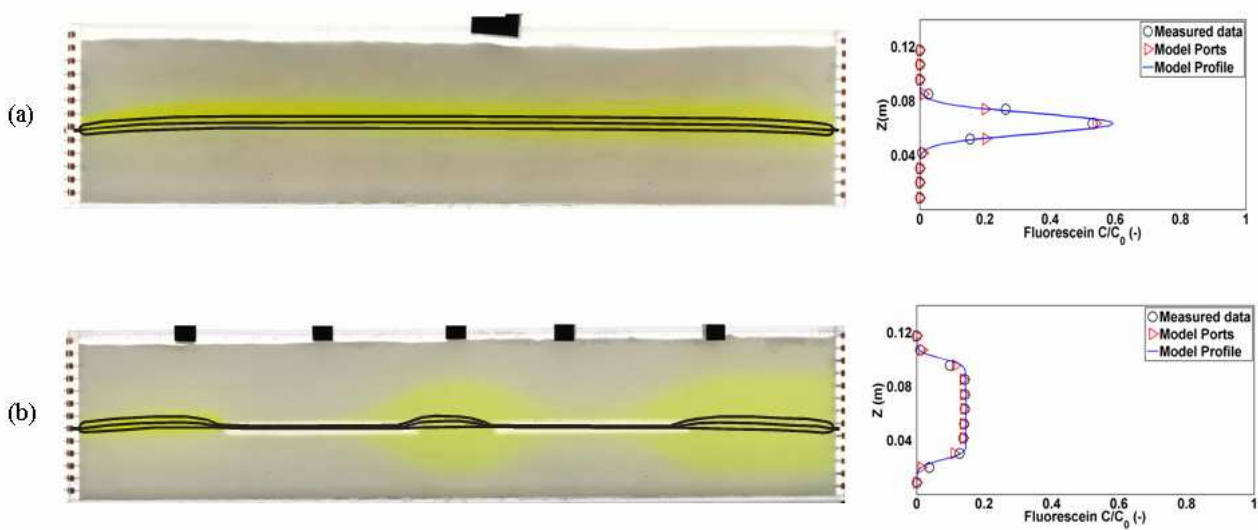


Figure 1.2: Steady-state fluorescein plumes in the homogeneous (a) and heterogeneous (b) tank and computed flow lines. On the right, measured triplicate fluorescein concentrations, normalized to the inlet concentration $C_0=30$ mg/L (circles), simulated results at the outlet ports (triangles) and a vertical profile inside the tank 2 cm from the outlet (solid line).

Moment analysis of transient plumes. Transient flow conditions in the homogeneous porous medium setup were established by using an additional peristaltic pump and resulted in oscillating fluorescein plumes. Snapshots at different times were taken for two experiments corresponding to a different frequency of flow oscillations (Fig.1.3). Fig. 1.3a shows the results at different times ($t_1=2.82$, $t_2=2.94$, and $t_3=3.00$ days) for an oscillating period of half the travel time of the solute in the tank and Fig. 1.3b shows the plumes corresponding to an oscillation period of a quarter of the travel time for $t_1=0.71$, $t_2=0.78$ and $t_3=0.88$ days. In the same figure, the corresponding outcomes of conservative transport simulations are reported.

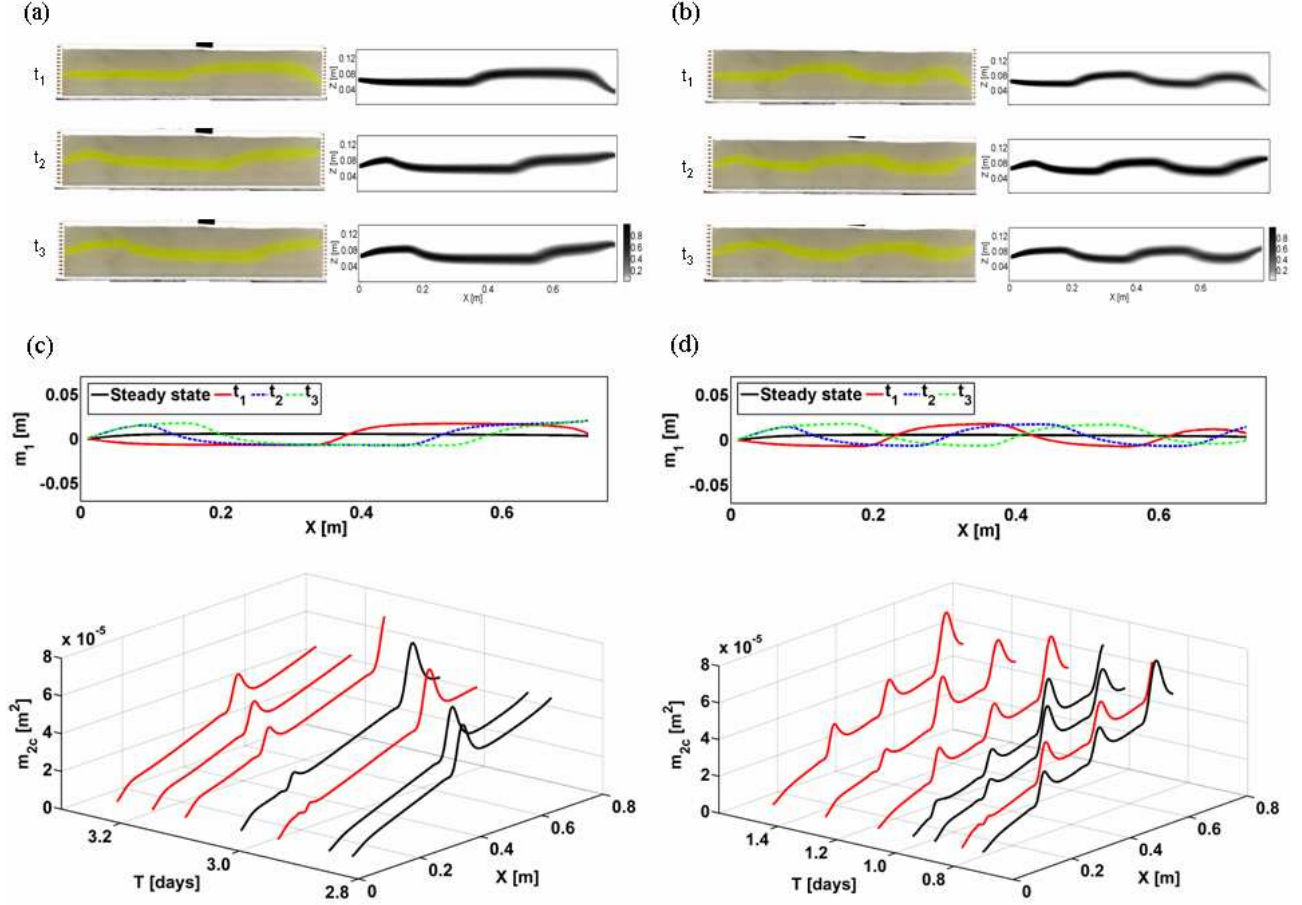


Figure 1.3: Observed and simulated fluorescein plumes corresponding to changes of boundary conditions of half- and a quarter of the solute travel time in the tank (a and b). Computed first and second central spatial moments in the homogeneous system (c and d). In the plots of the second central spatial moments the black solid lines correspond to the time of the pictures

We computed the spatial moments of the corresponding simulated concentrations. In a three-dimensional saturated porous medium, the raw spatial moments of the concentration distribution $C(x, y, z, t)$ are defined as (Aris, 1956):

$$M_{ijk}(t) = \int_{-\infty}^{+\infty} \int_{-\infty}^{+\infty} \int_{-\infty}^{+\infty} nC(x, y, z, t) x^i y^j z^k dx dy dz \quad (1.5)$$

where n represents the porosity and x , y and z the spatial coordinates. We calculated the zeroth, first and second spatial moments of the fluorescein distribution for the steady-state experiment and for the transient setups at the times for which the pictures and the outcomes of the numerical modeling were available. In our application, the concentration distribution is uniform over the width of the domain (W_y). Also, the size of the cross-section (L_z) is limited so that the integration in the lateral coordinates is bounded. The first moment normalized by the zeroth one represents the location of the center of gravity of the solute plume. For the continuous-injection experiments, the normalized first spatial moment in the vertical direction was calculated as:

$$m_1(x) = \frac{\int_0^{W_y} \int_0^{L_z} z \cdot c(x, y, z) dy dz}{\int_0^{W_y} \int_0^{L_z} c(x, y, z) dy dz} \quad (1.6)$$

which is computed for each column of the computational domain.

The results corresponding to the different times shown in Fig. 1.3a and b are reported in Fig. 1.3c and d. The normalized first moments of the transient plumes change their position in comparison to the steady-state fluorescein plume (black solid line) with the same phase as applied in the flow boundary conditions.

The normalized second central spatial moment is a measure of the spreading of the concentration distribution about its center of gravity and its value in the vertical transverse direction was calculated as:

$$m_{2c}(x) = \frac{\int_0^{W_y} \int_0^{L_z} (z - m_1(x))^2 \cdot c(x, y, z) dy dz}{\int_0^{W_y} \int_0^{L_z} c(x, y, z) dy dz} \quad (1.7)$$

Fig. 1.3c and 1.3d show the normalized second central moments for each vertical section along the length of the tank at different times. Under transient conditions the second central spatial moments increase where the plume bends. In fact, in these zones, the longitudinal dispersion is acting in a direction that is no more horizontal but presents a significant component also in the vertical transverse direction (Kinzelbach and Ackerer, 1986; Goode and Konikow, 1990). Several authors (e.g. Kitanidis 1994, Cirpka 2002) pointed out the difference between plume spreading and mixing, with the former concept related to the change of the plume shape whereas the latter referred to the change of volume occupied by the solute. However, in the homogeneous flow-through setup, both plume spreading and dilution are described by local dispersion coefficients, and the computed second central spatial moments increase with time (Fig. 1.3c and 1.3d). These findings suggest that the second central spatial moments, representing the fluorescein plume spreading, can be assumed as a good proxy for quantifying plume mixing in the homogeneous system. This conclusion clearly does not apply for heterogeneous porous media, where plume spreading does not represent a measure of mixing (or dilution), as can be observed in Fig. 1.4. The plot shows the computed second central transverse moments in the homogeneous and heterogeneous systems under steady-state flow conditions. When the plume is focused inside the high-permeability inclusions, its second central transverse moment decreases while its actual dilution cannot decrease because dilution is an irreversible process.

Quantification of mixing enhancement by the Dilution Index. Since second central spatial moments are inadequate to quantify plume mixing and dilution in heterogeneous porous media, another measure of these processes is required in order to perform a quantitative analysis of the experimental results. We refer here to the concept of dilution index introduced by Kitanidis (1994). In its original form, the dilution index is defined as:

$$E(t) = \exp \left[- \int_V p(\vec{x}, t) \ln(p(\vec{x}, t)) dV \right] \quad (1.8)$$

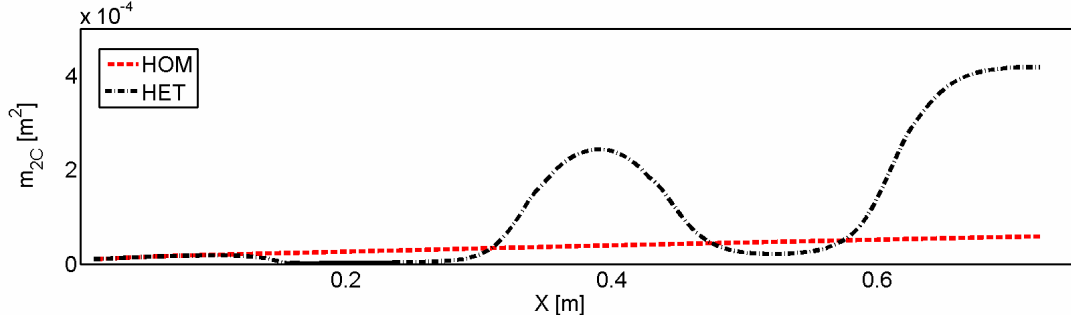


Figure 1.4: Normalized second central spatial moments in the transverse direction computed for the homogeneous and heterogeneous setups.

where $p(\bar{x}, t)$ is the distribution function of the solute (concentration normalized by the total mass of the solute in the domain).

The illustrative explanation of the original dilution index is the effective volume occupied by a solute cloud. This is a useful property for the analysis of mixing when the compound is introduced as an individual slug, and when the concentration distribution in the entire domain is observable at any given time of interest. However, the original dilution index gives no indication how the dilution of the solute increases with the travel distance when the compound is continuously injected into the flow domain, as occurred in our experimental setups. Therefore, we define a modified dilution index that can be obtained in a cross section perpendicular to the mean direction of flow and expresses an effective discharge over which the solute mass flux is distributed.

In the following, the reference framework is that of solute flux. While in the discussion of the original volume-related dilution index, dilution was defined as “the act of distributing solute mass over a larger volume” (Kitanidis, 1994), we address dilution as the act of distributing a given solute mass flux over a larger water flux. The concentrations considered are local flux concentrations, that is, the solute mass flux in the direction normal to the control plane divided by the specific discharge in that direction. As is well known, the difference between flux and resident concentration lies in the normal gradient component of the resident concentration times the bulk dispersivity (Kreft and Zuber, 1978). At the local scale, this difference is negligible in advection dominated transport.

Computing the dilution index involves integration. In the volume-related dilution index, this was an integral over the volume of the domain. In our flux-related framework, we compute the integral over the water flux which can be expressed as integral of the quantity to be integrated times the normal component of the local specific discharge over the cross-sectional area.

We start the analysis by considering the total solute mass flux:

$$F(x) = \int_{-\infty}^{+\infty} \int_{-\infty}^{+\infty} c(x, y, z) \cdot q_x(x, y, z) dy dz \quad (1.9)$$

where $c(x, y, z)$ is the flux-related concentration and $q_x(x, y, z)$ is the normal component of the specific discharge with respect to a cross-sectional area in the plane y - z .

A flux related density function of the solute mass can be defined as the ratio between the concentration and the mass flux:

$$p_Q(x, y, z) = \frac{c(x, y, z)}{F(x)} \quad (1.10)$$

which has units of an inverse discharge, and expresses the probability that a solute particle, in the cross-section at distance x , is within a certain fraction of the water flux. It can easily be shown that,

p_Q is a true flux related density function since its integral over the whole water flux crossing the control plane is unity:

$$\int_{-\infty}^{+\infty} \int_{-\infty}^{+\infty} p_Q(x, y, z) \cdot q_x(x, y, z) dydz = 1 \quad (1.11)$$

Then, the flux-related dilution index becomes:

$$E_Q(x) = \exp \left[- \int_{-\infty}^{+\infty} \int_{-\infty}^{+\infty} p_Q(x, y, z) \cdot \ln(p_Q(x, y, z)) \cdot q_x(x, y, z) dydz \right] \quad (1.12)$$

which has units of a discharge.

$E_Q(x)$ quantifies an effective volumetric flux transporting the solute flux at the longitudinal position x . In a conservative system at steady-state $E_Q(x)$ can only increase with travel distance because transverse dispersion distributes the solute flux over a larger water flux. In contrast, the cross-sectional area over which the solute flux is transported may decrease in regions of converging flow.

In our application, the integration in the lateral coordinates is bounded, and the flux-related dilution index can be written as:

$$E_Q(x) = \exp \left[- \int_0^{W_y} \int_0^{L_z} p_Q(x, y, z) \cdot \ln(p_Q(x, y, z)) \cdot q_x(x, y, z) dydz \right] \quad (1.13)$$

In a system with finite cross-section, the upper limit of the flux-related dilution index $E_{Q(x)}$ is the total discharge passing through the system:

$$E_Q^{\max}(x) = Q = \int_0^{W_y} \int_0^{L_z} q_x(x, y, z) dydz \quad (1.14)$$

in which $E_Q(x) = E_Q^{\max}(x)$ requires a uniform concentration distribution over the cross-section.

In analogy to the volume-related dilution index of Kitanidis (1994), we may define a flux-related reactor ratio $M_Q(x)$, by normalizing $E_Q(x)$ with $E_Q^{\max}(x)$:

$$M_Q(x) = \frac{E_Q(x)}{E_Q^{\max}(x)} \quad (1.15)$$

which cannot exceed the value of unity.

Fig. 1.5 shows the computed flux-related dilution indices $E_Q(x)$ and reactor ratios $M_Q(x)$ as function of travel distance for both the homogeneous and heterogeneous cases. It can be observed that for the homogeneous steady-state plume (Fig. 1.2a) the dilution index increases monotonically at a moderate rate along the flow direction. For the heterogeneous setup (Fig. 1.2b) the same behavior observed in the homogeneous system characterizes the portion of porous medium close to the inlet (same grain size). When the plume is focused into the first high-permeability inclusion, it is significantly diluted as can be noticed by the rapid increase of the dilution index. A plateau is reached between the two inclusions and further dilution takes place in the second zone. In this zone the increase of the dilution index is not as pronounced as in the first inclusion since the plume entering into the second high-permeability zone is already partially mixed with surrounding water.

Using the flux-related dilution index as a measure of mixing, the degree of mixing of the fluorescein plume at the end of the heterogeneous tank is 2.46 times higher than in the homogeneous setup.

In the given application, the original volume-related dilution index would have been no useful measure of mixing, because we consider a steady-state concentration distribution of a continuously injected compound. This would yield a single value of an effective volume occupied by the plume. How the degree of mixing increases with travel distance could not be quantified. Likewise, modifying the dilution-index to a cross-sectional quantity without weighting by the water flux would have failed to capture the physical process of transverse mixing taking place in the heterogeneous system. In fact, the shrinking of the plume in the high-permeability inclusion would have led to a decrease in the cross-section related dilution index at distances downstream of the high-permeability inclusions. This would have not been correct since, as mentioned above, dilution is an irreversible process and, under steady-state conditions, its measure should increase with the travel distance. Using the flux-related dilution index this physical constraint is fulfilled. In the high-permeability inclusions, the streamtubes get narrower leading to a smaller cross-sectional area, but transverse exchange makes the particles in the plume sample a larger fraction of the water flux.

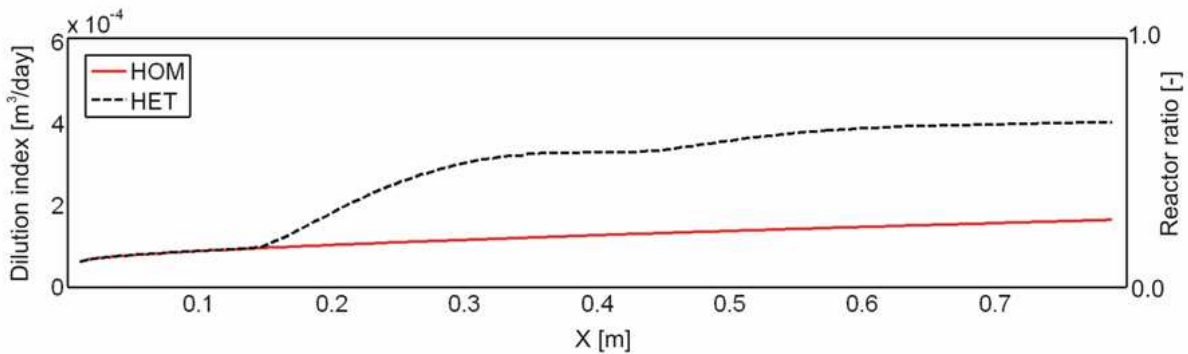


Figure 1.5: Comparison between the computed dilution index and reactor ratio for the homogeneous and heterogeneous setups.

We applied the concept of flux-related dilution index also to the transient experiments in the homogeneous setup. The results corresponding to two different oscillation frequencies are shown in Fig. 1.6. According to the computed values of dilution index, local mixing enhancements occur where the plume bends following the oscillating flow field. The mixing enhancements increase with time, as the signal propagates in the flow-through system. These findings, similar to the outcome of the second central spatial moments analysis, demonstrate that transient flow fields cause local mixing enhancements in comparison with the analogous steady-state setup.

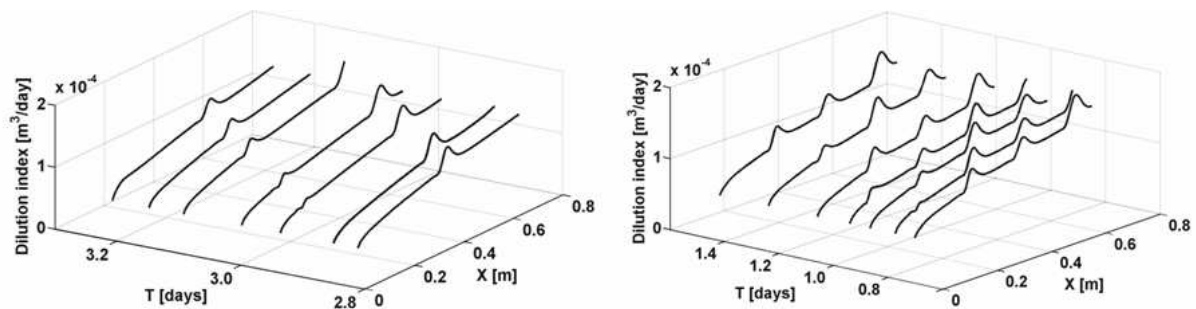


Figure 1.6: Dilution index computed at different time in the transient setups, for the two distinct frequencies of flow oscillations.

1.3.2 Reactive Experiments

Steady-state plumes. We performed reactive experiments by establishing an alkaline (0.004 mol/L NaOH) plume in an acidic ambient solution (0.01 mol/L HCl). Both solutions were amended with a concentration of 5.92×10^{-6} mol/L of bromophenol blue as pH indicator. The selected aqueous acid/base reaction is very fast, therefore it represents a suitable example for the investigation of mixing-controlled reactions in saturated porous media. The reaction between the acidic and alkaline solution reduces to water hydrolysis since the sodium and chloride ions behave as conservative compounds (spectator ions). The pH indicator added to both solutions behaves as a weak acid and undergoes the reaction $\text{HIn} \leftrightarrow \text{H}^+ + \text{In}^-$.

Titration experiments of 0.01 mol/L HCl solutions were performed with increasing volumes of alkaline solutions with different NaOH concentrations. The results plotted in Fig. 1.7 show the titration curves obtained with 0.004, 0.022 and 0.030 mol/L NaOH. The symbols (\times) represent the measured pH whereas the continuous line shows the values computed with the speciation code PHREEQC-2 (Parkhurst and Appelo, 1999). X_{alk} is the volumetric fraction of the alkaline solution in the mixture of the acidic and alkaline solutions, also denoted mixing ratio. A pH of 4.6, where the color change of the pH indicator is complete, was reached for mixing ratios of $X_{Alk}=0.712$, $X_{Alk}=0.309$, and $X_{Alk}=0.249$ (dashed lines) for the experiments with 0.004, 0.022 and 0.030 mol/L NaOH, respectively.

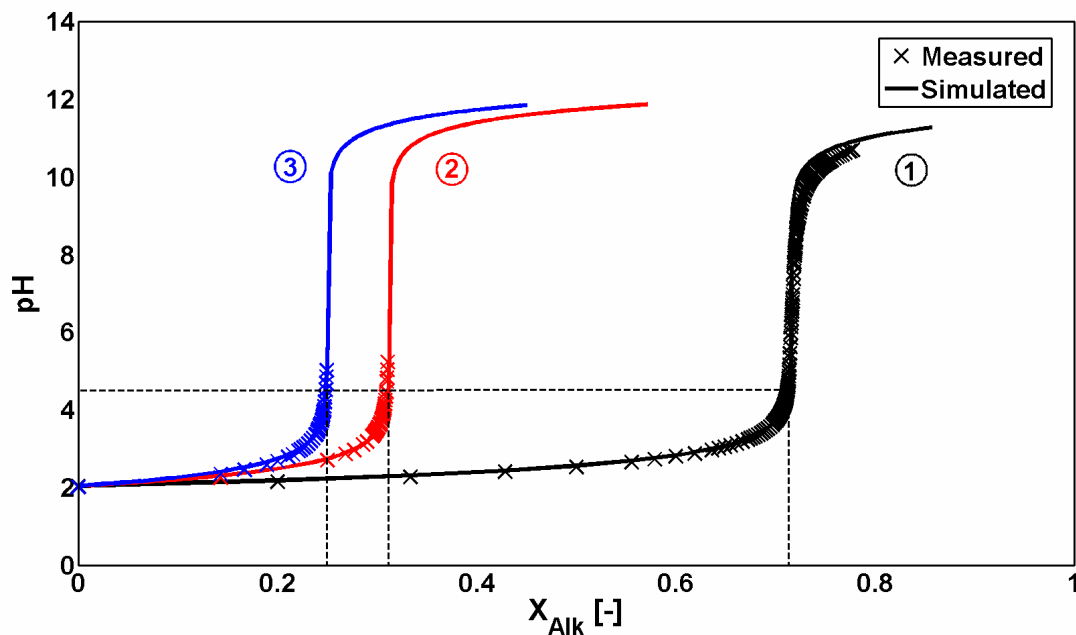


Figure 1.7: Titration of 0.01 mol/L HCl solutions with alkaline solutions of 0.004, 0.022 and 0.030 mol/L NaOH (case 1, 2 and 3, respectively) using bromophenol blue (5.92×10^{-6} mol/L) as pH indicator.

A steady-state alkaline plume was first established in the homogeneous tank by injecting the 0.004 mol/L NaOH solution in two adjacent central inlet ports and the ambient acidic solution (0.01 mol/L HCl) in the surrounding ports. The same procedure was repeated in the heterogeneous system. As shown in Fig. 1.8a and b, the plume shapes and lengths are quite different in the two systems: while in the homogeneous porous medium the plume extends for more than half the tank length, in the heterogeneous setup it appears to vanish as soon as it reaches the first high-permeability inclusion. As shown above for the conservative tracer, the focusing of flow causes an enhancement of mixing which leads, in the reactive case, to an enhanced acid/base reaction. This

results in a considerably shorter alkaline plume. A successive increase of the concentration of the inlet alkaline solution in the heterogeneous system resulted in longer plumes. For example, Fig. 1.8c shows a plume (0.022 mol/L NaOH) that travels through the first high-permeability inclusion and vanishes as it enters the second inclusion. Fig. 1.8d shows an alkaline plume (0.030 mol/L NaOH) traveling along the entire tank length.

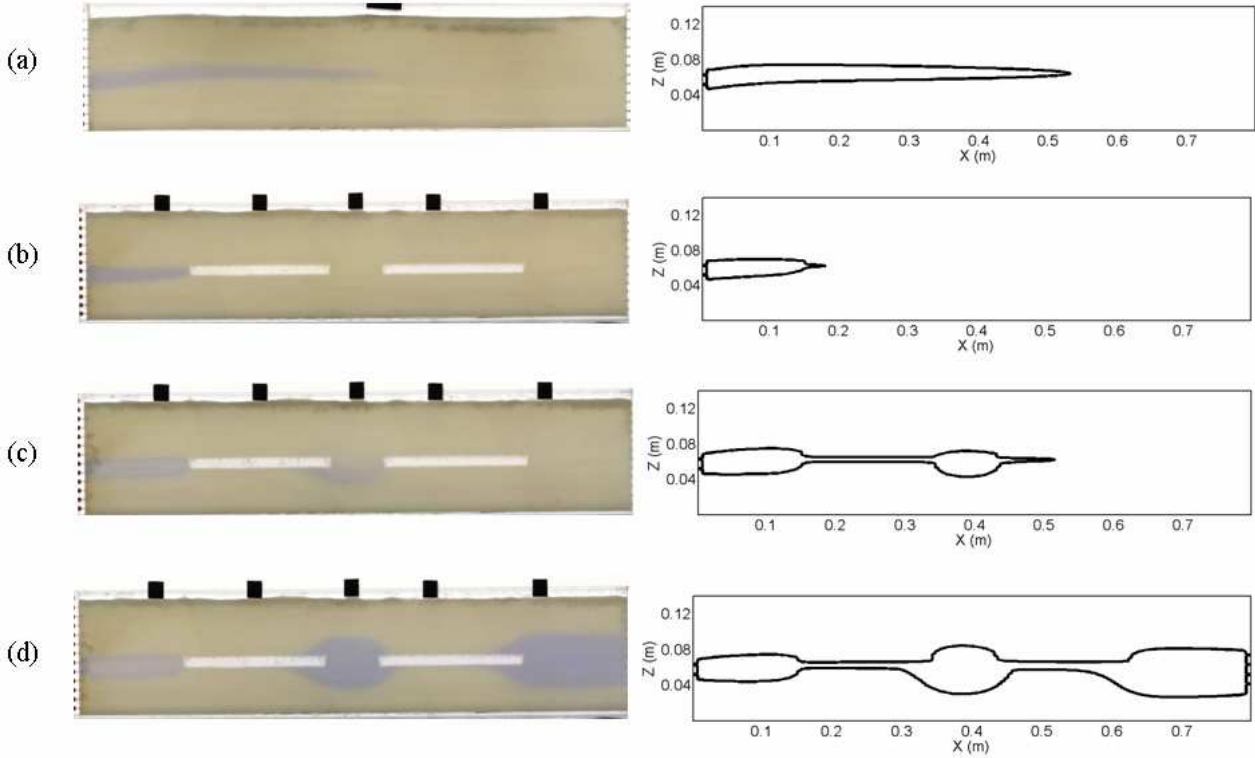


Figure 1.8: Reactive plumes observed in the homogeneous and heterogeneous setup (left) and simulated with the numerical model PHT3D (contour lines corresponding to $\text{pH}=4.6$). Plumes (a) and (b) were established injecting a concentration of 0.004 mol/L of NaOH, whereas (c) and (d) with 0.022 and 0.030 mol/L NaOH, respectively.

We performed forward numerical modeling of the reactive experiments with the multi-component reactive transport code PHT3D (Prommer et al., 2003). The simulations were conducted using the flow and transport parameters summarized in Table 1.1, except for the transverse dispersivity that was estimated following Cirpka et al. (2006). According to this method, the measured steady-state plume length in the homogeneous setup can be used to estimate the transverse dispersion coefficient by:

$$D_T = \frac{\nu Y^2}{16L(\text{inverf}(X))^2} \quad (1.16)$$

where ν is the seepage velocity, L is the plume length, Y is the injection height and X is the volume fraction corresponding to a specific pH value for which the plume can be visualized ($\text{pH}=4.6$ in our application). Assuming a standard linear model for transverse dispersion, as explained above, transverse dispersivity can be estimated according to equation 1.3. The value of α_T (2.3×10^{-5} m) determined for the reactive experiments was of the same order of magnitude but higher than the one obtained in the conservative tracer experiments conducted in the same porous medium (1.4×10^{-5} m).

The outcome of the reactive simulations are reported in Fig. 1.8 (right) and are consistent with the observed results.

Analysis of reaction enhancement. Numerical simulations were performed in order to quantify the reaction enhancement in the heterogeneous tank in comparison to the homogeneous porous medium. The reactive system for this analysis was simplified to the instantaneous reaction between two dissolved reaction partners A and B giving the dissolved reaction product C:



The concentration of the reactants and product were calculated using the analytical solution of Cirpka and Valocchi (2007) after the numerical computation, in both the homogeneous and heterogeneous setups, of the transport of a conservative species (i.e. the volumetric mixing ratio of the reactants' solutions).

Figure 1.9 shows the calculated mass fluxes of the product C of the instantaneous mixing-controlled reaction (equation 1.17) taking place in the homogeneous and heterogeneous setups, where B is introduced in the central inlet port at a concentration ten times higher than that of reactant A (0.01 mol/L) in the ambient water. With these concentrations the plume of compound B reaches the outlet of the tank in both the homogeneous and heterogeneous porous media. The production of C can only take place at the fringe of the plume where reactants A and B mix by hydrodynamic transverse dispersion. The increasing trend of the product mass flux is similar to the one observed for the dilution index for a conservative compound. The mixing enhancement in the first high-permeability inclusion causes a significant reaction enhancement as can be noticed by the steep increase of the product mass flux. The influence of the second coarse grain inclusion is clearly less important and the rate of increase of the product mass flux is comparable, and almost parallel, to that observed in the homogeneous system. This result reflects that, after the first inclusion, the plume of B is spread out and its successive focusing into the second high-permeability zone is less effective. The flowlines carrying the compound B are brought closely together inside the second inclusion, whereas the contact with the flowlines of the ambient groundwater, carrying the other reaction partner A, takes place mostly outside the coarse material. Therefore, the reactive zone turned out to be located outside the second inclusion and does not provide a significant reaction enhancement compared to the homogeneous setup. Other reactive transport simulations were performed assuming a setup similar to the experimental heterogeneous tank but with different locations of the second inclusion. Fig. 1.9a shows a scenario where the second high-permeability inclusion was shifted 3.2 cm towards the bottom of the tank. In Fig. 1.9b the second inclusion was divided into two thinner zones (each one with a thickness of half the experimental inclusion) located symmetrically with respect to the longitudinal axis of the inclusions in the experimental flow-through system. As can be noticed in Fig. 1.9c, the different location of the high-permeability inclusions resulted in different mass fluxes of the product. For the configuration shown in Fig. 1.9a, a higher product mass flux was calculated. This reaction enhancement is caused by the focusing of the lower fringe of the plume in the second high-permeability inclusion. In this case, both flowlines from the plume and from the surrounding ambient water converge into the second high-permeability zone resulting in a more effective mixing of A and B in the second half of the tank. The product mass flux additionally increases when the second inclusion is divided into two thinner zones (Fig. 1.9b), thus resulting in a more effective focusing of both the lower and the upper plume fringes.

The reaction enhancement factor (RF) was the parameter selected for the quantification of the reaction enhancement in the heterogeneous setups. RF is defined as the ratio between the mass flux of a reaction product in a heterogeneous porous medium and the product mass flux in the equivalent homogeneous system (Werth et al., 2006). In our application, we calculated the reaction enhancement factor, based on the outcome of the numerical flow and transport simulations, as:

$$RF = \frac{\int_0^L \int_0^{W_y} \int_0^{L_z} q_{HET}(L, y, z) \cdot c_{C,HET}(L, y, z) dydz}{\int_0^L \int_0^{W_y} \int_0^{L_z} q_{HOM}(L, y, z) \cdot c_{C,HOM}(L, y, z) dydz} \quad (1.18)$$

where $q_{HET}(L, y, z)$ and $q_{HOM}(L, y, z)$ are the water fluxes computed by the flow model at the outlet cells of the heterogeneous and homogeneous domains, respectively; $c_{C,HET}(L, y, z)$ and $c_{C,HOM}(L, y, z)$ are the concentrations of the product at the outlet.

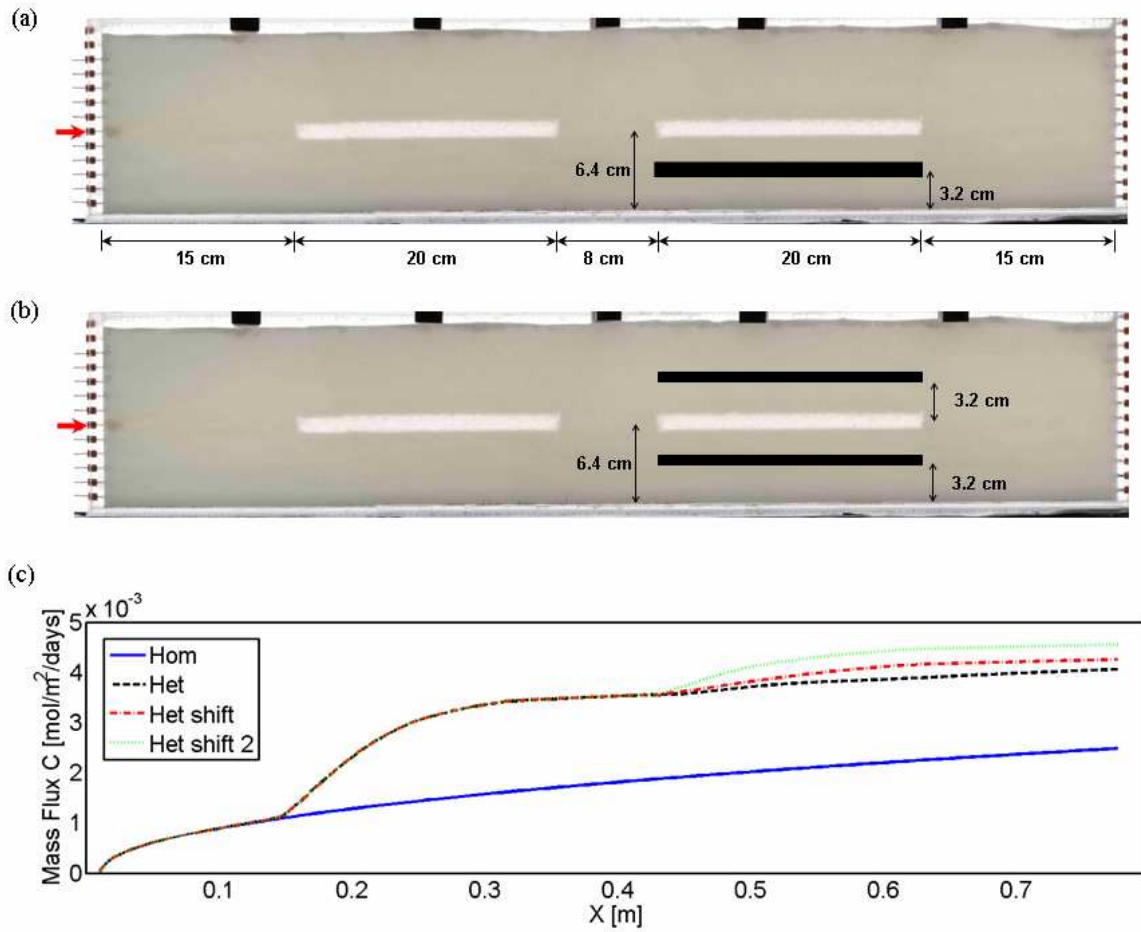


Figure 1.9: Heterogeneous tank and virtual shift of the second high-permeability inclusion (a and b). Calculated product mass fluxes along the homogeneous and heterogeneous porous media (c).

The reaction enhancement factor in the heterogeneous experimental setup was calculated to be 1.64. This means that the focusing of flow in the high-permeability inclusions and its consequent increase of mixing result in considerable higher mass fluxes of a product of an instantaneous, mixing-controlled reaction in the heterogeneous tank compared to the analogous homogeneous porous medium. An increase of RF from 1.64 to 1.72 was obtained when the second coarse grain size zone was shifted (Fig. 1.9a), therefore resulting in a more efficient focusing of the lower reactive fringe of the plume in the second high-permeability inclusion (Table 1.2). A higher increase of RF (8.9%), in comparison with the experimental heterogeneous setup, was calculated for the configurations shown in Fig. 1.9b.

Setup	Inclusions	Flux C [$\text{mol}/\text{m}^2/\text{d}$]	RF
HOM – experimental	-	2.5×10^{-3}	1.00
HET – experimental	2 in line	4.1×10^{-3}	1.64
HET – simulated	2 shifted	4.3×10^{-3}	1.72
HET - simulated	3 shifted	4.5×10^{-3}	1.80

Table 1.2: Product Mass Fluxes and Reaction Enhancement Factors

Reactive experiments were conducted also under transient flow conditions. In analogy to the conservative transport experiments using fluorescein, an alkaline plume was established in the homogeneous porous medium under oscillating flow conditions. The oscillating flow field was induced by using different flow rates at the inlet and outlet ports as described above. Pictures of the alkaline plume were taken at different times. The oscillating plumes generally showed a plume length comparable to the one of an analogous experiment in the same homogeneous setup but under steady-state conditions. Snapshots of the transient plumes after 1.6 days (a) and 2.1 days (b) from the beginning of the experiment are shown in Fig. 1.10, together with the simulated contours at pH=4.6.

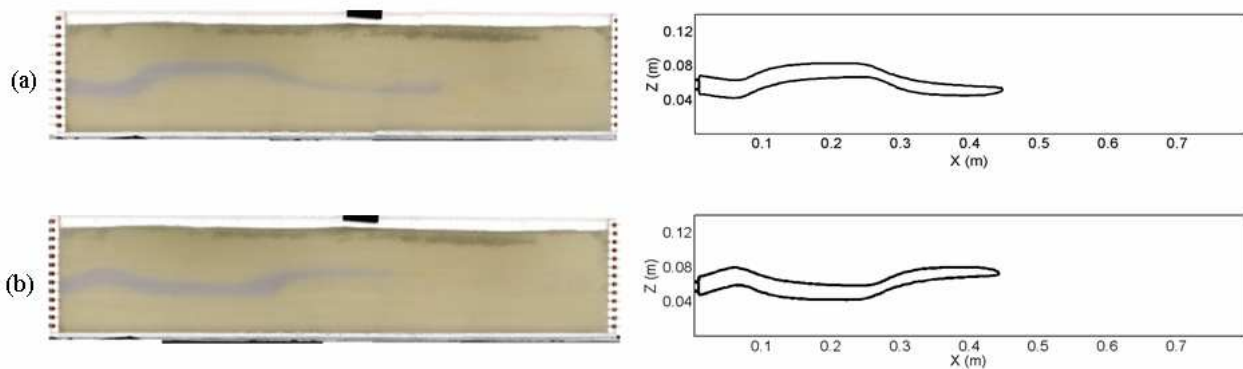


Figure 1.10: Observed and simulated (contour at pH=4.6) transient reactive plumes.

A quantitative comparison of reaction enhancement between the transient and steady-state experiments was done on the basis of the outcome of numerical simulations. In analogy with the analysis carried out in the heterogeneous setup, the instantaneous reaction (equation 1.17), with injection of the same alkaline and acidic solutions, was considered. Thus, an alkaline transient plume stretching over the whole domain was obtained. The mass fluxes of the product C, generated by mixing and reactions at the plume fringe, were calculated along the length of the flow-through system. Fig. 1.11 shows spatial profiles of the product mass flux in the homogeneous tank under steady-state and transient conditions, respectively. Similarly to what was observed by calculating the second central spatial moment of a conservative tracer (Fig. 1.3c and 1.3d), the mass flux of the reaction product shows local increase compared to the steady-state setup. In fact, the profile taken under transient conditions shows mixing enhancement corresponding to the points where the reactive plume bends as a consequence of the flow field induced by the pumps' switch. However, these local mixing and reaction enhancements are less relevant compared to the ones computed for the heterogeneous system (dash-dot line).

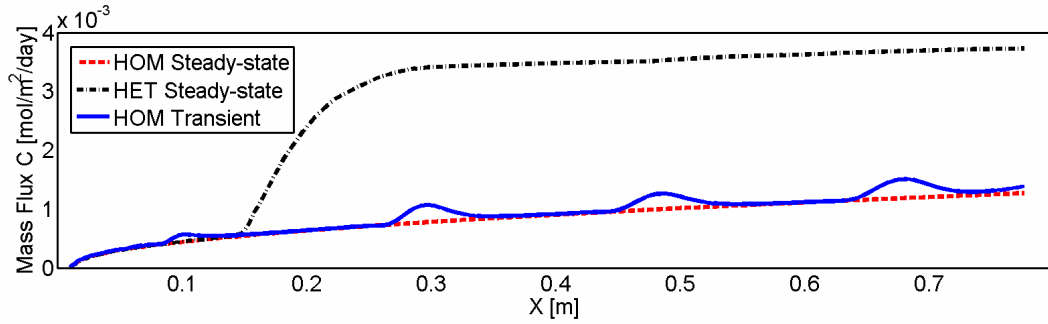


Figure 1.11: Product mass fluxes in the homogeneous tank under steady-state (dash line) and transient conditions (solid lines). The dash-dot line represents the product mass flux in the heterogeneous system at steady-state.

1.4 CONCLUSIONS

In this paper we experimentally investigated the effects of physical heterogeneity and transient flow conditions on mixing and mixing-controlled reactions in saturated porous media. The laboratory experiments were performed using both conservative and reactive tracers and the interpretation of the measured data and observed plume behavior was aided by forward numerical modeling. Conservative and reactive non-sorbing compounds were selected in order to limit the investigation to mixing caused by transverse hydrodynamic dispersion.

Mixing and reaction enhancements were caused by both transient flow fields and flow focusing into high-permeability inclusions compared to analogous homogeneous setups under steady-state flow conditions. However, for both conservative and reactive tracers, the contribution of porous medium heterogeneity, in the form of geometrically well-defined high-permeability inclusions, was distinctly more significant. The results of this study demonstrate the importance of flow focusing, suggested in the theoretical work of Werth et al. (2006), for the development of dissolved plumes in groundwater. For plumes whose behavior is controlled by diffusive/dispersive mixing-controlled reactions at the plume fringe, the amount of flow focusing, caused by the permeability contrast between the different materials, is of utmost importance in determining the plume development and length. Moreover, the extent to which the reactive fringe is focused considerably contributes to the degree of mixing enhancement. This depends on the geometry of the porous medium and, in particular, on the location of high-permeability inclusions.

For conservative and reactive non-sorbing compounds, oscillating flow fields only cause local mixing enhancements where the groundwater flow changes its principal direction. For the investigated settings, these enhancements were significantly lower than those obtained by plume focusing and mixing in the high-permeability inclusions.

Forward conservative and reactive transport modeling showed a good agreement with the measured concentrations and the observed behavior of the plumes. Based on the outcome of the numerical simulations, a quantitative analysis of the different experiments was possible. The transverse spatial moments of the plume were calculated for the conservative experiments, whereas for the reactive experiments the quantitative analysis was based on the computed fluxes of the product of an instantaneous mixing-controlled reaction. In particular, the definition of a flux-related dilution index proved to be of significant importance for quantifying mixing in both homogeneous and heterogeneous porous media. In the latter systems the second central spatial moments fail to describe plume mixing and a clear distinction between plume spreading and dilution is necessary.

Although the absolute values of the computed parameters are likely to be specific for the simplified experimental settings used in our study; important outcomes have a broader significance. For instance, the analysis based on the dilution index for the conservative tracer and on product mass fluxes for the reactive experiments, clearly shows the major contribution of the first high-permeability inclusion on mixing and reaction enhancement in the heterogeneous setup. In this zone, the rate of dilution increases considerably, as an “undiluted plume”, characterized by sharp gradients at the fringes, is effectively mixed with the surrounding clean water. These findings suggest the importance of focusing of the reactive fringe close to contamination sources for groundwater plumes. For organic contaminant plumes undergoing fringe biodegradation processes, the microbial activity is expected to be enhanced in high-permeability zones located close to contaminant sources and hot-spots, provided that the high contaminant concentrations do not inhibit the activity of the microorganisms and that ambient groundwater, rich in dissolved electron acceptors, is also focused into the high-permeability inclusions. This behavior was observed in experiments on biodegradation of organic contaminants in flow-through laboratory experiments (Cirpka et al., 1999; Bauer et al., 2009a and 2009b).

Oscillating flow fields, cause only limited and local mixing enhancements for conservative and reactive non-sorbing tracers as considered in our experimental investigation. Some previous modeling studies (e.g. Prommer et al., 2002; Cirpka et al., 2005) suggest a more significant one-time chromatographic mixing event for sorbing organic compounds. However, the mixing enhancement can entail a decrease of the overall contaminant degradation if the microbial populations mediating the transformations are not able to react sufficiently fast to the changes of environmental conditions caused by transient flow.

REFERENCES

- Anneser, B., Einsiedl, F., Meckenstock, R.U., Richters, L., Wisotzky, F., Griebler, C., 2008. High-resolution monitoring of biogeochemical gradients in a tar oil-contaminated aquifer. *Appl. Geochem.* 23, 1715-1730.
- Aris, R., 1956. On the dispersion of a solute in a fluid flowing through a tube. *Proc. R. Soc. London, Ser. A*, 235, 67-78.
- Attinger, S., M. Dentz, Kinzelbach, W., 2004. Exact transverse macro dispersion coefficients for transport in heterogeneous porous media, *Stochastic Environmental Research and Risk Assessment* 18, 9-15.
- Bauer, R.D., Maloszewski P., Zhang, Y., Meckenstock, R.U., Griebler, C., 2008. Mixing-controlled aerobic and anaerobic biodegradation of toluene in porous media – results from two-dimensional laboratory experiments. *J. Contam. Hydrol.* 96, 150-168.
- Bauer, R.D., Rolle, M., Eberhardt, C., Grathwohl, P., Bauer, S., Kolditz, O., Meckenstock, R.U., Griebler, C., 2009a. Enhanced biodegradation by hydraulic heterogeneities in petroleum hydrocarbon plumes. *J. Contam. Hydrol.* 105, 56-68.
- Bauer, R.D., Rolle, M., Kürzinger, P., Grathwohl, P., Meckenstock, R.U., Griebler, C., 2009b. Two-dimensional flow-through microcosms – Versatile test systems to study biodegradation processes in porous aquifers. *J. Hydrol.* 369, 284-295.
- Boving, T, Grathwohl, P. (2001): Matrix diffusion coefficients in sandstones and limestones: Relationship to permeability and porosity. *J. Cont. Hydrol.* 53, 85-100.
- Cirpka, O.A., 2002. Choice of dispersion coefficients in reactive transport calculations on smoothed fields. *J. Contam. Hydrol.* 58, 261-282.
- Cirpka, O.A., 2005. Effects of sorption on transverse mixing in transient flows. *J. Contam. Hydrol.* 78, 207-229.
- Cirpka, O.A., Frind, E.O., Helmig, R., 1999. Numerical simulation of biodegradation controlled by transverse mixing. *J. Contam. Hydrol.* 40, 159-182.
- Cirpka, O.A., Attinger, S., 2003. Effective Dispersion in Heterogeneous Media under Random Transient Flow Conditions. *Water. Resour. Res.* 39, 9, 1257, doi:10.1029/2002WR001931.
- Cirpka, O.A., Olsson, Å., Ju, Q., Rahman, M.A., Grathwohl, P., 2006. Determination of transverse dispersion coefficients from reactive plume lengths. *Ground Water* 44, 212-221.
- Cirpka, O.A., Valocchi, A.J., 2007. Two-dimensional concentration distribution for mixing-controlled bioreactive transport in steady state. *Adv. Water Resour.* 30, 1668-1679.
- Davis, G.B., Barber, C., Power, T.R., Thierrin, J., Patterson, B.M., Rayner, J.L., Wu, Q., 1999. The variability and intrinsic remediation of a BTEX plume in anaerobic sulphate-rich groundwater. *J. Contam. Hydrol.* 36, 265-290.

- Dentz, M., Kinzelbach, H., Attinger, S., Kinzelbach, W., 2000. Temporal behavior of a solute cloud in a heterogeneous porous medium I: Point-like injection, *Water Resour. Res.* 36, 3591-3604.
- Dentz, M., and Carrera, J., 2003. Effective dispersion in temporally fluctuating flow through a heterogeneous medium, *Phys. Rev. E.* 68, 036310.
- Domenico, P.A., Palciauskas, V., 1982. Alternative boundaries in solid waste management. *Ground Water* 20, 303-311.
- Domenico, P.A., Robbins, G.A., 1985. A new method of contaminant plume analysis. *Ground Water* 23, 476-485.
- Fiori, A., Dagan, G., 2000. Concentration fluctuations in aquifer transport: a rigorous first-order solution and applications. *J. Contam. Hydrol.* 45, Pages 139-163.
- Goode, D.J., Konikow, L.F., 1990. Apparent dispersion in transient groundwater flow. *Water Resour. Res.* 26, 2339-2351.
- Grathwohl, P., 1998. Diffusion in natural porous media: contaminant transport, sorption/desorption, and dissolution kinetics. Kluwer Academic Publishers, Boston, MA, USA.
- Ham, P.A.S., Schotting, R.J., Prommer, H., Davis, G.B., 2004. Effects of hydrodynamic dispersion on plume lengths for instantaneous bimolecular reactions. *Adv. Water Resour. Res.* 27, 803-813.
- Huang, W.E., Oswald, S.E., Lerner, D.N., Smith, C.C., Zheng, C., 2003. Dissolved oxygen imaging in a porous medium to investigate biodegradation in a plume with limited electron acceptor supply. *Environ. Sci. Technol.* 37, 1905-1911.
- Kinzelbach, W., Ackerer, P., 1986. Modélisation de la propagation d'un champ d'écoulement. *Hydrogéologie* 2, 197-206.
- Kitanidis, P.K., 1994. The concept of the dilution index. *Water Resour. Res.* 30, 2011-2026.
- Klenk, I., Grathwohl, P., 2002. Transverse vertical dispersion in groundwater and at the capillary fringe. *J. Contam. Hydrol.* 58, 111-128.
- Kreft, A., Zuber, A., 1978. On the physical meaning of the dispersion equation and its solutions for different initial and boundary conditions. *Chem. Eng. Sci.* 33(11), 1471-1480.
- Lerner, D.N., Thornton, S.F., Spence, M.J., Banwart, S.A., Bottrell, S.H., Higgs, J.J., Mallinson, H.E.H., Pickup, R.W., Williams, G.M., 2000. Ineffective natural attenuation of degradable organic compounds in a phenol-contaminated aquifer. *Ground Water* 38, 922-928.
- Liedl, R., Valocchi, A.J., Dietrich, P., Grathwohl, P. (2005): The finiteness of steady-state plumes. *Water Resources Research* 41, 1-8, W12501, doi:10.1029/2005WR004000.
- Maier, U., Grathwohl, P., 2006. Numerical experiments and field results on the size of steady state plumes. *J. Contam. Hydrol.* 85, 33-52.

- Mayer, K.U., Benner, S.G., Frind, E.O., Thornton, S.F., Lerner, D.N., 2001. Reactive transport modeling of processes controlling the distribution and natural attenuation of phenolic compounds in a deep sandstone aquifer. *J. Contam. Hydrol.* 53, 341-368.
- McDonald, M.G., Harbaugh, A.W., 1988. A modular three-dimensional finite-difference groundwater flow model. Technical Report. U.S. Geological Survey Techniques of Water Resources Investigations.
- Olsson, A., Grathwohl, P., 2007. Transverse dispersion of non reactive tracers in porous media: A new nonlinear relationship to predict dispersion coefficients. *J. Contam. Hydrol.* 92, 149-161.
- Parkhurst, D.L., C.A.J. Appelo, C.A.J., 1999. User's guide to PHREEQC – A computer program for speciation, reaction-path, 1D-transport, and inverse geochemical calculations. Technical Report 99-4259, US Geol. Survey Water-Resources Investigations Report, 1999.
- Pollock, D.W., 1994. A particle tracking post-processing package for modflow: the U.S. Geological Survey finite-difference ground-water flow model. User's guide for modpath/modpath-plot, version 3. Of 94-464, U.S. Geol. Survey, Reston, VA.
- Prommer, H., Barry, D.A., Davis, G.B., 2002. Modelling of physical and reactive processes during biodegradation of a hydrocarbon plume under transient groundwater flow conditions. *J. Contam. Hydrol.* 59, 113-131.
- Prommer, H., Barry, D.A., Zheng, C., 2003. PHT3D – A MODFLOW/MT3DMS based reactive multi-component transport model. *Ground Water* 42, 247-257.
- Prommer, H., Anneser, B., Rolle, M., Einsiedl, F., Griebler, C., 2009. Biogeochemical and Isotopic Gradients in a BTEX/PAH Contaminant Plume: Model-based Interpretation of a High-Resolution Field Data Set. *Environ. Sci. Technol.* (in press).
- Rahman, M.A., Jose, S.C., Nowak, W., Cirpka, O.A., 2005. Experiments on vertical transverse mixing in a large-scale heterogeneous model aquifer. *J. Contam. Hydrol.* 80, 130-148.
- Rees, H.C., Oswald, S.E., Banwart, S.A., Pickup, R.W., Lerner, D.N., 2007. Biodegradation processes in a laboratory-scale groundwater contaminant plume assessed by fluorescence imaging and microbial analysis. *Appl. Environ. Microbiol.* 73, 3865-3876.
- Rolle, M., Eberhardt, C., Grathwohl, P., 2008a. Influence of flow focusing on transverse mixing in heterogeneous porous media: laboratory experiments and model-based interpretation. *IAHS Red Book Series* 324, 348-355.
- Rolle, M., Clement, T.P., Sethi, R., Di Molfetta, A., 2008b. A Kinetic Approach for Simulating Redox-controlled Fringe and Core Biodegradation Processes in Groundwater: Model Development and Application to a Landfill Site in Piedmont, Italy. *Hydrological Processes* 22, 4905-4921.
- Scheidegger, A.E., 1961. General theory of dispersion in porous media, *J. Geophys. Res.* 66(4), 3273-3278.
- Schirmer, M., Durrant, G.C., Molson, J.W., Frind, E.O., 2001. Influence of transient flow on contaminant biodegradation. *Ground Water* 39, 276-282.

Srinivasan, V., Clement T.P., Lee K.K., 2007. Domenico model – Is it valid? *Ground Water*, 45, 136-146.

Sudicky, E.A., 1986. A natural-gradient experiment on solute transport in a sand aquifer: Spatial variability of hydraulic conductivity and its role in the dispersion process. *Water Resour. Res.* 22, 2069-2082.

Tuxen, N., Albrechtsen, H.-J., Bjerg P.L., 2006. Identification of a reactive degradation zone at a landfill leachate plume fringe using high resolution sampling and incubation techniques. *J. Contam. Hydrol.* 85, 179–194.

Werth, C.J., Cirpka, O.A., Grathwohl, P., 2006. Enhanced mixing and reaction through flow focusing in heterogeneous porous media. *Water Resour. Res.* 42, W12414, doi:10.1029/2005WR004511.

Willingham, T.W., 2006. Analysis of solute mixing at the pore-scale using micromodels and lattice-Boltzmann finite volume modeling. PhD Dissertation, University of Illinois at Urbana Champaign.

Willingham, T.W., Werth C.J., Valocchi A.J., 2008. Evaluation of the effects of porous media structure on mixing-controlled reactions using pore-scale modeling and micromodel experiments. *Environ. Sci. Technol.* 42, 3185–3193; DOI 10.1021/es7022835.

Zheng, C., Wang, P.P., 1999. MT3DMS: A modular three-dimensional multispecies model for simulation of advection, dispersion, and chemical reactions of contaminants in groundwater systems. Documentation and user's guide. Contract report SERDP-99-1. U.S. Army Engineer Research and Development Center, Vicksburg, MS.

Chapter 2

Transverse mixing of conservative and reactive tracers in porous media: quantification through the concepts of flux-related and critical dilution indices²

Abstract

The correct quantification of mixing is of utmost importance for modeling reactive transport in porous media and for assessing the fate and transport of contaminants in the subsurface. An appropriate measure of mixing in heterogeneous porous formations should correctly capture the effects on mixing intensity of various processes at different scales, such as local dispersion and the mixing enhancement due to heterogeneities. In this work, we use the concept of flux-related dilution index as a measure of transverse mixing. This quantity expresses the dilution of the mass flux of a conservative tracer solution over the total discharge of the system and is particularly suited to address problems where a compound is continuously injected into the domain. We focus our attention on two-dimensional systems under steady-state flow conditions and investigate both conservative and reactive transport in homogeneous and heterogeneous porous media at different scales. For mixing-controlled reactive systems, we introduce and illustrate the concept of critical dilution index, which represents the amount of mixing required for complete degradation of a continuously emitted plume undergoing decay upon mixing with ambient water. We perform two-dimensional numerical experiments at bench and field scales in homogeneous and heterogeneous conductivity fields. These numerical simulations show that the flux-related dilution index quantifies mixing and that the concept of critical dilution index is a useful measure to relate the mixing of conservative tracers to mixing-controlled degradation of reactive compounds.

²Reproduced from: Chiogna, G., O. A. Cirpka, P. Grathwohl, and M. Rolle (2011), Transverse mixing of conservative and reactive tracers in porous media: Quantification through the concepts of flux-related and critical dilution indices, *Water Resources Research*, 47, W02505, doi:10.1029/2010WR009608. Copyright 2010 American Geophysical Union.

2.1 INTRODUCTION

A detailed characterization of mixing in geologic formations and fixed-bed reactors is relevant in order to correctly quantify and describe reactive processes in porous media. In particular, many biodegradation reactions may be limited by the availability of reaction partners. Under steady-state flow and transport conditions, dissolved reactants come into contact through transverse mixing, which is determined by dilution processes in the directions perpendicular to flow (i.e., processes which increase the entropy and decrease the peak concentration of conservative solutes). In particular, we consider steady-state two-dimensional transport of two reacting species continuously injected in parallel. In homogenous media, transverse mixing is determined by molecular diffusion and dispersion, while in heterogeneous formations, this local mixing process is enhanced by flow focusing within high-permeability inclusions [Bear, 1972; Kitanidis, 1994; Werth *et al.*, 2006; Rolle *et al.*, 2009]. The Darcy-scale processes can be investigated through laboratory experiments and are typically modeled by Fickian dispersion. Although different theories and empirical expressions were proposed to compute the components of the local dispersion tensor [e.g., Scheidegger, 1961; Bear., 1972; Klenk and Grathwohl, 2002], a general agreement exists about the order of magnitude of these parameters.

The enhancement of transverse mixing due to the presence of advective heterogeneities is more difficult to quantify. The focusing of streamlines in high-conductivity zones is known to be one of the mechanisms that enhance transverse mixing since it reduces the transverse mixing length, increasing the mass flux across streamlines [Werth *et al.*, 2006, Rolle *et al.*, 2009]. However, a quantitative parameter to capture this effect would require field-scale experiments in which the heterogeneities are very well characterized; such experiments are unfortunately not feasible and usually the details of the flow field remain widely unknown. Furthermore, the presence of heterogeneities may stretch and squeeze the plume, and leads to meandering [e.g., Rahman *et al.*, 2005]. However, as pointed out by Kitanidis [1994], these processes do not directly contribute to physical mixing. Squeezing and stretching are mass displacements connected with advection mechanisms, and hence they are not strictly mixing or demixing processes, even if they affect the second central transverse moments of the plume [Rahman *et al.*, 2005; Rolle *et al.*, 2009]. Meandering causes an increase of the uncertainty of the plume's first transverse moment, but does not contribute to a net increase in transverse mixing. Stochastic analysis has dealt mainly with ensemble behavior of spatial moments in order to quantify dispersion in heterogeneous formations. Half the rate of change of second-central moments of the ensemble concentration defines the ensemble dispersion tensor [Gelhar and Axness, 1983; Dagan, 1984; Neuman *et al.*, 1987], which does not quantify mixing properly; in fact it is still affected by the uncertainty of tagging the plume center (i.e. it is affected by meandering). Although commonly used, ensemble dispersion is not a measure of pure mixing. Another possibility is to define so-called effective dispersion. The conceptual model underlying the effective dispersion tensor differs from ensemble dispersion in the order of taking spatial moments and averaging over all realizations. In effective dispersion, the second central moments of each realization are evaluated first, and the ensemble average of the second central moments is obtained subsequently [Kitanidis, 1988; Dagan, 1990, 1991; Rajaram and Gelhar, 1993a, 1993b, 1995; Dentz *et al.*, 2000a]. It is possible to define effective transverse dispersion coefficients for wide plumes [e.g., Dentz *et al.*, 2000b]. In this case both the irregular plume shape and the smooth transition of concentration from the plume centre to the surrounding are quantified. Only the latter property is related to actual mixing of the plume with ambient water, while the former quantifies an average squeezing and stretching. Effective transverse dispersion coefficients can also be defined for point-like injections [Dentz *et al.*, 2000a; Cirpka, 2002; Dentz and Carrera, 2003, 2005]. As claimed by Cirpka [2002], this is a good measure of mixing for reactive transport in case of complete mixing at the Darcy scale [Tartakovsky *et al.* 2009], since the scale of chemical transformation is the local one and in this way it is possible to quantify mixing.

Unfortunately, this measure is not applicable to individual plumes, it is not a measure for plumes of finite width, and it is affected by very high uncertainty. The mentioned stochastic approaches consider expected ensemble behavior and cannot cover the uncertainty of mixing and thus the variability of observable mixing in real measurements.

In multi-species (bio)reactive transport [e.g., *Cirpka and Valocchi, 2007, Prommer et al., 2009*], the limiting step for the reaction is the mixing between the different reactive compounds, if this process is slower than the (bio)chemical reaction. At steady state, the reaction partners must be mixed into the plume from the sides, hence the most important components of the dispersion tensor are the transverse ones [*Cirpka et al., 1999a; Liedl et al., 2006*]. The mixing processes of real interest are the ones at the pore-scale [*Willingham et al., 2008, 2010*] since reactions occur at a narrow reactive fringe, as shown by field scale measurements [*Lerner et al., 2000; Anneser et al., 2008*] as well as by laboratory bench-scale experiments [*Bauer et al., 2009*]. In order to estimate the length of a reactive plume in heterogeneous flow fields, we have to estimate the effect of advective heterogeneities and in particular of flow focusing on the enhancement of mixing and reaction [*Werth et al., 2006; Rolle et al., 2009*]. Hence, we have to consider a process at a larger scale than the pore one.

Kitanidis [1994] proposed to quantify mixing processes in groundwater by measuring the entropy of the plume, introducing the concept of the dilution index. This kind of measurement was applied to determine mixing of conservative tracers at the laboratory [e.g., *Ursino et al., 2001; Moroni et al. 2006; Rossi et al., 2007, 2008*] and at the field scale [e.g., *Thierrin and Kitanidis, 1994*]. The dilution index was also used in pore-scale modeling [e.g., *Cao and Kitanidis, 1998*]; in modeling studies in heterogeneous porous media [*Beckie, 1998; Kapoor and Kitanidis, 1996, 1998; Pannone and Kitanidis, 1999; McLaughlin and Ruan, 2001*], and even to determine numerical dispersion of transport codes [*Chilakapati and Yabusaki, 1999*]. Recently, this measure was applied in pore-scale multi-component reactive transport simulations [*Tartakovsky et al., 2009*]. The dilution index was modified by *de Rooij et al. [2006]* to apply it to breakthrough curves obtained by multi-compartment sampler data and later used by *Bloem et al. [2009]* for the interpretation of field experiments. *Bear and Sun [1998]* slightly modified the dilution index in order to account for changes in the porosity of the system, which was assumed constant by *Kitanidis [1994]*.

The dilution index as implemented by *Kitanidis [1994]* is a useful measure in case of a slug injection, while for continuous injections a flux-related dilution index appears to be more appropriate [*Rolle et al., 2009*]. In this work we further develop the concept of flux-related dilution index, providing analytical expressions to compute its value in homogeneous porous media, and comparing it with the volumetric dilution index presented by *Kitanidis [1994]* (Section 2.2). More importantly, we focus our attention on the reactive case (Section 2.3): we define the effective transverse dispersion coefficient needed in an equivalent homogeneous system to match the reactive behavior in a heterogeneous one, and we relate it to the dilution of a conservative tracer. This is accomplished through the introduction of the critical dilution index. This parameter quantifies the degree of mass flux dilution required to obtain complete degradation of a reactive plume emitted from a continuous line source. In Section 2.4, we present the results of numerical simulations of laboratory bench-scale systems and larger binary heterogeneous flow fields to show the applicability of the flux-related and critical dilution indices.

2.2 FLUX-RELATED DILUTION INDEX FOR CONSERVATIVE TRANSPORT

The flux-related dilution index $E_Q [L^3T^{-1}]$, introduced by *Rolle et al.* [2009], describes dilution “as the act of distributing a given solute mass flux over a larger water flux” and quantifies how the continuous mass flux of a conservative compound is mixed in a given flow field. The concentrations considered are local flux concentrations (i.e., the solute mass flux perpendicular to the control plane, divided by the specific discharge in the same direction), which differ slightly from the resident concentrations [*Kreft and Zuber, 1978*]. In contrast, the original dilution index of *Kitanidis* [1994] considered dilution as “the act of distributing (a finite slug of) solute mass over a larger volume”. The possibility to work with mass fluxes, instead of a finite mass, allows investigating how the dilution of a solute flux increases with travel distance when the compound is continuously injected into the flow domain. An ad-hoc transfer of the original dilution index to the situation of a continuously emitting source would be to consider the distribution of solute mass over a larger cross-sectional area perpendicular to the mean direction of flow. Such a concept would fail in the presence of heterogeneities where the cross-sectional area of a plume may shrink and expand due to spatially variable advection alone. In fact, as derived in Appendix A weighting the dilution index with the flow velocity is necessary to obtain a measure of mixing [*Rolle et al., 2009; Chiogna et al., 2010a*]. Both formulations of the dilution index intend to quantify mixing by the exponent of the entropy of the system. Entropy in this case has to be interpreted as a local spatial measure of dilution, and not as a thermodynamic quantity [*Beckie, 1998*]. In Table 2.1, we compare the distribution functions, the different definitions of the volumetric and flux-related dilution indices and of the reactor ratios (the normalized version of the dilution indices for a bounded domain). We also compare the rate of increase of the dilution index with time and of the flux-related dilution index with distance; the derivation of the latter is summarized in Appendix A. The concentration of the tracer solution is expressed by $c [ML^{-3}]$, the cross-sectional area by $A [L^2]$, the volume by $V [L^3]$, the porosity by $n [-]$, the specific-discharge component in the x direction by $q_x [LT^{-1}]$ and the total discharge by $Q_x [L^3T^{-1}]$. We assume that the flow is generally oriented in the x -direction, and that q_x is positive throughout the domain (i.e., we do not consider cases in which strong heterogeneity contrasts may cause a local flow reversal).

The volumetric dilution index introduced by *Kitanidis* [1994] is a function of time, while the flux-related dilution index of *Rolle et al.* [2009] is a function of space. It can be noticed that the rate of increase of both indices is the same, with the important difference that for the first one we consider the time derivative, while for the second one we consider the spatial derivative in the flow direction. The rate of increase of the entropy depends critically on the shape of the plume and on its interfacial area [*Kitanidis, 1994*] in both concepts. The property of being a monotonic increasing function is a necessary condition for both formulations of the dilution index. This allows to capture the essential characteristics of dilution processes which are irreversible and lead to a continuous increase of the entropy of the plume in both homogeneous and heterogeneous flow fields.

The volumetric expression for the dilution index can be restricted to a cross-sectional dilution index $E_{cs} [L^2]$, obtained by considering only the transverse coordinates (i.e., we integrate the entropy over a cross section of the domain instead over the whole volume, see Appendix B). At steady state in a homogeneous domain, the interpretation of the flux-related dilution index is strongly related to the cross-sectional dilution index and therefore with the original volumetric expression introduced by *Kitanidis* [1994]. In this context, we may transfer the longitudinal coordinate x of the cross-section to the equivalent travel time x/v . Then the flux-related dilution index in a uniform medium scales linearly with the cross-sectional dilution index by a factor of q_x (Appendix B):

$$\frac{E_Q(x)}{q_x(\mathbf{x})} = E_{cs}(x). \quad (2.1)$$

For a line source of width w [m] in y direction in an unbounded two-dimensional domain at steady state, we can express the flux-related dilution index as a function of the inverse transverse Péclet number (ε_y) defined as:

$$\varepsilon_y = \frac{nxD_t}{q_x w^2} \quad (2.2)$$

where n [-] is the porosity of the system, D_t [$L^2 T^{-1}$] is the local transverse dispersion coefficient and the flow is oriented in the x direction.

For this geometry, we obtain the following expression of $E_Q(\varepsilon_y)$ (Appendix C):

$$E_Q(\varepsilon_y) = wZq_x \left(1 - \sqrt{\frac{4\pi\varepsilon_y}{4\pi\varepsilon_y + 1}} + \sqrt{4\pi \exp(1)\varepsilon_y} \right) \quad (2.3)$$

where Z [L] is the thickness of the system in direction z .

This analytical expression (Eq. 2.3) is in very good agreement with the result obtained from a numerical computation of the flux-related dilution index for a line source in a 2-D unbounded homogeneous domain (Figure 2.1).

In Appendix C, we briefly illustrate other analytical expressions of the flux-related dilution index for different homogeneous flow domains (with the flow oriented in the x -direction) and boundary conditions.

	Volumetric Dilution index [Kitanidis, 1994]	Flux-related dilution index [Rolle et al., 2009]
Density function	$p(\mathbf{x}, t) = \frac{c(\mathbf{x}, t)}{\int_V c(\mathbf{x}, t) dV} \left[\frac{1}{L^3} \right]$ $\int_V p(\mathbf{x}, t) dV = 1$	$p_Q(\mathbf{x}) = \frac{c(\mathbf{x})}{\int_A q_x(\mathbf{x}) \cdot c(\mathbf{x}) dydz} \left[\frac{T}{L^3} \right]$ $\int_A p_Q(\mathbf{x}) \cdot q_x(\mathbf{x}) dydz = 1$
Dilution Index	$E(t) = \exp\left(-\int_V p(\mathbf{x}, t) \cdot \ln(p(\mathbf{x}, t)) dV\right) \left[L^3 \right]$	$E_Q(x) = \exp\left(-\int_A p_Q(\mathbf{x}) \cdot \ln(p_Q(\mathbf{x})) \cdot q_x(\mathbf{x}) dydz\right) \left[\frac{L^3}{T} \right]$
Reactor Ratio	$M(t) = \frac{E(t)}{V} \quad [-]$	$M_Q(x) = \frac{E_Q(x)}{Q_x} \quad [-]$
Rate of increase	$\frac{d \ln(E)}{dt} = -\int_V p \nabla \ln p^T \mathbf{D} \nabla \ln p dV \left[\frac{1}{T} \right]$	$\frac{d \ln(E_Q)}{dx} = -\int_A p_Q \nabla \ln p_Q^T n \mathbf{D} \nabla \ln p_Q dydz \left[\frac{1}{L} \right]$

Table 2.1: Definition and properties of the Volumetric Dilution Index $E(t)$ and the Flux-related Dilution Index $E_Q(x)$.

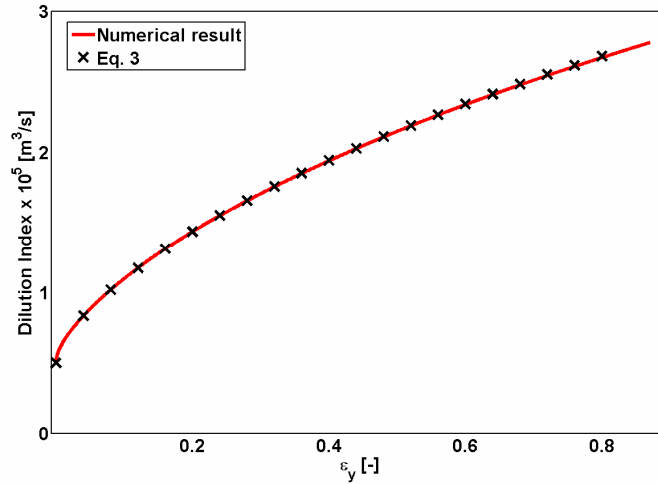


Figure 2.1: Comparison between the values of the dilution index computed numerically and analytically (Eq. 2.3) for a line source in a 2-D unbounded homogeneous domain.

2.3 CRITICAL DILUTION INDEX FOR REACTIVE TRANSPORT

2.3.1 Reactive transport problem

For simplicity, we restrict our analysis to conservative and reactive transport in a two-dimensional domain under steady-state conditions. We assume an instantaneous bimolecular complete reaction of the form $aA + bB \rightarrow cC$ (where a , b and c are the stoichiometric coefficients) so that the reaction rate is controlled only by the mixing process between the species A and B . The reacting compound A is injected through a continuous line source at the inflow boundary while B is introduced from its sides into the domain with the ambient groundwater. Figure 2.2 shows two examples of the heterogeneous flow fields at different scales considered in this work. The continuous line source of compound A is highlighted on the left boundary of the domain.

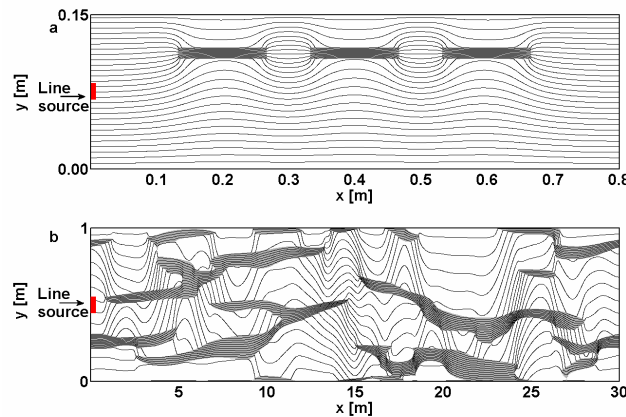


Figure 2.2: Streamlines computed for a bench-scale (a) and a field-scale (b) binary heterogeneous porous media. The gray zones where the streamlines converge are the high-conductivity inclusions.

Assuming that aqueous diffusion coefficients are identical for all reactive species, we can simplify the problem by considering a virtual conservative compound X , denoted the mixing ratio of

the plume [De Simoni *et al.*, 2005, 2007; Cirpka and Valocchi, 2007], introduced with unit concentration through the line source:

$$\begin{aligned}
\mathbf{v} \cdot \nabla X - \nabla \cdot (\mathbf{D} \nabla X) &= 0 \\
\mathbf{n} \cdot (\mathbf{v} X - \mathbf{D} \nabla X) &= \mathbf{n} \cdot \mathbf{v} \quad \text{along } \Gamma_{\text{in}}^A \\
\mathbf{n} \cdot (\mathbf{v} X - \mathbf{D} \nabla X) &= 0 \quad \text{along } \Gamma_{\text{in}}^B \\
\mathbf{n} \cdot \mathbf{D} \nabla X &= 0 \quad \text{along } \Gamma_{\text{nf}} \cup \Gamma_{\text{out}}
\end{aligned} \tag{2.4}$$

Where the seepage velocity \mathbf{v} is mainly oriented in the x direction and is expressed as $v = qn^{-1}$ [LT^{-1}] (for simplicity hereafter we will leave the subscription x), Γ_{in}^A and Γ_{in}^B are the fractions of the inflow boundary where compounds A respectively B are introduced, Γ_{nf} is a no-flow boundary, and Γ_{out} the outflow boundary. The local transverse dispersion coefficient D_t is defined following the non-linear empirical parameterization recently proposed by Chiogna *et al.* [2010b]:

$$D_t = D_p + \frac{vd}{\sqrt{Pe + 123}}, \tag{2.5}$$

In which D_p [L^2T^{-1}] is the pore diffusion coefficient, i.e., the ratio between the aqueous diffusion coefficient D_{aq} [L^2T^{-1}] and the tortuosity factor of the porous medium τ [-] (in this work we assume $\tau = n^{-1}$), d [L] is the grain size diameter, and $Pe = vd/D_{aq}$ [-] is the grain-Péclet number.

The mixing ratio can be converted to concentrations of reactive compounds by [Cirpka and Valocchi, 2007]:

$$\begin{aligned}
C_A &= \begin{cases} XC_A^{\text{in}} - \frac{a}{b}(1-X)C_B^{\text{amb}} & \text{if } X \geq X_{\text{crit}} \\ 0 & \text{if } X < X_{\text{crit}} \end{cases} \\
C_B &= \begin{cases} (1-X)C_B^{\text{amb}} - \frac{b}{a}XC_A^{\text{in}} & \text{if } X < X_{\text{crit}} \\ 0 & \text{if } X \geq X_{\text{crit}} \end{cases} \\
C_C &= \begin{cases} \frac{c}{a}XC_A^{\text{in}} & \text{if } X < X_{\text{crit}} \\ \frac{c}{b}(1-X)C_B^{\text{amb}} & \text{if } X \geq X_{\text{crit}} \end{cases}
\end{aligned} \tag{2.6}$$

in which C_A^{in} [ML^{-3}] and C_B^{amb} [ML^{-3}] are the inlet concentration of compound A and the inlet (and ambient) concentration of compound B , respectively, and X_{crit} is the critical mixing ratio at which both reactive-species concentrations are zero:

$$X_{\text{crit}} = \frac{aC_B^{\text{amb}}}{aC_B^{\text{amb}} + bC_A^{\text{in}}} \tag{2.7}$$

For the homogeneous case with the source width w [L], X will satisfy the two-dimensional analytical solution for the transport of a conservative species continuously injected by a line source [Domenico and Palciauskas, 1982]:

$$X(x, y) = \frac{1}{2} \left[\operatorname{erf} \left(\frac{y + \frac{w}{2}}{2\sqrt{D_t} \frac{x}{v}} \right) - \operatorname{erf} \left(\frac{y - \frac{w}{2}}{2\sqrt{D_t} \frac{x}{v}} \right) \right] \quad (2.8)$$

As pointed out by *Srinivasan et al.*[2007], this approximate analytical solution is subject to some limiting constraints. In this work we assume that those constraints are met and we rely on the applicability of Eq. 2.8.

2.3.2 Definition and derivation of the critical dilution index

In section 2.2, we have defined the flux-related dilution index, which measures the degree of dilution of a continuously emitted conservative tracer undergoing steady-state transport. We can now try to answer the following questions:

1. How are the dilution of a conservative and a reactive compound related?
2. Which information can be extrapolated from a conservative plume to a reactive plume?
3. How much mixing is required to achieve the complete degradation of a reactive plume?

The plume length of the injected compound A , is defined as the minimal distance L [L] from the source in the average flow direction at which $C_A = 0$ over the entire cross-sectional profile perpendicular to the average flow direction [*Cirpka et al.*, 2006]. The mixing ratio exactly has the value $X = X_{crit}$ where the concentration of both A and B are zero. For the homogeneous case, and when Eq. 2.8 is valid, we obtain [*Cirpka et al.*, 2006]:

$$L = \frac{vw^2}{16D_t \operatorname{inverf}(X_{crit})^2} \quad (2.9)$$

In case of an instantaneous reaction (i.e., the reaction occurs immediately upon mixing), the boundary of the plume is defined by $X = X_{crit}$, stemming from the stoichiometry of the reaction, the inflow and ambient concentrations. This distance of the farthest downstream point with $X = X_{crit}$ (i.e., the plume length), depends on hydraulic parameters (e.g., dispersion coefficient, heterogeneity) but the required amount of mixing between A and B will be similar for any hydraulic setting.

We now define the critical dilution index as the amount of mixing required for complete degradation of a reactive compound that is continuously injected into a porous medium and reacts with another compound injected in parallel. We conjecture that the required amount of mixing is unique (or at least affected by a negligible variance) when the aqueous diffusion coefficients (and hence the transverse dispersion coefficients) of the different reaction partners are the same. We define the critical dilution index as the value of the flux-related dilution index of a given conservative tracer at the length L of the reactive plume in the same flow field and for the same mass flux. For the homogeneous case, it is possible to demonstrate analytically that the value of the critical dilution index depends on the mass flux of the solute and on the critical mixing ratio (Appendix D).

Figure 2.3 shows the plume of a conservative compound in a homogeneous flow field: the white contour represents the normalized concentration $C(x, y)/C_0 = X_{crit}$, i.e., the boundary of a reactive plume. It is worth noticing that the $C(x, y)/C_0$ profile at a cross section before the end of reactive plume exhibits the value of X_{crit} at two locations and the reactive plume extends farther into the domain (Figure 2.3A). At a cross section beyond the end of the reactive plume, the concentration

ratio never reaches the value of X_{crit} (i.e., the reactive plume never reaches that distance). At the distance where the reactive plume ends, the transverse normalized concentration value $C(L,y)/C_0$ has the critical mixing ratio X_{crit} as its maximum (Figure 2.3B). This behavior also holds for heterogeneous cases. At steady state, the maximum of the normalized concentration of a conservative compound (i.e., the mixing ratio) will always be a continuously decreasing function with distance; and the length of a reactive plume is uniquely related to a particular maximum, corresponding to the critical mixing ratio (X_{crit}). Quite obviously, since the total mass flux of the conservative compound does not change with distance, a decrease of the maximum concentration requires the distribution over a larger water flux, that is, dilution. We conjecture that the relationship between the degree of dilution and the maximum concentration does not vary significantly with the specific flow field.

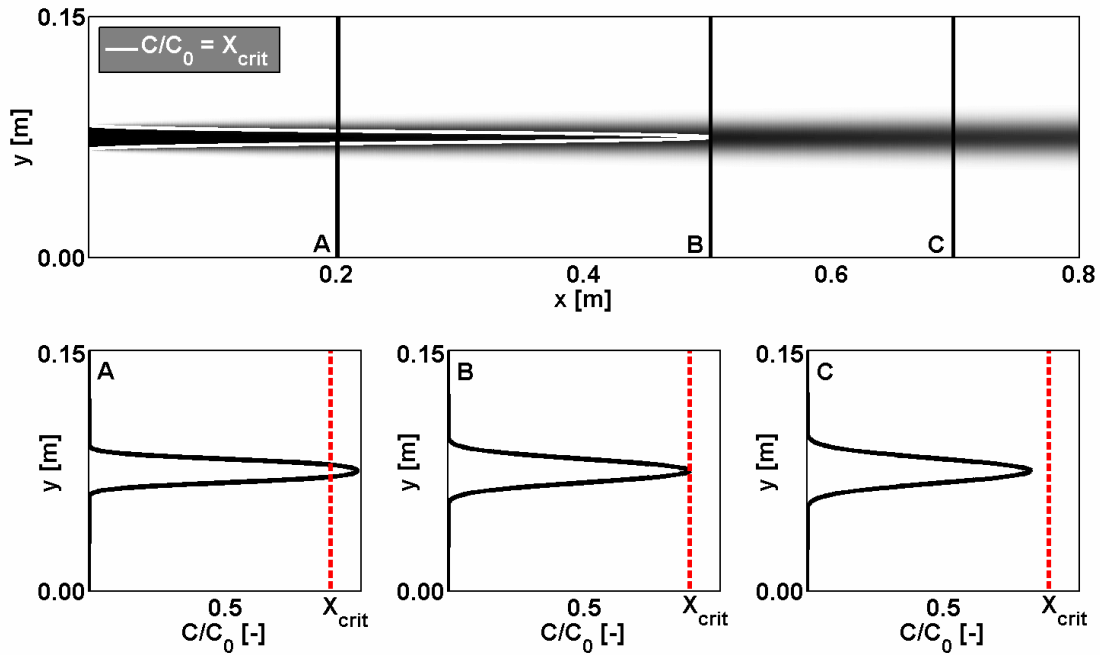


Figure 2.3: Conservative plume in a homogenous bench-scale domain (upper panel). The critical mixing ratio X_{crit} determines the boundary of the reactive plume (white contour line, upper panel). The vertical profiles of the normalized concentration of the conservative plume are compared with the critical mixing ratio at different cross-sections (i.e. 0.2 m, 0.5 m and 0.7 m in the lower panels A, B and C respectively).

Considering a continuous injection through a line source under steady-state flow conditions, we obtain for the critical dilution index, as a first order approximation:

$$CDI = E_Q(L) = \frac{E_Q(0)}{X_{crit}} \exp(1/2) \quad (2.10)$$

As discussed in Appendix C, Eq. 2.10 applies under the assumptions of validity of the analytical solutions Eq. 2.8 and Eq. 2.9.

No analytical solution is available to predict the concentration distribution in heterogeneous flow fields. However, in order to directly compare the critical dilution index of the homogeneous porous media (Eq. 2.10) with any heterogeneous setup we construct an equivalent homogeneous system. We define this system as the equivalent homogenous domain characterized by (i) the same injected solute mass flux as in the heterogeneous case and (ii) an effective transverse dispersion

coefficient leading to the same reactive plume length as in the heterogeneous domain. Using Eq. 2.9 and assuming we know the plume length of the heterogeneous case, the effective transverse dispersion coefficient of the equivalent homogeneous system will be:

$$D_{t,eff} = \frac{v \cdot w^2}{16L \cdot \text{inverf}(X_{crit})^2} \quad (2.11)$$

This definition of the effective dispersion coefficient differs from that proposed by *Kitanidis* [1988] and *Dentz et al.* [2000a], which relates to spatial moments of the plume. We have to point out that the effective transverse dispersion coefficient of the equivalent system will be usually larger than the mean local transverse dispersion coefficient because it includes effects of heterogeneity on mixing, but it does not quantify the spreading, the stretching and the meandering of the plume in the heterogeneous case. By construction, at distance L the equivalent homogeneous system will exhibit a maximum of X equal to the critical value X_{crit} . We expect in general that in a spatially variable permeability field the degree of mixing will be different than in a homogeneous one. However, at the end of the reactive plume, according also with the results of *Valocchi et al.* [2010], we conjecture that the dilution undergone by a conservative tracer is very similar for the homogeneous and any heterogeneous case. In fact, given the same mass flux and inflow concentrations at the boundary, we expect to obtain values for the critical dilution index very close to each other, independently from the heterogeneity of the system. Hence, as long as the flux-related dilution index does not reach the critical dilution index value, the plume will propagate farther both into the heterogeneous and into the homogeneous domains.

The concept of critical dilution index establishes a relationship between the dilution of a conservative tracer and the behavior of a compound undergoing a reaction. Furthermore it quantifies, for a given mass flux and a given reaction stoichiometry, to which extent a reactive species should be mixed with ambient water in order to be completely degraded. The advantage of the critical dilution index is that it connects a well known physical quantity, i.e., the entropy generated by mixing, with the possibility to predict at which distance a reactive plume will be completely degraded.

2.4 TRANSPORT SIMULATIONS AT DIFFERENT SCALES

We perform two kinds of numerical experiments: in the first one, two-dimensional laboratory bench-scale experiments [e.g., *Bauer et al.*, 2009; *Rolle et al.*, 2009, *Rolle et al.*, 2010] are simulated both under homogeneous and heterogeneous conditions; while in the second one, we perform two-dimensional field-scale simulations in heterogeneous systems. The parameters of the numerical examples are summarized in Table 2.2.

In the heterogeneous bench-scale experiment, three high-permeability inclusions (each 0.14 m long and 0.01 m wide) are placed at a distance of 0.13 m, 0.33 m and 0.53 m from the inflow boundary. Ten cases are considered, each one differing from the previous one by shifting the lenses 0.01m upwards, the first one being aligned with the center line of the tank. In the field-scale simulations, the heterogeneities are stochastically generated: irregularly shaped high-permeability inclusions are created using an auxiliary normal distributed variable with zero mean, Gaussian covariance function, longitudinal correlation length of 2 m and lateral correlation length of 0.1 m, as described in *Werth et al.* [2006]. In order to simulate naturally occurring inclusions where the bottom surfaces are more curved than the top surfaces, a cut-off value for the auxiliary variable is set to represent the 40% quantile and as a further constraint its vertical gradient component must be positive in the elements belonging to a high-conductivity lens. Both in the field- and in the bench-

scale simulations, the heterogeneous field is binary, the system is confined, fixed head boundary conditions are applied at the left- and right-hand side boundaries, and the mass flux of the injected solution is identical in all realizations. Heterogeneities thus lead to variations of the source width between the realizations, but we can define an effective source width by the width in an equivalent homogeneous medium [*de Barros and Nowak, 2010*].

Bench-scale domain dimension [m³]	0.8×0.01×0.13 (L×W×H)	Discretization [cells]	600×1×1000
Field-scale domain dimension [m³]	30×1×1 (L×W×H)	Stoichiometric coefficients a=b=c	1
Tortuosity factor [-]	2.5	D_{aq} [m ² s ⁻¹]	0.8×10 ⁻⁹
d coarse sand [m]	0.78×10 ⁻³	Field-scale specific discharge [m³s⁻¹]	5×10 ⁻⁵
d fine sand [m]	0.25×10 ⁻³	Bench-scale specific discharge [m³s⁻¹]	0.75×10 ⁻⁵
K coarse sand [ms⁻¹]	6.14×10 ⁻³	K fine sand [ms⁻¹]	6.14×10 ⁻⁴

Table 2.2: *Model parameters*

The steady-state flow problem for hydraulic head h and stream function ψ :

$$\begin{aligned}
 -\nabla \cdot (K\nabla h) &= 0 \\
 -\nabla \cdot \left(\frac{1}{K} \nabla \psi \right) &= 0
 \end{aligned}
 \tag{2.12}$$

is computed on a rectangular mesh grid by Finite Elements.

For the transport problem (Eq. 2.4), the domain is discretized into 600×1000 Finite Volumes with streamline-oriented cells constructed by the approach of *Cirpka et al.* [1999b,c]. The discharge is identical in all stream tubes. Figure 2.2 illustrates that streamlines are focused in inclusions of high-conductivity (light gray), leading to narrow elongated cells in that region. Orienting the grid in the flow direction avoids numerical transverse dispersion caused by diagonal fluxes between the cells; hence, no artificial-mixing entropy is generated through numerical errors. The transport problem is solved using the UMFPAK direct solver of Matlab[®] [*Davis and Duff, 1997*]. Since we work under the assumption that all species are characterized by the same aqueous diffusion coefficient we can use the post-processing procedure of *Cirpka and Valocchi* [2007] in order to evaluate the reactive concentration values for compounds A , B and C (Eq. 2.7) from the mixing ratio X . The ambient concentration of compound B is kept constant, i.e., $C_B^{amb} = 1$, while the inlet concentration C_A^{in} of compound A is varied in order to obtain different values for X_{crit} . The stoichiometric coefficients a , b and c are set to unity.

2.4.1 Results of conservative transport simulations

Figure 2.4 shows simulated plumes for different homogeneous and heterogeneous porous media at the bench-scale. The behavior of the flux-related reactor ratio (M_Q) in a homogeneous setup is compared with the results of three heterogeneous cases. In the first heterogeneous domain (Figure 2.4 HET A), in which the plume is focused in the high-conductivity inclusions, the concentration is

distributed over a larger water flux and hence the value of M_Q shows a steep increase, i.e., the increase in dilution leads to an effective mixing enhancement. The high-conductivity zones are almost in line with the source so that the whole mass flux of the injected conservative tracer solution is diluted in the first inclusion. In the second heterogeneous case (Figure 2.4 HET B), the lenses are shifted towards the upper part of the system and just the upper fringe of the plume is focused. The reduced focusing of the mass flux leads to a smoother increase in the flux-related reactor ratio. The effectiveness of the focusing decreases after each inclusion: the plume leaving the high-conductivity zone spreads over a wider region which is focused in a less efficient way by the successive inclusion (i.e., the mass flux involved in the flow focusing process decreases with the number of inclusions). In the last case (Figure 2.4 HET C), the plume is just meandering, but no effective focusing happens due to the presence of the heterogeneities, since the mass flux of the tracer solution does not pass through the inclusions. In this case the mixing in the heterogeneous case is even slightly less effective than in the homogeneous one because the heterogeneities exclusively cause expansion of the plume. However the flux-related reactor ratio is always a monotonically increasing function, while for example the second central spatial moment would decrease in the high conductivity inclusions as shown by *Rolle et al.* [2009].

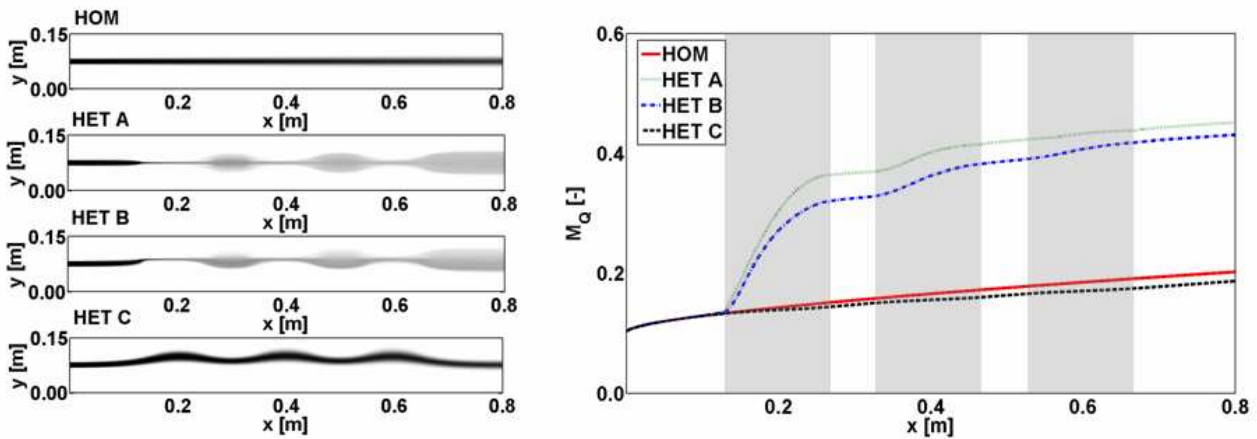


Figure 2.4: Conservative plumes in the homogeneous bench-scale model (HOM) and in three heterogeneous cases (HET A, HET B and HET C). The panel on the right shows the computed reactor ratios (the gray regions indicate the location of the high permeability inclusions).

In the field-scale setup, the plume can be focused by a higher number of high-conductivity lenses than in the bench-scale scenario. The average outcomes over 1000 realizations of binary heterogeneous flow fields, generated as previously described, are shown in Figure 2.5 as solid line, and the light gray shaded stripe indicate the range of ± 1 standard deviation. While single realizations show a step-like increase in the reactor ratio (similar to the bench-scale simulations), the reactor ratio averaged over the entire ensemble of realizations behaves like the reactor ratio for a homogeneous system and can be fitted by Eq. 2.3. From the fitted inverse Péclet number we can evaluate the value of the effective transverse dispersion coefficient $D_{t,eff} = 3.7 \times 10^{-8} \text{ m}^2 \text{ s}^{-1}$. This coefficient represents the geometric mean of the effective mixing of the system due to local transverse dispersion enhanced by flow focusing. For a hydraulic conductivity contrast of 10, the mean value of the local dispersion coefficient, averaged over the entire domain, ($D_t = 6.3 \times 10^{-9} \text{ m}^2 \text{ s}^{-1}$) is 6 times smaller than the effective one. We can thus conclude that, over the ensemble average, the flow focusing effect increased the mixing capacity of the system by almost an order of magnitude. This result is in good agreement with the outcomes of reactive transport modeling studies at contaminated sites equipped with high-resolution monitoring wells (e.g. *Prommer et al.*, 2006 and 2009). For instance, in the coal tar contaminated aquifer studied by *Prommer et al.* (2009), the best

fit of the measured biogeochemical and isotopic gradients was obtained using a $D_t=8.85\times 10^{-8}$ m²/s in the reactive transport simulations carried out in a two-dimensional homogeneous domain.

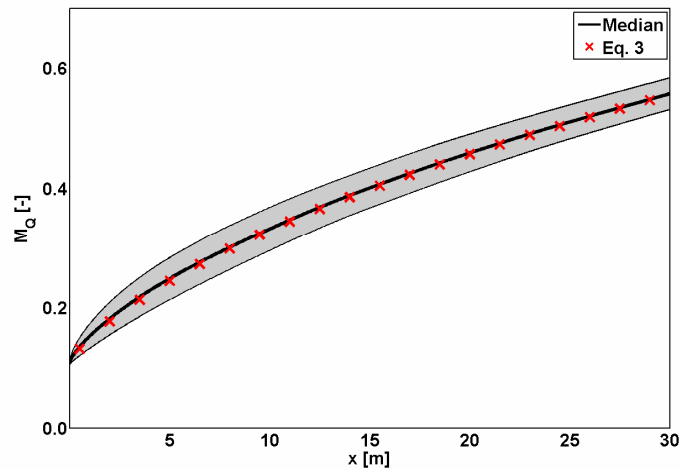


Figure 2.5: Average reactor ratio over 1000 realizations of the field scale model. Light gray shaded region represent ± 1 standard deviation.

2.4.2 Results of reactive transport simulations

For a reactive system, we need to verify the validity of the definition of the equivalent homogeneous system given in section 2.3.2. Starting with the bench-scale simulations, we consider some of the scenarios presented in Figure 2.4 (i.e. the HOM, HET B and HET C cases) with an inlet concentration of compound A, emitted from the source, equal 1/6 of the ambient concentration of compound B in the ambient groundwater. Figure 2.6 shows the contour boundaries of the three reactive plumes and the dilution indices of the conservative tracer in the same system. In case HET B, the mass flux of A is focused in the inclusions, the mixing is enhanced in an efficient way and the resulting plume is much shorter (0.15 m) than in the homogeneous setup. In case HET C, which presents the same high-permeability inclusions as HET B only shifted towards the upper boundary, the plume is bended due to the heterogeneous flow field and just a negligible part of the fringe is focused, whereas the bulk plume exhibits only expansion due to the heterogeneities. As a result, the plume is even longer (0.78 m) than the homogeneous one (0.59 m). We conclude that knowing the overall degree of heterogeneity is not sufficient to quantify effects on mixing of an individual plume; one must know how the mass flux of the plume is affected by the flow field: if the plume is expanded rather than focused, then a heterogeneous system may even reduce the dilution of the plume.

It can be noticed that, for a given mass flux of A, no difference can be detected between the values of the flux-related dilution index (i.e., the amount of mixing) at the length L of the reactive plume. This shows that even in extreme cases (complete focusing of the plume and bending with negligible focusing of a single fringe of the plume), the critical dilution index has the same value. We have to point out that, in order to correctly quantify the value of the critical dilution index, the numerical dispersion of the code must be negligible. In fact, the value of E_Q is the exponential of the entropy of the system and hence even a small numerical error may strongly affect this quantity if computed through numerical simulations.

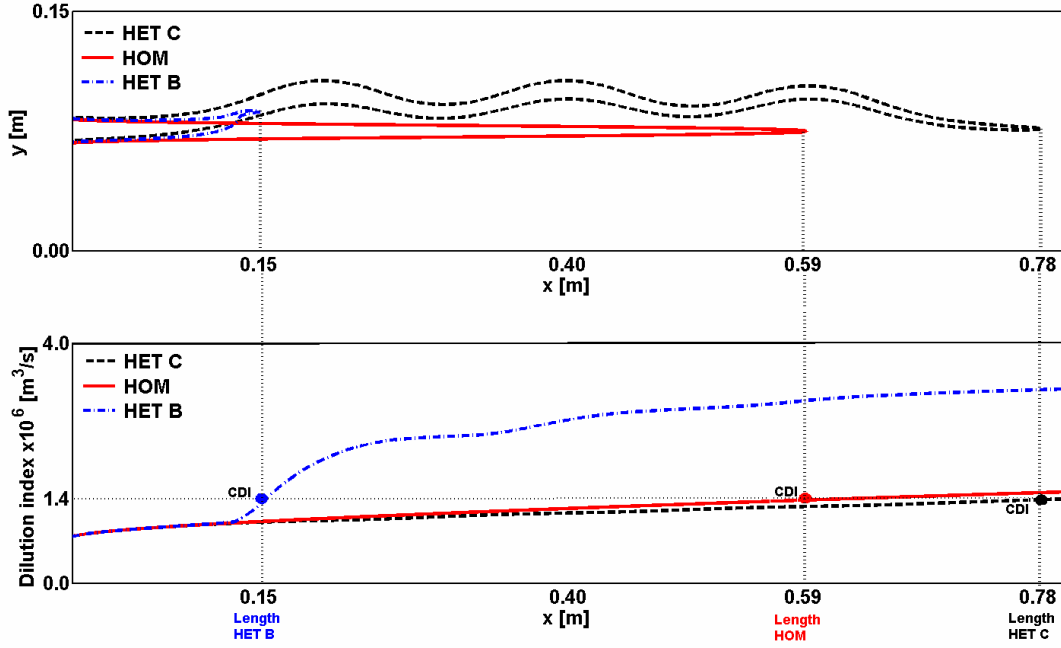


Figure 2.6: Contours of three reactive plumes (upper panel) and their flux-related and critical dilution index (lower panel).

In order to test the conjecture that the value of the critical dilution index does not depend significantly on the heterogeneity of the system, we generate 1000 random conductivity fields with a conductivity contrast of 10, as previously described. These realizations are performed at the larger field scale. The statistical analysis of the results (i.e. a chi squared goodness of fit test) shows that the values of the reactive plume length and the related effective transverse dispersion (Eq. 2.11) are lognormal distributed (Figure 2.7). The smaller the value of X_{crit} , the longer is the plume and hence the plume can sample a higher number of heterogeneities of the flow field before the end of the reactive plume is reached. This reduces the variability of the effective transverse dispersion coefficient and of the plume length within the ensemble of realizations (in fact $\sigma_{\ln(L)}$ and $\sigma_{\ln(D_{t,eff})}$ must be equal due to Eq. 2.11). On the contrary, the shorter the plume (i.e., the larger X_{crit}) the larger is the variability of the effective transverse dispersion coefficient among the realizations. For the same reason for small values of X_{crit} (i.e., long plumes) we obtain a slightly higher geometric mean of the effective transverse dispersion coefficients derived in the heterogeneous cases (Eq. 2.11) and hence we have a slight dependency of $D_{t,eff}$ on X_{crit} .

X_{crit}	Geometric mean of the plume length L [m]	Geometric mean of the effective transverse dispersion coefficient $D_{t,eff} \times 10^7$ [m ² /s]	$\sigma_{\ln(D_{t,eff})}$ and $\sigma_{\ln(L)}$
conservative	-	0.38	-
0.4	16.1	0.36	0.2
0.5	10.1	0.35	0.3
0.6	6.5	0.34	0.4

Table 2.3: Relationship between X_{crit} , plume length and effective transverse dispersion coefficient, with the standard deviation of the logarithm of their distribution $\sigma_{\ln(L)}$ and $\sigma_{\ln(L)}$, respectively.

Table 2.3 shows this slight dependence of $D_{t,eff}$ on X_{crit} , and thus on the reaction stoichiometry and the concentrations of the reaction partners in the inflow. It is worth to notice that the determination of the effective dispersion coefficient using the flux-related dilution index (i.e. for conservative transport) and analyzing the reactive cases leads to very close results. Other methods to determine an up-scaled dispersion coefficient usually are not able to predict a correct effective dispersion coefficient for reactive transport [Cirpka, 2002]. In the numerical simulations, the value of the logarithm of the flux-related dilution index (i.e., the entropy of the conservative mass flux) at the end of the plume for the heterogeneous case and the equivalent homogeneous case remain almost identical, showing an average difference of $\pm 0.4\%$. That is, in most cases, the distributions of p_Q for the homogeneous and the heterogeneous cases have not only the same maximum (per construction) but also the same entropy, so that the concept of the critical dilution index appears valid. Although it is mathematically possible to construct distributions with significantly different entropy but identical maximum, our numerical experiment indicates that physical constraints of solute transport (e.g. diffusive nature of governing equation, typical values of the parameters involved such as the velocity and the local dispersion coefficient, natural heterogeneity patterns, etc.) strongly limit and generally avoid the occurrence of such distributions.

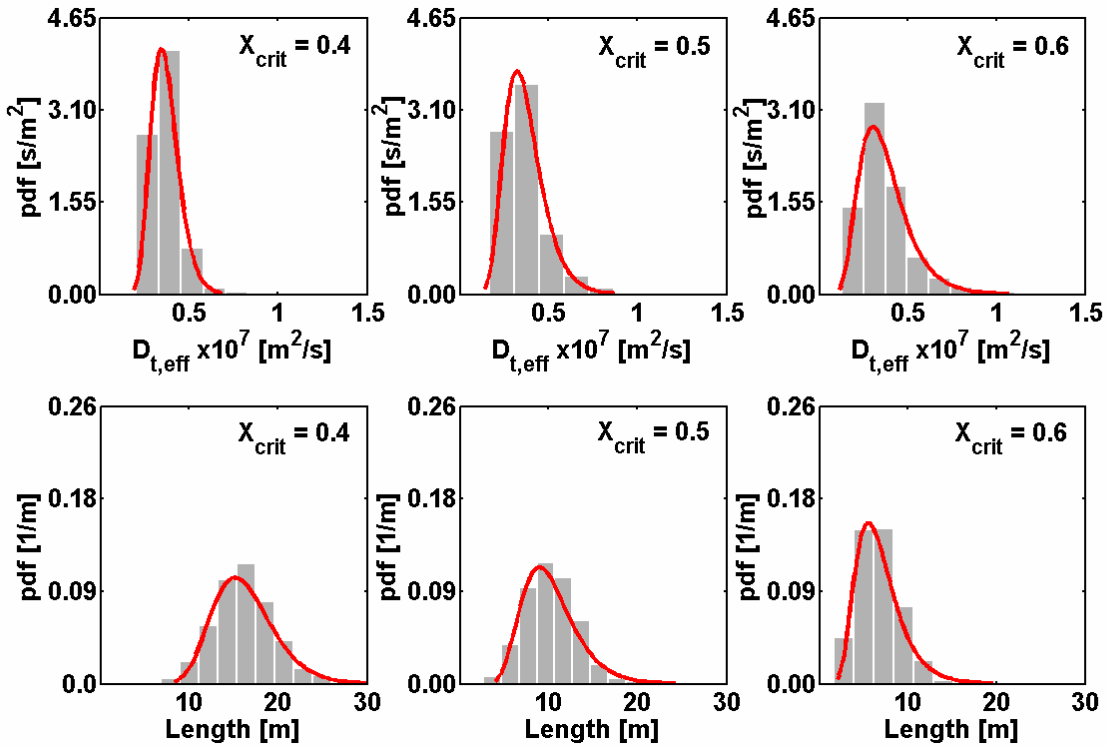


Figure 2.5: Probability density functions and histograms of the effective transverse dispersion coefficient (upper row) and of the reactive plume length (lower row) computed over the ensemble of 1000 realizations of field scale heterogeneous domains, for different values of X_{crit} .

Taking the geometric mean over the ensemble of realizations, the relation between X_{crit} , L and the effective transverse dispersion coefficient $D_{t,eff}$ is the same as Eq. 2.11 (Figure 2.7):

$$LD_{t,eff} = \frac{vw^2}{16\text{inverf}(X_{crit})^2} \quad (2.13)$$

in which w is the effective width of the line source in the equivalent homogeneous case, $D_{t,eff}$ is the geometric mean of the effective transverse dispersion coefficient of the equivalent homogeneous

systems and L the geometric mean of the length of plumes in the heterogeneous simulations. The average seepage velocity v is constant for all realization, since we keep the discharge of the system constant. The product between the plume length and the effective dispersion coefficient is per construction univocally determined for a given X_{crit} (Figure 2.8).

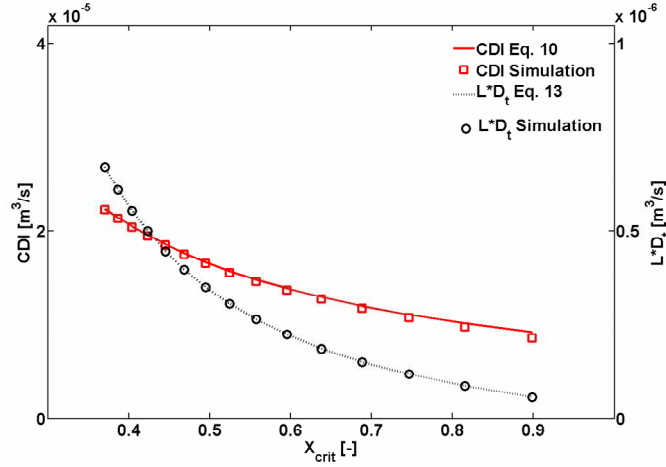


Figure 2.8: Relations between CDI and X_{crit} and between the product LD_t and X_{crit} . The geometric mean over 1000 realizations is plotted for the numerical simulations' results.

The results of the simulations confirm that the critical dilution index and the critical mixing ratio are related as predicted by Eq. 2.10 (Figure 2.8) for a given mass flux at the source. There is a small deviation from the expected values for high X_{crit} (i.e. short plumes) that can be explained by the fact that Eq. 2.10 is a first-order approximation for small values of X_{crit} . We have to consider furthermore that the validity of the analytical solution of *Domenico and Palciauskas* [1982] is not given in the proximity of the source [*Srinivasan et al.*, 2007].

Table 2.4 lists results for three different conductivity contrasts. These results indicate that the critical dilution index remains constant if the mass flux of the injected compound is the same; it only depends on the critical mixing ratio of the system (Table 2.4), as correctly predicted by Eq. 2.10. Hence, the definition given for the equivalent homogeneous system is reasonable since it allows obtaining a very good approximation for the dilution required for complete reaction of a plume even in heterogeneous systems with different permeability contrasts. The distributions of the plume length and of the effective transverse dispersion coefficient are affected by a higher uncertainty if the conductivity contrast is higher. For instance, given a conductivity contrast of 10, $\sigma_{\ln(L)}$ varies between 0.2 and 0.3, for $X_{crit}=0.4$ and $X_{crit}=0.5$ respectively; while for a conductivity contrast of 30 and the same values of X_{crit} , the variance $\sigma_{\ln(L)}$ of the log plume length varies between 0.3 and 0.4. Heterogeneous fields with higher conductivity contrast (and thus more effective flow focusing), result generally in shorter plumes and higher effective dispersion coefficients. We can notice that the effective transverse dispersion coefficient in this setup increases almost linearly with the permeability contrast.

	$K_{\text{high}}/K_{\text{low}} = 10$			$K_{\text{high}}/K_{\text{low}} = 20$			$K_{\text{high}}/K_{\text{low}} = 30$		
$X_{\text{crit}} [-]$	0.40	0.45	0.50	0.40	0.45	0.50	0.40	0.45	0.50
$D_{t,\text{eff}} \times 10^7 [\text{m}^2\text{s}^{-1}]$	0.36	0.35	0.35	0.68	0.67	0.66	0.96	0.91	0.87
Length [m]	16.1	12.5	10.19	8.4	6.5	5.2	5.9	4.8	3.9
$\text{CDI} \times 10^4 [\text{m}^3\text{s}^{-1}]$	0.21	0.18	0.17	0.21	0.18	0.17	0.21	0.18	0.17

Table 2.4: Influence of the hydraulic conductivity contrast ($K_{\text{high}}/K_{\text{low}}$) on $D_{t,\text{eff}}$, the plume length L , and the critical dilution index CDI for different X_{crit} (geometric mean values).

2.5 CONCLUSIONS

In this study, we illustrated the concept of flux-related dilution index, which is an appropriate measure to quantify mixing in both homogeneous and heterogeneous systems into which a conservative solute is continuously injected. For reactive systems, we introduced the critical dilution index, which is the degree of mixing required for the complete degradation of a reactive plume in case of instantaneous complete bimolecular reactions. In homogenous systems, the critical dilution index can be computed analytically. In order to transfer the concept of the critical dilution index to heterogeneous porous media, we have defined an equivalent homogeneous system in which the effective transverse dispersion coefficient is the one which matches the length of the plume. The results of the numerical simulations show that in this way it is possible to extend the use of the critical dilution index to heterogeneous systems. The newly defined effective transverse dispersion coefficient of the equivalent homogenous porous medium depends on the permeability contrast of the system and, via the critical mixing ratio, on the stoichiometry of the reaction, as well as the inflow and ambient concentrations. The local dispersion coefficient can be substantially smaller than the effective dispersion coefficient derived as fitting parameter to simulate the behavior of reactive plumes in heterogeneous formations. In our opinion, the apparent scale dependency of the transverse dispersion coefficient which appears in the interpretation of field scale plumes is caused by the difficulty to capture correctly the flow field when flow focusing effects caused by advective heterogeneities are the dominant mixing-enhancement process. Furthermore, we showed that information about the mass flux of a solute are of utmost importance in order to predict the fate of contaminant plumes. The performed theoretical and numerical analysis helps to answer the questions we posed in section 2.3.2:

1. The mixing of a conservative and of a reactive tracer can be quantitatively related to each other by the concept of critical dilution index in moderately heterogeneous aquifers and for instantaneous complete bimolecular reactions.

2. The flux-related dilution index of the system can be calculated from a conservative tracer. Under the assumption of instantaneous, mixing-controlled reactions, we can predict where a reactive plume generated by a continuous source will end if we know the critical dilution index of the system. In heterogeneous systems, information about the mass flux is required in order to correctly estimate the dilution of steady state plumes, whereas the knowledge of the spatial concentration distribution alone is not sufficient.

3. The amount of mixing required to completely degrade a reactive plume is well approximated by the value of the critical dilution index, a quantity which is exclusively controlled by the critical mixing ratio of the system and by the mass flux of the injected reactive species. The critical dilution index is defined over a cross section of the domain. Hence, it is not required to map the whole heterogeneity of an aquifer system, if we can quantify the mass flux of a plume over the cross section where the critical value for dilution is reached.

As already pointed out by *Kitanidis* [1994], the possibility to define a dilution index has a significant impact on many engineering applications, such as the design and optimization of in-situ remediation applications. With this work, we have added important information in order to answer the question whether it is possible to predetermine how much mixing is necessary to let a contaminant plume degrade. The determination of the critical dilution index and of the flux-related dilution index may be challenging in practical applications, due to the difficulties in measuring mass fluxes, determining the geometry of the source, and estimating the concentrations of the reaction partners. Nonetheless, any reactive transport model contains this information either as an input (e.g. initial concentration of the reactive species, source geometry) or they can be easily computed (such as the mass fluxes of the different chemical species). So the direct computation of the critical and the flux-related dilution indices, which can be performed on the basis of only conservative transport, will be useful when assessing plume development and/or potential remediation interventions on the basis of a modeling study.

The study of the behavior of the critical dilution index in cases of different reaction kinetics, of non-complete equilibrium reactions, of reaction partners with different aqueous diffusion coefficients and when the effects of transient flow on the effective dispersion tensor are relevant [e.g. *Cirpka and Attinger*, 2003, *Dentz and Carrera*, 2005] requires further investigations.

APPENDIX A: Transport of the entropy density

In this appendix, we derive the transport equation for the entropy density $p_Q \cdot \ln(p_Q)$ of a conservative component. In case of steady state transport, the probability density function p_Q as defined in Table 2.1, must satisfy the following conservation equation:

$$\nabla \cdot (\mathbf{q}p_Q - n\mathbf{D}\nabla p_Q) = 0 \quad (2.14)$$

Multiplying Eq. 2.14 by $\ln p_Q$ and applying the chain-rule of differentiation we obtain the following equation for the advective and dispersive fluxes:

$$\ln p_Q \nabla \cdot (\mathbf{q}p_Q) = \nabla \cdot (\mathbf{q}p_Q \ln p_Q) - \nabla \cdot (\mathbf{q}p_Q) \quad (2.15)$$

$$\ln p_Q \nabla \cdot (n\mathbf{D}\nabla p_Q) = \nabla \cdot (n\mathbf{D}\nabla(p_Q \ln p_Q)) - \nabla \cdot (n\mathbf{D}\nabla p_Q) - \frac{1}{p_Q} (\nabla p_Q)^T n\mathbf{D}(\nabla p_Q) \quad (2.16)$$

Hence, combining Eqs. 2.14, 2.15 and 2.16, we obtain an advection-dispersion equation for the entropy with a source term:

$$\nabla \cdot (\mathbf{q}p_Q \ln p_Q - n\mathbf{D}\nabla p_Q \ln p_Q) = -p_Q \nabla \ln p_Q^T n\mathbf{D}\nabla \ln p_Q \quad (2.17)$$

Integrating Eq. 2.17 over the unbounded cross section perpendicular to the main direction of the flow we obtain (remembering that we defined $q=q_x$):

$$\frac{d}{dx} \int_{-\infty}^{\infty} (\mathbf{q}p_Q \ln p_Q - \mathbf{e}_1^T n\mathbf{D}\nabla p_Q \ln p_Q) dydz = - \int_{-\infty}^{\infty} p_Q \nabla \ln p_Q^T n\mathbf{D}\nabla \ln p_Q dydz = - \int_{-\infty}^{\infty} \frac{1}{p_Q} \nabla p_Q^T n\mathbf{D}\nabla p_Q dydz \quad (2.18)$$

In the advection dominated case we can neglect the second term of the left hand side integrand, so that the rate of increase of the flux-related dilution index respect to the main direction of the flow is:

$$\frac{dF_{p_Q \ln p_Q}}{dx} \approx \frac{d}{dx} \int_{-\infty}^{\infty} (\mathbf{q}p_Q \ln p_Q) dydz = \frac{d \ln E_Q}{dx} = - \int_{-\infty}^{\infty} p_Q \nabla \ln p_Q^T n\mathbf{D}\nabla \ln p_Q dydz \quad (2.19)$$

Where $F_{p_Q \ln p_Q}$ is the total entropy flux integrated over a cross sectional area.

APPENDIX B: Relationship between flux-related and cross-sectional dilution indices in homogeneous cases

In this appendix, we show how to relate the flux-related dilution index to the cross-sectional dilution index in a homogeneous porous medium. The flux-related dilution index is defined as:

$$E_Q(x) = \exp \left[- \int_A p_Q(\mathbf{x}) \cdot \ln(p_Q(\mathbf{x})) \cdot q_x(\mathbf{x}) dydz \right] \quad (2.20)$$

In a homogeneous domain, the volumetric flux is uniformly distributed along the cross section, so we can write:

$$E_Q(x) = \exp \left[- \int_A \frac{p(\mathbf{x})}{q_x(\mathbf{x})} \cdot \ln \left(\frac{p(\mathbf{x})}{q_x(\mathbf{x})} \right) \cdot q_x(\mathbf{x}) dydz \right] \quad (2.21)$$

And hence:

$$E_Q(x) = \exp \left[- \int_A (p(\mathbf{x}) \cdot \ln(p(\mathbf{x})) - p(\mathbf{x}) \cdot \ln(q_x(\mathbf{x}))) dydz \right] = E_{cs}(x) q_x(\mathbf{x}) \quad (2.22)$$

If we now change to a coordinate system moving with velocity v , so that $x = vt$, we obtain:

$$E_Q(x) = E_{cs}(vt) q_x(vt) \quad (2.23)$$

APPENDIX C: Flux-related dilution index for a line source in homogeneous two-dimensional domains and analytical expressions for other remarkable cases

In the following, we derive the semi-analytical equation to express the flux-related dilution index in case of a line source and we present some analytical expression for other remarkable cases. We assume that the value of the flux-related dilution index can be expressed by a nested radical of the form:

$$E_Q(L) = wZq_x \left(1 + \sqrt{ax + (n+a)^2 + x\sqrt{a(x+n) + (n+a)^2 + (x+n)\sqrt{\dots}}} \right) \quad (2.24)$$

where w is the source width in y direction and Z is the thickness of the system in direction z . The fitted coefficients a , x and n have the following values:

$$\begin{aligned} a &= 0 \\ n &= \sqrt{4\pi \exp(1) \varepsilon_y(L)} \\ x &= -\sqrt{\frac{4\pi \varepsilon_y}{4\pi \varepsilon_y + 1}} \end{aligned} \quad (2.25)$$

Where ε_y is defined as in (4) i.e. $\varepsilon_y = nx D_t / (q_x w^2)$.

We note that the nested radical is the general formulation of the Ramanujan identity [Ramanujan, 1911], which can be simplified through:

$$E_Q(\varepsilon_y) = wZq_x \left(1 - \sqrt{\frac{\varepsilon_y}{\varepsilon_y + \exp(1)}} + \sqrt{4\pi \exp(1) \varepsilon_y} \right) \quad (2.26)$$

Eq. 2.26 converges for the limit $w \rightarrow 0$ to the expected analytical solution given by Eq. 2.31, for the limit $x \rightarrow 0$ to the dilution index at the source (i.e., the value of the exponential of the entropy of

a uniform distribution), and it fits in an excellent way the results of the numerical simulations (Figure 2.1).

It is worth noticing that the inverse Péclet number can be expressed as:

$$\varepsilon_y(L) = \frac{1}{16 \operatorname{inverf}(X_{crit})^2} \quad (2.27)$$

if we are far enough from the source zone (i.e. the hypothesis underlying Eq. 2.8 are satisfied [Srinivasan *et al.*, 2007]). This requirement is satisfied for small values of X_{crit} . If we truncate the Taylor expansion of the $\operatorname{inverf}(X_{crit})$ at its first order we obtain:

$$\operatorname{inverf}(X_{crit}) = \frac{1}{2} \sqrt{\pi} X_{crit} + O(X_{crit}^3) \quad (2.28)$$

It is now straightforward to compute the first-order approximation for the critical dilution index:

$$CDI \equiv E_Q(L) = \frac{E_Q(0)}{X_{crit}} \exp(1/2) \quad (2.29)$$

This value is exactly the value of the critical dilution index we have to expect for a Gaussian plume. Hence Eq. 2.14 satisfies the convergence for long plumes to a Gaussian shape.

The values of $E_Q(x)$ for the case of uniform flow with a continuous point injection can be computed from the analytical expressions given by Kitanidis [1994] (Eqs. 2.26 and 2.27). In a 3-D unbounded domain with uniform flow in direction x , we obtain for a point-like injection:

$$E_Q(x) = 4\pi \exp(1) x n D_t \quad (2.30)$$

where n [-] is the porosity of the system and $D_t [L^2 T^{-1}]$ is the local transverse dispersion coefficient.

In a two-dimensional domain with thickness $Z [L]$, we obtain for an injection over the thickness:

$$E_Q(x) = \exp(1/2) Z \sqrt{4\pi x n D_t q_x} \quad (2.31)$$

That is, in the unbounded 3-D uniform case, the flux-related dilution index increases linearly with distance, whereas in the case of 2-D flow we obtain an expression scaling with the square-root of travel distance.

APPENDIX D: Uniqueness of the critical dilution index in homogeneous media

In this appendix, we compute the critical dilution index in the homogeneous case and prove its uniqueness independent from the transverse dispersion coefficient. We consider the same reactive system (i.e. same stoichiometric coefficients, same flow conditions, same source geometry, etc.) for two different transverse dispersion coefficients (e.g. two packed beds with two distinct grain sizes) and we work under the hypothesis that the validity conditions of Eq. 2.8 and Eq. 2.9 apply.

The plume length L is different, since it depends on the transverse dispersion coefficients:

$$L_1 = \frac{vw^2}{16D_{t1}inverf(X_{crit})^2} \quad (2.32)$$

$$L_2 = \frac{vw^2}{16D_{t2}inverf(X_{crit})^2}$$

We consider the analytical solution [Domenico and Palciauskas, 1982] for the two conservative cases, with initial concentration C_0 [ML^{-3}]:

$$\frac{C_i(x, y)}{C_0} = \frac{1}{2} \left[erf \left(\frac{y + \frac{w}{2}}{2\sqrt{D_{ti} \frac{x}{v}}} \right) - erf \left(\frac{y - \frac{w}{2}}{2\sqrt{D_{ti} \frac{x}{v}}} \right) \right] \quad i = 1, 2 \quad (2.33)$$

If we compute the concentration of the conservative tracer at $x=L_1$ and $x=L_2$ we obtain:

$$\frac{C_1(L_1, y)}{C_0} = \frac{1}{2} \left[erf \left(\frac{y + \frac{w}{2}}{2\sqrt{\frac{w^2}{16inverf(X_{crit})}}} \right) - erf \left(\frac{y - \frac{w}{2}}{2\sqrt{\frac{w^2}{16inverf(X_{crit})}}} \right) \right] \quad (2.34)$$

The same procedure can be applied to compute the concentration for the second case:

$$\frac{C_2(L_2, y)}{C_0} = \frac{1}{2} \left[erf \left(\frac{y + \frac{w}{2}}{2\sqrt{\frac{w^2}{16inverf(X_{crit})}}} \right) - erf \left(\frac{y - \frac{w}{2}}{2\sqrt{\frac{w^2}{16inverf(X_{crit})}}} \right) \right] \quad (2.35)$$

So we demonstrated that:

$$C_1(L_1, y) = C_2(L_2, y) \quad (2.36)$$

We compute the probability density function for the flux-related dilution index:

$$p_Q(x, y) = \frac{C(x, y)}{\int q_x C(x, y) dx dy} \quad (2.37)$$

And we notice that:

$$p_{Q_1}(L_1, y) = \frac{C_1(L_1, y)}{\int q_x C_1(L_1, y) dy} = \frac{C_2(L_2, y)}{\int q_x C_2(L_2, y) dy} = p_{Q_2}(L_2, y) \quad (2.38)$$

Hence, it is straightforward to demonstrate that the critical dilution index must assume the same value in homogenous porous media:

$$CDI(L_1) = E_Q(L_1) = E_Q(L_2) = CDI(L_2) \quad (2.39)$$

REFERENCES

- Anneser, B., F. Einsiedl, R.U. Meckenstock, L. Richters, F. Wisotzky, and C. Griebler (2008), High-resolution monitoring of biogeochemical gradients in a tar oil-contaminated aquifer, *Appl. Geochem.*, 23, 1715-1730.
- Bauer, R.D., M. Rolle, S. Bauer, C. Eberhardt, P. Grathwohl, O. Kolditz, R.U. Meckenstock, and C. Griebler (2009), Enhanced biodegradation by hydraulic heterogeneities in petroleum hydrocarbon plumes, *J. Contam. Hydrol.*, 105, 56-68.
- Bear, J. (1972), *Dynamics of fluids in porous media*; Dover: New York, USA.
- Bear, J. and Y. Sun, (1998), Optimization of pump-treat-inject (PTI) design for the remediation of a contaminated aquifer: multi-stage design with chance constraints, *J. Contam. Hydrol.*, 29, 225-244.
- Beckie, R.D. (1998), Analysis of scale effects in large-scale solute transport models, in *Scale Dependence and Scale Invariance in Hydrology*, edited by G. Sposito Ed., pp.314 – 334, Cambridge University Press, New York.
- Bloem, E., F.A.N. Hogervorst and G.H. de Rooij (2009), A field experiment with variable-suction multi-compartment samplers to measure the spatio-temporal distribution of solute leaching in an agricultural soil, *J. Contam. Hydrol.*, 105, 131–145.
- Bolster, D., F. J. Valdés-Parada, T. LeBorgne, M. Dentz, and J. Carrera (2010), Mixing in confined stratified aquifers, *J. Contam. Hydrol.*, in Press.
- Cao, J, and P. K. Kitanidis (1998), Pore-scale dilution of conservative solutes: An example, *Water Resour. Res.*, 34(8), 1941-1949.
- Chilakapati, A., and S. Yabusaki (1999), Nonlinear reactions and nonuniform flows, *Water Resour. Res.*, 35(8), 2427-2438.
- Chiogna G., M. Rolle, O.A. Cirpka and P. Grathwohl, (2010a), Modeling mixing-controlled reactive transport: importance of compound dependent hydrodynamic and (hydro)mechanical transverse dispersion, paper presented at XVIII International Conference on Computational Methods in Water Resources, CMWR, Barcelona, Spain (accepted).
- Chiogna, G., C. Eberhardt, P. Grathwohl, O.A. Cirpka and M. Rolle (2010b), Evidence of compound-dependent hydrodynamic and mechanical transverse dispersion by multitracer laboratory experiments, *Environ. Sci. Technol.*, 44(2), 688-693, doi: 10.1021/es9023964.
- Cirpka, O.A. (2002), Choice of dispersion coefficients in reactive transport calculations on smoothed fields, *J. Contam. Hydrol.*, 58, 261-282.
- Cirpka, O.A., and S. Attinger (2003) Effective dispersion in heterogeneous media under random transient flow conditions, *Water Resour. Res.* 39(9): 1257.
- Cirpka, O.A. and A.J. Valocchi (2007), Two-dimensional concentration distribution for mixing-controlled bioreactive transport in steady state, *Adv Water Resour.*, 30 (6-7), 1668-1679.

- Cirpka, O. A., E. O. Frind, and R. Helmig (1999a), Numerical simulation of biodegradation controlled by transverse mixing, *J. Contam. Hydrol.*, 40(2), 159–182.
- Cirpka, O. A., E. O. Frind, and R. Helmig (1999b), Streamline-oriented grid-generation for transport modelling in two-dimensional domains including wells, *Adv. Water Resour.*, 22(7), 697–710.
- Cirpka, O. A., R. Helmig, and E. O. Frind (1999c), Numerical methods for reactive transport on rectangular and streamline-oriented grids, *Adv. Water Resour.*, 22(7), 711–728.
- Cirpka, O.A., A. Olsson, Q. Ju, A. Rahman and P. Grathwohl (2006), Determination of transverse dispersion coefficients from reactive plumes lengths, *Ground Water*, 44 (2), 212-221.
- Dagan, G. (1984), Solute transport in heterogeneous porous formations, *J. Fluid Mech.* 145: 151-177.
- Dagan, G. (1990), Transport in heterogeneous porous formations: Spatial moments, ergodicity, and effective dispersion, *Water Resour. Res.*, 26(6): 1281-1290.
- Dagan, G. (1991), Dispersion of a passive solute in nonergodic transport by steady velocity-fields in heterogeneous formations, *J. Fluid Mech.* 233: 197-210.
- Davis, T.A., and I.S. Duff (1997), An unsymmetric-pattern unifrontal method for sparse LU factorization, *SIAM J. Matrix anal. Appl.*, 18(1), 140-158.
- de Barros, F.P.J., and W. Nowak (2010), On the link between contaminant source release conditions and plume prediction uncertainty, *J. Contam. Hydrol*, (in press)
- De Rooij, G.H., O.A. Cirpka, F. Stagnitti, S.H. Vuurens, and J. Boll (2006), Quantifying minimum monolith size and solute dilution from multi-compartment percolation sampler data, *Vadose Zone J.*, 5, 1086-1092.
- De Simoni, M., J. Carrera, X. Sanchez-Vila, and A. Guadagnini (2005), A procedure for the solution of multi-component reactive transport problems, *Water. Resour. Res.*, 41, W11410, doi:10.1029/2005WR004056.
- De Simoni, M., X. Sanchez-Vila, J. Carrera, and M.W. Saaltink (2007), A mixing ratios-based formulation for multicomponent reactive transport, *Water Resour. Res.*, 43, W07419; doi:10.1029/2006WR005256.
- Dentz, M. and Carrera, J. (2003) Effective dispersion in temporally fluctuating flow through a heterogeneous medium, *Phys. Rev. E* 68 (3): 036310.
- Dentz, M., and J. Carrera (2005), Effective solute transport in temporally fluctuating flow through heterogeneous media, *Water. Resour. Res.*, 41, W08414, doi: 10.1029/2004WR003571.
- Dentz, M., H. Kinzelbach, S. Attinger, and W. Kinzelbach (2000a), Temporal behavior of a solute cloud in a heterogeneous porous medium 1. Point-like injection, *Water Resour. Res.*, 36(12): 3591-3604.

- Dentz, M., H. Kinzelbach, S. Attinger, and W. Kinzelbach.(2000b) Temporal behavior of a solute cloud in a heterogeneous porous medium 2. Spatially extended injection, *Water Resour. Res.*, 36(12): 3605-3614.
- Domenico, P.A., and V.V. Palciauskas (1982), Alternative boundaries in solid waste management, *Ground Water*, 20 (3), 303-311.
- Gelhar, L. W., and C.L. Axness (1983), Three-dimensional stochastic analysis of macrodispersion in aquifers, *Water Resour. Res.*, 19 (1), 161-180.
- Kapoor, V. and P.K: Kitanidis (1996), Concentration fluctuations and dilution in two-dimensionally periodic heterogeneous porous media, *Transp. Porous Media*, 22, 91-119.
- Kapoor, V. and P.K: Kitanidis (1998), Concentration fluctuations and dilution in aquifers, *Water Resour. Res.*, 34(5), 1181-1193.
- Kitanidis, P.K. (1988), Prediction by the method of moments of transport in heterogeneous formations, *J. Hydrol.* 102(1-4): 453-473.
- Kitanidis, P.K. (1994), The concept of dilution index, *Water Resour. Res.*, 30 (7), 2011-2026.
- Klenk, I.D., and P. Grathwohl (2002), Transverse vertical dispersion in groundwater and the capillary fringe. *J. Contam. Hydrol.*, 58(1-2), 111-128.
- Kreft, A., and A. Zuber (1978), On the physical meaning of the dispersion equation and its solutions for different initial and boundary conditions, *Chem. Eng. Sci.*, 33(11), 1471-1480.
- Lerner, D.N., S.F. Thornton, M.J. Spence, S.A. Banwart, S.H. Bottrell, J.J. Higgo, H.E.H. Mallinson, R.W. Pickup, and G.M. Williams (2000), Ineffective natural attenuation of degradable organic compounds in a phenol-contaminated aquifer, *Ground Water*, 38, 922-928.
- Liedl, R., A. J. Valocchi, P. Dietrich, and P. Grathwohl (2005), Finiteness of steady state plumes, *Water Resour. Res.*, 31, 1-8.
- Luo, J., M. Dentz, J. Carrera, and P. Kitanidis (2008), Effective reaction parameters for mixing controlled reactions in heterogeneous media, *Water. Resour. Res.*, 44, W02416, doi: 10.1029/2006WR005658.
- McLaughlin, D., and F. Ruan (2001), Macrodispersivity and large-scale hydrogeologic variability, *Transp. porous media*, 42, 133-154.
- Moroni, M., N. Kleinfelder, and J.H. Cushman (2007), Analysis of dispersion in porous media via matched-index particle tracking velocimetry experiments, *Adv. Water Res.*, 30, 1-15.
- Neuman, S.P., C.L. Winter, and C.M. Newman (1987), Stochastic theory of field-scale Fickian dispersion in anisotropic porous media, *Water Resour. Res.* 23(3): 453-466.
- Pannone, M., and P.K. Kitanidis (1999), Large-time behavior of concentration variance and dilution in heterogeneous formations, *Water Resour. Res.*, 35(3), 623-634.

Prommer, H., Tuxen, N. and P. Bjerg (2006), Fringe-controlled natural attenuation of phenoxy acids in a landfill plume: integration of field-scale processes by reactive transport modelling, *Environ. Sci. Technol.*, 40, 4732-4738.

Prommer, H., B. Anneser, M. Rolle, F. Einsiedl, and C. Griebler (2009), Biogeochemical and isotopic gradients in a BTEX/PAH contaminant plume: model-based interpretation of a high-resolution field data set, *Environ. Sci. Technol.*, 43, 8206-8212.

Rahman, A.M., S. Jose, W. Nowak, and O.A. Cirpka (2005), Experiments on vertical transverse mixing in a large-scale heterogeneous model aquifer. *J. Contam. Hydrol.*, 3-4, 80, 130-148. doi:10.1016/j.jconhyd.2005.06.010.

Rajaram, H., and L.W. Gelhar, (1993a) Plume scale-dependent dispersion in heterogeneous aquifers 1. Lagrangian analysis in a stratified aquifer, *Water Resour. Res.* 29(9): 3249-3260.

Rajaram, H., and L.W. Gelhar, (1993b) Plume scale-dependent dispersion in heterogeneous aquifers 2. Eulerian analysis and three-dimensional aquifers, *Water Resour. Res.* 29(9): 3261-3276.

Rajaram, H., and L.W. Gelhar, (1995) Plume-scale dispersion in aquifers with a wide range of scales of heterogeneity, *Water Resour. Res.* 31(10): 2469-2482.

Ramanujan, S. (1911), Question No. 298. *J. Indian Math. Soc.*.

Rolle, M., C. Eberhardt, G. Chiogna, O.A. Cirpka, and P. Grathwohl (2009), Enhancement of dilution and transverse reactive mixing in porous media: Experiments and model-based interpretation, *J. Contam. Hydrol.*, 110, 130-142.

Rolle, M., G. Chiogna, R. Bauer, C. Griebler and P. Grathwohl (2010), Isotopic fractionation by transverse dispersion: flow-through microcosms and reactive transport modeling study, *Environ. Sci. Technol.*, 44, 6167-6173.

Rossi, M., P. Lehmann, N. Ursino, O. Ippisch and H. Flüher (2007), Solute mixing during imbibition and drainage in a macroscopically heterogeneous medium, *Water Resour. Res.*, 43, doi: 10.1029/2005WR004038.

Rossi, M., O. Ippisch, and H. Flüher (2008), Solute dilution under imbibition and drainage conditions in a heterogeneous structure: Modeling of a sand tank experiment, *Adv Water Resour.*, 31, 1242-1252.

Scheidegger, A.E. (1961), General theory of dispersion in porous media, *J. Geophys. Res.*, 66(4), 3273-3278.

Srinivasan, V., T.P. Clement, and K.K. Lee (2007), Domenico solution – is it valid?, *Ground Water*, 45, 136-146.

Stueben, K. (2001), A review of algebraic multigrid, *J. Comput. Appl. Math.*, 128(1-2), 281-309.

Tartakovsky, A.M., G.D. Tartakovsky and T.D. Scheibe (2009), Effects of incomplete mixing on multicomponent reactive transport, *Adv Water Resour.*, 32(11), 1674-1679.

- Thierrin, J., and P.K Kitanidis (1994), Solute dilution at the Borden and Cape Cod groundwater tracer tests, *Water Resour. Res.*, 30(11), 2883-2890.
- Ursino, N., T. Gimmi and H. Flühler (2001), Dilution of non reactive tracers in variably saturated sandy structures, *Adv Water Resour*, 24, 877-885.
- Valocchi, A. J., K. Nakshatrala and M. Massabò, (2009), Reactions Along Transverse Mixing Zones in Heterogeneous Aquifers: Using Effective Dispersion Coefficients and Multi-Scale Finite Element Methods, paper presented at AGU fall meeting, San Francisco, USA.
- Werth, C.J., O.A Cirpka, and P. Grathwohl (2006), Enhanced mixing and reaction through flow focusing in heterogeneous porous media, *Water Resour. Res.*, 42, W12414; doi: 10.1029/2005WR004511.
- Willingham, T.W., C.J. Werth, and A.J. Valocchi (2008), Evaluation of the effects of porous media structure on mixing-controlled reactions using pore-scale modeling and micromodel experiments, *Environ. Sci. Technol.*, 42, 3185-3193.
- Willingham, T., C. Zhang, C.J. Werth, A.J. Valocchi, M. Oostrom, and T.W. Wiestma (2010), Using dispersivity values to quantify the effects of pore-scale flow focusing on enhanced reaction along transverse mixing zone, *Adv. Water Res.*, 33, 525-535.

Chapter 3

Evidence of compound-dependent hydrodynamic and mechanical transverse dispersion by multi-tracer laboratory experiments³

Abstract

Mass transfer, mixing, and therefore reaction rates during transport of solutes in porous media strongly depend on dispersion and diffusion. In particular, transverse mixing is a significant mechanism controlling natural attenuation of contaminant plumes in groundwater. The aim of the present study is to gain a deeper understanding of vertical transverse dispersive mixing of reaction partners in saturated porous media. Multi-tracer laboratory experiments in a quasi two-dimensional tank filled with glass beads were conducted and transverse dispersion coefficients were determined from high resolution vertical concentration profiles. We investigated the behavior of conservative tracers (i.e. fluorescein, dissolved oxygen and bromide), with different aqueous diffusion coefficients, in a range of grain-related Péclet numbers between 1 and 562. The experimental results do not agree with the classical linear parametric model of hydrodynamic dispersion, in which the transverse component is approximated as the sum of pore diffusion and a compound-independent mechanical dispersion term. The outcome of the multi-tracer experiments clearly indicates a non-linear relation between the dispersion coefficient and the average linear velocity. More importantly, we show that transverse mechanical dispersion depends on the diffusion coefficient of the compound, at least at the experimental bench-scale. This result has to be considered in reactive-transport models, because the typical assumption that two reactants with different aqueous diffusive properties are characterized by the same dispersive behavior does not hold anymore.

³ Reproduced with permission from: Chiogna, G., C. Eberhardt, P. Grathwohl, O.A. Cirpka and M. Rolle (2010), Evidence of compound dependent hydrodynamic and mechanical transverse dispersion by multitracer laboratory experiments, *Environmental Science & Technology*, 44(2), 688-693, doi: 10.1021/es9023964. Copyright 2009 American Chemical Society.

3.1 INTRODUCTION

Dispersion in porous media is a process of utmost importance in many scientific disciplines and technical applications, including contaminant hydrology, water treatment, oil reservoir engineering and chemical engineering. Hydrodynamic dispersion can be described as the sum of two simultaneous contributions: pore diffusion, resulting from Brownian motion, and mechanical dispersion, resulting from variations of local velocities in the porous medium, both in magnitude and direction (1).

The efforts to describe dispersion of solutes in uniform porous media began more than 100 years ago (2), with major developments in the '60s and '70s. An overview of the principal dispersion theories is given in the textbooks of Bear (1, 3). Two main approaches to hydrodynamic dispersion can be distinguished: exact mathematical methods which solve the governing flow and transport equations for some simplified boundary conditions (4) and statistical methods, for which the description of transport through a porous medium is based on probability distributions and averaging procedures to obtain macroscopic properties (e.g. refs. 5-9). The development of these statistical methods led to the description of dispersion as a tensorial property (6, 9). For a Cartesian coordinate system oriented along the principal flow direction, the dispersion tensor can be simplified to a second-order diagonal tensor in which components in the longitudinal (parallel to the flow) and transverse (perpendicular to the flow) directions can be distinguished.

The transverse dispersion components, typically smaller than the longitudinal ones, are very important for transverse mixing, which is a process of major interest for the spreading and mixing of contaminant plumes in groundwater (e.g. refs. 10-12). Since reactions take place at the microscopic (pore) scale, pore-scale dispersion was identified to be a critical process for overall contaminant degradation (13). Therefore, many recent studies addressed the topic of transverse dispersive mixing using both experimental and modeling approaches. At the laboratory scale, flow-through experiments have been performed to investigate mixing and mixing controlled abiotic and microbially mediated reactions in porous media (e.g. refs. 11, 14-16). At the field scale, high-resolution site investigations (17) showed the importance of mixing-controlled reactions occurring at the narrow (mm-cm) fringes of organic contaminant plumes. Mathematical modeling studies using both numerical (e.g. refs. 10, 18) and analytical techniques (e.g. refs. 12, 19, 20) focused on transport and mixing-controlled reactions. At the pore scale, microfluidic experiments (21) and pore-scale simulations (e.g. refs. 22, 23) were recently carried out to investigate mixing for well-defined porous media geometries.

Reactions in porous media require mixing of the reaction partners as well as pore scale transport of the reaction product(s). Depending on reaction pathways, a multitude of different compounds and species undergo dispersion processes. Thus the goal of this study is to investigate the dispersive behavior of different compounds by performing multi-tracer laboratory flow-through experiments. Conservative tracer tests were carried out at different velocities with the simultaneous continuous injection of at least two compounds in a homogeneous isotropic porous medium. We chose this simplified experimental set up in order to reduce the complexity of the problem and to gain insights into the fundamental physics that govern transverse dispersion of solutes in saturated porous media. An improvement in the description of the diffusive/dispersive behavior of different compounds is of primary importance in order to quantify and understand mixing-controlled reactions (e.g. in groundwater or in chemical flow-through reactors), which require the simultaneous presence of the reactive partners at the location where the reaction occurs.

3.2 THEORETICAL BACKGROUND

Hydrodynamic dispersion coefficients have been used to describe dispersion of solutes in porous media. These coefficients are defined as the additive contribution of a pore diffusion coefficient, D_p [L^2T^{-1}], and a mechanical dispersion coefficient, D_{mech} [L^2T^{-1}]. Therefore the coefficient of hydrodynamic dispersion in transverse direction D_t can be written as:

$$D_t = D_p + D_{mech} \quad (3.1)$$

However, as already pointed out by Bear (1), a clear separation of the two contributions is rather artificial since hydrodynamic dispersion includes both processes in an inseparable form.

Velocity ranges in which pore diffusion or mechanical dispersion is dominating are commonly distinguished (1, 23) by the value of the dimensionless Péclet number (Pe):

$$Pe = \frac{v d}{D_{aq}}, \quad (3.2)$$

in which v [LT^{-1}] is the flow velocity in the porous medium, d [L] is the length of a pore channel, represented by the average grain size (diameter), and D_{aq} [L^2T^{-1}] is the diffusion coefficient of the compound in water.

In porous media, molecular diffusion of solutes can only occur in the pore space. Considering the diminished cross sectional area available for diffusion, the tortuous nature of the pores, and the size of the pores, the pore diffusion coefficient is smaller than the free aqueous diffusion coefficient. In most practical cases, the tortuosity and pore size distribution are unknown and the pore diffusion coefficient is derived from empirical correlations as a function of the aqueous diffusion of the solute, and the porosity n [-] of the medium (24, 25). Under water-saturated conditions D_p can be approximated as:

$$D_p \approx D_{aq} n \quad (3.3)$$

Mechanical dispersion, considered as a pore-scale process, quantifies the scattering of the particles in the porous medium due to the presence of the grains and the fluctuations about the average velocity of the fluid. Conceptualizing random walks in a network of capillaries, the transverse mechanical dispersion was defined as a quantity linearly proportional to the velocity and to the grain size (e.g. refs. 7, 26). Nowadays it is commonly accepted (e.g. 27) to define this term with the linear parametric model proposed by Scheidegger (9):

$$D_{mech} = \alpha_t v \quad (3.4)$$

where the transverse dispersivity α_t [L] is a property of the porous medium assumed proportional to the grain size under some restrictive assumptions (28). If we accept this description, it seems that we can treat molecular diffusion and mechanical dispersion as two separate phenomena, that is, D_{mech} is identical for all compounds. Consequently two different compounds will show the same dispersive behavior at high velocities, where the contribution of pore diffusion to the overall dispersion is negligible.

Based on a statistical approach with spatial averaging on a representative elementary volume (REV), Bear and Bachmat (5) theoretically derived the following expression for the transverse component of the dispersion tensor:

$$D_t = D_p + \alpha_t v f(Pe, \delta) \quad (3.5)$$

where $f(Pe, \delta)$ is defined as:

$$f(Pe, \delta) = \frac{Pe}{Pe + 2 + 4 \cdot \delta^2} \quad (3.6)$$

$$\delta = \frac{d}{a} \quad (3.7)$$

in which d [L] is the length of a pore channel and a [L] its hydraulic radius. The value of the ratio δ can range between 4 to 10 (8, 29). The introduction of the function $f(Pe, \delta)$ was justified by physical considerations about the relative rate of growth of the volume occupied by a moving elementary mass of solute in a porous medium. This function implies a compound-dependency of the mechanical dispersion term. Bear and Bachmat also considered the possibility of introducing a non-integer exponent in order to reproduce nonlinear effects observed in experimental studies (e.g. refs. 16, 29-35). This approach clearly points out that molecular diffusion is a key process inseparable from mechanical dispersion; only diffusion allows transfer of molecules from a streamline to another.

The parametric model of Eq. 3.5 allows overcoming inconsistencies of Eq. 3.3. with experimental results. Several recent studies clearly indicate the non-linearities (16, 23, 29-35) and temperature dependencies (34) of the transverse dispersion over large velocity ranges and at large values of Pe . Therefore, this study focuses on well-controlled experiments to elucidate the compound dependency of mechanical transverse dispersion as a function of flow velocity. To our knowledge this is the first study, which is specifically dedicated to this phenomenon.

3.3 MATERIAL AND METHODS

The experimental setup consists of a quasi two-dimensional flow-through system, made of glass, Teflon and alumina, with inner dimensions: 77.3 cm \times 14.0 cm \times 1.1 cm (L \times H \times W). The tank is equipped with 10 equally spaced (1.2 cm) inlet and outlet ports connected to three high precision peristaltic pumps (IPC-N, Ismatec, Glattburg, Switzerland), which allow maintaining constant flow boundary conditions, as illustrated in Fig. 3.1. We used Tygon™ tubes for all ports, except the inlet port of the tracer where a Fluran™ tube was used to minimize atmospheric oxygen diffusion into the tube. Similar setups were recently used for flow-through experiments with conservative and reactive tracers (e.g. ref. 33) and to study coupled transport and biodegradation processes (e.g. refs. 14, 15).

Oxygen concentration gradients were measured at three oxygen-sensitive polymer stripes (10 cm \times 0.5 cm, PreSens, Germany) attached to the inner wall of the tank (Fig. 3.1), at a distance of 40.5 cm (A1), 57 cm (A2) and 74 cm (A3) from the inlet.

Before the injection into the tank, the tracer solution passed through a vial equipped with an oxygen-sensitive membrane spot to check the inlet oxygen concentration.

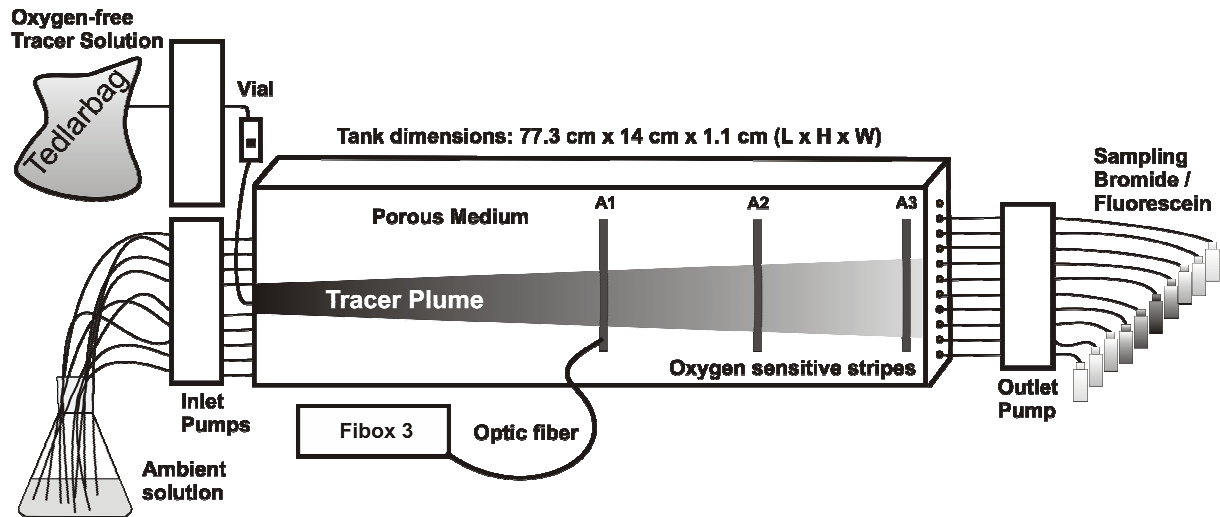


Figure 3.1: *Experimental setup.*

The tank was homogeneously filled with glass beads with diameters ranging between 0.5 mm and 0.75 mm (Fisher Scientific GmbH, Germany). During the filling procedure, the water level was always maintained above the height of the glass beads in order to avoid trapping of air into the porous medium. In the experiments the water table was kept below the surface of the porous medium, thus maintaining an unsaturated zone on top of the aquifer to avoid a shortcut of the tracer along a free water surface. The porosity of the system was determined from evaluation of breakthrough curves of the injected solutes, obtaining an average value of 0.39.

We performed tracer tests with a bromide solution (42.7 mg/l or 20 mg/l) depleted in oxygen and a sodium fluorescein solution (20 mg/l) depleted in oxygen at different seepage velocities. The oxygen depletion was performed by stripping the solutions with nitrogen-gas and then storing them in a gastight Tedlar bag (Alltech, Germany). Hence three different tracers (i.e. fluorescein, bromide and oxygen) with characteristic aqueous diffusion coefficients were selected. Fluorescein is often used as conservative tracer and has, at 22°C, an aqueous diffusion coefficient (D_{aq}) of $4.8 \times 10^{-10} \text{ m}^2/\text{s}$ (determined after Worch (36)). This value is similar to those of many organic pollutants frequently found in contaminated groundwater. Bromide and oxygen are characterized by considerably higher aqueous diffusion coefficients of $1.96 \times 10^{-9} \text{ m}^2/\text{s}$ and $1.97 \times 10^{-9} \text{ m}^2/\text{s}$ at 22°C, respectively (36, 37, 38).

The tracer solution was injected into the middle port (port 6, counted from the bottom of the tank). The other 9 ports were used for the injection of the ambient solution: tap water when we applied fluorescein as tracer and Millipore water in case of bromide. The oxygen concentration in those ambient solutions was in equilibrium with the atmosphere.

After steady-state conditions were reached (i.e. after the exchange of at least two pore volumes) water samples for fluorescein or bromide measurements were taken at the outlet ports (Fig. 3.1) and analyzed by UV-spectrometry and ion-chromatography (Dionex DX-120, Germany), respectively. The oxygen concentrations were measured at 45 points along the 3 oxygen-sensitive polymer stripes from outside with a non-invasive optode technique using an optical fiber as a light guide between the oxygen meter (Fibox 3, PreSens, Germany) and the sensor foil (Fig. 3.1). The principle of the sensor operation is based on quenching of luminescence caused by collision between molecular oxygen and luminescent dye molecules

in the excited state. The oxygen sensing is a luminescence lifetime detector. The detection limit is at 0.015 mg/l dissolved oxygen.

The injected solutions containing fluorescein and bromide were depleted in oxygen and were injected separately for each selected flow velocity. In this way, two compounds (fluorescein and oxygen, or bromide and oxygen, respectively) could always be measured during the same experimental run at a given flow velocity. The good agreement between the measured value of the transverse dispersion coefficient for oxygen during the runs with the oxygen/fluorescein solution and the oxygen/bromide solution guarantees the same hydraulic conditions of the system. The fact that the plume simultaneously carried two compounds allowed studying the effect of molecular diffusion on transverse dispersion without disturbance by non-identical experimental conditions (flow rates, packing, etc.) which may occur in individual tests with only one compound. The relative experimental error for the determined transverse dispersion coefficient can be estimated in the order of 15%. Further details about the measurements of each compound are reported in the supporting information.

The determination of the transverse dispersion coefficients was performed by applying the analytical solution of the 2-D steady-state advection-dispersion equation neglecting longitudinal dispersion:

$$v \frac{\partial C}{\partial x} - D_t \frac{\partial^2 C}{\partial z^2} = 0 \quad (3.8)$$

in which C is the concentration [ML^{-3}], x [L] is the coordinate in the direction of the flow and z [L] is the transverse coordinate. This equation is applicable, as pointed out in ref. (39), since longitudinal dispersion is negligible under steady-state conditions at a sufficient distance from the source.

As boundary condition, we consider a line source determined by the continuous injections of two constant concentration solutions:

$$C(x=0, z) = \begin{cases} C_0 & \forall |z| < \frac{W}{2} \\ C_1 & \forall |z| > \frac{W}{2} \end{cases} \quad (3.9)$$

where C_1 is the uniform ambient concentration of the compound, C_0 is the concentration in the injected tracer solution, and W [L] is the source width (1.2 cm in our experimental setup).

In a semi-infinite domain, the general solution to the problem is (adapted after 40):

$$C(x, z) = C_1 + \frac{C_0 - C_1}{2} \left[\operatorname{erf} \left(\frac{z + \frac{W}{2}}{2\sqrt{D_t \frac{x}{v}}} \right) - \operatorname{erf} \left(\frac{z - \frac{W}{2}}{2\sqrt{D_t \frac{x}{v}}} \right) \right] \quad (3.10)$$

This analytical solution was fitted to the measured data points using the Nelder-Mead simplex algorithm in which the dispersion coefficient D_t and a shift a , which accounts for the usually small deviation of the plume centerline from the injection port, were the fitting parameters.

3.4 RESULTS AND DISCUSSION

Concentration profiles of the conservative tracers at different flow velocities (1 m/d, 3.5 m/d, 9.5 m/d, 16.5 m/d) are shown in Fig. 3.2. In order to compare the results for the three different tracers and to eliminate systematic errors due to the different measurement techniques the data are plotted as normalized concentrations, defined as $(C-C_1)/(C_0-C_1)$, along the vertical cross-section. Measured solute concentrations at the outlet ports (fluorescein and bromide) and at the last oxygen sensitive stripe A3 (oxygen), respectively, are shown by markers, whereas the lines indicate the fitted analytical solution. A remarkable difference in the physical displacement of fluorescein and the compounds with larger aqueous diffusion coefficient (bromide and oxygen) can be clearly noticed for all seepage velocities. The role played by D_{aq} is obvious at low flow velocities, where the dispersion process is dominated by diffusion, but the difference is still relevant at higher flow velocities, as it can be clearly seen from the difference in the peak concentration. A higher value of the dispersion coefficient leads to a broader Gaussian concentration profile with lower concentration peak at the same flow velocity.

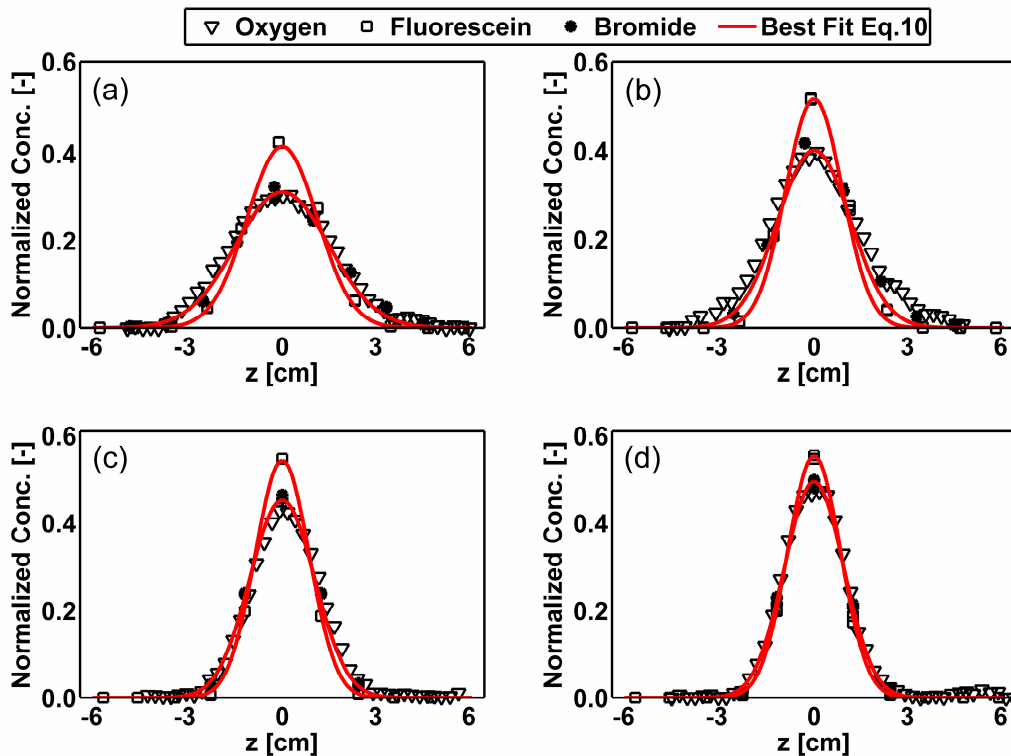


Figure 3.2: Comparison of vertical concentration profiles for oxygen, fluorescein and bromide at flow velocities of 1 m/d (a), 3.5 m/d (b), 9.5 m/d (c) and 16.5 m/d (d). Solid lines represent the best fit obtained with Eq. 3.10 for the different compounds.

Fig 3.3A shows the average values of the hydrodynamic transverse dispersion coefficient as function of velocity for all compounds. The plot clearly shows that the measured concentrations of the different solutes follow a distinct pattern. For the entire range of velocities investigated, the dispersion coefficients of bromide and oxygen are found to be significantly higher than the ones of fluorescein. This behavior is observed also for high velocities, for which mechanical dispersion should be the dominant process (corresponding to Péclet numbers $Pe > 5$ (1)). The theoretical ratio between the transverse dispersion coefficients

for the three compounds analyzed in this study is plotted in Fig. 3.3B as a function of the seepage velocity. It can be noticed that the biggest difference for the ratios of bromide/fluorescein and oxygen/fluorescein is expected at low velocities, where pore diffusion dominates transverse hydrodynamic dispersion. For the porous medium (average grain size of 0.625 mm) and the compounds (ratio between the high D_{aq} and the low D_{aq} of ≈ 4) used in this study, the ratio between the transverse dispersion coefficients has a minimum (≈ 1.36) at 5.3 m/d. At higher velocities the ratios of transverse dispersion coefficients increase again with velocity. This clearly indicates that also the mechanical contribution to transverse dispersion is compound specific.

We interpreted these experimental results with the theoretical model proposed by Bear and Bachmat (5) because it already predicts a compound dependent mechanical dispersion. An exponent β is introduced in order to account for the non-linearities reported in previous studies (e.g. refs. 10, 16, 29-35) and it is assumed to be a fitting parameter in the following evaluation of the experimental data. In the model of Bear and Bachmat (5), it is assumed that the relative rate of growth of the volume occupied by a moving elementary mass of solute in a porous medium is linearly dependent on the characteristic velocities in the pore channels. The introduction of an exponent $\beta \neq 1$ is based on the hypothesis that the physical law for the volume growth rate may be non-linear:

$$D_t \approx D_p + D_{aq} \left(\frac{Pe^2}{Pe + 2 + 4 \cdot \delta^2} \right)^\beta \quad (3.11)$$

Eq. 3.11 has been used to evaluate the relationship between the measured D_t of each compound and the Péclet number. We fitted parameters β and δ by minimizing the squared residuals of the modeled and measured D_t values. The results are summarized in Table 3.1.

Compound	β [-]	δ [-]	χ^2
Fluorescein	0.52	5.5	1.1
Oxygen	0.49	5.4	1.3
Bromide	0.53	5.8	1.1

Table 3.1: Values for β , δ and the reduced chi-squared coefficient χ^2 .

Average values of 0.5 and 5.5 were determined for the exponent (β) and for the ratio (δ) between the length and the width of a pore channel, respectively. The estimated uncertainty for these parameters is in the order of 10%. The obtained δ values were not significantly different from each other suggesting that the model is consistent with the experimental results. In fact, as mentioned above, the homogeneous porous medium used was the same in all experiments, and δ is supposed to be a property of the porous medium alone. A dependence of transverse dispersion on the velocity characterized with an exponent lower than one is in agreement with other experimental studies (16, 31, 32, 33, 40) and pore-scale modeling results (23). The continuous lines reported in Fig. 3.3A represent the calculated values of D_t with the proposed parametric model (Eq. 3.12) for oxygen, bromide and fluorescein.

Based on the outcome of the multi-tracer experiments, the relationship describing the hydrodynamic transverse dispersion in the given domain can be written as a function of the Péclet number:

$$D_t = D_p + D_{aq} \sqrt{\left(\frac{Pe^2}{Pe + 2 + 4 \cdot (5.5)^2} \right)} = D_p + v \frac{d}{\sqrt{Pe + 123}} \quad (3.12)$$

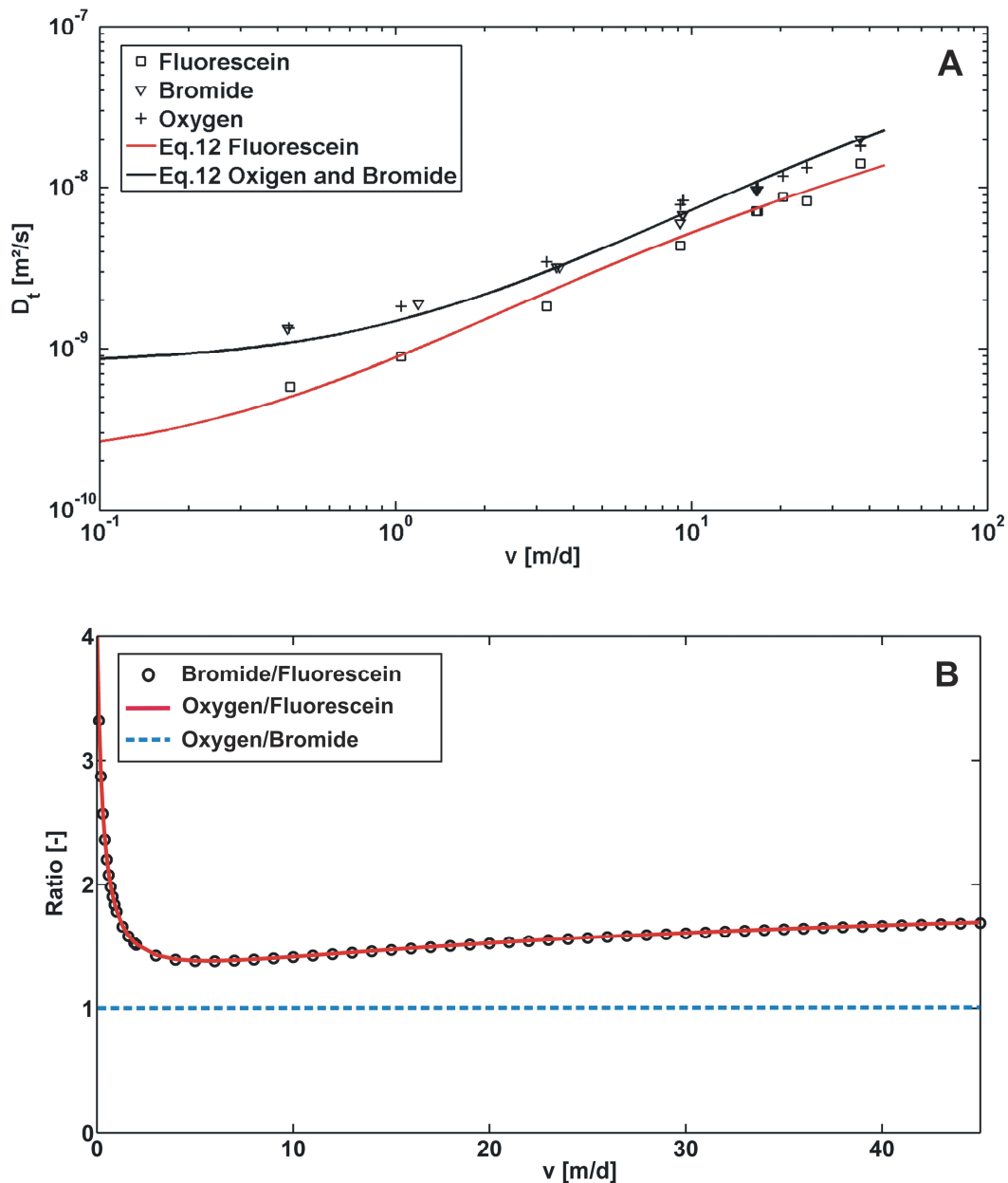


Figure 3.3: A) Transverse dispersion coefficients for fluorescein, bromide and oxygen as a function of the seepage velocity; lines represent the non linear parametric model (Eq. 3.12), in which bromide and oxygen (black lines) almost overlap because of similar D_{aq} ; B) Ratio between the transverse dispersion coefficients of the different compounds in a wide range of seepage velocities.

At the limit of low flow velocities, pore diffusion is the dominant process. This holds for velocities up to ~ 1 m/d, depending on the compound and on the grain size of the matrix. Mechanical dispersion begins to be the dominant process at ~ 10 m/d. For compounds which diffuse faster, these velocities are higher, while for compounds with lower diffusion properties these velocities are smaller. The limit for very high flow velocities should be handled carefully, since Darcy's law holds only for Reynold's number $Re = \frac{vd}{N} \leq 1$ ($N \approx 1 \times 10^{-6} \text{ m}^2/\text{s}$ being the kinematic viscosity of water) which, in the given domain, requires velocities < 150 m/d. The experimental results of this study and the new parametric model proposed (Eq. 3.12) were compared with literature data (30, 32, 33, 42, 43, 44), with grain sizes up to 1.25 mm and Péclet numbers up to 10^4 . This range covers all cases of practical interest for flow in natural porous media. These literature data relate to flow-through experiments performed using tracer compounds with different aqueous diffusion coefficients, such as chloride ($D_{aq} = 2.03 \times 10^{-9} \text{ m}^2/\text{s}$), trichloroethene (TCE, $D_{aq} = 8.4 \times 10^{-10} \text{ m}^2/\text{s}$), and fluorescein ($D_{aq} = 4.8 \times 10^{-10} \text{ m}^2/\text{s}$). In Fig. 3.4 the literature values of transverse dispersion coefficients and the measurements of this study are shown as a standard dimensionless plot. All data points appear to merge into a single line, as predicted by Eq. 3.12, since D_t is normalized by D_{aq} and plotted as a function of Pe . This graphical representation should be interpreted with caution since both values plotted (i.e. D_t / D_{aq} and Pe) are inversely proportional to D_{aq} , so that the compound-dependence of D_t is not obvious.

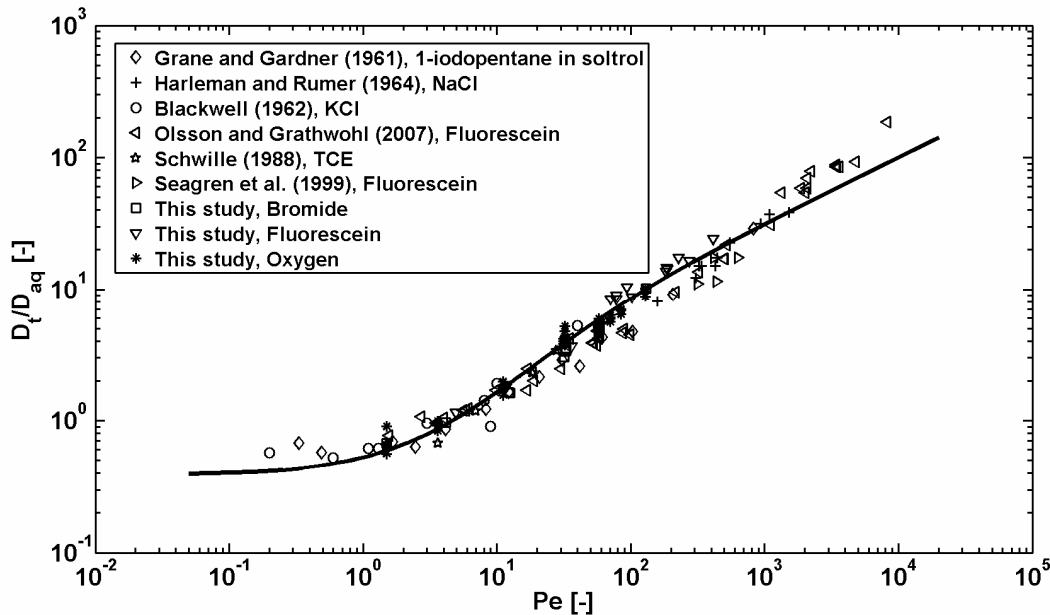


Figure 3.4: Dimensionless scatter plot of literature data (points) on transverse dispersion coefficients (D_t) compared with the new relationship (Eq. 3.12).

The comparison with previously published literature data allows generalizing the conclusions of this study to a wider range of compounds and grain sizes, even if the value of the parameters β and particularly δ may depend on the porous medium. The ratio between the length of a pore and its width depends on the geometry and the homogeneity of the grains that

compose the porous material, while we suggest that the value for the exponent β should be kept constant. This value is in qualitative agreement with the outcomes of Klenk and Grathwohl (29) and the concept of incomplete mixing in the pores. The validity of Eq. 3.12 for each compound allows one to use the same empirical relation to describe transverse dispersion for different tracer solutions. This is an important outcome of this work, since standard power law fitting (e.g. 32, 33) would lead to different coefficients for distinct compounds therefore preventing the formulation of a general empirical relationship.

The experimental evidence that transverse dispersion always depends on the compound-specific molecular diffusion coefficient implies that physical mixing is also compound specific at any flow velocity. This outcome is relevant for mixing-controlled reactive transport in groundwater. The interpretation of experimental studies such as (16), (45), (46) and (47) could be improved by the introduction of a compound-dependent dispersion coefficient. Thus, a compound-specific description of transverse dispersion should be implemented in numerical codes simulating transport processes both at the laboratory and at the field scale. For instance, the efficient solution of transport and mixing-driven chemical and biochemical processes based on the distribution of mixing ratios (i.e. conservative species) recently introduced into the groundwater literature (19, 48, 49) may need to be reconsidered since this approach is based on the assumption that the dispersive behavior of all reaction partners is identical. Additional effort is required to quantitatively assess the influence of compound-dependent local-scale mixing in heterogeneous porous media. At the current state of knowledge, it is not clear to which extent compound-dependent behaviors will prevail in the macroscopic description of mixing at layer scales.

REFERENCES

- (1) Bear, J. *Dynamics of fluids in porous media*; Dover: New York, USA, 1972.
- (2) Slichter, C. Field measurement of the rate of movement of underground waters. *U.S. Geol. Surv. Tech. Rep. Water Supply* **1905**, Pap., 140.
- (3) Bear, J. *Hydraulics of groundwater*; Dover: New York, USA, 1979.
- (4) Taylor, G.I. Dispersion of soluble matter in solvent flowing slowly through a tube. *Proc. Roy. Soc. A.* **1953**, 1137 (219), 186-203.
- (5) Bear, J.; Bachmat, Y. A generalized theory on hydrodynamic dispersion in porous media. IASH Symp. Artificial Recharge and management of aquifers, Haifa, Israel IASH, P.N. **1967** 72, 7-16.
- (6) Bear, J. On the tensor form of dispersion in porous media. *J. Geophys. Res.* **1961**, 66, 1185-1197.
- (7) De Josselin de Jong, G. Longitudinal and transverse diffusion in granular deposits. *Eos Trans. AGU* **1958**, 39, 67-74.
- (8) Saffman, P.G. Dispersion due to molecular diffusion and macroscopic mixing in flow through a network of capillaries. *J. Fluid Mech.* **1960**, 2, 194-208.
- (9) Scheidegger, A.E. General theory of dispersion in porous media. *J. Geophys. Res.* **1961**, 66(4), 3273-3278.
- (10) Cirpka, O.A.; Frind, E.O.; Helming, R. Numerical simulation of biodegradation controlled by transverse mixing. *J. Contam. Hydrol.* **1999**, 40 (2), 159-182.
- (11) Cirpka, O.A.; Olsson, A.; Ju, Q.; Rahman, A.; Grathwohl, P. Determination of transverse dispersion coefficients from reactive plumes lengths. *Ground Water* **2006**, 44 (2), 212-221.
- (12) Liedl, R.; Valocchi A. J.; Dietrich P.; Grathwohl P. Finiteness of steady state plumes. *Water Resour. Res.* **2005**, 31, W12501; DOI 10.1029/2005WR004000.
- (13) Kitanidis, P.K. The concept of dilution index. *Water Resour. Res.* **1994**, 30 (7), 2011-2026.
- (14) Bauer, R.D.; Rolle, M.; Bauer, S.; Eberhardt, C.; Grathwohl, P.; Kolditz, O.; Meckenstock, R.U.; Griebler, C. Enhanced biodegradation by hydraulic heterogeneities in petroleum hydrocarbon plumes. *J. Contam. Hydrol.* **2009** 105, 56-68.
- (15) Bauer, R.D.; Rolle, M.; Kürzinger, P.; Grathwohl, P.; Meckenstock, R.U.; Griebler, C. Two-dimensional flow-through microcosms: versatile test systems to study biodegradation processes in porous aquifers. *J. Hydrol.* **2009** 369, 284-295.

- (16) Huang, W.E.; Oswald, S.E.; Lerner, D.N.; Smith, C.C.; Zheng, C. Dissolved oxygen imaging in a porous medium to investigate biodegradation in a plume with limited electron acceptor supply. *Environ. Sci. Technol.* **2003**, 37, 1905-11.
- (17) Anneser, B.; Einsiedl, F.; Meckenstock, R.U.; Richters, L.; Wisotzky, F.; Griebler, C. High-resolution monitoring of biogeochemical gradients in a tar oil-contaminated aquifer. *Appl. Geochem.* **2008**, 23, 1715-1730.
- (18) Prommer, H.; Tuxen, N.; Bjerg, P. Fringe-controlled natural attenuation of phenoxy acids in a landfill plume: integration of field-scale processes by reactive-transport modeling. *Environ. Sci. Technol.* **2006**, 40 (15), 4732-4738.
- (19) Cirpka, O.A.; Valocchi, A.J. Two-dimensional concentration distribution for mixing-controlled bioreactive transport in steady state. *Advances Water Resour.* **2007**, 30 (6-7), 1668-1679.
- (20) Werth, C.J., Cirpka, O.A.; Grathwohl, P. Enhanced mixing and reaction through flow focusing in heterogeneous porous media. *Water Resour. Res.* **2006**, 42, W12414; DOI 10.1029/2005WR004511.
- (21) Willingham, T.W.; Werth C.J.; Valocchi A.J. Evaluation of the effects of porous media structure on mixing-controlled reactions using pore-scale modeling and micromodel experiments. *Environ. Sci. Technol.* **2008**, 42 (9), 3185-3193; DOI 10.1021/es7022835
- (22) Acharya, R. C.; Valocchi, A. J.; Werth, C. J.; Willingham, T.W. Pore-scale simulation of dispersion and reaction along a transverse mixing zone in two-dimensional porous media. *Water Resour. Res.* **2007**, 43, W10435; DOI 10.1029/2007WR005969.
- (23) Bijeljic, B.; Blunt, M.J. Pore-scale modelling of transverse dispersion in porous media. *Water Resour. Res.* **2007**, 43, W12S11; DOI 10.1029/2006WR005700.
- (24) Boving, T.; Grathwohl, P. Tracer diffusion coefficients in sedimentary rocks correlation to porosity and hydraulic conductivity. *J. Contam. Hydrol.* **2001**, 53, 85-100.
- (25) Grathwohl, P. *Diffusion in natural porous media: contaminant transport, sorption/desorption, and dissolution kinetics*; Kluwer Academic Publishers: Boston, MA, USA, 1998.
- (26) Saffman, P.G. A theory of dispersion in porous media. *J. Fluid Mech.* **1959**, 6(3), 321-349.
- (27) Freeze, R.A.; Cherry, J.A. *Groundwater*; Prentice-Hall International: NJ, USA, 1979.
- (28) Scheidegger, A.E. Statistical hydrodynamics in porous media. *J. Appl. Phys.* **1954**, 25, 994-1001.
- (29) Klenk, I.D.; Grathwohl, P. Transverse vertical dispersion in groundwater and the capillary fringe. *J. Contam. Hydrol.* **2002**, 58, 111-128.
- (30) Blackwell, R.J. Laboratory studies of microscopic dispersion phenomena. *Soc. Petrol. Engrs. J.* **1962**, 225,1-8.

- (31) Carvalho, J.F.R.; Delgado J.M.P.Q. Lateral dispersion in liquid flow through packed beds at $Pe < 1400$. *American Institute for chemical engineering* **2000**, 46 (5), 1089-1095.
- (32) Harleman, D.; Rumer R. Longitudinal and lateral dispersion in an isotropic porous medium. *J. Fluid Mech.* **1963**, 16, 385-394.
- (33) Olsson, A.; Grathwohl P. Transverse dispersion of non reactive tracers in porous media: A new nonlinear relationship to predict dispersion coefficients. *J. Contam. Hydrol.* **2007**, 92, 149-161.
- (34) Delgado, J.M.P.Q.; Carvalho, J.F.R. Measurement of the coefficient of transverse dispersion in flow through packed beds for a wide range of values of the Schmidt number. *Transport in porous media* **2001**, 44, 165-180.
- (35) Gutierrez, M.N. Aspects of transverse dispersion in porous media. Ph.D. Dissertation, Universiteit Utrecht, Netherland, 2009.
- (36) Worch, E. Eine neue Gleichung zur Berechnung von Diffusionskoeffizienten gelöster Stoffe. *Vom Wasser*, **1993**, 81, 289-297.
- (37) Atkins, P.W. *Physical Chemistry*, 4th, ed; Oxford University Press: Oxford, UK, 1990.
- (38) Cussler, E.L. *Diffusion, mass transfer in fluid systems*; Cambridge university press: New York, USA, 1984.
- (39) Srinivasan, V.; Clement, T.P.; Lee, K.K. Domenico solution – is it valid?. *Ground Water* **2007**, 45, 136-146.
- (40) Domenico, P.A.; Palciauskas, V.V. Alternative boundaries in solid waste management. *Ground Water* **1982**, 20 (3), 303-311.
- (41) Delgado, J.A. critical review of dispersion in packed beds. *Heat Mass Transfer* **2006**, 42(4), 279-310.
- (42) Grane, F.E.; Gardner, G.H.F. Measurements of transverse dispersion in granular media. *J. Chem. Eng. Data* **1961**, 6 (2), 283-287.
- (43) Seagren, E.A.; Rittmann, B.E.; Valocchi, A.J. An experimental investigation of NAPL pool dissolution enhancement by flushing. *J. Contam. Hydrol.* **1999**, 37, 111 - 137.
- (44) Schwille, F. *Chlorinated solvents in porous and fractured media – model experiment*; Lewis Publishers: Boca Raton, FL, 1988.
- (45) Nambi, M.I.; Werth, J.; Sanford, R.A.; Valocchi, A.J. Pore-scale analysis of anaerobic halo-respiring bacterial growth along the transverse mixing zone of an etched silicon pore network. *Environ. Sci. Technol.* **2003**, 37 (24), 5617-5624.
- (46) Gramling, M.C.; Harvey, C.F.; Meigs L.C. Reactive transport in porous media: a comparison of model prediction with laboratory visualization. *Environ. Sci. Technol.* **2002**, 36 (11), 2508-2514.
- (47) Raje S.D.; Kapoor, V. Experimental study of bimolecular reaction kinetics in porous media. *Environ. Sci. Technol.* **2000**, 34 (7), 1234-1239.

- (48) De Simoni, M.; Sanchez-Vila, X.; Carrera J.; Saaltink M.W. A mixing ratios-based formulation for multicomponent reactive transport. *Water Resour. Res.* **2007**, 43, W07419; doi:10.1029/2006WR005256.
- (49) Saaltink, M.W.; Carrera, J.; Ayora, C. On the behaviour of approaches to simulate reactive transport. *J. Contam. Hydrol.* **2001**, 48, 213-235.

S1. SUPPORTING INFORMATION: Measurements of transverse dispersion coefficient.

S1.1 Fluorescein tracer experiments

Values of the aqueous diffusion coefficient of fluorescein vary in the literature. Most of the studies report values close to $5 \times 10^{-10} \text{ m}^2/\text{s}$ (Nugent and Jain, 1984; Radomsky, 1990; Himmelsbach et al., 1998; Huang, 2001; Zhou et al., 2007). In this work, a value of $4.8 \times 10^{-10} \text{ m}^2/\text{s}$, for a temperature of $22 \text{ }^\circ\text{C}$, was computed with the empirical equation proposed by Worch (1993):

$$D_{aq} = 3.595 \cdot 10^{-14} \frac{T}{\eta M^{0.53}}, \quad (3.13)$$

(where M [g/mol] is the molecular weight of the compound, η [Pa·s] is the dynamic viscosity of the fluid, and T [K] is the temperature).

Fluorescein concentrations were determined over 7 orders of magnitude with a fluorescence spectrometer, hence the expected steep concentration profiles can be measured with high accuracy. The concentration of sodium fluorescein used in the tracer experiments was 20 mg/l . The solutions were depleted in oxygen by stripping with nitrogen gas. The oxygen depleted solution was stored in a Tedlar gastight sampling bag (Alltech Assoc. Incorp., Germany).

In order to measure the transverse concentration profile of the plume, samples from the outflow ports were taken after the establishment of a steady state flow regime. The fluorescein concentration C [M/L^3] for each of the 10 samples was normalized by the injection concentration (C_0 [M/L^3]) and plotted against the lateral distance relative to the injection port as shown in Fig. 3.5.

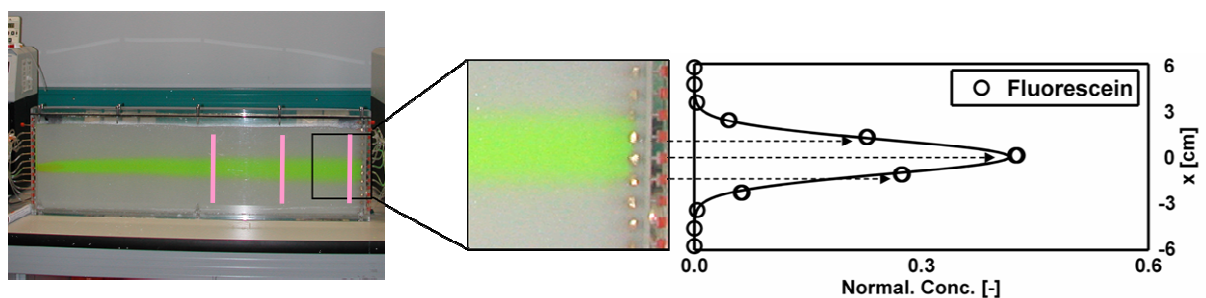


Figure 3.5: Experimental setup with a fluorescein plume at steady state flow conditions in a homogeneous porous medium; the continuous line represents the analytical solution, which is fitted to the fluorescein concentrations measured at the outlet ports to determine the transverse dispersion coefficient (modified after Olsson and Grathwohl, 2007).

S1.2 Bromide tracer experiments

The NaBr solutions (25.7 mg/l and 55 mg/l corresponding to a bromide concentration of 20 mg/l and 42.7 mg/l, respectively), were prepared by dilution of NaBr salt with Millipore water and depleted in oxygen as explained for the fluorescein tracer solution. The bromide concentration in the samples from the outlet ports was determined by ion chromatography (Dionex DX-120, Germany).

The self-diffusion coefficient of bromide, in standard conditions, is $2.08 \times 10^{-9} \text{ m}^2/\text{s}$ (Atkins, 1990). We corrected this value, following Eq. 3.13, taking into account the experimental temperature conditions ($T = 22^\circ\text{C}$, $1.96 \times 10^{-9} \text{ m}^2/\text{s}$). We conducted few tests at the same velocity using CaCl_2 (13.9 mg/l, prepared with Millipore water) as ambient fluid to investigate potential ionic effects on the dispersion of bromide. The results showed no appreciable differences between the two setups.

S1.3 Measurement with oxygen as tracer

We used oxygen in the multi-tracer experiments as additional conservative tracer. The oxygen concentrations were measured with a non-invasive optode technique (fiber optic oxygen meter, PreSens GmbH, Regensburg, Germany). Three stripes of oxygen sensitive polymer were glued inside the tank to the inner wall at a distance of 40.5 cm (stripe A1), 57 cm (stripe A2) and 74 cm (stripe A3) from the inlet. The concentrations were measured scanning the stripes from outside of the tank through the glass wall using an optical fiber as a light guide between the oxygen meter and the sensor foil. The measurement can be conducted on line and allows rapidly to check if the plume is stable. Moreover, the technique is precise (see Table 3.2 for the relative error of each measurement) and non invasive, since no sampling at the outlet is required. This method allows a better spatial resolution compared to the conventional sampling at the 10 outlet ports, because 45 points could be measured along the 10 cm long stripes.

$\langle v \rangle \times 10^{-5} [\text{m/s}]$	$\langle D_t \rangle \times 10^{-9} [\text{m}^2/\text{s}]$	Relative Error %
0.51	1.35	18.8
1.21	1.83	6.3
3.75	3.45	8.0
10.80	8.19	8.7
19.26	9.99	8.0
23.60	11.75	5.1
28.40	13.22	4.6
43.15	18.1	8.8

Table 3.2: Average values and relative errors of transverse hydrodynamic dispersion coefficients determined from oxygen measurements. The relative error is computed as the ratio between the standard deviation of the measurements and their average value.

The solutions of fluorescein and bromide, injected in the central inlet port (port 6), were depleted in oxygen, as previously described whereas the ambient water injected from the other ports was in equilibrium with the atmosphere. The good agreement between the measured value of the transverse dispersion coefficient for oxygen during the runs with the oxygen/fluorescein solution and the oxygen/bromide solution guarantees the same hydraulic

conditions of the system. Furthermore it can be observed (Fig. 3.6) that each of the stripes provides a reliable result independently on the position in the tank.

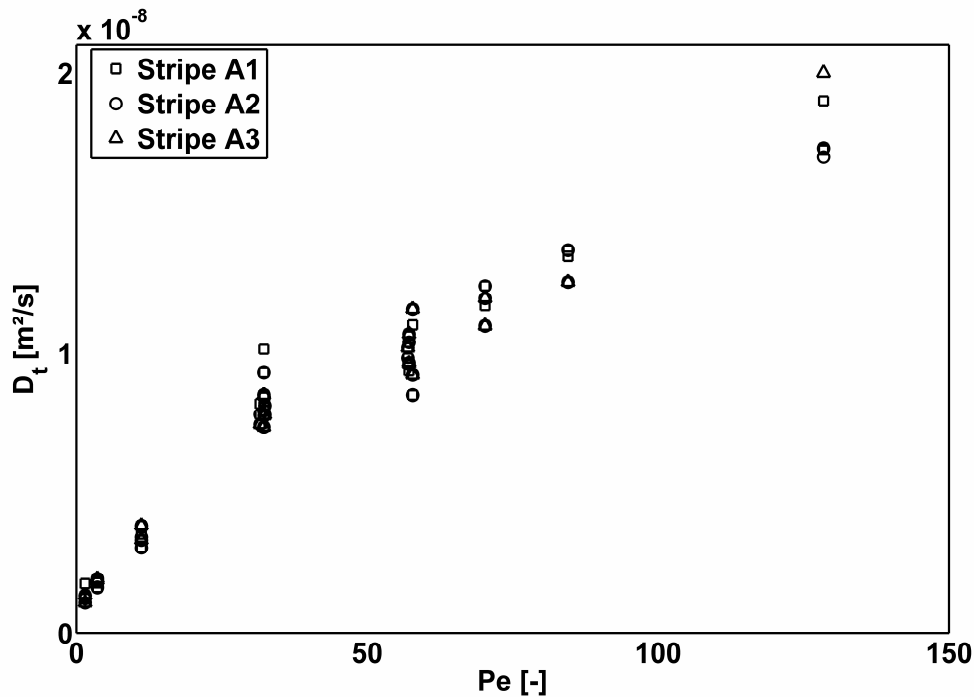


Figure 3.6. *Reproducibility of transverse dispersion coefficients determined for oxygen measured at different positions of the oxygen sensitive stripes (distance from inlet: A1=40.5cm, A2=57cm, A3=74cm).*

The value for the aqueous diffusion coefficient is given in literature for standard conditions $2.1 \times 10^{-9} \text{ m}^2/\text{s}$ and was corrected for temperature according to Eq. 3.13 ($1.97 \times 10^{-9} \text{ m}^2/\text{s}$).

In some experiments oxygen-depleted solutions of fluorescein (20 mg/l) and bromide (25.7 mg/l) were injected simultaneously. In these cases all three compounds could be determined for the same experiment. However, bromide could not be directly measured in the presence of fluorescein which had to be filtered out. Therefore, the measurement analysis of samples containing simultaneously bromide and fluorescein turned out to be an extremely time consuming procedure, and was, therefore, discarded for most of the other experimental runs.

S1.4 Experimental Data

The complete list of the experimental runs and the relative dispersion coefficient measured for the different compounds is reported in Table 3.3, while in Figure 3.7 we show the normalized plot (i.e. $D_t/D_{aq} [-]$ vs $Pe [-]$) of our experimental data.

Compound	$v \times 10^{-5}$ [m/s]	Pe [-]	$D_t \times 10^{-9}$ [m²/s]	$D_{aq} \times 10^{-9}$ [m²/s]
Fluorescein	10.6	138	4.34	0.48
	19.2	249	6.87	
	23.6	307	8.72	
	28.4	370	8.26	
	43.2	562	14.1	
	19.4	253	7.11	
	19.2	250	7.33	
	1.21	15.8	0.90	
	3.75	48.9	1.82	
	12.0	157	6.90	
	0.51	6.65	0.58	
Bromide	10.6	31.9	6.00	1.96
	19.2	57.5	8.54	
	43.2	130	20.0	
	19.4	58.4	10.8	
	19.2	57.7	9.65	
	19.4	58.4	9.64	
	10.9	32.6	6.67	
	10.9	32.6	6.62	
	10.8	32.5	6.85	
	10.8	32.5	6.85	
	0.50	1.51	1.33	
	1.39	4.16	1.90	
	4.16	12.5	3.20	
	4.06	12.2	3.23	
O₂ stripe A3	10.6	31.6	7.46	1.97
	19.2	57.0	10.2	
	23.6	70.3	11.0	
	23.6	70.3	12.0	
	28.4	84.5	12.5	
	43.2	128	20.8	
	19.4	57.8	9.22	
	19.4	57.8	11.6	
	19.2	57.2	9.60	
	19.2	57.2	9.65	
	19.2	57.2	9.65	
	19.2	57.2	10.7	
	10.9	32.4	7.80	
	10.9	32.4	7.78	

Compound	$v \times 10^{-5}$ [m/s]	Pe [-]	$D_t \times 10^{-9}$ [m ² /s]	$D_{aq} \times 10^{-9}$ [m ² /s]
O₂ stripe A3	10.8	32.2	8.49	1.97
	1.21	3.60	1.88	
	1.21	3.60	1.95	
	3.75	11.2	3.85	
	3.75	11.2	3.33	
	3.75	11.2	3.85	
	3.75	11.2	3.33	
	0.51	1.51	1.36	
	0.51	1.51	1.10	
	43.2	128	17.5	
O₂ stripe A2	19.2	57.0	9.83	1.97
	23.6	70.3	12.4	
	28.4	84.5	13.7	
	43.2	128	17.3	
	19.4	57.8	8.49	
	19.2	57.2	9.66	
	19.2	57.2	10.4	
	10.9	32.4	8.13	
	10.9	32.4	8.41	
	10.8	32.3	9.30	
	10.8	32.3	7.95	
	1.21	3.60	1.86	
	1.21	3.60	1.64	
	3.75	11.2	3.05	
	3.75	11.2	3.44	
	3.75	11.2	3.05	
	3.75	11.2	3.05	
	3.75	11.2	3.05	
	0.51	1.51	1.25	
	0.51	1.51	1.26	
10.6	31.658	8.19		
19.2	57.0	9.65		
23.6	70.3	11.7		
O₂ stripe A1	28.4	84.5	13.5	1.97
	43.2	128	17.3	
	19.4	57.9	11.0	
	19.2	57.2	9.36	
	19.2	57.2	10.6	
	10.9	32.4	7.80	

Compound	$v \times 10^{-5}$ [m/s]	Pe [-]	$D_t \times 10^{-9}$ [m ² /s]	$D_{aq} \times 10^{-9}$ [m ² /s]
O ₂ stripe A1	10.9	32.4	8.15	1.97
	10.8	32.2	10.2	
	10.8	32.2	8.09	
	1.21	3.60	1.80	
	3.75	11.2	3.55	
	3.75	11.17	3.55	
	0.51	1.51	1.77	

Table 3.3: Measured transverse dispersion coefficients D_t at different velocities v and for compounds with different aqueous diffusion coefficients D_{aq} . The porosity of the system is 0.39 and the grain size is 0.5-0.75 mm.

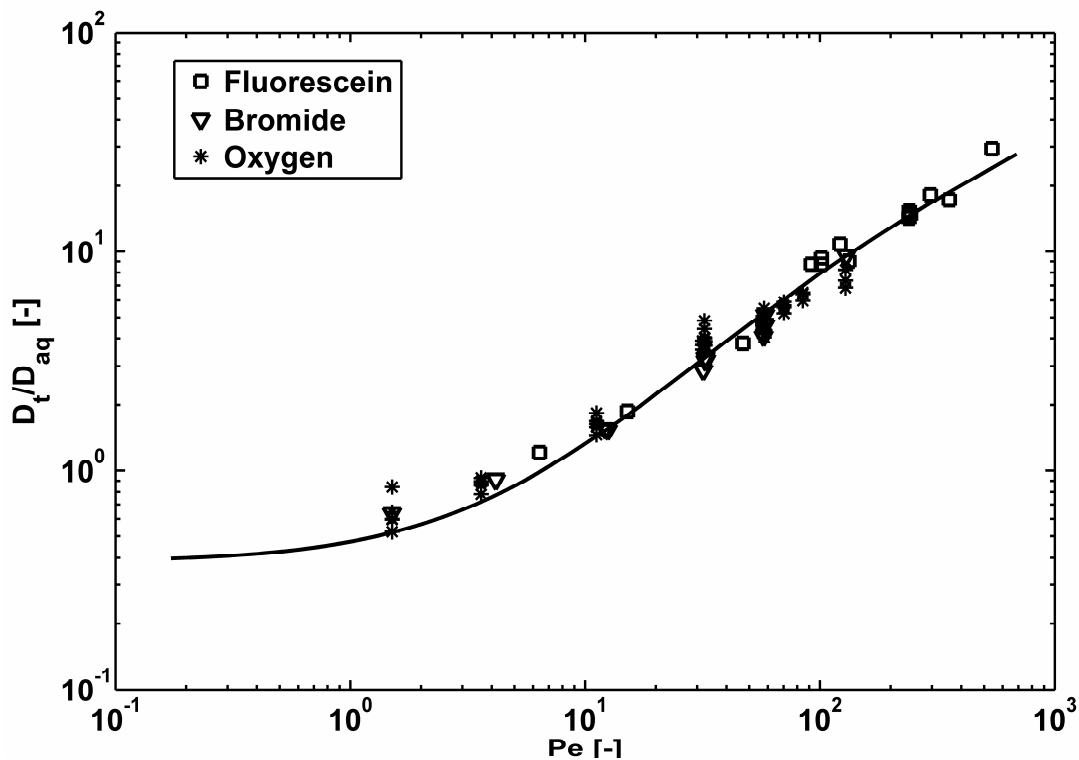


Figure 3.7: Normalized transverse dispersion coefficients for fluorescein, bromide and oxygen (O₂); lines represent the non linear parametric model (Eq. 3.12).

References

Himmelsbach, T.; Hötzl, H.; Maloszewski, P. Solute transport processes in a highly permeable fault zone of Lindau fractured rock test site. *Ground Water* **1998**, 36(5), 792-800.

Huang, W. The role of transverse mixing of electron acceptors and carbon substrates in natural attenuation. PhD Dissertation, University of Sheffield, 2001.

Nugent, L.J.; Jain, R.K. Extravascular diffusion in normal and neoplastic tissues. *Cancer Research* **1984**, 44, 238-244.

Radomsky, M.L.; Whaley, K.J.; Cone, R.A.; Saltzman, W.M. Macromolecules released from polymers – diffusion into unstirred fluids. *Biomaterials* **1990**, 11(9), 619-624.

Worch, E. Eine neue Gleichung zur Berechnung von Diffusionskoeffizienten gelöster Stoffe. *Vom Wasser* **1993**, 81, 289-297.

Zhou, Q.; Liu, H.H.; Molz, J.F.; Zhang, Y.; Bodvarsson, G.S. Field-scale effective matrix diffusion coefficient for fractured rock: Results from literature survey. *Journal of Contaminant Hydrology* **2007**, 93, 161–187; doi:10.1016/j.jconhyd.2007.02.002.

Chapter 4

Isotopic fractionation by transverse dispersion: flow-through microcosms and reactive transport modeling study⁴

Abstract

Flow-through experiments were carried out to investigate the role of transverse dispersion on the isotopic behavior of an organic compound during conservative and bioreactive transport in a homogeneous porous medium. Ethylbenzene was selected as model contaminant and a mixture of labeled (perdeuterated) and light isotopologues was continuously injected in a quasi two-dimensional flow-through system. We observed a significant fractionation of ethylbenzene isotopologues during conservative transport at steady state. This effect was particularly pronounced at the plume fringe and contrasted with the common assumption that physical processes only provide a negligible contribution to isotope fractionation. Under the experimental steady state conditions, transverse hydrodynamic dispersion was the only process that could have caused the observed fractionation. Therefore, the measured isotope ratios at the outlet ports were interpreted with different parameterization of the transverse dispersion coefficient. A non-linear compound specific parameterization showed the best agreement with the experimental data. Successively, bioreactive experiments were performed in two subsequent stages: a first oxic phase, involving a single strain of ethylbenzene degraders and a second phase with aerobic and anaerobic (i.e. ethylbenzene oxidation coupled to nitrate reduction) degradation. Significant fractionation through biodegradation occurred exclusively due to the metabolic activity of the anaerobic degraders. We performed analytical and numerical reactive transport simulations of the different experimental phases which confirmed that both the effects of physical processes (diffusion and dispersion) and microbially-mediated reactions have to be considered to match the observed isotopic fractionation behavior.

⁴ Reproduced with permission from: Rolle, M., G. Chiogna, R. Bauer, C. Griebler and P. Grathwohl (2010), Isotopic fractionation by transverse dispersion: flow-through microcosms and reactive transport modeling study, *Environmental Science & Technology*, 44, 6167-6173. Copyright 2010 American Chemical Society.

4.1 INTRODUCTION

The release of organic pollutants into the subsurface is a significant and widespread environmental problem that frequently causes persistent groundwater contamination. Understanding the physical and biogeochemical processes that determine the transport and fate of contaminants is a major challenge and represents an important requirement to quantify the effectiveness of natural attenuation and/or engineered remediation of contaminated aquifers.

In the last decade, compound specific isotope analysis (CSIA) has emerged as a tool to assess in situ biodegradation of organic contaminant plumes (1-3). CSIA has been most frequently applied to carbon isotopes for a number of organic contaminants including BTEX, MTBE and chlorinated hydrocarbons, but is also applicable to other elements such as hydrogen, oxygen, nitrogen, sulfur, chlorine and bromine (4). The method is based on the assumption that (bio)chemical transformations are responsible for significant shifts in the isotopic composition of dissolved organic compounds, whereas mass transfer (e.g. sorption) and transport processes (e.g. advection, diffusion and dispersion) only cause much smaller isotopic changes (5). The changes in stable isotope fractionation are typically described by the Rayleigh equation which expresses the variation of the isotope ratio as a function of the initial isotope value of the compound, the normalized concentration of the residual contaminant and a fractionation factor (6). Several studies pointed out limitations of the Rayleigh equation and suggested different approaches to extend its validity (7-9). These methods often include conservative and/or reactive transport modeling which allows dealing with spatial heterogeneity of physico-chemical aquifer properties and with complex reaction networks. The interpretation of isotope data with the aid of mathematical modeling was applied at different field sites (10-12).

Recent studies pointed out the important active and/or confounding role of physical transport processes on isotope fractionation. Kopinke et al. (13) observed, in their laboratory experiments, significant carbon isotope fractionation of organic contaminants due to sorption on humic acids. In a column study under unsaturated conditions Bouchard et al. (14) measured isotope changes during volatilization of petroleum hydrocarbons. Aeppli et al. (15) showed that mass-transfer limitations, for transfer of chlorinated compounds from nonaqueous phase liquids to the aqueous phase, influence the observed carbon isotope fractionation associated with contaminant biodegradation. Eggenkamp and Coleman (16) investigated the isotope fractionation during diffusive transport of chlorine and bromine at different temperatures. The importance of diffusion for isotope fractionation in groundwater is also the main outcome of the numerical modeling investigation presented by LaBolle et al. (17).

In this study, we also focus our attention on the importance of physical processes on stable isotope patterns. The objective of our investigation is to quantify the role of transverse hydrodynamic dispersion during conservative and reactive transport of different contaminant isotopologues in saturated porous media. Dispersion is a key process controlling the spreading and effective mixing of contaminant plumes in groundwater (18). In particular, the transverse component plays an important role for mixing-controlled reactions frequently observed at the fringe of organic contaminant plumes (19). To the best of our knowledge, no experimental study has yet been dedicated to the effect of transverse dispersion on isotopic shifts during contaminant transport in saturated porous media. The approach followed in this work is based on conservative and bioreactive tracer experiments using different ethylbenzene isotopologues carried out in a quasi two-dimensional flow-through system. Different transverse dispersion parameterizations are used to interpret the conservative and reactive (i.e. aerobic and anaerobic) experimental results. A reactive transport model incorporating the physical- and

reaction-specific fractionation behavior was developed to describe and interpret the observed isotope ratios.

4.2 MATERIAL AND METHODS

4.2.1 *Experimental Setup*

Tracer experiments were carried out in a quasi two-dimensional flow-through system in a saturated porous medium (20-23). The flow-through system (0.785m×0.011m×0.14m) is equipped with 12 ports (with diameter 0.75 mm), spaced 1.2 cm, at the inlet and at the outlet (Fig. 4.5 Supporting Information). The system was homogeneously packed using middle sand with an average grain diameter of 0.256 mm. Clean sand was used to avoid sorption of the organic contaminant to the solid matrix. After the establishment of steady state flow conditions, at an average seepage velocity of 1.2 m/day corresponding to a residence time of 15.7 hours, an ethylbenzene plume with an inflow concentration of 300 μM was injected through the central inlet port. The plume consisted of a mixture of non-labeled ethylbenzene- h_{10} and perdeuterated ethylbenzene- d_{10} (ratio of 3:1). The light and heavy isotopologues underwent conservative transport under identical hydraulic conditions. When the plume reached steady state (i.e. after the exchange of at least two pore volumes), samples were taken daily at each outlet port during the conservative experimental phase (day 1-4).

Ethylbenzene concentrations and isotope ratios were determined by GC-MS analysis (see Supporting Information).

The reactive phases of the experiment (i.e. day 4-11 and 11-18, respectively) were performed by inoculating the system with two different microbial strains: an aerobic degrader (*Pseudomonas putida* F1) and an anaerobic degrader (i.e. *Aromatoleum aromaticum* EbN1) in two successive stages. These microbial strains are able to degrade ethylbenzene using oxygen and nitrate as electron acceptor, respectively. Their metabolic pathways show a significantly different fractionation behavior (24). Dissolved oxygen and nitrate were continuously provided with the ambient water (Table 4.1); therefore optimal conditions for ethylbenzene degradation are established at the plume fringes where the reactions partners are brought into contact by transverse mixing. No alteration of the hydraulic properties due to microbial growth (25) was observed during the experiment.

Table 4.1 summarizes the principal characteristics of the experimental setup including the flow and transport parameters, the inlet concentrations and the biokinetic parameters obtained in batch experiments. A schematic illustration of the experimental setup is provided in the Supporting Information (Fig. 4.5) as well as further details on the experimental procedure and measurements.

Flow and Transport Parameters		Inlet Concentrations	
Tank dimensions (L×W×H) [m]	0.785×0.011×0.14	Ethylbenzene [μM] (central port)	300
Number active inlet/outlet ports	11/10	Ratio: Deuterated/Light	0.25/0.75
Ports spacing [m]	0.012	Ethylbenzene [μM] (ambient water)	0
Total flow rate [m ³ s ⁻¹]	9.67×10 ⁻⁹	Oxygen [μM] (ambient water)	285
Seepage velocity [m s ⁻¹]	1.39×10 ⁻⁵	Oxygen [μM] (central port)	100 [^]
Porosity [-]	0.48	Nitrate [μM] (ambient water)	360
Porous medium tortuosity [-]	3 [*]	Nitrate [μM] (central port)	0
Hydraulic conductivity [m s ⁻¹]	4.11×10 ⁻⁴	Bromide [μM] (central port)	625
D _{aq} ^L Ethylbenzene [10 ⁻⁹ ×m ² s ⁻¹]	1.0082 [#]		
D _{aq} ^H Ethylbenzene [10 ⁻⁹ ×m ² s ⁻¹]	0.9613 [#]		
D _{aq} Oxygen [10 ⁻⁹ ×m ² s ⁻¹]	2.1 [§]		
D _{aq} Nitrate [10 ⁻⁹ ×m ² s ⁻¹]	1.9 [§]		

Biokinetic Parameters	Aerobic	Anaerobic
k _{max} [d ⁻¹]	13.1	3.1 ^{&}
K _{Substrate} [μM]	10	11.4
K _{Electron Acceptor} [μM]	3	70
k _{dec} [d ⁻¹]	0.1	0.02 ^{&}
k _{ihh} [μM]	30	30
Yield [μmol _X /μmol _S]	1.26	1.05
F _{gr} [μmol _{EA} /μmol _S]	4.2	4.2
F _{dec} [μmol _{EA} /μmol _S]	6.3	4.2
X _{max} [μmol L ⁻¹]	250	250
Fractionation factor, α	0.996	0.569
[*] estimated value based on (26)		
[#] determined according to Eq. 4.4 at T=298.15 K		
[§] from (26) at T=298.15 K		
[^] minimum oxygen concentration that was possible to obtain without the addition of a reducing agent		
^{&} determined as fitting parameters for the simulation of the last experimental phase		

Table 4.1: Experimental setup: flow and transport parameters, inlet concentrations and biokinetic parameters.

4.2.2 Conservative transport modeling

In a two-dimensional homogeneous domain, under steady state conditions, the analytical solution for a line source (27, 28) describes the distribution of a conservative species:

$$\frac{C(x, z)}{C_0} = \frac{1}{2} \left[\operatorname{erf} \left(\frac{z + \frac{W}{2}}{2\sqrt{D_t} \frac{x}{v}} \right) - \operatorname{erf} \left(\frac{z - \frac{W}{2}}{2\sqrt{D_t} \frac{x}{v}} \right) \right]. \quad (4.1)$$

where C [ML⁻³] is the solute concentration, v [ML⁻¹] is the seepage velocity, D_t [L²T⁻¹] the transverse dispersion coefficient and C_0 [ML⁻³] is the concentration of the injected tracer solution; x [L] and z [L] are the longitudinal and transverse coordinates, respectively and W [L] represents the source width. In our experimental setup we observed an effective source width of 1.2 cm, resulting from the rapidly diverging flowlines at the inlet ports.

In this section we focus our attention on conservative transport of ethylbenzene during the first abiotic phase of the experiment. In a previous study (29) we investigated, in a similar flow-through system, the simultaneous transport of non-reactive tracers (i.e. bromide, fluorescein and oxygen) over a wide range of flow velocities. The light and heavy ethylbenzene isotopologues are considered as distinct species and their steady state distribution is described by Eq. 4.1. The only parameter which is different in the mathematical description of transport of the two isotopologues is the transverse dispersion coefficient D_t .

Dispersion Parameterization. The hydrodynamic dispersion coefficient, describing solute dispersion in porous media, includes the additive contribution of pore diffusion D_p and mechanical dispersion (30). Pore diffusion is defined as the solute aqueous diffusion coefficient divided by a tortuosity factor, taking into account that molecular diffusion can only take place in the pore space. Mechanical dispersion quantifies the spreading due to the variation of local velocities in the complex, tortuous structure of a porous medium and is often described as the product of the seepage velocity and the dispersivity (31). Therefore, the classical description of transverse hydrodynamic dispersion reads as:

$$D_t = D_p + \alpha_t v \quad (4.2)$$

where α_t [L] is the transverse dispersivity, assumed a constant property of the porous medium.

Based on the outcome of multitracer experiments carried out in a similar laboratory setup, a new non-linear parameterization of transverse dispersion was recently proposed by Chiogna et al. (29):

$$D_t = D_p + v \frac{d}{\sqrt{Pe + 123}} \quad (4.3)$$

where d [m] is the porous medium grain size and $Pe=(vd)/D_{aq}$ is the Péclet number. Compared to the classical description of transverse dispersion, D_t in the new model depends non-linearly on the seepage velocity and the aqueous diffusion coefficient affects both the pore diffusion and the mechanical dispersion terms. The latter property is particularly significant for transport of isotopic species, since distinct isotopologues are characterized by different D_{aq} .

Aqueous Diffusion Coefficients. As pointed out by Richter et al. (32), the effect of different isotopic masses on the diffusion of neutral species in water is not yet well documented nor completely understood. Little data are available for deuterated and non-deuterated hydrocarbons. Mills (33) measured a ratio of aqueous diffusion coefficients between light and perdeuterated benzene of 1.057 and observed that this is in agreement with the inverse square root mass relation: ${}^L D_{aq} / {}^H D_{aq} = \sqrt{{}^H m / {}^L m}$. We obtained similar results for ethylbenzene using the correlation proposed by Worch (34):

$$D_{aq} = 3.595 \cdot 10^{-14} \frac{T}{\eta M^{0.53}} \quad (4.4)$$

where M [g·mol⁻¹] is the molar mass of the compound, η [Pa·s] is the dynamic viscosity of the fluid, and T [K] is the absolute temperature.

Using this empirical correlation, considering $\eta=0.897 \times 10^{-3}$ [Pa·s] and $T=298.15$ [K], aqueous diffusion coefficients of 1.0082×10^{-9} m²s⁻¹ and 0.9613×10^{-9} m²s⁻¹ were determined

for the light (^Lethylbenzene, MW=106.17 amu) and the heavy, perdeuterated isotopologue (^Hethylbenzene, MW=116.17 amu), respectively.

4.2.3 Reactive transport modeling

Reactive transport simulations were performed in order to investigate the effects of coupled transport and biodegradation processes on isotope signatures. A finite volume method using a streamline oriented grid was applied to simulate the reactive transport of different isotopologues. The features of the code were extensively described in previous studies (35-36). Different parameterizations of transverse dispersion (Eq. 4.2 and 4.3) were implemented in the code together with a reaction network including the biodegradation reactions and the dynamics of the microbial strains inoculated in the flow-through system. Dispersion is described with a second order tensor oriented in the principal directions (i.e. diagonal). The transverse component is expressed with the non linear parameterization given in Eq. 4.3. The longitudinal component (not sensitive in our experimental setup) is described following the classical linear parameterization (Eq. 4.2), where the longitudinal dispersivity was estimated equal to the average grain size ($\alpha_L = 0.256$ mm). The reactive processes are included as sink/source terms in the governing transport equations. The system of equations was solved implicitly with an operator split approach, used to decouple the physical transport from the reactive terms.

The reaction network consists of four mobile species: the light and labeled substrate isotopologues (i.e. ^Lethylbenzene, ^Hethylbenzene), two dissolved electron acceptors (i.e. oxygen and nitrate), and two immobile species: the aerobic and denitrifying microbial strains, assumed to be attached to the solid matrix.

The specific rates of contaminant removal can be expressed with multiple-Monod formulations that for the aerobic (aer) and nitrate-reducing (den) cases read as:

$$r_{S,aer} = k_{max,aer} \left(\frac{c_S}{c_S + K_S} \right) \left(\frac{c_{O_2}}{c_{O_2} + K_{O_2}} \right) \quad (4.5)$$

$$r_{S,den} = k_{max,den} \left(\frac{c_S}{c_S + K_S} \right) \left(\frac{c_{NO_3}}{c_{NO_3} + K_{NO_3}} \right) \left(\frac{k_{inh}}{k_{inh} + c_{O_2}} \right) \quad (4.6)$$

in which $k_{max,aer}$ and $k_{max,den}$ [T^{-1}] are the maximum specific degradation rates, c_S , c_{O_2} and c_{NO_3} [ML^{-3}] the concentrations of the substrate (i.e. sum of the labeled and non-labeled isotopologues) and the electron acceptors. K_S , K_{O_2} and K_{NO_3} [ML^{-3}] are the half-saturation constants of the organic contaminant, oxygen and nitrate, respectively. A term expressing the inhibition of oxygen concentration was included in the specific rate of contaminant removal by denitrification.

Isotope fractionation during degradation is described incorporating different kinetic expressions for the light and heavy species. The degradation of the light ethylbenzene isotopologue is described as the product of the overall substrate degradation rate corrected by the ratio between the light isotopologue ($^L c_S$) and the total ethylbenzene concentration (6):

$$\frac{\partial ^L c_S}{\partial t} = -r_{S,aer} X_{aer} \left(\frac{^L c_S}{c_S} \right) - r_{S,den} X_{den} \left(\frac{^L c_S}{c_S} \right) \quad (4.7)$$

where X_{aer} and X_{den} are the concentration of the two considered biomasses [ML^{-3}].

Similarly, the degradation rate of the heavy isotopologue ($^H c_S$) is based on the overall rate corrected by the proportion of the heavy isotopologue and a kinetic isotope fractionation factor (α), relating the isotope ratio of the instantaneous product to the isotope ratio of the substrate (see Supporting Information for further detail):

$$\frac{\partial {}^H c_S}{\partial t} = -r_{S,aer} X_{aer} \left(\frac{{}^H c_S}{c_S} \right) \alpha_{aer} - r_{S,den} X_{den} \left(\frac{{}^H c_S}{c_S} \right) \alpha_{den} \quad (4.8)$$

The dynamics of the biomasses is described by the contribution of a growth and a decay term:

$$\frac{\partial X_{aer}}{\partial t} = \left[r_{S,aer} Y_{S,aer} \left(\frac{{}^L c_S}{c_S} + \frac{{}^H c_S}{c_S} \alpha_{aer} \right) \left(1 - \frac{X_{aer}}{X_{max,aer}} \right) - k_{dec,aer} \right] X_{aer} \quad (4.9)$$

$$\frac{\partial X_{den}}{\partial t} = \left[r_{S,den} Y_{S,den} \left(\frac{{}^L c_S}{c_S} + \frac{{}^H c_S}{c_S} \alpha_{den} \right) \left(1 - \frac{X_{den}}{X_{max,den}} \right) - k_{dec,den} \right] X_{den} \quad (4.10)$$

in which $Y_{S,aer}$ and $Y_{S,den}$ [$M_X M_S^{-1}$] are the substrate yield coefficients and $k_{dec,aer}$ and $k_{dec,den}$ [T^{-1}] are the specific decay rates. The terms $(1-X/X_{max})$ are introduced to limit the simulated biomass growth, especially close to the continuous supply of contaminant and electron acceptor at the inlet of the system (37).

The removal rate of the electron acceptors is expressed by the additive contribution of oxygen and nitrate consumption during degradation of the light and heavy substrate isotopologues and during biomass decay:

$$\frac{\partial c_{O_2}}{\partial t} = -r_{S,aer} X_{aer} \left(\frac{{}^L c_S}{c_S} + \frac{{}^H c_S}{c_S} \alpha_{aer} \right) F_{aer,gr} - k_{dec,aer} X_{aer} F_{aer,dec} \quad (4.11)$$

$$\frac{\partial c_{NO_3}}{\partial t} = -r_{S,den} X_{den} \left(\frac{{}^L c_S}{c_S} + \frac{{}^H c_S}{c_S} \alpha_{den} \right) F_{den,gr} - k_{dec,den} X_{den} F_{den,dec} \quad (4.12)$$

where F_{aer} and F_{den} are stoichiometric coefficients of electron acceptor consumption for aerobic degradation and denitrification, respectively.

4.3 RESULTS AND DISCUSSION

4.3.1 *Conservative Transport Experiments*

The results of the conservative tracer runs performed in the first phase of the experiment are shown in Fig. 4.1. The data at consecutive days show a consistent pattern indicating fractionating behavior. Significant differences in the ratio between the heavy and light isotopologues concentrations were observed at the different sampling locations. During conservative transport, under steady state conditions, transverse hydrodynamic dispersion is the only process that can cause the observed fractionation. In fact, differences in aqueous diffusion coefficients result in a different physical transverse displacement of the two isotopic species. The light molecules are characterized by a higher D_{aq} which facilitates a more effective mixing across different streamlines and results in an enrichment of this species at the plume fringe. In order to interpret the measured data, we used the steady state analytical solution (Eq. 4.1) to describe the behavior of the two ethylbenzene isotopologues. As discussed in section 4.2.2, we considered different parameterizations of the transverse dispersion coefficient of the two isotopologues, described as different species undergoing conservative transport. Figure 4.1 shows the calculated isotopic ratio at the end of the flow-through domain. Modeling was performed in a forward mode and the only adjusted parameter was the ratio between the heavy to light isotopologue at the plume source which was set to 0.225/0.775 instead of the nominal 0.25/0.75. This adjustment was required in order to take into account that the nominal concentration ratio between the ethylbenzene isotopologues was not perfectly matched while preparing the plume solution. Therefore, a solution slightly depleted in the heavy ethylbenzene isotopologue was injected in the flow-through system. The classical transverse dispersion parameterization (Eq. 4.2), without distinction between the different aqueous diffusion coefficients of the light and labeled isotopologues, does not produce any shift in the ratio between the heavy and light species at the outlet of the flow-through system. Equation 4.2 was successively applied considering an isotopologue-specific pore diffusion term. We used the aqueous diffusion coefficients ${}^L D_{aq}=1.0082\times 10^{-9}$ m²/s and ${}^H D_{aq}=0.9613\times 10^{-9}$ m²/s, calculated with the empirical correlation proposed by Worch (Eq. 4.4). The mechanical dispersion term was the same for both transported species, with a transverse dispersivity $\alpha_T=7.6\times 10^{-5}$ m determined from bromide tracer experiments in the same experimental setup. This value was calculated with the classical linear parameterization (Eq. 4.2), taking into account the diffusion coefficient of bromide and using the fitting procedure described in a previous study (21). The different pore diffusion terms for the light and heavy species cause a shift of the isotopic ratio at the plume fringe but less pronounced than the one observed. A more satisfying agreement with the experimental data was achieved when we used the new empirical formulation of transverse dispersion (Eq. 4.3), since it considers the effects of the different aqueous diffusion coefficients on both the pore diffusion and the mechanical dispersion terms.

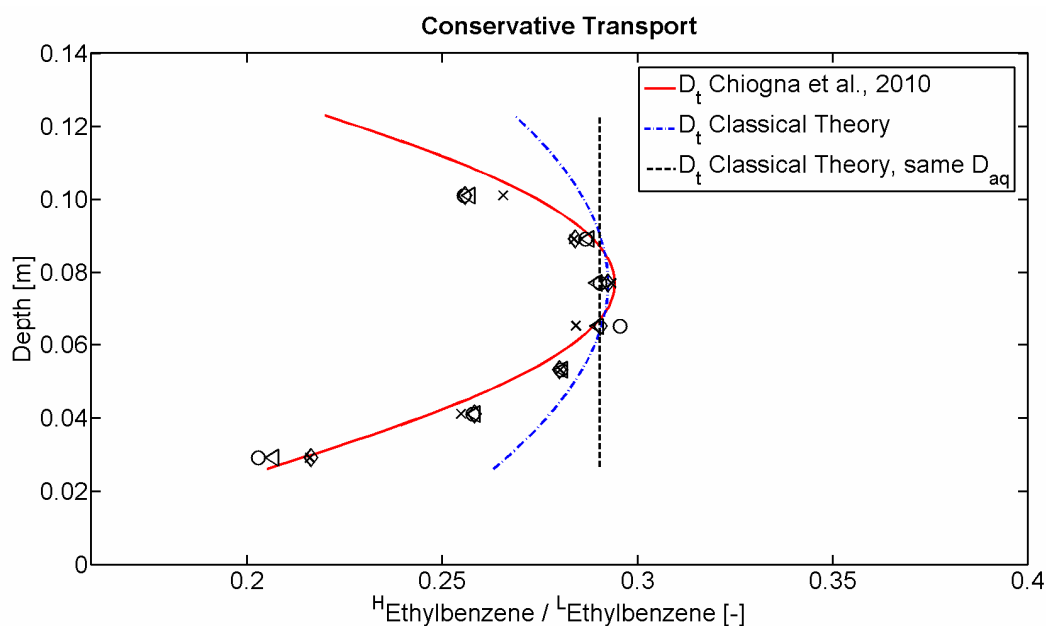
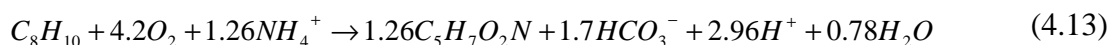


Figure 4.1: Vertical profiles of isotopologues ratios measured at the outlet ports (symbols representing days 1-4 of the experiment: crosses, triangles, circles and diamonds, respectively) and simulated with the analytical solution centered along the plume axis (Eq. 4.1), using different transverse dispersion parameterizations.

4.3.2 Reactive Transport Experiments

Aerobic Degradation. An aerobic ethylbenzene degrading strain, *Pseudomonas putida* F1, was injected at day 4. The aerobic biodegradation process established in the saturated porous medium is a typical mixing-controlled reaction requiring mixing of the ethylbenzene plume with the ambient groundwater rich in dissolved oxygen. Therefore, the microbially-mediated ethylbenzene degradation takes place predominantly at the plume fringe where the electron donor and the electron acceptor are brought into contact by transverse dispersion. Contaminant degradation coupled to active biomass growth can be summarized by the following redox reaction:



where the biomass is conceptualized as a chemical species ($C_5H_7O_2N$), and the portions of substrate's electrons used for cells synthesis during the aerobic process is assumed to be 0.6 (38).

The degraders' kinetic parameters for aerobic degradation of ethylbenzene were studied in batch systems and are reported in Table 4.1. A mixture of light and deuterated ethylbenzene, with the same ratio used in the flow-through experiments (3:1), was provided as sole carbon and energy source. An average value of the fractionation factor $\alpha_{er}=0.996$ was determined in triplicate experiments (data not shown). This value is very low, considering the fact that hydrogen isotope fractionation factors for mixtures of labeled and non-labeled compounds (i.e. toluene) were found up to 3 orders of magnitude greater than the ones typically reported for $^{13}C/^{12}C$ (39-40). Therefore, it can be safely assumed that *P. putida* F1 does not significantly fractionate between the light and deuterated ethylbenzene during aerobic degradation, as it is also documented for this strain with aerobic toluene degradation (24). A

lack of extensive fractionation was observed during the entire aerobic degradation phase of the flow-through experiment. In fact, the ratio of heavy to light isotopologues measured at the outlet ports (Fig. 4.2) shows a similar pattern to the one observed during the conservative run of the first experimental phase (Fig. 4.1), with a significant decrease at the plume fringes and a slight increase in the plume core. The reactive transport modeling study substantiates the observed behavior. Simulations carried out with the isotopologue-specific transverse dispersion parameterization (Eq. 4.3) and the kinetic parameters for aerobic degradation (Table 4.1) allow capturing the observed behavior at the outlet of the flow-through system (Fig. 4.2). The considerable decrease of the isotopologues ratio at the plume fringes is due to the more efficient transverse displacement of the light species compared to the heavy one, whereas in the plume core the labeled isotopologue is enriched. This fringe- and core-specific behavior of the isotope ratio cannot be described with a reactive transport formulation using the same reaction kinetic parameters but a transverse dispersion parameterization non-specific for the heavy and light isotopologues (e.g. Eq. 4.2 with same D_{aq} for the light and heavy species).

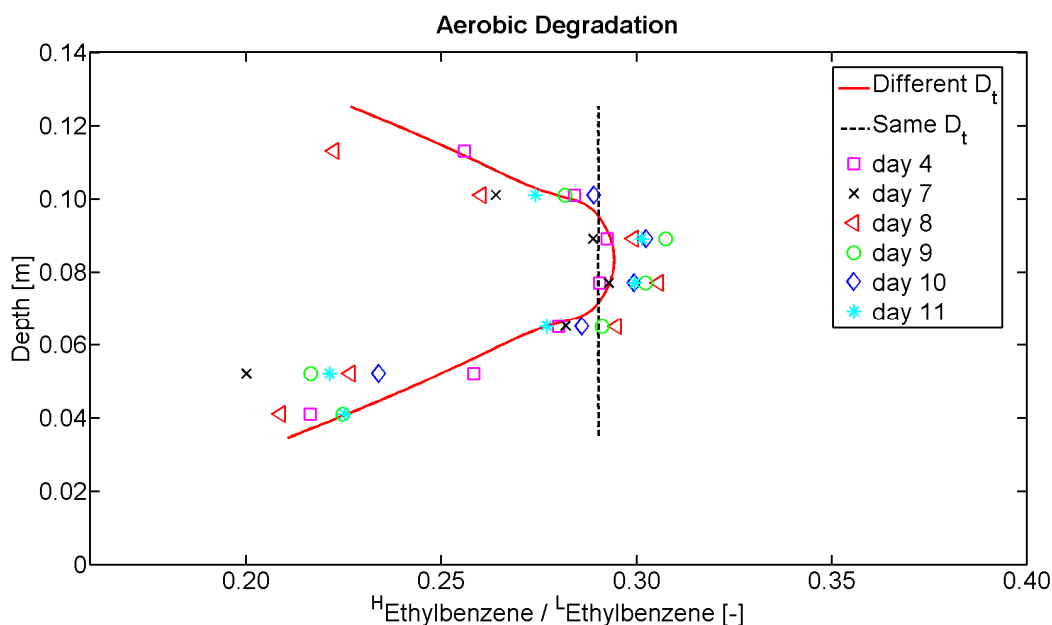
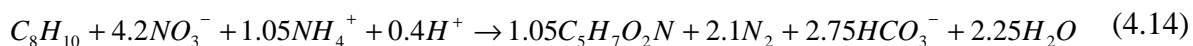


Figure 4.2: Isotopologues ratio during aerobic degradation. Symbols represent the ratios of measured concentrations. The solid and dash lines are the result of the reactive transport modeling with different transverse dispersion parameterizations: Eq. 4.3 (solid) and Eq. 4.2 (dash), respectively.

Aerobic and Anaerobic Degradation. The anaerobic degrader, *Aromatoleum aromaticum* EbN1, was inoculated in the flow-through system at day 11. This strain is able to degrade ethylbenzene under nitrate reducing conditions. Similarly to aerobic degradation, also the ethylbenzene oxidation coupled to nitrate reduction is a process taking place at the plume fringe. Assuming an electron transfer fraction of 0.5 from the oxidizable substrate to the synthesis of new cellular material (38), and the formula $C_5H_7O_2N$ representing the biomass of the anaerobic degraders, the degradation of ethylbenzene can be summarized as:



The metabolic pathway of ethylbenzene oxidation by *A. aromaticum* EbN1 produces a significant isotope fractionation. The fractionation factor for the mixture of labeled and light

ethylbenzene injected in the flow-through experiments was determined in batch cultures with nitrate as electron acceptor. An average value of $\alpha_{den}=0.596$ was obtained from triplicate experiments (data not shown). After the injection of the denitrifying strain (day 11), the concentrations measured at the outlet ports show a significant fractionation due to the metabolic activity of the denitrifying bacteria (Fig. 4.3).

As expected, an increased fractionation is observed at the plume fringe where nitrate from the ambient solution mixes with ethylbenzene, therefore providing favorable conditions for the metabolic activity of EbN1. The observed ratio of the labeled/light isotopologues shows an interesting transient trend. Increasing ratios were observed at subsequent observations (day 14 and day 15) where the anaerobic activity increased and stabilized at higher values towards the end of the experiment (day 16, 17 and 18).

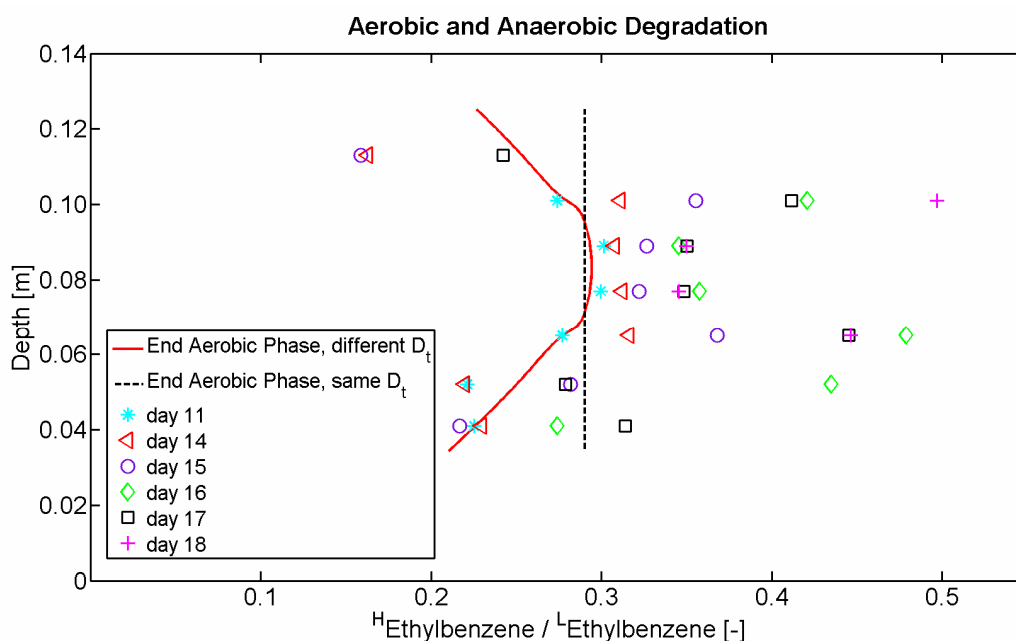


Figure 4.3: Isotopic ratios measured (symbols) during the aerobic-anaerobic phase (day 11-18) and simulated profiles (lines) at the end of the aerobic phase (day 11).

The observed transient behavior of the isotope ratios was captured by the reactive transport simulations. This third experimental phase was simulated as a new stress period, starting from the computed species distribution at the end of the previous aerobic degradation phase. Ethylbenzene degradation was described as a sequential process coupled to the consumption of oxygen by *P. putida* F1 at the outer fringe and of nitrate by *A. aromaticum* EbN1. The sequential degradation is described using an inhibition constant (Eq. 4.6) set to a value of $k_{inh}=30 \mu\text{M}$. The comparison between the observed and simulated ratios of labeled and light ethylbenzene is shown in Fig. 4.4. Fractionation starts to be observed 3 days after the inoculation of the system with the anaerobic strain and becomes progressively more significant towards the end of the experiment. The simulated ratios show two distinct peaks corresponding to the active denitrifying fringe where the degradation activity of EbN1, and hence the fractionation of ethylbenzene is more significant. The three-dimensional representation of the transient isotopic behavior shows the results of a simulation considerably longer (30 days) than the actual experiment. In this spatio-temporal representation, the increase of the ratio of the labeled to light ethylbenzene and successive approaching of steady state conditions can be visualized.

On the basis of the measured isotopologues ratio at the outlet ports, the specific contribution of the anaerobic fractionating strain to the overall ethylbenzene degradation can

be assessed by the port-resolved application of a Rayleigh-type equation based on the measured isotopic ratios (see Supporting Information). For a more accurate estimation of biodegradation an initial isotope ratio taking into account the fractionating effects of transport processes (i.e. transverse mixing) should be selected (Fig. 4.8 Supporting Information). In fact, if we take a uniform value of the ratio (i.e. ratio at the source) neglecting the fractionation due to dispersion, an overestimation of biodegradation at the plume core and an underestimation at the fringes are introduced.

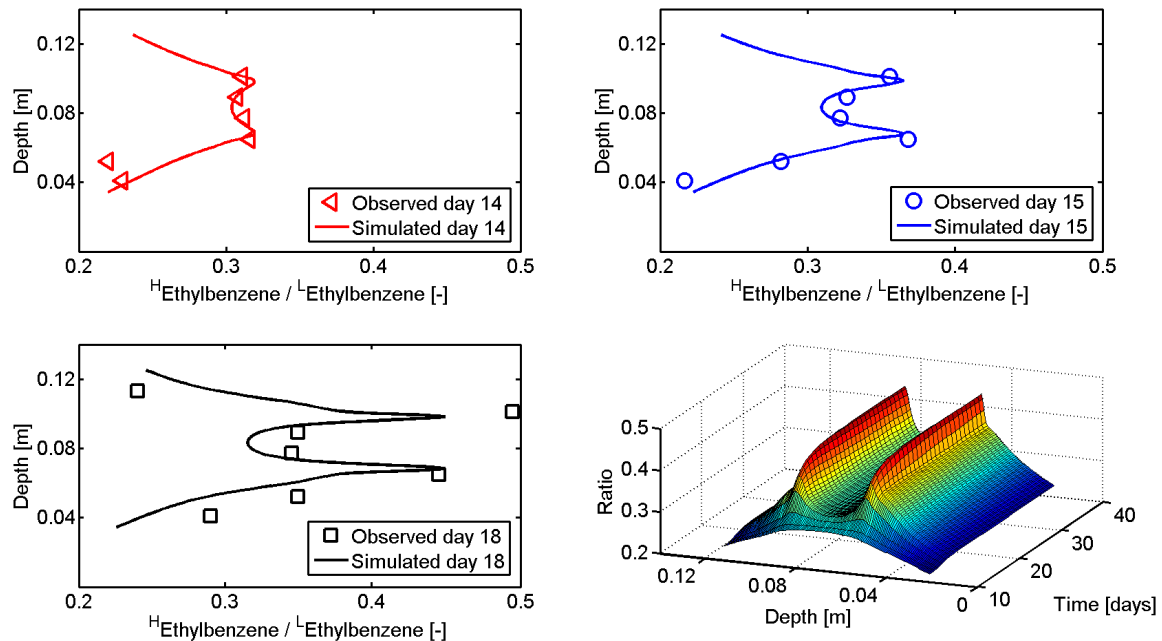


Figure 4.4: Transient evolution of the isotopic ratio due to the fractionating effects of transverse dispersion (parameterized according to Eq. 4.3) and biodegradation under nitrate-reducing conditions.

4.3.3 Environmental implications and significance

The outcomes of this study show a significant influence of transverse dispersion on isotopic fractionation during transport of a mixture of labeled and non-labeled ethylbenzene in a homogeneous porous medium. This finding contrasts with the common assumption that dispersive dilution of solutes does not cause fractionation of different isotopic species. Moreover, the effects observed during conservative transport experiments are also relevant for the interpretation of the measured isotopic ratios during the subsequent reactive transport phases, where ethylbenzene undergoes aerobic and anaerobic biodegradation. It has to be underlined that the results of the present laboratory study are obtained under very simplified conditions compared to a complex natural aquifer. Simplifying assumptions include the physical system (e.g. scale, homogeneous porous medium), the contaminant source (i.e. a single contaminant in a mixture of labeled and non-labeled isotopologues), the microbiological conditions (i.e. use of well-characterized pure cultures, optimal growth medium for the plume and ambient water solutions) and the geochemical conditions. In particular, we think it would be interesting to investigate the fractionating effect of transport processes also for non-labeled organic contaminants for which the differences of the masses

of the heavier and lighter isotopologues are smaller, thus resulting in more minute differences in the aqueous diffusion coefficients. Moreover, as suggested by a recent modeling study (16), differences on the physical displacement of light and heavy isotopic species can be enhanced in heterogeneous porous media. Preliminary simulations results indicate a still significant role of diffusive/dispersive processes also for non-labeled compounds; however this topic should be further explored using comprehensive modeling and experimental investigations.

Nonetheless this study, together with an emerging number of investigations of the role of physical processes on isotope fractionation (12-15), points to the need of considering both physical and reactive processes to achieve an improved interpretation of observed isotope data. This would probably lead to an increased effort for the evaluation of observed data, but could also open new possibilities of using stable isotope techniques to gain a better understanding of complex coupled reactive transport processes in porous media.

REFERENCES

- (1) Sherwood Lollar, B.; Slater, G. F.; Sleep, B.; Witt, M.; Klecka, G. M.; Harkness, M.; Spivack, J. Stable carbon isotope evidence for intrinsic bioremediation of tetrachloroethene and trichloroethene at area 6, Dover Air Force Base. *Environ. Sci. Technol.* **2001**, 35, 261–269.
- (2) Spence, M. J.; Bottrell, S. H.; Thornton, S. F.; Richnow, H. H.; Spence, K. H., Hydrochemical and isotopic effects associated with petroleum fuel biodegradation pathways in a chalk aquifer. *J. Cont. Hydrol.* **2005**, 79, 67-88.
- (3) Fischer, A.; Theuerkorn, K.; Stelzer, N.; Gehre, M.; Thullner, M.; Richnow, H. H., Applicability of stable isotope fractionation analysis for the characterization of benzene biodegradation in a BTEX-contaminated aquifer. *Environ. Sci. Technol.* **2007**, 41, 3689-3696.
- (4) Hunkeler, D.; Mekenstock, R. U.; Lollar, B. S.; Schmidt, T. C.; Wilson, J. T. A guide for assessing biodegradation and source identification of organic groundwater contaminants using compound specific isotope analysis (CSIA). Environmental Protection Agency (EPA) EPA600/R-08/148, 2008.
- (5) Hofstetter, T. B.; Schwarzenbach, R. P.; Bernasconi, S. M. Assessing transformation processes of organic compounds using stable isotope fractionation. *Environ. Sci. Technol.* **2008**, 42, 7737-7743.
- (6) Mariotti, A.; Germon, J. C.; Hubert, P.; Kaiser, P.; Letolle, R; Tardieux, A.; Tardieux, P. E. Experimental determination of nitrogen kinetic isotope fractionation : some principles ; illustrations for denitrification and nitrification processes. *Plant Soil* **1981**, 62, 413-430.
- (7) van Breukelen, B. M.; Hunkeler, D.; Volkering, F. Quantification of sequential chlorinated ethene degradation by use of a reactive transport model incorporating isotope fractionation. *Environ. Sci. Technol.* **2005**, 39, 4189-4197.
- (8) van Breukelen, B. M. Quantifying the degradation and dilution contribution to natural attenuation of contaminants by means of an open system Rayleigh equation. *Environ. Sci. Technol.* **2007**, 41, 4980–4985.
- (9) van Breukelen, B. M.; Prommer, H. Beyond the Rayleigh equation: reactive transport modeling of isotope fractionation effects to improve quantification of biodegradation. *Environ. Sci. Technol.* **2008**, 42, 2457-63.
- (10) Atteia, O.; Franceschi, M.; Dupuy, A. Validation of reactive model assumptions with isotope data: Application to the Dover case. *Environ. Sci. Technol.* **2008**, 42, 3289–3295.
- (11) Pooley, K. E; Blessing, M.; Schmidt, T. C.; Haderlein, S. B.; MacQuarrie, K. T. B.; Prommer, H. 2009 Aerobic biodegradation of chlorinated ethenes in a fractured bedrock aquifer: quantitative assessment by compound-specific isotope analysis (CSIA) and reactive transport modeling. *Environ. Sci. Technol.* **2009**, 43, 7458-7464.

- (12) Prommer, H.; Anneser, B.; Rolle, M.; Einsiedl, F.; Griebler, C. Biogeochemical and isotopic gradients in a BTEX/PAH contaminant plume: model-based interpretation of a high-resolution field data set. *Environ. Sci. Technol.* **2009**, 43, 8206-8212.
- (13) Kopinke, F. D.; Georgi, A.; Voskamp, M.; Richnow, H. H. Carbon isotope fractionation of organic contaminants due to retardation on humic substances: Implications for natural attenuation studies in aquifers. *Environ. Sci. Technol.* **2005**, 39, 6052–6062.
- (14) Bouchard, D.; Höhener, P.; Hunkeler, D. Carbon isotope fractionation during volatilization of petroleum hydrocarbons and diffusion across a porous medium: a column experiment. *Environ. Sci. Technol.* **2008**, 42, 7801–7806.
- (15) Aeppli, C.; Berg, M.; Cirpka, O. A.; Holliger, C.; Schwarzenbach, R. P.; Hofstetter T. B. Influence of Mass-Transfer Limitations on Carbon Isotope Fractionation During Microbial Dechlorination of Trichloroethene. *Environ. Sci. Technol.* **2009**, 43, 8813–8820.
- (16) Eggenkamp H. G. M.; Coleman M. L. The effect of aqueous diffusion on the fractionation of chlorine and bromine stable isotopes. *Geochim. Cosmochim. Acta* **2009**, 73, 3539–3548.
- (17) LaBolle, E. M., Fogg, G. E.; Eweis, J. B.; Gravner, J.; Leaist, D. G. Isotopic fractionation by diffusion in groundwater. *Water Resour. Res.* **2008**, 44, W07405, doi:10.1029/2006WR005264.
- (18) Kitanidis, P. K. The concept of dilution index. *Water Resour. Res.* **1994**, 30, 2011-2026.
- (19) Anneser, B.; Einsiedl, F.; Meckenstock, R. U.; Richters, L.; Wisotzky, F.; Griebler, C. High-resolution monitoring of biogeochemical gradients in a tar oil-contaminated aquifer. *Appl. Geochem.* **2008**, 23, 1715-1730.
- (20) Huang, W. E.; Oswald, S. E.; Lerner, D. N.; Smith, C. C.; Zheng, C. Dissolved oxygen imaging in a porous medium to investigate biodegradation in a plume with limited electron acceptor supply. *Environ. Sci. Technol.* **2003**, 37, 1905-11.
- (21) Bauer, R.D.; Rolle, M.; Bauer, S.; Eberhardt, C.; Grathwohl, P.; Kolditz, O.; Meckenstock, R. U.; Griebler, C. Enhanced biodegradation by hydraulic heterogeneities in petroleum hydrocarbon plumes. *J. Contam. Hydrol.* **2009**, 105, 56-68.
- (22) Bauer, R. D.; Rolle, M.; Kürzinger, P.; Grathwohl, P.; Meckenstock, R. U.; Griebler, C. Two-dimensional flow-through microcosms: versatile test systems to study biodegradation processes in porous aquifers. *J. Hydrol.* **2009**, 369, 284-295.
- (23) Rolle, M.; Eberhardt, C.; Chiogna, G.; Cirpka, O. A.; Grathwohl, P. Enhancement of dilution and transverse reactive mixing in porous media: experiments and model-based interpretation. *J. Contam. Hydrol.* **2009**, 110, 130–142.
- (24) Morasch, B.; Richnow, H. H.; Schink, B.; Vieth, A.; Meckenstock, R. U. Carbon and hydrogen stable isotope fractionation during aerobic bacterial degradation of aromatic hydrocarbons. *Appl. Environ. Microbiol.* **2002**, 68, 5191-5194.

- (25) Thullner, M.; Mauclaire, L.; Schroth, M. H.; Kinzelbach, W.; Zeyer, J. Interaction between water flow and spatial distribution of microbial growth in a two-dimensional flow field in saturated porous media. *J. Contam. Hydrol.* **2002**, *58*, 169-189.
- (26) Cussler, E. L. *Diffusion: Mass Transfer in Fluid Systems (Third Edition)*; Cambridge University Press: New York, USA, 2009.
- (27) Domenico, P. A.; Palciauskas, V. V. Alternative boundaries in solid waste management. *Ground Water* **1982**, *20*, 303-311.
- (28) Srinivasan, V.; Clement, T. P.; Lee, K. K. Domenico solution – is it valid? *Ground Water* **2007**, *45*, 136-146.
- (29) Chiogna, G.; Eberhardt, C.; Grathwohl, P.; Cirpka, O. A.; Rolle, M. Evidence of compound dependent hydrodynamic and mechanical transverse dispersion by multi-tracer laboratory experiments. *Environ. Sci. Technol.* **2010**, *44*, 688-693.
- (30) Bear, J. *Dynamics of fluids in porous media*; Dover: New York, USA, 1972.
- (31) Scheidegger, A. E. General theory of dispersion in porous media. *J. Geophys. Res.* **1961**, *66*, 3273-3278.
- (32) Richter, F. M.; Mendybaev, R. A.; Christensen, J. N.; Hutcheon, I. D.; Williams, R. W.; Sturchio, N. C.; Beloso Jr., A. D. Kinetic isotopic fractionation during diffusion of ionic species in water, *Geochim. Cosmochim. Acta* **2006**, *70*, 277–289.
- (33) Mills, R. Diffusion relationships in the binary system benzene-perdeuteriobenzene at 25 °C. *J. Phys. Chem.* **1976**, *80*, 888-890.
- (34) Worch, E. A new equation for the calculation of diffusion coefficients for dissolved substances. *Vom Wasser*, **1993**, *81*, 289-297.
- (35) Cirpka, O. A.; Frind, E. O.; Helmig, R. Streamline-oriented grid-generation for transport modelling in two-dimensional domains including wells. *Adv. Water Resour.* **1999**, *22*, 697–710.
- (36) Cirpka, O. A.; Frind, E. O.; Helmig, R. Numerical methods for reactive transport on rectangular and streamline-oriented grids. *Adv. Water Resour.* **1999**, *22*, 711–728.
- (37) Barry, D. A.; Prommer, H.; Miller, C. T.; Engesgaard, P.; Brun, P.; Zheng, C. Modelling the fate of oxidizable organic contaminants in groundwater. *Adv. Water Resour.* **2002**, *25*, 945-983.
- (38) Rittman, B. E.; McCarty P. L. *Environmental biotechnology: principles and applications*; McGraw-Hill: New York, USA, 2001.
- (39) Morasch, B.; Richnow, H. H.; Schink, B.; Meckenstock, R. U. Stable carbon and hydrogen isotope fractionation during microbial toluene degradation: mechanistic and environmental aspects. *Appl. Environ. Microbiol.* **2001**, *67*, 4842–4849.
- (40) Meckenstock, R. U.; Morasch, B.; Griebler, C.; Richnow, H. H. Stable isotope fractionation analysis as a tool to monitor biodegradation in contaminated aquifers. *J. Contam. Hydrol.* **2004**, *75*, 215–255.

S1. SUPPORTING INFORMATION: Experimental setup

Fig. 4.5 shows a schematic illustration of the experimental flow-through system, described in detail in previous studies (Bauer et al., 2008; 2009).

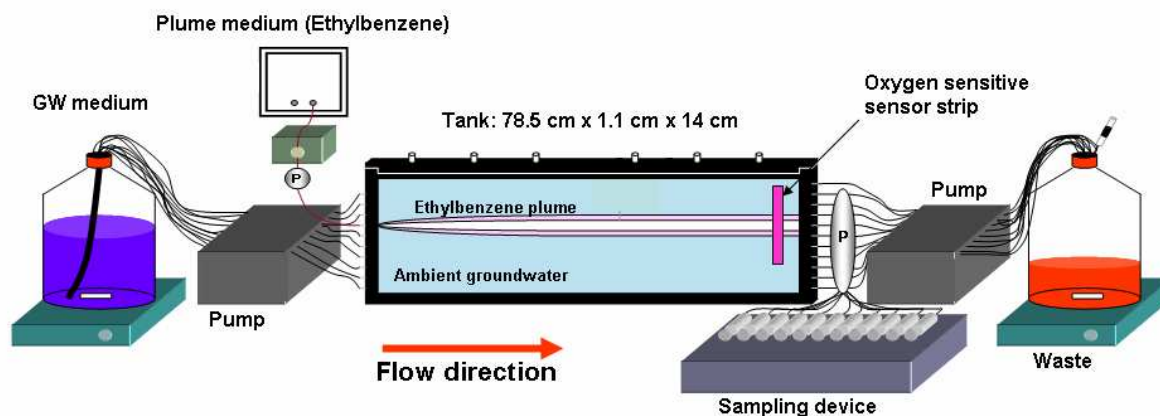


Figure 4.5: *Experimental setup (modified after Bauer et al., 2008).*

The plume medium was injected through a single inlet port with a concentration of 300 μM ethylbenzene, kept as constant as practically possible. Bromide (625 μM) was amended, as conservative tracer, to the plume medium. The ambient groundwater solution was prepared based on freshwater medium (Widdel and Bak, 1992) and contained high concentrations of dissolved electron acceptors (i.e. oxygen 285 μM and nitrate 360 μM). Ethylbenzene was measured by GC-MS (Finnigan Trace Ultra and Trace DSQ, Thermo Electron Cooperation, Waltham, MA, USA, with a DB-5MS column, 0.5 μm film thickness, 0.25 i.d., 30 m length, J&W Scientific, USA) after addition of internal standard and liquid-liquid extraction with cyclohexane. Sample injection was on split mode ($1:10 \text{ mL min}^{-1}$) and the flow rate of the carrier gas helium was 1 mL min^{-1} . The oven temperature was 40 $^{\circ}\text{C}$ for 1 min, then ramped first at a rate of 15 $^{\circ}\text{C min}^{-1}$ to 200 $^{\circ}\text{C}$ and then at a rate of 25 $^{\circ}\text{C}$ to 300 $^{\circ}\text{C}$ where it was held for 1.33 min.

The concentrations of ionic species (i.e. nitrate and bromide) were determined by ion-chromatography (Dionex AS3500, Idstein, Germany). Dissolved oxygen was measured with a non-invasive optode technique (Microx 1/FIBOX, PreSens, Regensburg, Germany) at an oxygen sensitive stripe located 3 cm from the outlet of the flow-through system. Detailed explanation of this technique can be found in Haberer et al., (2010). Measurements of the electron acceptors (i.e. oxygen and nitrate) during the conservative and reactive phases of the experiment are shown in Fig. 4.5. In the conservative phase the depletion of oxygen in the center of the plume is just due to the smaller concentration injected through the central inlet port ($\sim 1/3$ of the surrounding clean water, i.e. minimum oxygen concentration that was possible to obtain without the addition of a reducing agent) and the side diffusion/dispersion from the ambient groundwater. In the reactive phase oxygen is consumed in the central zone of the flow-through system occupied by the ethylbenzene plume. During ethylbenzene anaerobic degradation consumption of nitrate was observed in the central zone of the plume.

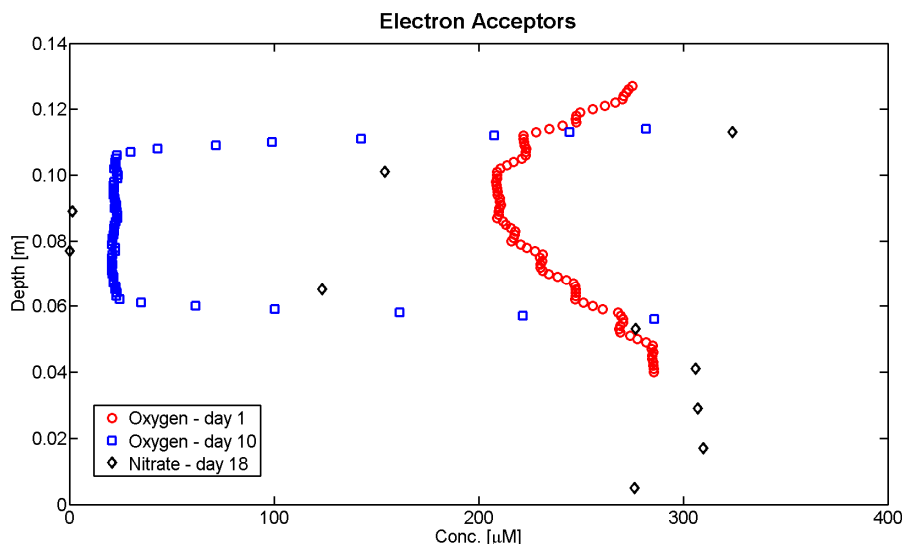


Figure 4.6: Electron acceptors concentrations measured at different phases of the flow-through experiment.

S1.1 Batch cultures

The aerobic ethylbenzene-degrading strain *P. putida* strain F1 was obtained from J. R. van der Meer, Dübendorf, Switzerland, and the anaerobic strain *A. aromaticum* EbN1 from F. Widdel, Bremen, Germany (Rabus and Widdel, 1995). Precultures of both strains were grown using ethylbenzene as sole carbon and energy source and oxygen and nitrate as electron acceptors for *P.putida* F1 and *A. Aromaticum* EbN1, respectively. All batch cultures were grown in half-filled 100 mL serum bottles sealed with butyl rubber stoppers (Maag Technik, Switzerland) and incubated in the dark. For the anaerobic strain, the headspace was flushed with an N_2/CO_2 (80/20) atmosphere. Before inoculation of the flow-through system the strains were grown to an $OD_{578}=0.08-0.1$ (corresponding to a concentration range $4-5 \times 10^7$ cells/mL) in batch cultures, with ethylbenzene as sole carbon and energy source. The inoculation of the flow-through system was performed continuously injecting the biomass suspension for 15 hours through the two ports surrounding the central inlet used for the injection of the ethylbenzene plume.

The isotopic behavior of the different microbial strains was also determined in batch cultures. Figure 4.7 shows the degradation of ethylbenzene by the anaerobic strain EbN1. The temporal decrease in contaminant concentrations is accompanied by a significant increase of the ratio between the perdeuterated and the non-labeled isotopologues.

The kinetic fractionation factor α during ethylbenzene degradation was determined by fitting the logarithmic form of the Rayleigh equation (4.15) to the experimental data. A value of $\alpha=0.596 \pm 0.019$ was obtained for the anaerobic, fractionating strain. Differently from what was recently reported for the toluene degradation experiments of Kampara et al. (2008) we did not observe a clear fractionation change caused by bioavailability limitations. This was probably due to the specific conditions at which our degradation experiments were performed and in particular the electron-acceptor limitation which resulted in only few data points available at low substrate concentrations.

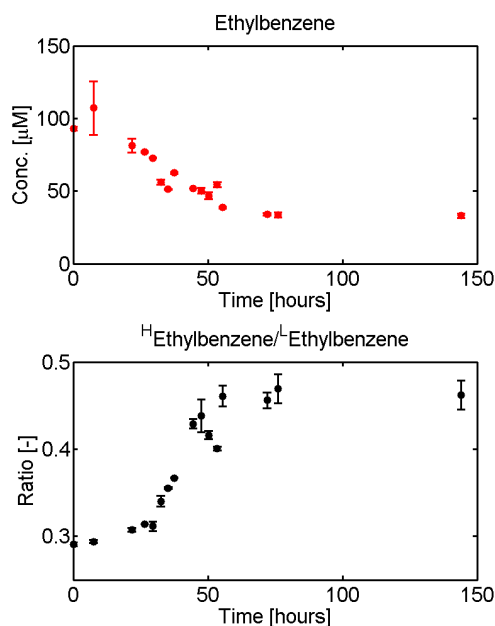


Figure 4.7: Ethylbenzene degradation and isotope ratio during batch experiments with the fractionating strain *A. aromaticum EbN1*.

S2 SUPPORTING INFORMATION: Calculation of biodegradation

Quantification of biodegradation based on isotope ratios is often performed using the Rayleigh equation (Mariotti et al., 1981), which can be generally written as:

$$\frac{R_t}{R_0} = \left(\frac{R_0 + 1}{R_t + 1} \cdot f \right)^{\alpha-1} \quad (4.15)$$

where R_t and R_0 are the ratios of heavy (H) to light species (L) at time t and $t=0$, respectively. f is the fraction of compound remaining and α is the kinetic fractionation factor which relates the isotope ratio of the increment of product which appears in an infinitely short time (instantaneous product) to the isotope ratio of the substrate:

$$\alpha = \frac{dH_p / dL_p}{H / L} \quad (4.16)$$

In natural systems, for important elements such as $^{13}\text{C}/^{12}\text{C}$ and $^{15}\text{N}/^{14}\text{N}$, Eq. (4.15) is often approximated as:

$$\frac{R_t}{R_0} = f^{\alpha-1}. \quad (4.17)$$

This equation has often been used for practical applications by changing the temporal dependency of the concentrations and isotope ratios into spatial dependency.

Based on the Rayleigh equation, biodegradation can be calculated as:

$$B = 1 - f \quad (4.18)$$

In the case of the flow-through experiments presented in this study, the amount of biodegradation at each outlet sampling port due to the activity of the fractionating nitrate-reducing strain was calculated from the measured isotopic ratios combining Eq. (4.15) and Eq. (4.18):

$$B_{port} = 1 - f = 1 - \frac{R_{port} + 1}{R_0 + 1} \cdot \left(\frac{R_{port}}{R_0} \right)^{1/(\alpha-1)} \quad (4.19)$$

where R_{port} is the ratio of the deuterated to light isotopologues measured at the outlet ports. R_0 was considered in two different ways:

- 1) ratio between deuterated and light ethylbenzene at the source (inlet port), assuming no fractionation due to dilution;
- 2) ratio between deuterated and light ethylbenzene measured at the end of the aerobic phase preceding the injection of the fractionating anaerobic degrader, therefore taking into account the fractionation contribution of transverse dispersion.

Fig. 4.8 shows the percentage of biodegradation calculated at the outlet ports at the different days of the experimental phase with active fractionation during anaerobic biodegradation. The results show that neglecting the fractionating contribution of dilution leads to overestimation of biodegradation in the plume core and underestimation at the fringes.

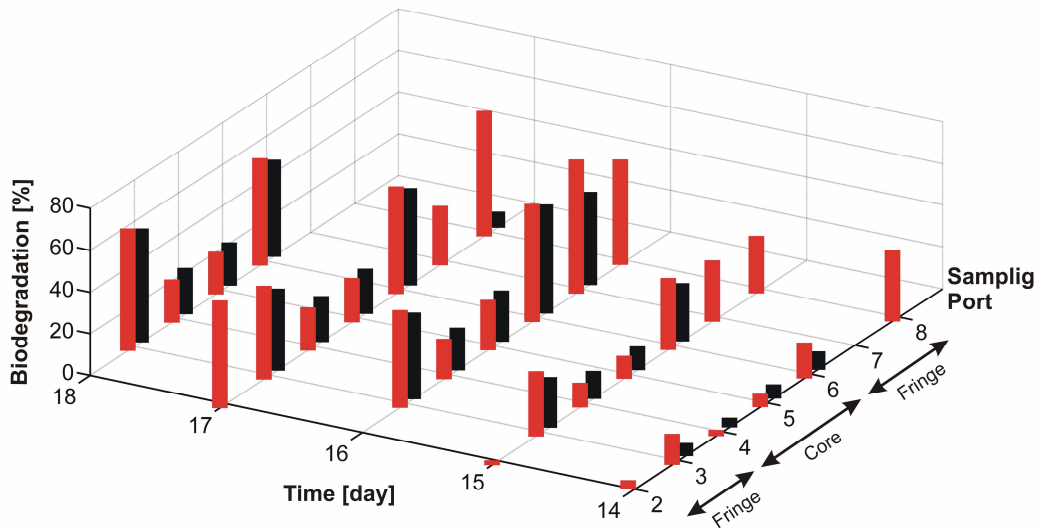


Figure 4.8: Biodegradation contribution of the anaerobic degraders calculated from the measured isotope ratios neglecting (black bars) and considering (red bars) the fractionation due to transverse dispersion.

References

Bauer, R. D.; Maloszewski, P.; Zhang, Y.; Meckenstock, R. U.; Griebl, C. Mixing-controlled aerobic and anaerobic biodegradation of toluene in porous media — results from two-dimensional laboratory experiments. *J. Contam. Hydrol.* **2008**, 96, 150–168.

Bauer, R. D.; Rolle, M.; Bauer, S.; Eberhardt, C.; Grathwohl, P.; Kolditz, O.; Meckenstock, R. U.; Griebler, C. Enhanced biodegradation by hydraulic heterogeneities in petroleum hydrocarbon plumes. *J. Contam. Hydrol.* **2009**, 105, 56-68.

Haberer, C.; Rolle, M.; Liu, S.; Grathwohl, P. A high-resolution non-invasive approach to determine oxygen transport across the capillary fringe and in the underlying groundwater. *J. Contam. Hydrol.* **2010** (submitted).

Kampara, M.; Thullner, M., Richnow, H. H.; Harms, H.; Wick, L. Y. Impact of bioavailability restrictions on microbially induced apparent stable isotope fractionation: 2. experimental observations. *Environ. Sci. Technol.* **2008**, 42, 6552-6558.

Mariotti, A.; Germon, J. C.; Hubert, P.; Kaiser, P.; Letolle, R.; Tardieux, A.; Tardieux, P. Experimental determination of nitrogen kinetic isotope fractionation: some principles; illustration for the denitrification and nitrification processes. *Plant Soil.* **1981**, 62, 413-430.

Rabus, R.; Widdel, F. Anaerobic degradation of ethylbenzene and other aromatic hydrocarbons by new denitrifying bacteria. *Arch. Microbiol.* **1995**, 163, 96-103.

Widdel, F.; Bak, F. Gram negative mesophilic sulfate reducing bacteria. In: Balows, H.G.T., Dworkin, M., Harder, W., Schleifer, K.H. (Eds.), *The Prokaryotes. A Handbook on the Biology of Bacteria: Ecophysiology, Isolation, Identification, and Applications.* Springer, New York, pp. 3352-3378, 1992.

Chapter 5

Relevance of local compound-specific transverse dispersion for conservative and reactive mixing in heterogeneous porous media⁵

Abstract

Different measures of dilution have been proposed to describe solute mixing in heterogeneous porous media. Most of these approaches lead to the definition of effective dispersion coefficients. In order to quantify mixing, these up-scaled parameters should account for both local-scale dispersion and effects of flow variability in heterogeneous formations (e.g., flow focusing in high-permeability and defocusing in low-conductivity inclusions). The correct quantification of mixing is particularly important for transport of compounds undergoing reactions. Recent results of laboratory-scale experiments showed a dependency of local transverse dispersion on molecular diffusion over a wide range of flow velocities, implying compound-specific transverse mixing even at intermediate and high Péclet numbers. The goal of this study is to assess the relevance of a compound-specific local-scale transverse dispersion on conservative and reactive mixing in heterogeneous domains at the field scale. We restrict our analysis to steady-state two-dimensional flow and transport with continuous injection by a line source. We present numerical simulations in heterogeneous domains with different characteristics of variability in the conductivity field, and apply as measures of solute mixing (1) the effective transverse dispersion coefficient derived from second central spatial moments, (2) a dispersion coefficient derived from flux-related second central spatial moments, (3) the scalar dissipation rate and (4) a dispersion coefficient derived from the flux-related dilution index. The results indicate compound-specific transverse mixing behavior also at the field scale which is particularly significant in case of low to moderately heterogeneous porous media. Moreover, we show that measures of dilution calculated in a flux-related framework result in an improved quantification of mixing processes and allow to define up-scaled parameters (*i.e.*, effective transverse dispersion coefficients) affected by a low degree of uncertainty. For mixing-controlled reactive transport we illustrate the importance of compound-dependent local effects on the length of reactive solute plumes.

⁵ Chiogna G., O.A. Cirpka, P. Grathwohl and M. Rolle, (2010), Relevance of local compound-specific transverse dispersion for conservative and reactive mixing in heterogeneous porous media, *Water Resources Research* (submitted).

5.1 INTRODUCTION

The investigation of dilution and mixing processes in porous media is of primary importance in many scientific disciplines (e.g., contaminant hydrology, chemical engineering, reservoir engineering, etc.) and technical applications (e.g., water treatment, groundwater risk assessment, nuclear waste storage). In subsurface environments such as groundwater systems, the complex interplay between physical and biogeochemical processes determines the transport and degradation of contaminant plumes. Insufficient mixing of reaction partners often limit (bio)chemical reactions thus controlling natural attenuation of dissolved contaminants and the performances of many engineered remediation interventions. Therefore, the correct characterization of mixing processes, i.e. those processes which affect both the entropy as well as the peak concentration of a plume, is a challenging but necessary prerequisite to accurately describe and assess reactive solute transport in natural porous formations. Modeling and experimental studies have shown the importance of mixing at the plume's fringe in determining the transport and fate of organic contaminants [e.g., *Cirpka et al.*, 1999a; *Lerner et al.*, 2000; *Maier and Grathwohl*, 2006; *Prommer et al.*, 2009; *Bauer et al.*, 2009; *Rolle et al.*, 2010].

In order to model and understand the physics behind mixing in porous media, it is necessary to define the scale of interest at which we aim to address a problem [*Bear*, 1972; *Dentz et al.*, 2010]. Porous media structures can be analyzed at the pore scale [e.g., *Cao and Kitanidis* 1998; *Li et al.*, 2006; *Tartakovsky et al.*, 2009; *Willingham et al.*, 2008, 2010], at the Darcy scale [e.g., *Berkowitz et al.*, 2000; *Ginn et al.*, 2001] or at the larger field scale [e.g., *Thierrin and Kitanidis*, 1994; *Heinz et al.*, 2003; *Englert et al.*, 2009; *Li et al.*, 2010]. Depending on the system we are interested in, we may focus just on one of these scales. Nevertheless there is always an influence of the smaller-scale processes on the larger scale [*Bear*, 1972]. The main goals of up-scaling procedures are i) to quantify this influence and ii) to define up-scaled parameters which are still capturing the significant physical properties at the lower scale [e.g. *Bear*, 1972; *Kitanidis*, 1988; *Dagan*, 1984, 1990, 1991; *Rajaram and Gelhar*, 1993a, 1993b, 1995; *Gelhar and Axness*, 1983; *Neuman et al.*, 1987; *Whitaker*, 1999]. Therefore up-scaling procedures aim at describing solute transport in complex systems such as natural porous formations through some relatively simple equations using up-scaled parameters. A detailed description of up-scaling approaches is beyond the scope of this study and we refer, for this purpose, to the recent review of *Dentz et al.* [2010].

Two fundamental steps can be identified in the up-scaling of mixing processes: 1) the up-scaling of flow and transport equations from the pore channels to the larger Darcy scale, where the most important physical quantities are averaged over a defined domain (i.e., a representative elementary volume) and 2) the up-scaling from the Darcy to the field scale. At the Darcy scale, the up-scaled quantity that describes dilution in homogenous porous media is the tensor of local hydrodynamic dispersion [*Bear*, 1972]. The components of this tensor are usually described as the sum of two processes: pore diffusion and mechanical dispersion [*Bear*, 1972; *Freeze and Cherry*, 1979]. Pore diffusion is described by the ratio between the aqueous diffusion coefficient of a compound and the tortuosity of the medium [*Grathwohl*, 1998; *Boving and Grathwohl*, 2001]. Mechanical dispersion takes into account the effects of variable velocity at the pore scale and quantifies how mixing of a solute is affected by this process at the Darcy scale [*Bear*, 1972]. For a Cartesian coordinate system oriented in the principal flow direction, the dispersion tensor can be simplified to a second order diagonal tensor in which components in the longitudinal (parallel to the flow) and transverse (perpendicular to the flow) directions can be identified. The transverse dispersion components, typically smaller than the longitudinal one [e.g. *Bijeljic and Blunt*, 2007], determine transverse mixing, which is the process of major interest for the transport of

contaminant plumes from continuous sources under steady state flow and transport conditions [e.g. *Cirpka et al.*, 1999a; *Ham et al.*, 2004; *Liedl et al.*, 2005]. Since reactions are taking place at the microscopic (pore) scale [e.g. *Steeffel et al.*, 2005], a correct quantification of Darcy-scale dispersion and its influence on solute dilution was identified to be of critical importance in modeling transport of contaminant plumes [*Kitanidis*, 1994].

At the field scale, the effects of spatially varying advection, caused by the heterogeneity of the formations, have to be considered in the description of mixing processes. In particular, flow focusing in high-permeability zones was shown to cause a significant enhancement of mixing [e.g., *Werth et al.*, 2006, *Rolle et al.*, 2009]. This enhancement is caused by converging streamlines in high-permeability inclusions increasing the probability of a solute particle to cross a given number of streamlines, therefore resulting in enhanced dilution. Conversely, defocusing in low-permeability zones can reduce the rate of increase in mixing [e.g., *Chiogna et al.*, 2010c]. The permeability contrast and the location of the inclusions strongly influence the effectiveness of mixing. Up-scaled parameters to measure dilution at the field scale need to account for both local-scale dispersion and effects of flow variability in heterogeneous formations.

In this work, we study the effects of a new compound-specific parameterization of the local transverse dispersion coefficient, obtained as a result of multi-tracer laboratory experiments [*Chiogna et al.*, 2010a] on dilution and reactive transport at field scales. This parameterization differs from the classical linear expression [*Scheidtgerger*, 1961] because it retains a significant dependence of transverse dispersion on molecular diffusion also at higher velocities. Up to now, this feature was neglected by most up-scaling approaches. We show through numerical experiments the impact of this compound dependency on field-scale dispersive mixing. For the interpretation of conservative transport simulations we consider the following measures of dilution: (1) the effective dispersion coefficient [e.g., *Cirpka*, 2002; *Dentz and Carrera*, 2005], (2) a newly defined effective dispersion coefficient based on flux-related second central moments, (3) the scalar dissipation rate [e.g., *Kitanidis*, 1994; *Beckie*, 1998, *De Simoni et al.*, 2005], and (4) the flux-related dilution index [*Rolle et al.*, 2009]. In the reactive cases, we quantify mixing using the concept of critical dilution index [*Chiogna et al.*, 2010c], the length of the reactive plume and the flux of the mixing ratio squared (which is directly related to the scalar dissipation rate).

5.2 PROBLEM STATEMENT

In this work, we perform conservative and reactive transport simulations of continuously injected solutes in a two-dimensional domain (100 m long and 3 m thick) representing a vertical cross-section of a confined aquifer under steady-state flow and transport conditions (Figure 5.1). In the reactive case we consider an instantaneous bimolecular complete reaction of the form $f_A A + f_B B \rightarrow f_C C$, with f_A , f_B , and f_C being stoichiometric coefficients. By this choice, the reaction is controlled only by mixing of the reactive species A and B [*Luo et al.*, 2008]. This reactive system represents mixing-controlled degradation of an organic contaminant (A) under aerobic conditions, where oxygen (B) acts as oxidant. The reactive species A is continuously injected through a line source perpendicular to the main flow direction, while the reaction partner B is introduced parallel to A into the domain with the ambient groundwater (Figure 5.1).

The numerical approach used to solve flow and transport can be summarized as follows [see also *Chiogna et al.*, 2010b]: (a) generation of a conductivity field on a regular grid, (b) simulation of hydraulic head, and stream function values, (c) construction of a streamline-

oriented grid, (d) simulation of conservative and reactive solute transport on the streamline-oriented grid.

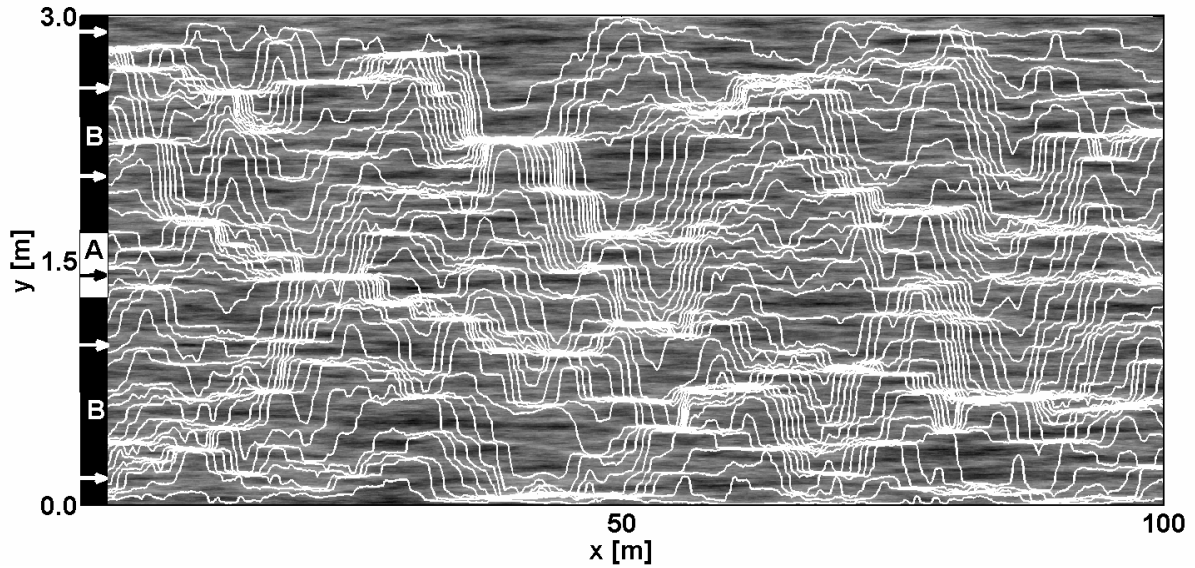


Figure 5.1: *Principal model setup. White area at the left boundary: injection source of compound A; adjacent black regions: injection zones of compound B. White lines: streamlines illustrating how flow is focused in high-permeability inclusions.*

5.2.1 Generation of heterogeneous conductivity fields

We generate four different types of heterogeneous conductivity fields: two of them are binary, characterized by different permeability contrasts, while the other two are the Gaussian equivalent fields associated to the binary ones, as explained in the following paragraphs (Figure 5.2). All these fields have the same integral scales $l_x = 3.9$ m and $l_y = 0.02$ m, in the horizontal and vertical directions, respectively. For each field we consider an ensemble of 100 Monte Carlo realizations.

Binary fields

The binary fields are generated following *Werth et al.* [2006]: a periodic auxiliary multi-Gaussian field $a(\mathbf{x})$ with zero mean, standard deviation of unity, and Gaussian covariance function is generated on a 1000×500 grid using the spectral approach of *Dykaar and Kitanidis* [1992]. In order to obtain the binary fields, we define a cutoff value of the auxiliary variable a : points exhibiting a -values exceeding the 40% quantile and with a positive vertical gradient component $\partial a / \partial y$ fall into high-conductivity inclusions, while all other points fall into the low-conductivity matrix. The $\partial a / \partial y$ criterion leads to shapes of the inclusions with straighter top than bottom surfaces [*Heinz et al.*, 2003].

The hydraulic conductivity value of the porous matrix is 6.14×10^{-4} m s⁻¹ and remains constant in both binary cases, whereas the conductivity value in the heterogeneous lenses K_{high} varies: in the first type of binary fields we set a contrast between high and low conductivity regions $K_{\text{Ratio}} = 100$ (i.e. $K_{\text{high}} = 6.14 \times 10^{-2}$ m s⁻¹); while in the second case we select a lower permeability contrast: $K_{\text{Ratio}} = 25$ (i.e. $K_{\text{high}} = 15.35 \times 10^{-3}$ m s⁻¹).

Gaussian equivalent fields

For the binary fields with $K_{\text{Ratio}}=100$ we construct equivalent continuous multi-Gaussian fields with identical covariance functions of log hydraulic conductivity, and the same is done for the binary fields with $K_{\text{Ratio}}=25$. Since the (original) binary field is in both cases periodic, the covariance function can conveniently be evaluated by taking the Fourier transform of the binary log-conductivity field, multiplying it with its complex conjugate and performing the inverse Fourier transformation. Multi-Gaussian fields generated with this covariance function exhibit the same variance as the binary fields (i.e. $\sigma_{\ln K}^2=3.2$ and $\sigma_{\ln K}^2=1.6$ for the $K_{\text{Ratio}}=100$ and the $K_{\text{Ratio}}=25$ binary cases, respectively). However, since the binary fields don't exhibit intermediate log-conductivity values, the range of conductivity values in the equivalent continuous fields must be substantially larger (up to 7 and 6 orders of magnitude in case of $K_{\text{Ratio}}=100$ and of $K_{\text{Ratio}}=25$, respectively) to achieve the same variance. In this way, higher conductivity contrasts can occur in the equivalent continuous fields.

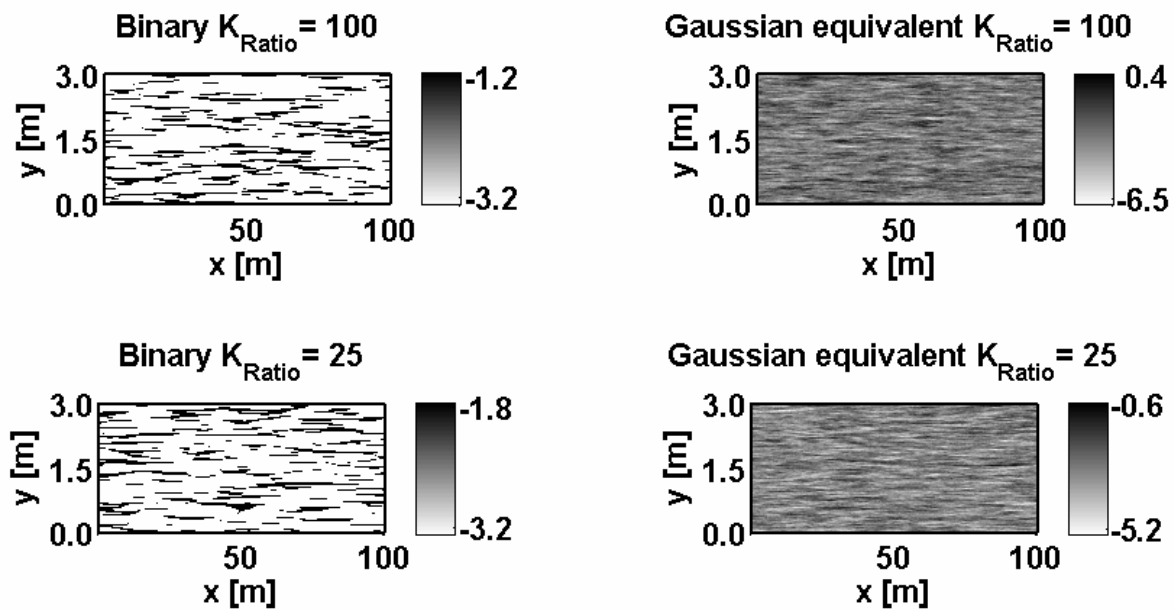


Figure 5.2: Examples of the flow fields studied. The gray scale indicates the values of $\log_{10}(K)$.

5.2.2 Governing equations

Groundwater flow

We consider two-dimensional flow in a confined aquifer. No-flow boundaries are applied at the top and bottom boundaries, while the hydraulic head is fixed at the left- and right-hand side boundaries. The steady-state flow problem for hydraulic head ϕ and stream function ψ for a given conductivity field K reads as:

$$\begin{aligned}
-\nabla \cdot (K\nabla\phi) &= 0 \\
-\nabla \cdot \left(\frac{1}{K} \nabla\psi \right) &= 0
\end{aligned} \tag{5.1}$$

Eq. 5.1 is solved numerically on a rectangular grid by bilinear Finite Elements, applying Dirichlet boundary conditions on the left- and right-hand side for the head-problem. The value of the hydraulic gradient is adjusted to obtain the same discharge Q_{in} [L^2T^{-1}] between different realizations ($Q_{in} = 5 \times 10^{-5} \text{ m}^2\text{s}^{-1}$). In the stream-function problem, the top and bottom boundaries have fixed values, in which the value difference equals the total volumetric flux through the domain. With the simulated values of ϕ and ψ , we can construct streamline-oriented grids using the approach of *Cirpka et al.* [1999b].

Conservative and reactive transport

Steady-state transport of a conservative tracer is described by the advection-dispersion equation:

$$\mathbf{v} \cdot \nabla C - \nabla \cdot (\mathbf{D} \nabla C) = 0 \tag{5.2}$$

in which C is the concentration [ML^{-3}] of a conservative species, \mathbf{v} [LT^{-1}] is the seepage velocity mainly oriented in the x direction, and \mathbf{D} [L^2T^{-1}] is the local hydrodynamic dispersion tensor. As boundary conditions, we assume fixed values at the inflow boundary, and zero dispersive flux at all other boundaries:

$$\begin{aligned}
C &= 1 && \text{along } \Gamma_{in}^A \\
C &= 0 && \text{along } \Gamma_{in}^B \\
\mathbf{n} \cdot \mathbf{D} \nabla C &= 0 && \text{along all other boundaries}
\end{aligned} \tag{5.3}$$

in which Γ_{in}^A and Γ_{in}^B are two complementary fractions of the inflow boundary Γ_{in} .

Reactive transport is described by the following system of partial differential equations:

$$\begin{aligned}
\mathbf{v} \cdot \nabla C_A - \nabla \cdot (\mathbf{D}_A \nabla C_A) &= -f_A \mathbf{r}_A \\
\mathbf{v} \cdot \nabla C_B - \nabla \cdot (\mathbf{D}_B \nabla C_B) &= -f_B \mathbf{r}_B \\
\mathbf{v} \cdot \nabla C_C - \nabla \cdot (\mathbf{D}_C \nabla C_C) &= f_C \mathbf{r}_C
\end{aligned} \tag{5.4}$$

with boundary conditions:

$$\begin{aligned}
C_A &= C_{Ain} & C_B &= 0 & C_C &= 0 & \text{along } \Gamma_{in}^A \\
C_A &= 0 & C_B &= C_{Bin} & C_C &= 0 & \text{along } \Gamma_{in}^B \\
\mathbf{n} \cdot \mathbf{D}_i \nabla C_i &= 0 & & & & & i = A, B, C \text{ along all other boundaries}
\end{aligned} \tag{5.5}$$

in which C_i [ML^{-3}] (with $i = A, B, C$) are the concentrations of the different reactive species and \mathbf{r}_i are the reaction rates. The inlet concentrations of compounds A and B are indicated by C_{Ain} [ML^{-3}] and C_{Bin} [ML^{-3}], respectively. \mathbf{D}_i is the local dispersion tensor specific for each compound. Due to the conditions of the problem (i.e. steady-state, advection-dominated

transport), the longitudinal component of the dispersion tensor is not a sensitive parameter [e.g., *Liedl et al.*, 2005]. The transverse component determining local-scale transverse mixing is parameterized following a non-linear compound-dependent parameterization [*Chiogna et al.*, 2010a]:

$$D_t = D_p + v \frac{d}{\sqrt{\text{Pe} + 123}} \quad (5.6)$$

where D_p [L^2T^{-1}] is the pore diffusion coefficient, defined as the ratio between the aqueous diffusion coefficient, D_{aq} [L^2T^{-1}], and the tortuosity of the porous medium, d [L] is the average grain size and $\text{Pe} = v \times d / D_{aq}$ [-] denotes the Péclet number. The parameterization of the local transverse dispersion coefficient in Eq. 5.6 requires the grain size at each location in the domain. In our application, we reconstruct it from the local conductivity values using the relation of *Hazen* [1892]:

$$d \approx A\sqrt{K} \quad (5.7)$$

with the proportionality constant $A = 0.01 \text{ m}^{0.5} \text{ s}^{0.5}$. The tortuosity $\tau = 2.5$ [-] and the porosity $n = 0.4$ [-] are kept constant throughout the domain. It may be noted that D_t as parameterized in Eq. 5.6 is compound-specific at all velocities because the mechanical dispersion component depends via the Péclet number on the molecular diffusion coefficient of the solute. Eq. 5.6 was empirically derived through a number of multitracer bench-scale experiments [*Chiogna et al.*, 2010a], but is in agreement with several experimental studies clearly indicating compound-specific transverse dispersion even at intermediate and large velocity ranges [e.g. *Carvahlo and Delgado*, 2000; *Klenk and Grathwohl*, 2002; *Olsson and Grathwohl*, 2007; *Haberer et al.*, 2010].

The transport problem is solved on the previously described streamline-oriented grids using the Finite Volume scheme of *Cirpka et al.* [1999c]. The resulting system of equations is solved using the direct solver UMFPACK implemented in Matlab [*Davis and Duff*, 1997]. Instead of keeping a constant geometrical width w [L] of the source, we fix the volumetric flux (10% of the total flux) over which we inject the solute A in all realizations. Heterogeneities thus lead to variations of the source width between the realizations, but an effective source width could be defined over the ensemble of the realizations [*de Barros and Nowak*, 2010]. The inlet concentration of compound B is defined as C_{Bin} and set to 1 [ML^{-3}], while the inlet concentration of A is defined as C_{Ain} and set to 1.5 [ML^{-3}]. The stoichiometric coefficients f_A , f_B , and f_C are set to unity and the aqueous diffusion coefficients of A and C are close to those of many organic pollutants ($D_{aq,A} = D_{aq,C} = 0.8 \times 10^{-9} \text{ m}^2\text{s}^{-1}$), while the one of B is that of oxygen ($D_{aq,B} = 2.1 \times 10^{-9} \text{ m}^2\text{s}^{-1}$) [*Cussler*, 2009].

5.2.3 Solution of reactive transport

In this section, we briefly describe the two approaches we use to solve the reactive transport problem. The first one is a purely numerical method, in which we perform a Picard iteration for the reactive term of Eq. 5.4. The second one is a well known semi-analytical approach for the case of compound-independent dispersion, in which Eq. 5.2 is solved for the mixing ratio of the system and the concentrations of the reactive species are obtained by post-processing.

Numerical iterative solution

We are not aware of closed-form solutions of mixing-controlled reactive transport in heterogeneous media in case of compound-specific local transverse dispersion. Thus, under these conditions, we use an iterative numerical approach. As initial guess, we solve the transport equations neglecting the reactions ($r_i=0$). We define $\mathbf{M}_{mob,i}$ as the mobility matrix for each specie i , resulting from discretizing the divergence of advective-dispersive fluxes by the Finite Volume Method on the streamline-oriented grids:

$$\mathbf{v} \cdot \nabla C_i - \nabla \cdot (\mathbf{D}_i \nabla C_i) \xrightarrow{\text{discretization}} \mathbf{M}_{mob,i} \mathbf{C}_i \quad i = A, B, C \quad (5.8)$$

in which \mathbf{C}_i denotes the vector of discrete concentration values of compound i in all cells. Then, we proceed with the numerical computation of the reactive transport problem through a Picard loop which consists of 6 steps, as summarized in Algorithm 5.1.

while $\mathbf{C}_i^{\kappa+1} - \mathbf{C}_i^\kappa > 0 \quad i = A, B, C$

Step 1: $\mathbf{C}_i^{\kappa+1} = s\mathbf{C}_i^\kappa + (1-s)\mathbf{M}_{mob,i}^{-1} \left(\mathbf{b}_i + \frac{\mathbf{r}_A^\kappa + \mathbf{r}_B^\kappa}{2} \right) f_i \quad i = A, B, C$

Step 2: $\mathbf{C}_A^{\kappa+1} = 0 \quad \text{if} \quad \frac{\mathbf{C}_A^{\kappa+1}}{f_A} < \frac{\mathbf{C}_B^{\kappa+1}}{f_B}; \quad \mathbf{C}_B^{\kappa+1} = 0 \quad \text{if} \quad \frac{\mathbf{C}_A^{\kappa+1}}{f_A} > \frac{\mathbf{C}_B^{\kappa+1}}{f_B};$

Step 3: $\tilde{\mathbf{r}}_i = \frac{\mathbf{M}_{mob,i} \mathbf{C}_i^{\kappa+1} - \mathbf{b}_i}{f_i} \quad i = A, B, C$

Step 4: $r_A^{tot} = \sum_{N_{cells}} \tilde{\mathbf{r}}_A; \quad r_B^{tot} = \sum_{N_{cells}} \tilde{\mathbf{r}}_B;$

step 5: $\mathbf{r}_A^{\kappa+1} = \frac{\tilde{\mathbf{r}}_A}{2} \left(\frac{r_B^{tot}}{r_A^{tot}} + 1 \right); \quad \mathbf{r}_B^{\kappa+1} = \frac{\tilde{\mathbf{r}}_B}{2} \left(\frac{r_A^{tot}}{r_B^{tot}} + 1 \right);$

step 6: increase κ by 1

end while

Algorithm 5.1: *Solution of multi-component, mixing-controlled, steady-state, reactive transport by Picard iteration.*

The reactive term in *step 1* $(r_A^\kappa + r_B^\kappa)/2$ is a sink term for C_A and C_B , while it is a source term for the product concentration C_C ; \mathbf{b}_i is the right-hand side vector resulting from the inlet boundary condition, and the factor s is a relaxation factor which was set to 0.9 in the following simulations. Since we consider an instantaneous bimolecular reaction, the two reacting compounds A and B cannot coexist:

$$C_A \cdot C_B = 0 \quad (5.9)$$

For each iteration κ , Eq. 5.9 implies that at each location C_A or C_B must be zero and the conditions in *step 2* have to be fulfilled [e.g., *Clement et al.*, 1998; *Cirpka and Valocchi*, 2007]. Furthermore the reactive terms for C_A and C_B must equal the fluxes across the interfaces of the cells in which the reaction takes place. So we start defining the reactive fluxes $\tilde{\mathbf{r}}_i$ for the reactive fringe of the plume as shown in *step 3*. The equality of the total

reactive fluxes of compound *A* and *B* over the entire computational domain has been given as a condition at the end of each loop (*steps 4* and *5*) to define the reaction rates to be used again in *step 1* of the following iteration. The iterative procedure terminates when the concentrations converge to a constant value.

Semi-analytical solution

As illustrated in the previous section, a numerical procedure is required when the aqueous diffusion coefficients of the species considered are different. However, when the aqueous diffusion coefficient is assumed identical for the reacting compounds, a semi-analytical approach can be applied. This method is based on the concept of the mixing ratio X [-], defined as the volumetric ratio of the injected solution in the mixture with ambient water (Cirpka and Valocchi, 2007). X behaves as a conservative component according to Eq. 5.2. This or similar approaches have been applied in several recent contributions [e.g., De Simoni et al., 2005, 2007; Chiogna et al. 2010c; Bellin et al. 2010] to which we refer for a detailed description of the solution strategy.

5.3 MEASURES OF DILUTION IN CONSERVATIVE TRANSPORT

We quantify mixing of a conservative tracer by four different measures of dilution: (1) the effective dispersion coefficient, (2) a newly defined flux-related effective dispersion coefficient, (3) the scalar dissipation rate, and (4) the flux-related dilution index. Since dilution directly leads to decreasing peak concentrations and increasing entropy of the plume, mass displacements connected with purely advective movements of the plume (e.g., squeezing and stretching of plumes in heterogeneous formations) cannot be considered as true mixing processes. This implies that the ensemble dispersion coefficient, quantifying the rate of change of second central moments of the ensemble-averaged concentration [Gelhar and Axness, 1983; Dagan, 1984; Neuman et al., 1987], are not considered, since they are widely affected by the uncertainty of determining the mean position of a plume [Kitanidis, 1988, 1994]. In particular, we analyze to which extent the above-mentioned measures of dilution retain the compound-specific behavior of local transverse dispersion. Since the values of effective transverse dispersion coefficients in similar flow fields were found to be approximately log-normal distributed [e.g. Chiogna et al., 2010c], we generally take the median of the dilution measure as characteristic value for the ensemble of realizations. In the following we will indicate with $D_{t\ low}$ the results obtained for a conservative tracer with the aqueous diffusion coefficient of compound *A* (i.e. typical organic pollutant), and with $D_{t\ high}$ the results obtained for a conservative tracer with the aqueous diffusion coefficient of compound *B* (i.e., oxygen).

5.3.1 Effective dispersion coefficient

Effective dispersion [Kitanidis, 1988; Dentz et al., 2000a] differs from ensemble dispersion in the order of computing second central moments and taking expected values. In ensemble dispersion the concentrations are averaged over the ensemble of realizations first, followed by computing second central moments of the ensemble concentration. In effective dispersion, by contrast, second central moments are computed in each realization first and averaged over the ensemble subsequently. By this procedure, uncertainties about the first

moments are factored out. Analytical expressions of effective dispersion have been derived for wide sources [e.g., *Dentz et al.*, 2000b] and for point-like injections [*Dentz et al.*, 2000a; *Cirpka*, 2002; *Dentz and Carrera*, 2005]. In the first case, the effective dispersion coefficient is affected by squeezing and stretching of plumes due to spatially variable velocity fields, while in the second case *Cirpka* [2002] claimed that effective dispersion is a good measurement of mixing.

Most studies on effective dispersion were performed for transient transport of a solute slug. Here, we consider steady-state transport in a system with continuous injection and exclusively analyze the transverse spatial moments. In this context, the normalized first transverse spatial moment of each realization M_1 [L] represents the location of the center of gravity of the solute plume as a function of the longitudinal travel distance:

$$M_1(x) = \frac{\int_0^H yC(x, y)dy}{\int_0^H C(x, y)dy} \quad (5.10)$$

Successively, we compute the normalized second central spatial moment of each realization M_{2C} [L²], which represents the spread of the concentration distribution about its center of gravity:

$$M_{2C}(x) = \frac{\int_0^H (y - M_1(x))^2 C(x, y)dy}{\int_0^H C(x, y)dy} \quad (5.11)$$

Finally, we calculate the effective dispersion coefficient D_t [L²T] as half the rate of increase in the mean flow direction x of the mean normalized second central spatial moment multiplied by the average flow velocity $\langle v \rangle$:

$$D_t = \frac{\langle v \rangle}{2} \frac{d\langle M_{2C} \rangle}{dx} \quad (12)$$

This definition is modified compared to the common expression of D_t for a pulse injection, where the dispersion coefficient equals half the time derivative of the normalized second central moment. The traditional expression, quite obviously, cannot be applied in steady-state transport because the time derivative vanishes in such settings.

Figure 5.3 shows the results of the second central spatial moments for the different heterogeneous fields. M_{2C} is normalized by its initial value at the line source and plotted as function of distance x , normalized by the integral scale in the direction of flow. This kind of normalization is chosen for practical reasons, as will become clearer in the next section. Besides the median, indicated by a bold line, we also show the range bounded by the 16 and 84 percentiles as shaded area. These percentiles would represent the mean plus/minus one standard deviation if M_{2C} was normally distributed.

The results exemplify that the transverse spatial second central moment obtained for two conservative species, introduced with the same volumetric flux but characterized by different aqueous diffusion coefficients, such as compound *A* and compound *B*, are different at a

statistically significant level. While the 16-84 percentiles of the two compounds overlap, a Wilcoxon rank sum test (always considered in this work within 95% confidence level) shows that the two datasets D_t low (i.e., compound A) and D_t low (i.e., compound B) are not samples from identical continuous distributions. We conclude that considering the compound-specific local transverse dispersion coefficient is required to correctly characterize the mean spatial second central moment of the plume ensemble, even though these moments exhibit high uncertainty.

In all four settings, the second central moment increases approximately linearly, resulting in two constant effective transverse dispersion coefficients, one for each compound. The values are listed in Table 5.1 along with other measures of dilution. In every single realization, the simulation with the higher D_{aq} -value resulted in a quicker increase of the second central moment, and this also results in distinctly different median values.

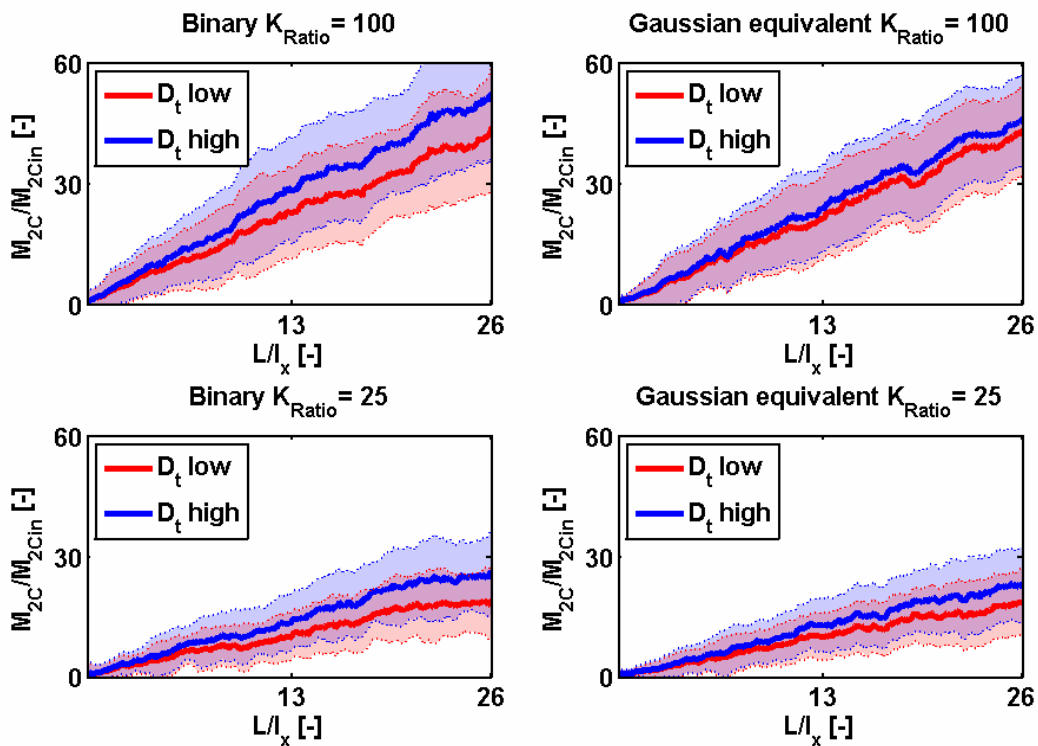


Figure 5.3: Second central transverse spatial moments of a conservative compound normalized by the value at the source (M_{2Cin}). Red: low transverse dispersion coefficient; blue: high transverse dispersion coefficient. Bold lines: median; shaded regions: 16 to 84 percentiles.

5.3.2 Flux-related effective dispersion coefficient

A key problem of traditional spatial moments analysis is that these moments are directly affected by spatial variability of advection, which is not a mixing process. Even though plume meandering is corrected for in effective dispersion, the advective squeezing of plumes in high-velocity regions and the stretching in low-velocity ones leads to changes in second central moments that are not directly related to mixing. In particular for plumes with finite initial width, effective dispersion includes a component of uncertainty in streamline positions rather than mass exchange between streamlines. In order to quantify the lateral exchange in

terms of volumetric flux rather than spatial coordinate, we therefore suggest taking normalized flux-related lateral moments defined as:

$$M_{q1}(\varphi) = \frac{\int_0^H \psi C(\varphi, \psi) d\psi}{\int_0^H C(\varphi, \psi) d\psi} \quad (5.13)$$

$$M_{q2C}(\varphi) = \frac{\int_0^H (\psi - M_{q1}(\varphi))^2 C(\varphi, \psi) d\psi}{\int_0^H C(\varphi, \psi) d\psi} \quad (5.14)$$

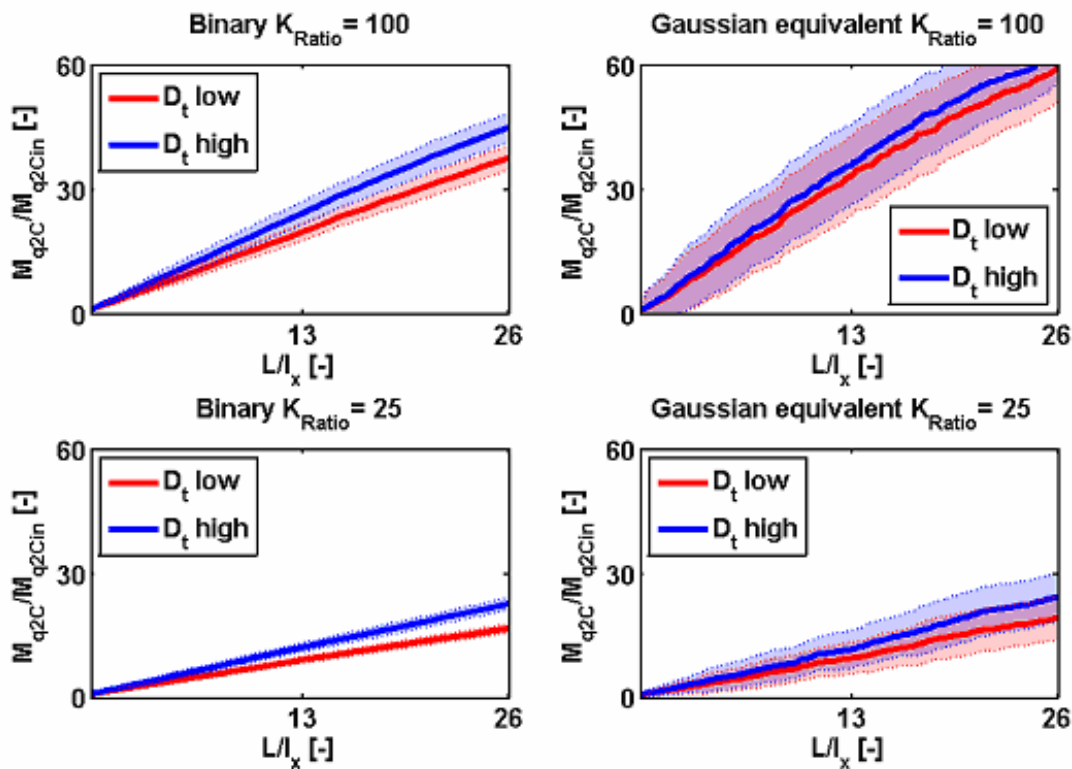


Figure 5.4: Flux-related second central transverse spatial moments of a conservative compound normalized by the value at the source (M_{q2Cin}). Red: low transverse dispersion coefficient; blue: high transverse dispersion coefficient. Bold lines: median; shaded regions: 16 to 84 percentiles.

Using the flux-related second central moment, the effect of the local transverse dispersion coefficient being compound specific is more pronounced (Figure 5.4). This is so, because the traditional spatial transverse moments are affected by plume squeezing and stretching, introducing additional uncertainty, independent of local transverse dispersion, whereas the flux-related moments are not. In Figures 5.3 and 5.4 we show the relative values of the two second moments considered (i.e., M_{2C}/M_{2Cin} and M_{q2C}/M_{q2Cin} , respectively). While the increase of the median of the second central moment and of the flux-related second central

moment has similar slopes, the ranges of the 16-84 percentiles are much narrower in the flux-related measures (Figure 5.4) than in traditional moments analysis (Figure 5.3).

In analogy to the framework in Cartesian coordinates, we can define an effective dispersion coefficient based on the flux-related second central moment:

$$D_t = \frac{\langle v \rangle}{2\langle q \rangle^2} \cdot \frac{d\langle M_{q2C} \rangle}{dx} \quad (5.15)$$

in which the scaling by $\langle q \rangle^2$ results from the transformation of the stream-function value ψ to lateral spatial coordinates.

Table 5.1 lists the values of the flux-related effective dispersion coefficients for the four different cases considered. The major difference to the traditional effective dispersion coefficient is the significant reduction of uncertainty, highlighting that a flux-related framework is better suited to quantify lateral mixing than traditional moments analysis [see also *Rahman et al.*, 2005].

5.3.3 Scalar dissipation rate

The scalar dissipation rate $-\nabla^T \mathbf{C} \mathbf{D} \nabla C$ of a conservative compound is a measure of mixing related to the total flux of the concentration squared [*Beckie*, 1998] and thus the concentration variance. In fact, if we multiply the steady-state advection-dispersion equation of a conservative compound (Eq. 5.2) by its concentration and apply the chain rule of differentiation, we obtain:

$$\frac{1}{2} \nabla \cdot (vC^2 - \mathbf{D} \nabla C^2) = -\nabla^T \mathbf{C} \mathbf{D} \nabla C \quad (5.16)$$

The integration of this equation over the entire cross-section of the domain gives the total flux of the concentration squared (F_C^2). As discussed below, *De Simoni et al.* [2005, 2007], *Bolster et al.* [2009, 2010], *Luo et al.* [2008], *Bellin et al.* [2010] among others, related the scalar dissipation rate to the reaction rate in reactive transport controlled by local dispersive mixing.

As already mentioned, the mixing ratio is a conservative quantity, so that twice the change of the total flux of the mixing ratio squared, F_X^2 , is identical to the scalar dissipation rate. We calculate F_X^2 by integrating the longitudinal advective and dispersive fluxes of X^2 over the entire cross-section of the domain. The results for the different heterogeneous fields are shown in Figure 5.5, exemplifying that the fluxes of the mixing ratio squared for compounds with different local transverse dispersion coefficients are distinct, even if they are close to each other.

A Wilcoxon rank sum test confirms the statistical difference between the two results. Note that the scalar dissipation rate does not directly lead to a definition of an effective dispersion coefficient, but there is an increasing interest in studying the properties of this quantity in order to address mixing problems in complex heterogeneous porous media [e.g. *Le Borgne et al.*, 2010a, *Le Borgne et al.*, 2010b].

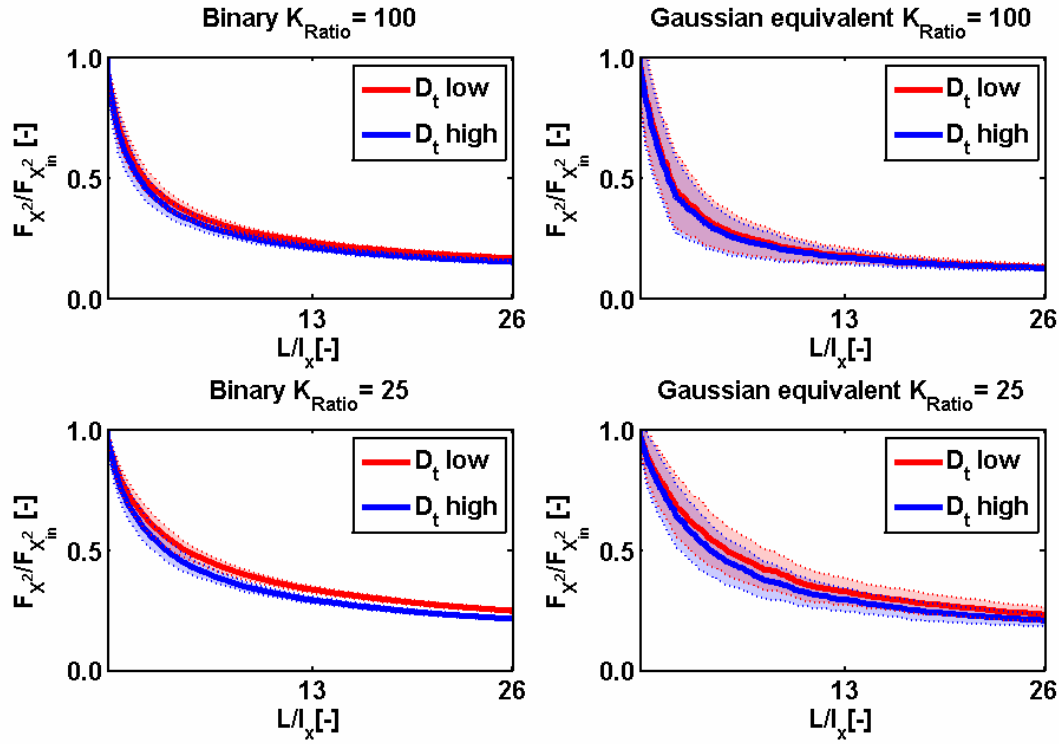


Figure 5.5: Flux of the mixing ratio squared normalized by the value at the source ($F_{X^2_{in}}$). Red: low transverse dispersion coefficient; blue: high transverse dispersion coefficient. Bold lines: median; shaded regions: 16 to 84 percentiles.

5.3.4 Flux-related dilution index

The flux-related dilution index was introduced by *Rolle et al.* [2009] and further developed by *Chiogna et al.* [2010c] in order to transfer the concept of volumetric dilution index [*Kitanidis, 1994*] to measure dilution of steady-state plumes developing from continuously emitting sources. In illustrative terms, it quantifies the effective volumetric flux over which a given solute flux is distributed. In a two-dimensional domain it is defined as:

$$E_Q(x) = \exp\left(-\int_0^H p_Q(\mathbf{x}) \cdot \ln(p_Q(\mathbf{x})) q_x(\mathbf{x}) dy\right) \quad (5.17)$$

in which the flux-related probability density p_Q is defined as:

$$p_Q(\mathbf{x}) = \frac{C(\mathbf{x})}{\int_0^H q_x(\mathbf{x}) \cdot C(\mathbf{x}) dy} \quad (5.18)$$

The reactor ratio is the normalized form of the flux-related dilution index defined as:

$$M_Q(x) = \frac{E_Q(x)}{Q_x} \quad (5.19)$$

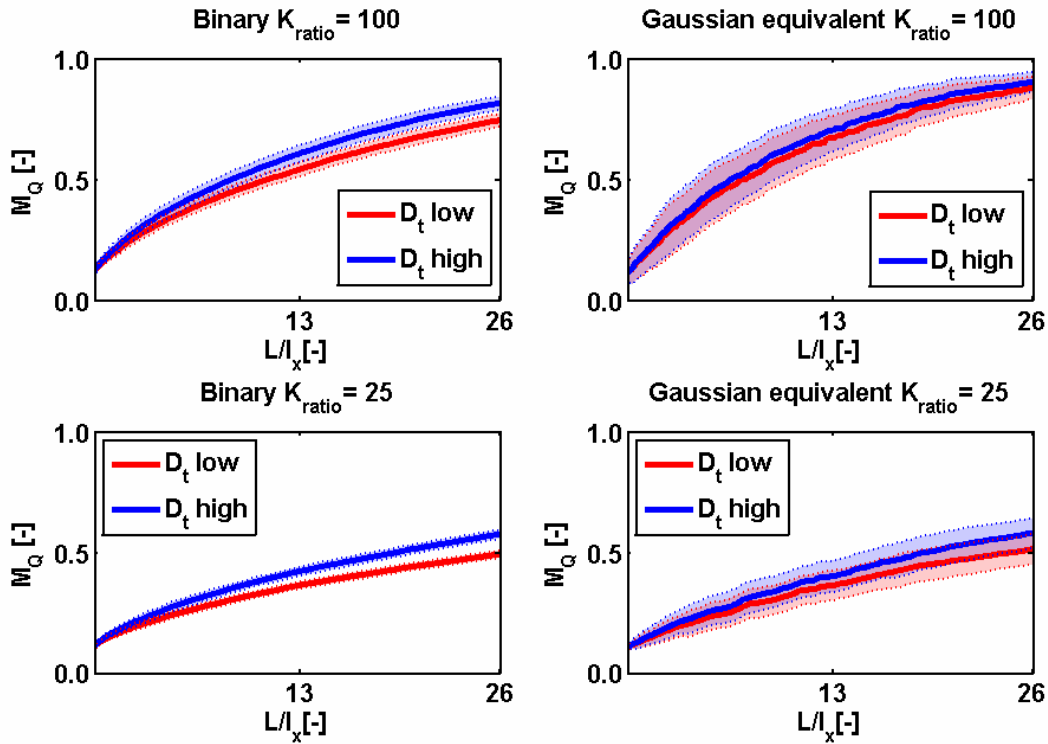


Figure 5.6: Reactor ratios. Red: low transverse dispersion coefficient; blue: high transverse dispersion coefficient. Bold lines: median; shaded regions: 16 to 84 percentiles.

Figure 5.6 shows values of the flux-related dilution index for all settings and both compounds as a function of dimensionless distance. Similarly to what we observed for the other measures of mixing, the results indicate compound-specific differences between tracers with different local transverse dispersion coefficients.

Averaging the values of the flux-related dilution index over the ensemble of realizations, we obtain a flux-related dilution index, which shows a similar dependence on distance as in a homogeneous equivalent system. Therefore, we can use the two-dimensional formulation of the semi-analytical expression given by *Chiogna et al.* [2010c] to estimate a value for an effective transverse dispersion coefficient (Eq. 5.20), using a best fit procedure (e.g. Nelder-Mead simplex algorithm).

$$E_Q(D_t) = wq_x \left(1 - \frac{\sqrt{\frac{nxD_t}{q_x w^2}}}{\sqrt{\frac{nxD_t}{q_x w^2} + \exp(1)}} + \sqrt{4\pi \exp(1) \frac{nxD_t}{q_x w^2}} \right) \quad (5.20)$$

The values of the calculated effective transverse dispersion coefficients, for compound A and B, are listed in Table 5.1. Like for the previous measures of mixing, these up-scaled values of D_t reflect differences of transverse dispersion at the local scale.

5.3.5 Discussion of conservative transport results

In the previous sections, we have quantified dilution of conservative tracers by different tools. All measures and all settings confirm that effective dispersion coefficients, quantifying transverse mixing in heterogeneous domains, should account for differences of aqueous diffusion coefficients among different compounds, at least in cases of low to moderate log-conductivity variability. Even in the case of high conductivity contrasts (e.g. $\sigma_{\ln K}=3.2$), the macroscopic solute mixing is affected by the differences in the aqueous diffusion coefficient at a statistically significant level. In highly variable media, however, the uncertainty of mixing caused by heterogeneity may be higher than the systematic difference caused by different molecular diffusion coefficients.

The results obtained for the effective dispersion coefficients derived by the flux-related dilution index and the flux-related second central moments are affected by a lower uncertainty than those based on traditional spatial moments. This outcome can easily be explained by advective plume squeezing and stretching which affects standard spatial moments, but is corrected for in the flux-weighted schemes. However the results presented in Table 5.1 show that for binary fields the effective dispersion coefficients derived with the three different methods are consistent (i.e. similar mean values), whereas more pronounced differences are obtained for the Gaussian equivalent cases. These differences can be explained by the different weight given to low concentrations in computing second central moments and the flux-related dilution index (Eqs. 5.11, 5.14, 5.17). The main advantage in using an effective dispersion coefficient derived from the flux-related dilution index is that it is affected by a lower variability than the values obtained analyzing the second central moments of the plume. The effect of flow focusing in high permeability inclusions is important, leading to an increase of approximately two orders of magnitude compared to the pore diffusion term of the local hydrodynamic transverse dispersion coefficient. Considering the results presented in Table 5.1, we can notice that a higher variance in the conductivity field leads to a higher enhancement factor.

Effective Disp. [m ² s ⁻¹]	Binary K _{Ratio} = 100	GaussianEquivalent K _{Ratio} = 100	Binary K _{Ratio} = 25	GaussianEquivalent K _{Ratio} = 25	Binary		GaussianEquivalent		
					Geom.mean	$\sigma_{\ln(D_t)}$	Geom.mean	$\sigma_{\ln(D_t)}$	
Second central moment									
D_{t low} case	5.4×10 ⁻⁸	1.9	7.9×10 ⁻⁸	1.9	2.9×10 ⁻⁸	1.9	2.4×10 ⁻⁸	1.9	
D_{t high} case	7.0×10 ⁻⁸	1.9	9.0×10 ⁻⁸	1.9	4.0×10 ⁻⁸	1.9	3.4×10 ⁻⁸	1.9	
Flux-related second moment									
D_{t low} case	5.9×10 ⁻⁸	0.2	6.0×10 ⁻⁸	0.9	2.5×10 ⁻⁸	0.1	2.2×10 ⁻⁸	0.7	
D_{t high} case	7.3×10 ⁻⁸	0.2	6.3×10 ⁻⁸	0.9	3.5×10 ⁻⁸	0.1	2.6×10 ⁻⁸	0.7	
Flux-related dilution index									
D_{t low} case	6.0×10 ⁻⁸	0.1	8.9×10 ⁻⁸	0.8	2.6×10 ⁻⁸	0.1	2.7×10 ⁻⁸	0.3	
D_{t high} case	7.4×10 ⁻⁸	0.1	9.7×10 ⁻⁸	0.8	3.5×10 ⁻⁸	0.1	3.4×10 ⁻⁸	0.4	

Table 5.1: Values of the field-scale effective transverse dispersion coefficients obtained from different measures of dilution. $D_{t low}$ represents the case for compound A (i.e., low value of D_{aq}) and $D_{t high}$ represents the case for compound B (i.e., high value of D_{aq}).

Hitherto we have focused our attention on the mean behavior of these measures of mixing and we have observed that they are all affected by a certain degree of uncertainty, which arises from the variability and uncertainty of the generated log-conductivity fields. In fact, in single realizations, the compound-specific local dispersion coefficient always influences the degree of mixing of the two compounds: the one with the lower aqueous diffusion coefficient always undergoes less mixing than the species with higher D_{aq} . In Figure 5.7 we show an example of the flux-related dilution index computed for single realizations. Figure 5.7 also shows that, in the binary case, the flux-related dilution index of the single realization behaves similarly to a homogeneous case (or the ensemble mean), showing the expected square root increase (Eq. 5.20) already after a few correlation lengths. On the contrary, in the Gaussian equivalent cases the step-like behavior indicates that permeability contrasts of some orders of magnitude act as hot spots of mixing.

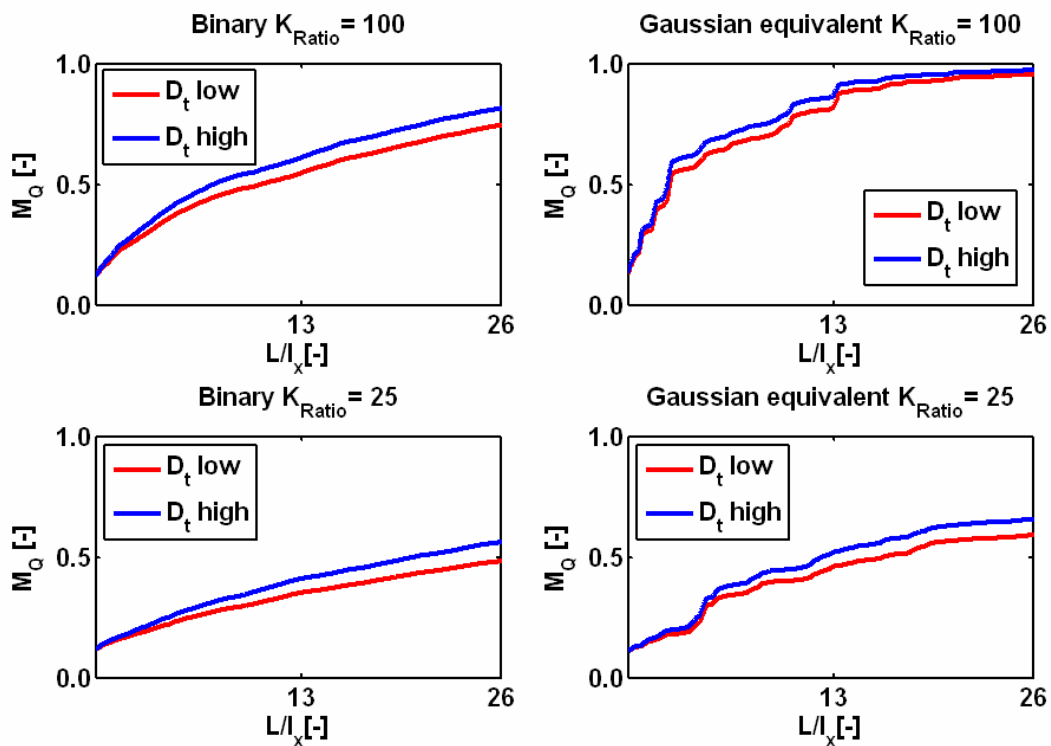


Figure 5.7: Reactor ratios for a single realization.

5.4 REACTIVE TRANSPORT

In this section, we focus our attention on mixing-controlled reactive transport, trying to extend the concepts discussed for conservative tracers to reactive systems. Like before, we discuss alternative measures of mixing, this time in the context of reactions triggered by mixing of reactants.

5.4.1 Length of steady-state reactive plumes

A parameter of utmost importance in practical applications is the length L [L] of a reactive plume, i.e. the distance from the source where the concentration of a contaminant becomes zero. The length of a steady state plume is important in groundwater risk assessment at contaminated sites. We performed numerical simulations to investigate the effects of compound-specific local transverse dispersion on the length of a reactive plume in the same heterogeneous flow fields as used for conservative transport. The results of the analysis are summarized in Table 5.2, where we report the geometric mean of the plume length computed over the ensemble of realizations and the standard deviation of its logarithm. Neglecting the compound dependence of the local transverse dispersion coefficients of the two reactive species (e.g., an organic substrate and an electron acceptor in a microbially-mediated oxidation-reduction reaction), we either overestimate or underestimate the plume length ($D_{t \text{ specific}}$ case). The latter was obtained using the compound-specific local dispersion coefficients and applying the iterative solution procedure described in Algorithm 5.1. In cases where we attribute the same local transverse dispersion coefficient to both reactants and hence we use the solution presented in section 5.2.3 for the reactive problem, we overestimate the plume length when using the lower D_{aq} for both reactants (indicated with $D_{t \text{ low}}$) or underestimate it in the other case (indicated with $D_{t \text{ high}}$). The differences are also evident for individual realizations: Figure 5.8 shows examples of steady state reactive plumes in the different flow fields. The blue contour line shows the outline of the injected reactive plume of A in case of $D_{t \text{ high}}$, the red line in case of $D_{t \text{ low}}$, while the green region shows the plume computed with the compound-specific local dispersion coefficients ($D_{t \text{ specific}}$). These results illustrate the relevance of a compound-specific parameterization of local transverse dispersion in order to correctly estimate the length of a contaminant plume. From Figure 5.8 and Table 5.2 it is also clear the influence of the variance of the conductivity field on the plume length: an higher variance (i.e., Binary and Gaussian equivalent fields with $K_{\text{Ratio}}=100$) leads to shorter plumes.

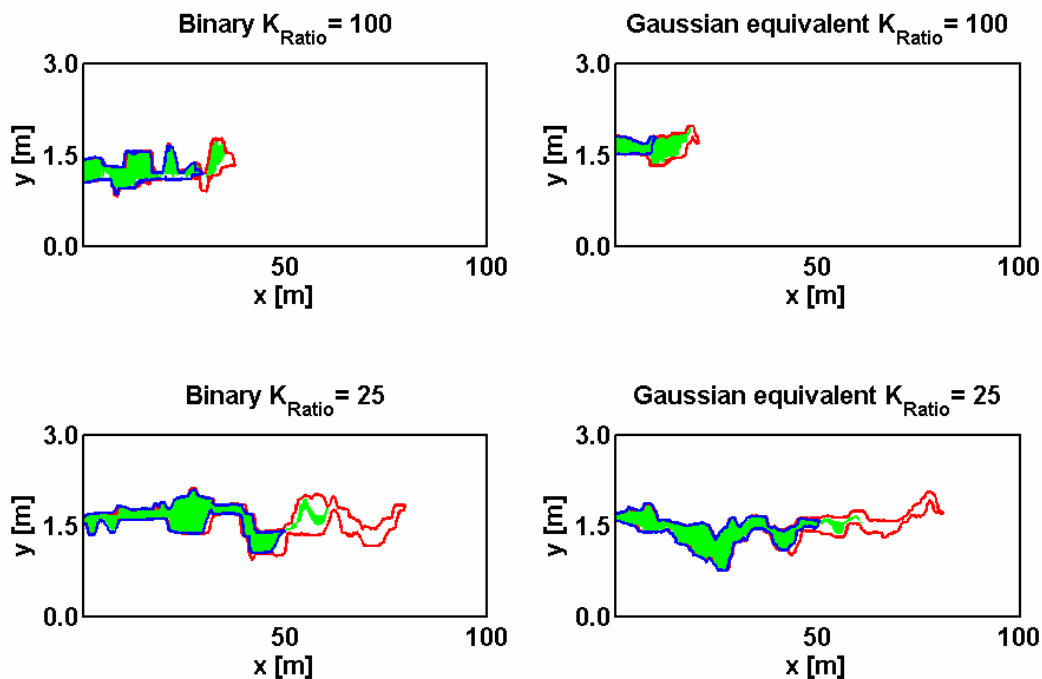


Figure 5.8: Example reactive plumes of the injected compound A. Red line: plume outline for $D_{t \text{ low}}$; blue line: plume outline for $D_{t \text{ high}}$; green area: plume extent for $D_{t \text{ specific}}$.

5.4.2 Measures of reactive mixing

In this section, we extend the concepts to quantify the dilution of a conservative tracer to a reactive system. Particular emphasis is put on the influence of compound-specific effects. In the following, we focus our attention on the flux-related dilution index and the scalar dissipation rate and we discuss how these measures can be related to the length of a reactive plume. The flux-related dilution index is chosen because it provides the approximation with the lowest variance for an effective transverse dispersion coefficient in the conservative case (Table 5.1), while the scalar dissipation rate is selected since it has been often related to the reaction rate in mixing-controlled reactive transport [e.g., *De Simoni et al.* 2005, 2007; *Bolster et al.*, 2009, 2010; *Luo et al.*, 2008; *Bellin et al.*, 2010].

For conservative tracers, the flux-related dilution index captures the compound-specific behavior leading to reliable and distinct up-scaled dispersion coefficients for different solutes. The flux-related dilution index can also be linked to the case of mixing-controlled reactive transport. Conceptualizing a homogeneous equivalent system with identical reactive plume length [*Chiogna et al.*, 2010c], we can define *a posteriori* (i.e., after performing a reactive transport simulation with defined local dispersion coefficients in a heterogeneous domain) an effective dispersion coefficient for a reactive system:

$$D_{t,eff} = \frac{v \cdot w^2}{16L \cdot \text{inverf}(X_{crit})^2} \quad (5.21)$$

in which X_{crit} [-] expresses the critical mixing ratio as defined by *Cirpka and Valocchi* [2007].

Table 5.2 lists the computed values of $D_{t,eff}$ for the case of compound-specific local transverse dispersion ($D_{t,specific}$) and the cases with identical local dispersion coefficient for both compounds ($D_{t,low}$ and $D_{t,high}$). The values of $D_{t,eff}$ calculated *a posteriori* for the reactive simulations in the different heterogeneous flow fields for the cases of $D_{t,low}$ and $D_{t,high}$ (Table 5.2) are in very good agreement with the results obtained from the conservative transport cases based on the flux-related dilution index (Table 5.1). On the contrary the value of $D_{t,specific}$ can not be predicted from conservative transport simulations and will depend on the stoichiometry of the reaction and on the concentrations of the reacting compounds. However, as shown in Table 5.2, the value of $D_{t,specific}$ calculated considering the different local dispersion properties of the reactants always lies in-between the effective dispersion coefficients obtained neglecting these effects ($D_{t,low}$ and $D_{t,high}$).

Furthermore, the flux-related dilution index allows to derive [*Chiogna et al.*, 2010c] a critical dilution index (CDI), which is the critical value of dilution needed to consume a contaminant plume upon mixing with ambient water:

$$CDI = E_Q(L) = \frac{E_Q(0)}{X_{crit}} \exp(1/2) \quad (5.22)$$

The CDI for the $D_{t,low}$ and $D_{t,high}$ cases is computed from the conservative transport simulation, considering the value of the flux-related dilution index at a distance L from the source, i.e. $E_Q(L)$. This approach is not directly applicable for the case of compound-specific local transverse dispersion because the two reactants would experience a different degree of dilution at the plume length L (i.e., different values of $E_Q(L)$) if they were transported as conservative tracers. Instead, we test whether the dispersion coefficients $D_{t,low}$ and $D_{t,high}$, computed from the values of the flux-related dilution indices for conservative transport of compounds A and B (Table 5.1), are good predictors of mixing-controlled reactive transport in

an equivalent homogeneous system. That is, we apply the iterative procedure outlined in Algorithm 5.1 to a homogeneous flow field using $D_{t\ low}$ and $D_{t\ high}$, computed as discussed above, as local transverse dispersion coefficients of compounds A and B , respectively, and compare the length of this reactive plume to the average length obtained in the heterogeneous cases $L(D_{t\ specific})$. The outcomes of these simulations are in perfect agreement with the mean values for $L(D_{t\ specific})$ presented in Table 5.2. Hence we can conclude that the up-scaled parameters derived from the flux-related dilution index of the two conservative species can be successfully applied for compound-specific reactive transport simulations to estimate the length of a reactive plume.

As shown in Section 5.3, the scalar dissipation rate is also a good measure of dilution. Various authors have used this quantity to relate the properties of a conservative component, such as the mixing ratio X , to a reactive system [De Simoni *et al.*, 2005, 2007; Luo *et al.*, 2008; Bolster *et al.*, 2010; among others]. These approaches require that all species involved experience the same local dispersion (implying identical aqueous diffusion coefficient of the different reactive species).

If we apply the chain rule of differentiation to the gradient of the product concentration C_c in Eq. 5.3, we obtain:

$$\nabla C_c = \frac{\partial C_c}{\partial X} \nabla X \quad (5.23)$$

Substituting Eq. 5.23 into the advection-dispersion-reaction equation of the reaction product C_c yields:

$$\mathbf{v} \cdot \frac{\partial C_c}{\partial X} \nabla X - \nabla \cdot \left(\mathbf{D} \frac{\partial C_c}{\partial X} \nabla X \right) = r_c \quad (5.24)$$

After some transformations, it can be shown [e.g. De Simoni *et al.*, 2005] that:

$$-\frac{\partial^2 C_c}{\partial X^2} \nabla X^T \mathbf{D} \nabla X = r_c \quad (5.25)$$

expressing that the reaction rates depends on the second derivative of the reactive species concentration with respect to the mixing ratio X times the scalar dissipation rate.

Substituting Eq. 5.25 into Eq. 5.24 and integrating over the entire cross-section perpendicular to the mean direction of flow yields [De Simoni *et al.*, 2005, 2007; Bolster *et al.*, 2010]:

$$\frac{dF_{C_c}^{tot}}{dx} = - \int_{\infty}^{\infty} \frac{\partial^2 C_c}{\partial X^2} \nabla X^T \mathbf{D} \nabla X dy \quad (5.26)$$

where $F_{C_c}^{tot}$ is the total flux of the reaction product. It may be worth noting that the rate of increase of the product mass flux is consistent with the rate of increase of the entropy of the system [Kitanidis, 1994; Beckie, 1998; Chiogna *et al.*, 2010c].

If the dependence of C_c on X was strictly quadratic, the following identity would hold:

$$\frac{dF_{C_c}^{tot}}{dx} = -\frac{\partial^2 C_c}{\partial X^2} \frac{dF_{X^2}^{tot}}{dx} \quad (5.27)$$

For non-quadratic relationships $C_c(X)$, the total fluxes of C_c and X^2 still might be approximately proportional to each other. Approximations equivalent to this one were made in the above cited studies [De Simoni *et al.*, 2005, 2007; Luo *et al.*, 2008; Bolster *et al.*, 2010]. Then, the flux of the mixing ratio squared can be used as a measure of mixing in reactive systems, too, and present another link between the mixing properties of conservative and reactive species.

We can define the end of a steady state plume as the first point along the groundwater flow direction at which the mass flux of the product $F_{C_c}^{tot}$ [MT^{-1}] will reach its maximum value:

$$F_{C_c}^{tot}(L) = \max(F_{C_c}^{tot}) \Rightarrow \left. \frac{dF_{C_c}^{tot}}{dx} \right|_L = 0 \quad (5.28)$$

Therefore, in relating mixing properties of conservative and reactive systems and in analogy to the concept of critical dilution index [Chiogna *et al.*, 2010c], we may define a critical value for the flux of the mixing ratio squared F_{X^2} . The results of the simulations for the different heterogeneous fields are reported in Table 5.2.

Both the flux-related dilution index and the mass flux of the mixing ratio squared are good measures of mixing in reactive systems. They also allow identifying, with little uncertainty, a critical value of mixing necessary to consume a reactive tracer plume but they require identical local mixing behavior of all reactants to establish a unique relationship between conservative dilution and reactive mixing. However, while, the mean value of the *critical* mass flux of the mixing ratio squared is affected by an higher degree of variability between the different explored scenarios, the mean value of the critical dilution index is practically constant between the four heterogeneous flow fields and for the D_t low and D_t high cases and equals the expected result given by Eq. 5.22 (Table 5.2). This can be explained since the value of critical dilution index given by Eq. 5.22 does not depend on any transport parameter, but just on the mass flux of a contaminant at the source ($E_Q(0)$) and the critical mixing ratio X_{crit} .

5.5 CONCLUSIONS

In this work we analyzed and compared different measures of dilution and mixing through numerical simulations of transport in heterogeneous flow fields. We have restricted our analysis to conservative and mixing-controlled reactive transport in cases of continuous injection of solutes under steady state flow and transport conditions. The following conclusions can be drawn from the results of this modeling study:

- 1) Measures of dilution calculated in a flux-related framework allow an improved quantification of mixing processes in porous media in comparison to measures based on conventional second central spatial moments. The results of our simulations show that quantities such as the flux-related second moment and the flux-related dilution index describe effective dilution processes without interference by purely advective mechanisms such as plume meandering, squeezing and spreading. As a consequence, the flux-related measures are characterized by a very low degree of uncertainty resulting in robust estimates of mixing-effective transverse dispersion coefficients. In

	Binary $K_{Ratio}=100$		GaussianEquivalent $K_{Ratio}=100$		Binary $K_{Ratio}=25$		GaussianEquivalent $K_{Ratio}=25$	
	Geom.mean	$\sigma_{ln(L)}$	Geom.mean	$\sigma_{ln(L)}$	Geom.mean	$\sigma_{ln(L)}$	Geom.mean	$\sigma_{ln(L)}$
Plume Length [m]								
$D_{t\ low}$ case	28	0.2	20	0.8	66	0.1	64	0.4
$D_{t\ specific}$ case	24	0.2	18	0.9	51	0.1	53	0.4
$D_{t\ high}$ case	22	0.2	17	0.9	48	0.1	50	0.4
	Geom.mean	$\sigma_{ln(D_t)}$	Geom.mean	$\sigma_{ln(D_t)}$	Geom.mean	$\sigma_{ln(D_t)}$	Geom.mean	$\sigma_{ln(D_t)}$
Effective disp. [m^2s^{-1}]								
$D_{t\ low}$ case	6.1×10^{-8}	0.2	8.3×10^{-8}	0.8	2.6×10^{-8}	0.1	2.7×10^{-8}	0.4
$D_{t\ specific}$ case	7.1×10^{-8}	0.2	9.2×10^{-8}	0.9	3.3×10^{-8}	0.1	3.2×10^{-8}	0.4
$D_{t\ high}$ case	7.4×10^{-8}	0.2	9.5×10^{-8}	0.9	3.5×10^{-8}	0.1	3.4×10^{-8}	0.4
	Geom.mean	$\sigma_{ln(CDI)}$	Geom.mean	$\sigma_{ln(CDI)}$	Geom.mean	$\sigma_{ln(CDI)}$	Geom.mean	$\sigma_{ln(CDI)}$
CDI [m^2s^{-1}]								
$D_{t\ low}$ case	2.06×10^{-5}	0.05	2.06×10^{-5}	0.18	2.06×10^{-5}	0.03	2.07×10^{-5}	0.10
$D_{t\ high}$ case	2.06×10^{-5}	0.06	2.04×10^{-5}	0.18	2.06×10^{-5}	0.04	2.06×10^{-5}	0.11
Eq. 5.22	2.06×10^{-5}		2.06×10^{-5}		2.06×10^{-5}		2.06×10^{-5}	
	Geom.mean	$\sigma_{ln(FX^2)}$	Geom.mean	$\sigma_{ln(FX^2)}$	Geom.mean	$\sigma_{ln(FX^2)}$	Geom.mean	$\sigma_{ln(FX^2)}$
$(F_X^2)_{crit}$ [ms^{-1}]								
$D_{t\ low}$ case	4.63×10^{-6}	0.03	4.73×10^{-6}	0.14	4.78×10^{-6}	0.01	4.87×10^{-6}	0.03
$D_{t\ high}$ case	4.57×10^{-6}	0.04	4.75×10^{-6}	0.16	4.72×10^{-6}	0.02	4.84×10^{-6}	0.04

Table 5.2: Geometric means of the reactive plume lengths (L), of the effective dispersion coefficient, of the critical dilution index (CDI) and of the critical flux of the mixing ratio squared. $D_{t\ low}$, $D_{t\ high}$ and $D_{t\ specific}$, represent the case of local low dispersion coefficients for all the species, local high dispersion coefficient for all the species and local compound-specific dispersion coefficient, respectively.

particular, as shown in Section 5.4.2, the effective transverse dispersion coefficients derived from conservative transport simulations using the flux-related dilution index can be directly applied for the description of reactive transport modeling in homogeneous equivalent systems.

- 2) The experimental evidence of compound-specific local dispersion of dissolved species with different aqueous diffusion coefficients is still relevant at field scales. In particular, for moderate to low heterogeneity flow fields the compound-specific behavior is significant not only in each individual realization, but also in a probabilistic average sense. The mean behavior over the ensemble of realizations leads to the identification of effective up-scaled parameters that still reflect the compound-specific local-scale properties.
- 3) In mixing-controlled reactive transport, some of the proposed measures of dilution of a conservative solute such as the flux-related dilution index and the flux of the mixing ratio squared allow to quantify reactive mixing. Critical values of these measures identify the amount of mixing required to consume a reactive plume and are directly related to the length of a steady state plume, a parameter of major importance in practical applications.
- 4) A consistent way of upscaling transverse mixing in mixing-controlled reactive transport of compounds with different aqueous diffusion coefficients is to evaluate an effective transverse dispersion coefficient of each compound from dilution-based

measures in conservative transport, and to apply these compound-specific effective transverse dispersion coefficients to mixing-controlled reactive transport in the equivalent homogeneous medium. Of course, it is also possible to evaluate *a posteriori* a mean effective transverse dispersion coefficient for all reacting compounds that matches the reactive plume length. This value must be between the effective coefficients of the two reactants. However, the weighting of the two effective coefficients will depend on the stoichiometry of the reaction and the concentrations of the reacting compounds.

This study points to the need of considering the local-scale compound-dependent transverse mixing also in studies at field scales, at least when mixing controlled reactions are in the focus. We assess that numerical codes and recently developed analytical methods for reactive transport based on the use of the mixing ratio [e.g., *De Simoni et al.* 2005, 2007; *Cirpka and Valocchi*, 2007; *Luo et al.*, 2008; *Bolster et al.*, 2010] may need to be further developed in order to capture this effect.

The possibility of identifying effective measures of mixing and, in particular, the link between dilution of conservative and reactive species, should be explored beyond the assumptions of the present study: including, for instance, transient conditions, different dynamics of compound release and more complex reaction kinetics. The present study also showed the advantage of working in a flux-related framework when attempting to quantitatively describe transverse mixing processes affecting solute transport in porous media. We think that further developments in this direction of theoretical concepts, numerical studies and possibly also experimental techniques (e.g. high-resolution measurements of mass fluxes) will contribute to advance our capability to understand and describe mixing processes in complex subsurface environments.

REFERENCES

- Bauer, R.D., M. Rolle, S. Bauer, C. Eberhardt, P. Grathwohl, O. Kolditz, R.U. Meckenstock, and C. Griebler (2009), Enhanced biodegradation by hydraulic heterogeneities in petroleum hydrocarbon plumes, *J. Contam. Hydrol.*, 105, 56-68.
- Bear, J. (1972), *Dynamics of fluids in porous media*; Dover: New York, USA.
- Beckie, R.D. (1998), Analysis of scale effects in large-scale solute transport models, in *Scale Dependence and Scale Invariance in Hydrology*, edited by G. Sposito Ed., pp.314 – 334, Cambridge University Press, New York.
- Bellin, A., G. Severino and A. Fiori (2010), On the local concentration pdf of solutes reacting upon mixing, *Water Resour. Res.* (in press)
- Berkowitz, B., H. Scher, and S. E. Silliman, (2000), Anomalous transport in laboratory-scale, heterogeneous porous media, *Water Resour. Res.*, 36(1), 149-158.
- Bijeljic, B. and Blunt, M.J (2007), Pore-scale modelling of transverse dispersion in porous media, *Water Resour. Res.*, 43, W12S11; DOI 10.1029/2006WR005700.
- Bolster, D., M. Dentz, M. and T. Le Borgne (2009), Solute dispersion in channels with periodically varying apertures, *Phys. Fluids*, 21, 056601.
- Bolster, D., F. J. Valdés-Parada, T. Le Borgne, M. Dentz, and J. Carrera (2010), Mixing in confined stratified aquifers, *J. Contam. Hydrol.*, (in press).
- Boving, T, and P. Grathwohl (2001), Matrix diffusion coefficients in sandstones and limestones: Relationship to permeability and porosity. *J. Contam. Hydrol.*, 53 (1-2), 85-100.
- Cao, J, and P. K. Kitanidis (1998), Pore-scale dilution of conservative solutes: An example, *Water Resour. Res.*, 34(8), 1941-1949.
- Carvalho, J.F.R. and J.M.P.Q. Delgado (2000), Lateral dispersion in liquid flow through packed beds at $Pe < 1400$. *American Institute for Chemical Engineering*, 46 (5), 1089-1095.
- Chiogna, G., C. Eberhardt, P. Grathwohl, O.A. Cirpka and M. Rolle (2010a), Evidence of compound dependent hydrodynamic and mechanical transverse dispersion by multitracer laboratory experiments, *Environ. Sci. Technol.*, 44(2), 688-693, doi: 10.1021/es9023964.
- Chiogna G., M. Rolle, O.A. Cirpka and P. Grathwohl, (2010b), Modeling mixing-controlled reactive transport: importance of compound dependent hydrodynamic and (hydro)mechanical transverse dispersion, paper presented at XVIII International Conference on Computational Methods in Water Resources, CMWR, Barcelona, Spain.
- Chiogna G., O.A. Cirpka, P. Grathwohl and M. Rolle, (2010c), Transverse mixing of conservative and reactive tracers in porous media: quantification through the concepts of flux-related and critical dilution indices, *Water Resour. Res.* (in press).
- Cirpka, O.A. (2002), Choice of dispersion coefficients in reactive transport calculations on smoothed fields, *J. Contam. Hydrol.*, 58, 261-282.

- Cirpka, O.A. and A.J. Valocchi (2007), Two-dimensional concentration distribution for mixing-controlled bioreactive transport in steady state, *Adv Water Resour*, 30 (6-7), 1668-1679.
- Cirpka, O. A., E. O. Frind, and R. Helmig (1999a), Numerical simulation of biodegradation controlled by transverse mixing, *J. Contam. Hydrol.*, 40(2), 159–182.
- Cirpka, O. A., E. O. Frind, and R. Helmig (1999b), Streamline-oriented grid-generation for transport modelling in two-dimensional domains including wells, *Adv. Water Resour.*, 22(7), 697–710.
- Cirpka, O. A., R. Helmig, and E. O. Frind (1999c), Numerical methods for reactive transport on rectangular and streamline-oriented grids, *Adv. Water Resour.*, 22(7), 711–728.
- Cirpka, O.A., A. Olsson, Q. Ju, A. Rahman and P. Grathwohl (2006), Determination of transverse dispersion coefficients from reactive plumes lengths, *Ground Water*, 44 (2), 212-221.
- Clement, T.P., Y. Sun., B.S. Hooker and J.N. Petersen (1998), Modeling Multi-species Reactive Transport in Groundwater Aquifers, *Groundwater Monitoring & Remediation*, 79-92.
- Cussler, E.L. (2009) Diffusion, mass transfer in fluid systems, Cambridge University Press, New York, USA.
- Dagan, G. (1984), Solute transport in heterogeneous porous formations, *J. Fluid Mech.* 145, 151-177.
- Dagan, G. (1990), Transport in heterogeneous porous formations: Spatial moments, ergodicity, and effective dispersion, *Water Resour. Res.*, 26(6): 1281-1290.
- Dagan, G. (1991), Dispersion of a passive solute in nonergodic transport by steady velocity-fields in heterogeneous formations, *J. Fluid Mech.* 233, 197-210.
- Davis, T.A., and I.S. Duff (1997), An unsymmetric-pattern unifrontal method for sparse LU factorization, *SIAM J. Matrix anal. Appl.*, 18(1), 140-158.
- de Barros, F.P.J., and W. Nowak (2010), On the link between contaminant source release conditions and plume prediction uncertainty, *J. Contam. Hydrol*, (in press)
- De Simoni, M., J. Carrera, X. Sanchez-Vila, and A. Guadagnini (2005), A procedure for the solution of multi-component reactive transport problems, *Water. Resour. Res.*, 41, W11410, doi:10.1029/2005WR004056.
- De Simoni, M., X. Sanchez-Vila, J. Carrera, and M.W. Saaltink (2007), A mixing ratios-based formulation for multicomponent reactive transport, *Water Resour. Res.*, 43, W07419; doi:10.1029/2006WR005256.
- Dentz, M., and J. Carrera (2005), Effective solute transport in temporally fluctuating flow through heterogeneous media, *Water. Resour. Res.*, 41, W08414, doi: 10.1029/2004WR003571.
- Dentz, M., H. Kinzelbach, S. Attinger, and W. Kinzelbach (2000a), Temporal behavior of a solute cloud in a heterogeneous porous medium 1. Point-like injection, *Water Resour. Res.*, 36(12), 3591-3604.

- Dentz, M., H. Kinzelbach, S. Attinger, and W. Kinzelbach.(2000b) Temporal behavior of a solute cloud in a heterogeneous porous medium 2. Spatially extended injection, *Water Resour. Res.*, 36(12), 3605-3614.
- Dentz, M, T. Le Borgne, A. Englert and B. Bijeljic (2010), Mixing, spreading and reaction in heterogeneous porous media: A brief review, *J. Contam. Hydrol.* (in press).
- Dykaar B. B. and P. K. Kitanidis (1992), Determination of the effective hydraulic conductivity for heterogeneous porous media using a numerical spectral approach 1. Method, *Water Resour. Res.*, 28 (4), 1155-1166.
- Englert, A., S. S. Bubbard, K. H. Williams, L. Li and C. I. Steefel (2009), Feedbacks between hydrological heterogeneity and bioremediation induced biogeochemical transformations, *Environ. Sci. Technol.*, 43, 5197 – 5204.
- Freeze, R.A.; Cherry, J.A. Groundwater; Prentice-Hall International: NJ, USA, 1979.
- Gelhar, L. W., and C.L. Axness (1983), Three-dimensional stochastic analysis of macrodispersion in aquifers, *Water Resour. Res.*, 19 (1), 161-180.
- Ginn, T. R., E. M. Murphy, A. Chilakapati and U. Seeboonruang (2001), Stochastic-convective transport with nonlinear reaction and mixing: application to intermediate-scale experiments in aerobic biodegradation in saturated porous media, *J. Contam. Hydrol.*, 48, 121-149.
- Grathwohl, P. (1998), Diffusion in natural porous media: contaminant transport, sorption/desorption, and dissolution kinetics; Kluwer Academic Publishers: Boston, MA, USA.
- Haberer, C.M., M. Rolle, S. Liu, O.A. Cirpka and P. Grathwohl (2010), A high-resolution non-invasive approach to quantify oxygen transport across the capillary fringe and within the underlying groundwater. *J. Contam. Hydrol.* (in press).
- Ham, P.A.S., R.J. Schotting, H. Prommer and G.B. Davis, G.B., (2004), Effects of hydrodynamic dispersion on plume lengths for instantaneous bimolecular reactions. *Adv. Water Resour.*, 27, 803–813.
- Hazen, A. (1892), Some physical properties of sands and gravels special reference to their use in filtration. *Ann. Rep. State Board of Health Mass.*, 24, 541-556.
- Heinz, J., S. Kleinedam, G. Teutsch, and T. Aigner (2003), Heterogeneity patterns of Quaternary glaciofluvial gravel bodies(SW-Germany): application to hydrogeology. *Sediment. Geol.*, 158, 1-23.
- Kapoor, V. and P.K. Kitanidis (1998), Concentration fluctuations and dilution in aquifers, *Water Resour. Res.*, 34(5), 1181-1193.
- Kitanidis, P.K. (1988), Prediction by the method of moments of transport in heterogeneous formations, *J. Hydrol.*, 102(1-4): 453-473.
- Kitanidis, P.K. (1994), The concept of dilution index, *Water Resour. Res.*, 30 (7), 2011-2026.
- Klenk, I.D. and P. Grathwohl (2002), Transverse vertical dispersion in groundwater and the capillary fringe. *J. Contam. Hydrol.*, 58, 1-2, 111-128.

- Le Borgne, T., M. Dentz, D. Bolster, J. Carrera, J.-R. de Dreuzy and P. Davy (2010) Non-Fickian mixing: Temporal evolution of the scalar dissipation rate in porous media, *Adv. Water Resour.* (in press).
- Lerner, D.N., S.F. Thornton, M.J. Spence, S.A. Banwart, S.H. Bottrell, J.J. Higgs, H.E.H. Mallinson, R.W. Pickup, and G.M. Williams (2000), Ineffective natural attenuation of degradable organic compounds in a phenol-contaminated aquifer, *Ground Water*, 38, 922-928.
- Li, L., C. A. Peters and M. A. Celia (2006), Upscaling geochemical reaction rates using pore-scale network modelling, *Adv. Water Resour.*, 29, 1351-1370.
- Li, L., C. I. Steefel, M. B. Kowalsky, A. Englert and S. S. Hubbard (2010), Effects of physical heterogeneities on mineral transformation and biomass accumulation during biostimulation experiments at Rifle, Colorado, *J. Contam. Hydrol.*, 112 (1-4), 45-63.
- Liedl, R., A. J. Valocchi, P. Dietrich, and P. Grathwohl (2005), Finiteness of steady state plumes, *Water Resour. Res.*, 31, 1-8.
- Luo, J., M. Dentz, J. Carrera, and P. Kitanidis (2008), Effective reaction parameters for mixing controlled reactions in heterogeneous media, *Water Resour. Res.*, 44, W02416, doi: 10.1029/2006WR005658.
- Maier, U. and Grathwohl, P. (2006): Numerical experiments and field results on the size of steady state plumes. *J. Contam. Hydrol.*, 85, 33-52.
- Neuman, S.P., C.L. Winter, and C.M. Newman (1987), Stochastic theory of field-scale Fickian dispersion in anisotropic porous media, *Water Resour. Res.* 23(3): 453-466.
- Olsson, A. and P. Grathwohl (2007), Transverse dispersion of non-reactive tracers in porous media: a new nonlinear relationship to predict dispersion coefficients. *J. Contam. Hydrol.*, 92, 3-4, 149-161.
- Prommer, H., B. Anneser, M. Rolle, F. Einsiedl, and C. Griebler (2009), Biogeochemical and isotopic gradients in a BTEX/PAH contaminant plume: model-based interpretation of a high-resolution field data set, *Environ. Sci. Technol.*, 43, 8206-8212.
- Rahman, A.M., S. Jose, W. Nowak, and O.A. Cirpka (2005), Experiments on vertical transverse mixing in a large-scale heterogeneous model aquifer. *J. Contam. Hydrol.*, 3-4, 80, 130-148. doi:10.1016/j.jconhyd.2005.06.010.
- Rajaram, H., and L.W. Gelhar, (1993a) Plume scale-dependent dispersion in heterogeneous aquifers 1. Lagrangian analysis in a stratified aquifer, *Water Resour. Res.*, 29(9): 3249-3260.
- Rajaram, H., and L.W. Gelhar, (1993b) Plume scale-dependent dispersion in heterogeneous aquifers 2. Eulerian analysis and three-dimensional aquifers, *Water Resour. Res.*, 29(9): 3261-3276.
- Rajaram, H., and L.W. Gelhar, (1995) Plume-scale dispersion in aquifers with a wide range of scales of heterogeneity, *Water Resour. Res.*, 31(10): 2469-2482.
- Rolle, M., C. Eberhardt, G. Chiogna, O.A. Cirpka, and P. Grathwohl (2009), Enhancement of dilution and transverse reactive mixing in porous media: Experiments and model-based interpretation, *J. Contam. Hydrol.*, 110, 130-142.

- Rolle, M., G. Chiogna, R. Bauer, C. Griebler and P. Grathwohl (2010), Isotopic fractionation by transverse dispersion: flow-through microcosms and reactive transport modeling study, *Environ. Sci. Technol.*, 44, 6167-6173.
- Steeffel, C. I., D. J. DePaolo and P. C. Lichtner (2005), Reactive transport modeling: An essential tool and a new research approach for the earth sciences. *Earth and Planetary Science Letters*, 240, 539-558.
- Scheidegger, A.E. (1961), General theory of dispersion in porous media, *J. Geophys. Res.*, 66(4), 3273-3278.
- Tartakovsky, A.M., G.D. Tartakovsky and T.D. Scheibe (2009), Effects of incomplete mixing on multicomponent reactive transport, *Adv. Water Resour.*, 32(11), 1674-1679.
- Thierrin, J., and P.K. Kitanidis (1994), Solute dilution at the Borden and Cape Cod groundwater tracer tests, *Water Resour. Res.*, 30(11), 2883-2890.
- Werth, C.J., O.A. Cirpka, and P. Grathwohl (2006), Enhanced mixing and reaction through flow focusing in heterogeneous porous media, *Water Resour. Res.*, 42, W12414; doi: 10.1029/2005WR004511.
- Willingham, T.W., C.J. Werth, and A.J. Valocchi (2008), Evaluation of the effects of porous media structure on mixing-controlled reactions using pore-scale modeling and micromodel experiments, *Environ. Sci. Technol.*, 42, 3185-3193.
- Willingham, T., C. Zhang, C.J. Werth, A.J. Valocchi, M. Oostrom, and T.W. Wiestma (2010), Using dispersivity values to quantify the effects of pore-scale flow focusing on enhanced reaction along transverse mixing zone, *Adv. Water Res.*, 33, 525-535.

Conclusions

The correct definition and quantification of an effective transverse dispersion coefficient at the field-scale is of primary importance in order to improve our capability to quantitatively describe reactive transport in aquifer systems. In fact, for plumes at steady state, transverse mixing is usually the process which limits degradation of the dissolved contaminants. The aim of this work was to investigate in detail the processes at the Darcy and at the field-scale which control transverse mixing. In the following, the main outcomes of this study are summarized.

- *Flow focusing and transient flow as enhancement factors for mixing.* Laboratory bench-scale experiments allow to quantify the relevance of different physical processes better than field-scale experiments since the experimental conditions are easier to control. The results presented in the first Chapter demonstrate what was suggested by *Werth et al.* [2006]: flow focusing in high-permeability inclusions significantly enhances mixing of conservative and reactive tracers. Moreover, the extent to which the reactive fringe is focused considerably contributes to the degree of mixing enhancement. This depends on the source width, the geometry of the porous medium, on the permeability contrast between the surrounding porous matrix and the high-permeability inclusions and, in particular, on their location. In the limiting case where a plume is just affected by meandering but it does not pass through a high-permeability zone, the heterogeneous nature of the field may even have a negative effect on mixing, as shown in Chapter 2. Compared to the effect of non-stationary flow conditions, flow focusing is more effective in terms of dilution enhancement of non-sorbing species, since oscillating flow fields only cause local mixing enhancement where the groundwater flow changes its principal direction. Based on the outcomes of the experimental study presented in Chapter 1, and its quantitative interpretation through a forward model, a further investigation of laboratory and field-scale synthetic scenarios was presented in Chapter 2. The outcomes of this second study regarding flow focusing as enhancement factor for dilution and mixing has shown that an effective transverse dispersion coefficient higher than the local-scale one has to be expected in heterogeneous field-scale domains. These results are in agreement with the evidences reported in the literature for high-resolution field-scale studies [e.g. *Prommer et al.*, 2009].
- *New measures of dilution.* Three new measures of dilution have been introduced in this work: the flux-related dilution index (based on the concept of dilution index introduced by *Kitanidis* [1994]), the flux-related second moment (based on the concept of effective dispersion introduced by *Kitanidis* [1988] and *Dentz and Carrera* [2003]) and the critical dilution index. The first two refer to mixing of conservative tracers while the third one addresses reactive problems. In Chapter 1, we observed the advantages of the use of the flux-related dilution index with respect to the second central moment in an experimental heterogeneous setup, where steady state conditions apply and there is a continuous injection of a tracer. While the second central moment analysis fails in capturing the points of major dilution in the medium, the flux-related dilution index is able to quantify the mixing enhancement due to flow focusing in high-permeability inclusions. The introduction of information about the mass fluxes drastically improve the quality of dilution measures, leading to a significant drop in the uncertainty of the effective transverse dispersion coefficients related to those quantities. This is particularly evident for the flux-related second moment analysis: compared with the standard second moment analysis the improvement presented in

Chapter 5 is evident. The property of the flux-related dilution index to capture in an effective way both the local effects of Darcy-scale dispersion as the effects of flow focusing in high-permeability inclusions is reflected in the effective dispersion coefficient that we can derive from this quantity. This parameter is in very good agreement with the required effective dispersion coefficient to simulate reactive transport, as shown in Chapters 2 and 5, while the one related with the moments of the plume underestimate this parameter. It has to be noticed, that, the values for the effective dispersion coefficient derived from the flux-related dilution index is generally in very good agreement with the transverse dispersion coefficients used in field-scale modeling studies [e.g., *Frind and Hokkanen, 1987; Prommer et al., 2006 and 2009*]. Furthermore it has been possible to quantify the amount of mixing required to completely extinguish a contaminant plume. This quantity was called critical dilution index and it was defined for instantaneous bimolecular complete reactions. As shown in Chapters 2 and 5, flux-related and critical dilution indices are directly related and through their analysis it is possible to link in an effective way conservative and reactive mixing. Both these quantities are based on the concept of information entropy of the plume. This approach in comparison to the traditional moment analysis, provides new and improved insights in terms of description of mixing processes. Another quantity considered to measure dilution is the scalar dissipation rate [*Beckie, 1998*], which is related to the rate of increase of the dilution index [*Kitanidis, 1994*], of the flux-related dilution index [*Chiogna et al., 2010*] and to the mass flux of a reaction product [e.g. *De Simoni et al., 2005*]. However, the main disadvantage of the dissipation rate is that it does not lead to an effective dispersion coefficient for field-scale simulations.

- *Compound-specific local transverse dispersion coefficient.* Laboratory bench-scale experiments are fundamental for the verification of theories and to improve our process understanding [*Oswald and Kinzelbach, 2004*]. In Chapter 3 we used them to verify if the classical representation of transverse mechanical dispersion given by *Scheidtger* [1961] was able to correctly predict the dispersive behavior of tracers characterized by different aqueous diffusion coefficients transported in the same porous medium. The outcomes of multi-tracer laboratory bench-scale experiments showed that local transverse dispersion is compound-specific even at high flow velocities, where the mechanical dispersion term is the dominant one and the same dispersive behavior was expected for different compounds. Hence different aqueous diffusion coefficients lead to different physical displacements of the solutes. This behavior is not only reflected, as expected, in the pore diffusion term but also in the mechanical dispersion term. The theoretical approach to this problem proposed by *Bear and Bachmat* [1967], predicted a similar effect which was parameterized through the introduction of a function of the Péclet number in the mechanical dispersion term, but no experimental evidences were provided in order to verify this specific point. Furthermore it was confirmed that local transverse dispersion does not increase linearly with the flow velocity, in agreement with previous experimental works [e.g., *Klenk and Grathwohl, 2002; Delgado, 2006; Olsson and Grathwohl, 2007*]. These results are particularly important in order to capture the behavior of reactive species with different aqueous diffusion coefficients (e.g. oxidation of hydrocarbons) and point to the need of considering compound-specific dispersion coefficients both in numerical codes as well as in analytical methods for reactive transport.

- *Effects of compound specific transverse dispersion on reactive transport and isotope fractionation.* In the experiments presented in Chapter 4 we focused our attention on the effects that the newly introduced parameterization of local transverse dispersion has both on conservative as well as on reactive transport in terms of stable isotopes analysis. We observed a significant fractionation of ethylbenzene isotopologues during conservative transport at steady state. This effect was particularly pronounced at the plume fringe and contrasted with the common assumption that physical processes only provide a negligible contribution to isotope fractionation. The compound-specific parameterization of local transverse dispersion coefficient introduced in Chapter 3 was able to predict and to correctly quantify this behavior. Successively, bioreactive experiments were performed in two subsequent stages: a first oxic phase, and a second phase with aerobic and anaerobic (i.e. ethylbenzene oxidation coupled to nitrate reduction) degradation. The outcomes of the performed analytical and numerical reactive transport simulations of the different experimental phases confirmed that both the effects of physical processes (diffusion and dispersion) and microbially-mediated reactions have to be considered to match the observed isotopic fractionation behavior.
- *Effects of compound-specific local transverse dispersion in field-scale scenarios.* In Chapter 5 we investigated if the compound-specific behavior of transverse dispersion observed at Darcy-scale is still relevant at the field scale and therefore should be considered in field-scale effective dispersion coefficients. The outcomes of Monte Carlo synthetic realizations of different heterogeneous flow fields point to the need of considering appropriate compound-dependent effective dispersion coefficients. All the measures of dilution investigated for conservative tracers (i.e., second moment analysis, flux-related second moment analysis, flux-related dilution index and scalar dissipation rate) captured the difference in mixing that exists at the local-scale for compounds characterized by different aqueous diffusion coefficients. This outcome is of particular importance in case of reactive transport modeling: the assumption of considering the same aqueous diffusion coefficient for different species led to a systematic underestimation or overestimation of the length of a contaminant plume. Moreover, an appropriate measure of mixing for reactive solutes as the critical dilution index provides a very good estimation of the amount of mixing required in order to completely extinguish a reactive plume. Furthermore, based on the concept of homogeneous equivalent system introduced in Chapters 2 and 5, it is possible to define an effective transverse dispersion coefficient for field-scale studies able to both correctly quantify the local-scale compound-specific effects and the field-scale flow focusing effects.

Based on the results of this work and following a similar approach based on both experimental investigations and numerical modeling studies, future research should particularly address the following open problems:

- *Quantification of the enhancement factor due to flow focusing.* A practical relation to quantify a priori the effective dispersion coefficient based on characteristic properties of the aquifer (e.g., statistic of the distribution of conductivity values or the characteristic values of high and low conductivity zones) is missing. This relationship could find application in analytical expressions like the one of *Liedl et al.* [2005], or *Cirpka et al.* [2006], which require an estimated value for the effective transverse dispersion coefficient at the field scale in order to predict the length of a reactive plume.

- *Generalization of the concept of critical dilution index.* It would be worth to investigate the applicability of the concept of critical dilution index for other kind of reaction kinetics (e.g. Michaelis-Menten) and to apply this concept for practical purposes such as assessing plume development and/or potential remediation interventions on the basis of modeling studies.
- *Generalization of the compound-specific transverse dispersion coefficient.* The outcomes of the experiments presented in Chapter 3 could be generalized performing further experiments using different grain sizes for the experimental setup. Furthermore, we can not overlook, from a theoretical point of view, the necessity of finding a sound up-scaling theory from the pore to the Darcy-scale able to explain the results of the experimental study.
- *Implementation of new laboratory bench-scale experiments.* The investigation of (compound-specific) mixing processes in three dimensional porous media has not been addressed yet in a comprehensive way neither from the experimental nor from the theoretical point of view. A new set of three dimensional laboratory bench-scale experiments could hence lead to new interesting and important insights about the processes which control mixing in transverse direction.
- *Development of new analytical solutions.* The introduction of a compound specific transverse dispersion coefficient requires a development of the actual (semi-)analytical methods for reactive transport based on the concept of mixing ratio [e.g., *Cirpka and Valocchi, 2007; De Simoni et al., 2005*] in order to obtain a more general solution to the problem.

The topic of mixing and reactions in porous media presents many intrinsic difficulties, especially when dealing with problems at the typical field-scale. This work added some new insights on the understanding of mixing and mixing-controlled processes by means of well-controlled high-resolution laboratory experiments and numerical simulations at the Darcy- and field-scales. Furthermore, an attempt was made to propose and develop new concepts and measures in order to improve our capability to describe and quantify mixing processes in complex heterogeneous porous formations.

REFERENCES

- Bear, J. and Y.A. Bachmat (1967), A generalized theory on hydrodynamic dispersion in porous media. IASH Symp. Artificial Recharge and management of aquifers, Haifa, Israel IASH, P.N. 1967 72, 7-16.
- Beckie, R.D. (1998), Analysis of scale effects in large scale solute transport models, in scale Dependence and scale Invariance in Hydrology, edited by G. Sposito Ed., pp.314 – 334, Cambridge University Press, New York.
- Chiogna G., O.A. Cirpka, P. Grathwohl and M. Rolle, (2010), Transverse mixing of conservative and reactive tracers in porous media: quantification through the concepts of flux-related and critical dilution indices, *Water. Resour. Res.* (accepted).
- Cirpka, O.A., A. Olsson, Q. Ju, A. Rahman and P. Grathwohl (2006), Determination of transverse dispersion coefficients from reactive plumes lengths. *Ground Water*, 44 (2), 212-221.
- De Simoni, M., J. Carrera, X. Sanchez-Vila, and A. Guadagnini (2005), A procedure for the solution of multi-component reactive transport problems, *Water. Resour. Res.*, 41, W11410, doi:10.1029/2005WR004056.
- Delgado, J. (2006) A. critical review of dispersion in packed beds. *Heat Mass Transfer*, 42(4), 279-310.
- Dentz, M. and Carrera, J. (2003), Effective dispersion in temporally fluctuating flow through a heterogeneous medium, *Phys. Rev. E* 68 (3): 036310.
- Frind, E.O. and G.E. Hokkanen (1987), Simulation of the Borden Plume using the alternating direction Galerkin technique, *Water Resour. Res.*, 23 (5), 918-930.
- Kitanidis, P.K. (1988), Prediction by the method of moments of transport in heterogeneous formations, *J. Hydrol.* 102(1-4): 453-473.
- Kitanidis, P.K. (1994), The concept of dilution index, *Water Resour. Res.*, 30 (7), 2011-2026.
- Klenk, I.D., and P. Grathwohl (2002), Transverse vertical dispersion in groundwater and the capillary fringe. *J. Contam. Hydrol.*, 58, 111-128.
- Liedl, R., A.J. Valocchi, P. Dietrich and P. Grathwohl (2005), Finiteness of steady state plumes. *Water Resour. Res.*, 31, W12501; DOI 10.1029/2005WR004000.
- Olsson, A. and P. Grathwohl (2007), Transverse dispersion of non reactive tracers in porous media: A new nonlinear relationship to predict dispersion coefficients. *J. Contam. Hydrol.*, 92, 149-161.
- Oswald, S.E. and W. Kinzelbach, (2004) Three-dimensional physical benchmark experiments to test variable-density flow model, *J. Hydrol.*, 290, 22-42.

Prommer H, N. Tuxen and P.L. Bjerg (2006), Fringe-controlled natural attenuation of phenoxy acids in a landfill plume: integration of field-scale processes by reactive transport modeling, *Environ. Sci. Technol*, 40 (15), 4732-4738.

Prommer, H., B. Anneser, M. Rolle, F. Einsiedl, and C. Griebler (2009), Biogeochemical and isotopic gradients in a BTEX/PAH contaminant plume: model-based interpretation of a high-resolution field data set, *Environ. Sci. Technol*, 43, 8206-8212.

Scheidegger, A.E. (1961), General theory of dispersion in porous media, *J. Geophys. Res.*, 66(4), 3273-3278.

Werth, C.J., O.A. Cirpka and P. Grathwohl (2006), Enhanced mixing and reaction through flow focusing in heterogeneous porous media. *Water Resour. Res.*, 42, W12414; DOI 10.1029/2005WR004511.

Worch, E. (1993), Eine neue Gleichung zur Berechnung von Diffusionskoeffizienten gelöster Stoffe. *Vom Wasser*, 81, 289-297.

Acknowledgements

This work was financed by a grant from the Deutsche Forschungsgemeinschaft (DFG) within the subproject “Diffusion/dispersion-limited mixing and reactions in saturated homogeneous and heterogeneous porous media.” of the Research Group FOR. 525 “Analysis and modeling of diffusion/dispersion-limited reactions in porous media”.

First and foremost I want to thank Dr.-Ing. Massimo Rolle: his precious help and guide gave me the chance to grow both from a scientific as well as from a personal point of view. “For the *shake* of simplicity” I will say that without his help and patience it would have been much more difficult to achieve this important goal.

I want to express my explicit gratitude to my supervisors Prof. Dr. Peter Grathwohl and Prof. Dr.-Ing. Olaf A. Cirpka, who provided excellent support to my work throughout these years and for their readiness for spontaneous discussions.

Furthermore I would like to thank Dr. Christina Eberhardt and Christina Haberer for their help in the experimental part of this study.

I greatly appreciated the fruitful discussions within the Environmental Fluid Mechanics and Hydrology Group of Prof. Dr. Peter Kitanidis at Stanford University, especially with David Hochstetler and Liu Yuan. I am also indebted to Prof. Grathwohl and Dr. Rolle for giving me this important exchange opportunity.

I would like to thank Prof. Dr.-Ing. Alberto Bellin and Prof. Dr. Andreas Kappler for their willingness to take part as examiner in my Ph.D. defence.

Thanks to all members of the Institute of Applied Environmental Geosciences for their cooperativeness and the great working atmosphere, and especially to the *Mensa team* (Ben, Jin Biao, Maik, Massimo, Claudius, Olaf, Raul and many others) who did not just help me to survive after so many lunches in the Mensa but to enjoy this period as well.

I want to thank all my friends, spread all around the world, for helping me out of occasional downs and for sharing with me many happy moments.

Sincere thanks are given to my parents, my sister and my brother-in-law with Giulia, who never stopped to encourage and sustain me in those long years, where the distance has strengthened our family.

In the end I want to thank Giorgia, the person who most shared with me feelings and experiences in the past four years, and has chosen to stay beside me, day by day, in our future life together.

Curriculum Vitae

Birth date: 23. October 1983

Birth place: Trento, Italy

Curriculum studiorum

- 09.2007 - 09.2009 Master Degree in Applied Environmental Geosciences – University of Tübingen Grade A (Excellent).
- Thesis: ‘The Relevance of Compound Dependent Dispersion Coefficients for Modeling of Mixing-Controlled Reactive Transport’.
- 04.2005 - 07.2007 Italian-German Double degree program in Physics (focus on computational physics and nanotechnologies):
- Diplom Physiker - University of Tübingen Average Note 1.6.
Laurea Specialistica in Fisica (Master Degree in Physics) - University of Trento, Grade 108/110.
- Thesis: ‘The Derivative Riemann Problem in Special Relativistic Hydrodynamics’.
- 09.2002 - 09.2005 Laurea breve in Fisica (Bachelor degree in Physics) - University of Trento; Grade 106/110
- Thesis (at ITC-Irst, SRD group): ‘Electric characterization of BJT silicon radiation detectors’.

List of Peer-Reviewed Publications

Chiogna G., O.A. Cirpka, P. Grathwohl, and M. Rolle, (2010), **Relevance of local compound-specific transverse dispersion for conservative and reactive mixing in heterogeneous porous media**. Water Resour. Res, (submitted).

Chiogna G., O.A. Cirpka, P. Grathwohl, and M. Rolle, (2010), **Transverse mixing of conservative and reactive tracers in porous media: quantification through the concepts of flux-related and critical dilution indices**. Water Resour. Res, (in press).

Rolle M., G. Chiogna, R. Bauer, C. Griebler and P. Grathwohl, (2010), **Isotopic fractionation by transverse dispersion: flow-through microcosms and reactive transport modeling study**, Environ. Science and Technology, 44, 6167-6173

Chiogna G., M. Rolle, O.A. Cirpka and P. Grathwohl, (2010), **Modeling mixing-controlled reactive transport: importance of compound dependent Hydrodynamic and (hydro)mechanical transverse dispersion**, CMWR (in press)

Chiogna G., C. Eberhardt, P. Grathwohl, O.A. Cirpka and M. Rolle, (2010), **Evidence of compound dependent hydrodynamic and mechanical transverse dispersion by multi-tracer laboratory experiments**, Environ. Science and Technology, 44, 666-693

Rolle, M., C. Eberhardt, G. Chiogna, O. A. Cirpka and P. Grathwohl, (2009), **Enhancement of dilution and transverse reactive mixing in porous media: experiments and model-based interpretation**, J. Cont. Hydrology, 110 (3-4), 130-142

Conference Proceedings and Posters

Chiogna, G., Rolle. M., Cirpka O.A. and Grathwohl, P. (2010) **Flux related and critical dilution indices: quantitative indicators of mixing and mixing-controlled reactions in heterogeneous porous media**, AGU Fall meeting, San Francisco

Rolle M., Chiogna G., Bauer R., Griebler C. and Grathwohl P. (2010) **Influence of transverse mixing on stable isotope fractionation: flow-through microcosms and reactive transport modeling study**, AGU Fall meeting, San Francisco.

Rolle M., Chiogna G., Eberhardt C., Haberer C., Griebler C., Cirpka O.A., and Grathwohl P. (2010) **Two-dimensional flow-through experiments: versatile test systems for a combined investigation of transport and reactive processes in porous media**, GQ, Zurich.

Chiogna, G., Rolle. M., Cirpka O.A. and Grathwohl, P. (2010) **Flux related and critical dilution index as tools to quantify mixing and mixing-controlled reactions in porous media**, IAHR, Valencia.

Chiogna, G., Rolle, M, Eberhardt, C., Cirpka, O.A. and Grathwohl, P. (2010) **Compound-dependent mechanical transverse dispersion and its relevance in modeling mixing-controlled reactive transport**, FHDGG, Tübingen*.

Rolle, M., Chiogna, G., Eberhardt, C. and Grathwohl, P. (2009) **Compound dependent hydrodynamic and (hydro)mechanical dispersion: evidence from multi-tracer laboratory experiments and transport simulations**, AGU Fall meeting, San Francisco.

Rolle. M, Eberhardt, C., Chiogna, G. and Grathwohl, P (2009) **Experimental investigation and numerical modeling of diffusion/dispersion limited reactions in saturated porous media**, TRePro II, Karlsruhe.

Chiogna, G., Eberhardt, C., Rolle. M and Grathwohl, P. (2009) **Dependence of Mechanical Dispersion on Aqueous Diffusion: Results From Multi-tracer Laboratory Experiments**, Aquaterra final conference, Tübingen.

Chiogna, G., Eberhardt, C., Rolle M. and Grathwohl, P. (2008) **Determination of vertical transverse dispersion with multi-tracer laboratory experiments (H51I-0995)**, AGU Fall meeting, San Francisco

* Best poster award.

Ergänzungsblatt zur Eigenleistung

Hiermit beantrage ich die kumulative Promotion im Fach Geowissenschaften mit dem folgenden Promotionsthema:

Transverse mixing of conservative and reactive tracers in porous media.


unter Zusammenfassung der im folgenden aufgeführten Publikationen und Manuskripte. Die Eigenanteile an diesen Publikationen sind in Prozent in der Tabelle angegeben und entsprechen der jeweiligen Beteiligung an 1) Idee und Fragenstellung 2) Datengenerierung 3) Auswertung und Interpretation und 4) Erstellung der Publikation.

Hauptbetreuer des Promotionsvorhabens ist Prof. Dr. Peter Grathwohl.

Peer-Reviewed Publikationen

1. Chiogna G., O.A. Cirpka, P. Grathwohl, and M. Rolle, (2010), Relevance of local compound specific transverse dispersion coefficients on conservative and reactive mixing: insights from a transport modeling study. Water Resour. Res (submitted)
2. Chiogna G., O.A. Cirpka, P. Grathwohl, and M. Rolle, (2010), Transverse mixing of conservative and reactive tracers in porous media: quantification through the concepts of flux-related and critical dilution indices. Water Resour. Res (in press)
3. Rolle M., G. Chiogna, R. Bauer, C. Griebler and P. Grathwohl, (2010), Isotopic fractionation by transverse dispersion: flow-through microcosms and reactive transport modeling study, Environ. Science and Technology, 44, 6167-6173.
4. Chiogna G., C. Eberhardt, P. Grathwohl, O.A. Cirpka and M. Rolle, (2010), Evidence of compound dependent hydrodynamic and mechanical transverse dispersion by multi-tracer laboratory experiments, Environ. Science and Technology, 44, 666-693.
5. Rolle, M., C. Eberhardt, G. Chiogna, O. A. Cirpka and P. Grathwohl, (2009), Enhancement of dilution and transverse reactive mixing in porous media: experiments and model-based interpretation, J. Cont. Hydrology, 110 (3-4), 130-142.

Publikation	Idee und Fragenstellung	Datengenerierung	Auswertung und Interpretation	Erstellung der Publikation
1	80 %	100 %	70 %	90 %
2	80 %	100 %	80 %	90 %
3	30 %	50 %	50 %	10 %
4	90 %	60 %	90 %	90 %
5	30 %	30 %	50 %	10 %



Gabriele Chiogna